

# Part 2

## Diffraction



# Diffraction in TEM

## CHAPTER PREVIEW

This chapter will set the stage for our discussion of imaging using diffraction contrast. Put simply, diffraction contrast arises because the intensity of the diffracted beams is different in different regions of the specimen. These variations may arise because of changing diffracting conditions or because of differences in specimen thickness. In our study of diffraction in the TEM, we will see spots—lots of them. Sometimes the ‘spots’ will be small faint points and other times they will be large disks, which themselves contain ‘structure’ and more information. Other patterns will contain lines that we will examine in Chapters 19–21.

We need to know how to use the information that these spot patterns (diffraction patterns or DPs) contain. We will discuss the practical question of how we can best record the DPs, so that we can maximize the information they contain, but we will not try to give a rigorous proof of every equation used. These DPs give direct crystallographic information about small areas of the specimen. This capability is one of the most important features of the TEM, because we can relate the crystallography to the images we see.

In reading this chapter you should remember our discussion of the scattering of waves using an array of slits (Chapter 2). Much of the analysis is geometrically the same as we found for visible light—it’s essentially the same physical optics. The big differences are that we have ‘modulated’ holes which are located in 3D space and both our wavelengths and the spacing of the ‘holes’ are very small.

A note on history: spot patterns in DPs have always been recorded using a photographic emulsion but many TEMs no longer have photographic plates. The CCD has a much greater dynamic range but you may need to record the DP using several different camera lengths. Plus—burning a hole in photographic film is one thing, doing the same to the CCD is another.

### 11.1 WHY USE DIFFRACTION IN THE TEM?

Let’s begin by looking at an experimental DP. The pattern shown in Figure 11.1, like those we introduced in Chapter 2, was recorded from a thin specimen, in this case silicon. The main features to note are there are many spots and the spots vary in intensity and size (these are related effects).

We can list some of the questions you might ask on first seeing such a DP.

- What is it?
- What can we learn from it?
- Why do we see it?
- What determines the scale? What determines the distances between the spots or the positions of the lines?

What do we want to know about our specimen? To a materials scientist, perfect crystals are often pretty

boring and can usually be better studied using such techniques as X-ray diffraction (for structural characterization), the electron microprobe (for chemical characterization), etc., although new EM techniques may change this situation. The TEM is the instrument of choice when the specimen is not perfect, particularly when the feature of interest is what makes the material imperfect or, paradoxically, useful!

The questions that we can address using DPs obtained in the TEM include the following

- Is the specimen crystalline? Crystalline and amorphous materials have very different properties.
- If it is crystalline, then what are the crystallographic characteristics (lattice parameter, symmetry, etc.) of the specimen?
- Is the specimen monocrystalline? If not, what is the grain morphology, how large are the grains, what is the grain-size distribution, etc.?



**FIGURE 11.1.** An experimentally observed DP showing the central, intense, direct beam and an array of diffraction spots from different atomic planes. Such a pattern, with sharply focused spots, is best obtained by underfocusing the beam.

Remember, however, that SADPs patterns are not always the most useful DPs, since CBED (Chapters 20 and 21) can give you other useful information. Nevertheless, we are emphasizing SADPs here, since we use them to explain the contrast in TEM images, in Part III.

## 11.2 THE TEM, DIFFRACTION CAMERAS, AND THE TV

The use of electron diffraction for materials studies began around 1930 using diffraction cameras which very much resembled X-ray tubes in their physical appearance. Later on, if you pursue TEM in depth, you will find many of the earlier texts on electron diffraction useful for gaining a deeper understanding of TEM. It will be helpful to bear in mind some of the historical circumstances behind these developments when reading some of these texts. For example, many articles show ray diagrams with the optic axis horizontal. One reason for this is that much of the early theoretical analysis was developed as an extension of X-ray diffraction (XRD) or by researchers who were actively using either X-ray or electron-diffraction cameras. In each case, the optic axis of the instrument was horizontal as is still the case for visible-light optical benches. The optic axis of all electron microscopes is now vertical although the beam may originate at either the top or the bottom of the column. Actually, more than one of the early TEMs, e.g., the Philips EM100, was built with the optic axis horizontal and the electron beam directed at the observer. This arrangement is similar to that used for television, but remember that in TEM we are using very high energy electrons ( $\geq 100$  keV rather than 20 keV used in a TV). References to some of the early texts, and their historical significance, are given at the end of this chapter. When you are reading early texts on TEM remember that many were written at a time when most TEMs operated at 100 kV. This fact may easily be overlooked but it affects many features of diffraction including the camera length.

We will be talking about *positions* of spots and *not their intensities* for most of the time in this book. This type of analysis differs from many X-ray studies. The reason that beam intensities are not measured in TEM is that the electron beams are diffracted many times in a typical TEM specimen. A similar, but not identical, situation actually occurs when producing powder patterns by X-ray diffraction (XRD); diffraction then occurs in many different grains at the same time. We can compare the electron-diffraction pattern with that encountered in XRD. In the X-ray case, if you have a single crystal, then you either have to rotate the crystal to 'see' all the beams or use 'white' radiation (i.e., essentially use a range of wavelengths). Electron diffraction is very different. We can use a single wavelength and still see many diffracted beams. The techniques differ also with respect to the time

- What is the orientation of the specimen or of individual grains with respect to the electron beam?
- Is more than one phase present in the specimen? If so, how are they oriented?

In general, if we see spots then the specimen is at least partly crystalline. (We'll discuss quasicrystals later.) The ability to determine crystallographic orientations locally (down to the nm level) gives TEM its great advantage over SEM and visible-light microscopes. Later on we can make this determination even more precise (to an accuracy of  $\sim 0.001^\circ$ ) using convergent-beam patterns, as we'll see in Chapter 21.

In this chapter we will restrict the discussion to the geometry of the spot patterns. These are necessarily associated with crystalline materials. We'll see that spot patterns provide a great deal of information themselves; they also provide the basis for understanding other DPs. We will find that standard DPs which are common to a group of materials allow us quickly to recognize particular orientations and even certain grain boundaries and twin boundaries, etc., without having to index the pattern from scratch. For example, in a particular orientation, all cubic crystals give the same array of spots although some of the spots may have no intensity! We will consider the intensity of the spots in Chapter 12.

it takes to record a DP on a photographic plate; XRD takes minutes or hours unless you have a synchrotron or a position-sensitive detector to count every photon, while electron-diffraction patterns can be recorded in  $<1$  second although longer is usually better because it means you will have 'spread the beam' (made the incident beam more parallel); for photographic film you'll use several seconds to a minute or more.

Much of the discussion of electron diffraction follows directly from the analysis of XRD. This has advantages and disadvantages, depending on whether or not you are familiar with XRD. Several references to XRD are given at the end of the chapter. When considering diffraction, remember that there are important differences between electrons and X-rays:

- Electrons have a much shorter wavelength than the X-rays commonly encountered in the research lab.
- Electrons are scattered more strongly because they interact with both the nucleus and the electrons of the scattering atoms through Coulomb forces.
- Electron beams are easily directed because electrons are charged particles.

It is particularly important that the electron beam can be deflected off the optic axis a short distance above the specimen and then pass through the specimen; this process of tilting the beam was described in Section 9.1.D. The most obvious effect of this deflection on the DP is that the whole DP is translated relative to the viewing screen. The more subtle effect results from the change in the direction of the incident beam with respect to the crystal lattice, as we will discuss in subsequent chapters.

### 11.3 SCATTERING FROM A PLANE OF ATOMS

If you go back to Chapter 3 on elastic scattering you'll see that we introduced the two different ways of thinking about diffraction: the Laue conditions and Bragg's law. In this chapter we'll derive Bragg's law again, introducing a vector notation that we'll use throughout the rest of the book. In Chapter 12, we'll do the same with the Laue conditions.

The simple diagram in Figure 11.2 shows an *initial* wavefront,  $W_I$ , being scattered by a plane of atoms to produce a *diffracted* wavefront,  $W_D$ . Whether or not  $W_D$  corresponds to a diffracted beam will depend on whether the atoms are scattering in phase, which itself is determined by the angles between the incident beam, the diffracted beam, and the diffracting planes. The conditions for the individual waves being in phase are known as the Laue conditions, which we introduced in Section 3.10.B. To analyze the situation

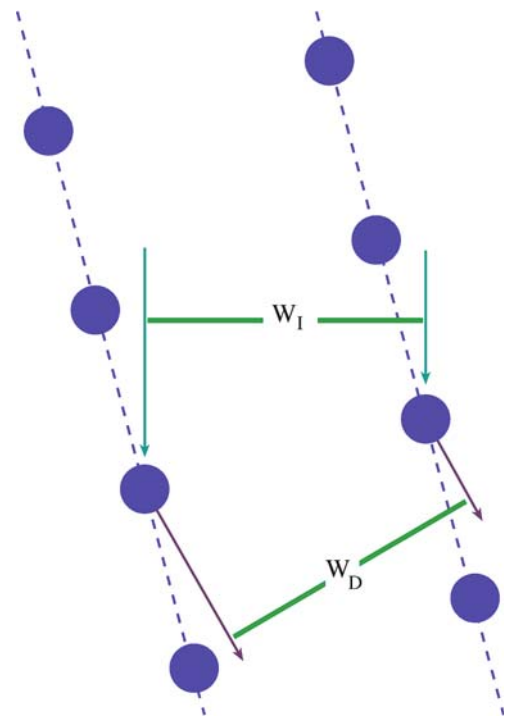


FIGURE 11.2. Scattering from two planes of atoms.  $W_I$  and  $W_D$  are the incident and diffracted wavefronts, respectively.

we first simplify the diagram as shown in Figures 11.3 and 11.4. These figures define the wave-propagation vectors, which we will refer to simply as the wave vectors or the  $\mathbf{k}$ -vectors. We begin by considering scattering from only two atoms.

Notice that we are already mixing the concepts of waves and beams.

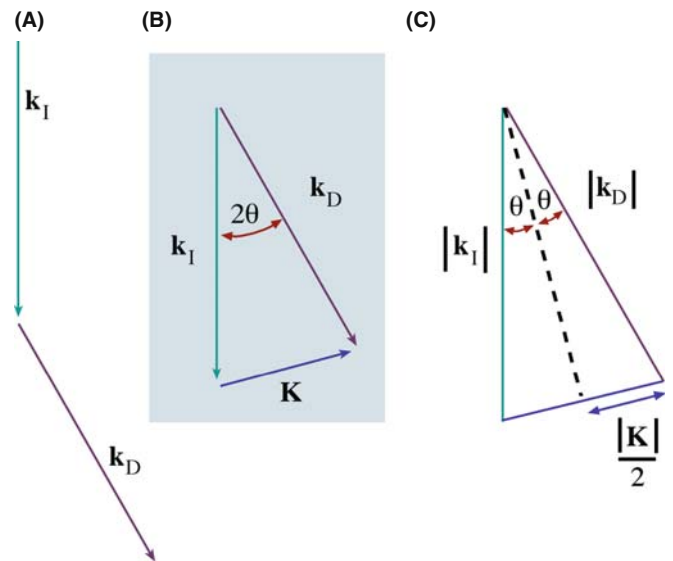
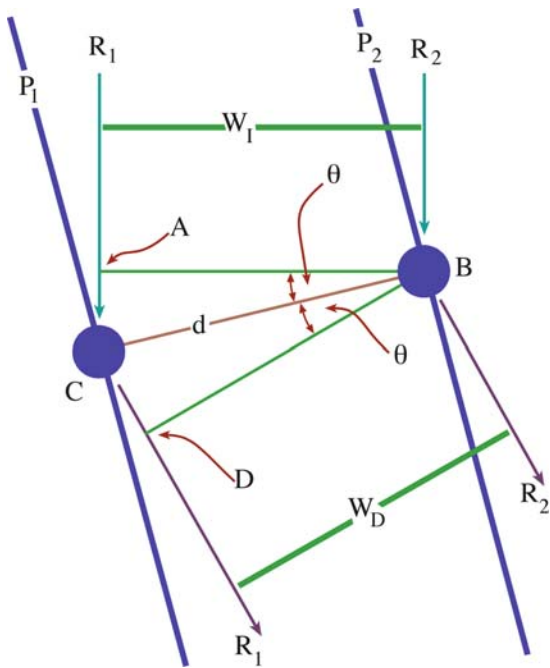


FIGURE 11.3. Definition of the scattering vectors: (A) the incident wavefront normal is  $\mathbf{k}_I$ , the diffracted wave normal is  $\mathbf{k}_D$ ; (B)  $\mathbf{K}$  is the difference vector ( $= \mathbf{k}_D - \mathbf{k}_I$ ); (C)  $\sin \theta$  is defined as  $\mathbf{K}/2\mathbf{k}_I$ .





**FIGURE 11.4.** Two beams are scattered from two points, C and B, which lie on different planes,  $P_1$  and  $P_2$ . The rays travel different distances giving a path difference of  $AC + CD$ .

We'll only consider plane wavefronts, i.e., the wavefront is flat and  $\mathbf{k}$  is normal to this wavefront. The diagrams in Figure 11.3A and B define vectors  $\mathbf{k}_I$ ,  $\mathbf{k}_D$ , and  $\mathbf{K}$  and gives us the following important equation (which is just vector addition)

$$\mathbf{K} = \mathbf{k}_D - \mathbf{k}_I \quad (11.1)$$

where  $\mathbf{k}_I$  and  $\mathbf{k}_D$  are the  $\mathbf{k}$ -vectors of the incident and diffracted waves, respectively. The vector  $\mathbf{K}$  is thus the change in  $\mathbf{k}$  due to diffraction. An important feature of this analysis is that this construction can be made for any  $\mathbf{k}_D$  and thus for any value of  $\mathbf{K}$ ; the angle  $\theta$  shown here need not be a Bragg angle.

Following our discussion in Section 3.10.B, we can always write that

$$|\mathbf{k}_I| = |\mathbf{k}_D| = \frac{1}{\lambda} = |\mathbf{k}| \quad (11.2)$$

providing the energy of the electron is unchanged during diffraction, i.e., the scattering process is elastic. From Figure 11.3C we can write an expression for  $\theta$  using simple trigonometry

$$\sin \theta = \frac{|\mathbf{K}|/2}{|\mathbf{k}_I|} \quad (11.3)$$

or

$$|\mathbf{K}| = \frac{2 \sin \theta}{\lambda} \quad (11.4)$$

$|\mathbf{K}|$ , like  $|\mathbf{k}_I|$ , has units of  $\text{nm}^{-1}$  if  $\lambda$  is measured in nm.  $\mathbf{K}$  and  $\mathbf{k}_I$  are then referred to as *reciprocal-lattice vectors*. Note that this scattering process is taking place inside the crystal and therefore the  $\mathbf{k}$ -vectors are all appropriate to the electrons inside the crystal (rather than in the vacuum).

#### EQUATION 11.4 IS VERY IMPORTANT

Whenever you see the term  $\sin \theta/\lambda$  remember that it is just  $\mathbf{K}/2$  and is thus related to a change in wave vector.

If we now extend this argument to consider the interference between waves scattered from two points (which you can visualize as being atom sites) then we have the situation sketched in Figure 11.4. This figure should remind you of the idea of constructive and destructive interference which we discussed back in Section 3.10. You will recognize that the geometry of Figure 11.4 is essentially a cross section of the two slits used by Young to demonstrate the wave nature of light (see also Section 2.10). We can then define two planes  $P_1$  and  $P_2$  to be normal to the vector  $\mathbf{CB}$  which has length  $d$ . The distance traveled by ray  $R_1$  is then larger than that traveled by ray  $R_2$  by the path difference  $AC + CD$ . Simple geometry shows that

$$AC + CD = 2d \sin \theta \quad (11.5)$$

which is the basis for Bragg's law, as we'll now see.

### 11.4 SCATTERING FROM A CRYSTAL

We introduced the Bragg angle in Figure 3.9 as the most important scattering angle in TEM; at the Bragg angle the electron waves interfere constructively. If we now analyze Figure 11.4 further, we see that when  $\theta$  equals the Bragg angle,  $\theta_B$ , equation 11.4 becomes

$$|\mathbf{K}| = \frac{2 \sin \theta_B}{\lambda} \quad (11.6)$$

When  $\theta$  is  $\theta_B$ , the path difference in equation 11.5 is  $n\lambda$ , where  $n$  is any integer, and the equation becomes

$$n\lambda = 2d \sin \theta_B \quad (11.7)$$

This is Bragg's law (equation 3.21). If  $n$  is 1

$$2 \sin \theta_B = \frac{\lambda}{d} \quad (11.8)$$

but we already know from equation 11.6 that, at the Bragg angle,

$$2 \sin \theta_B = \lambda |\mathbf{K}| \quad (11.9)$$

so when we are at the Bragg angle, the magnitude of the vector  $\mathbf{K}$  has a special value,  $\mathbf{K}_B$ ,

$$|\mathbf{K}_B| = \frac{1}{d} \quad (11.10)$$

and we define this vector,  $\mathbf{K}_B$ , to be  $\mathbf{g}$  so that

$$\mathbf{K}_B = \mathbf{g} \quad (11.11)$$

This sequence of steps may seem rather pedantic but the conclusion is extremely important. Bragg's law and the geometry used to 'prove' it will be used so frequently in our discussions that it is worthwhile to delve a little into what it really tells us. Although it is not really a valid treatment of the phenomenon we are seeing, Bragg's law gives us a very useful physical picture of the diffraction process because the diffracting planes appear to behave as mirrors for the incident electron beam. Therefore, the diffracted beams, or the spots in the DP, are often called 'reflections' and we sometimes refer to the vector  $\mathbf{g}$  as the diffraction vector. This derivation is simply geometry. In Section 12.3 we will derive the Laue equations and hence deduce Bragg's law from first principles.

### DIFFRACTION, NOT REFLECTION

Don't forget we are really dealing with diffraction, not reflection, and we derived Bragg's law by considering just two atoms. We still examine reflections, but they're not.

The reason that this derivation of Bragg's law is not really valid (it just gives the right answer) is that it really applies to scattering at a glancing angle where the beam exits the same surface as it enters, not transmission.

We mentioned earlier that the angles shown in all of our figures are exaggerated for the case of diffraction in the TEM. For example, for 111 planes in Cu,  $d$  is 0.21 nm;  $\lambda$  is 3.35 pm (0.00335 nm or 0.0335 Å) for 120-kV electrons; equation 11.8 then gives  $\theta = 7.97$  mrad (0.46°) for  $n = 1$ . As a rule of thumb, the Bragg angles of interest are usually no more than 1° when we are forming images (although important information may be present in DPs at much larger, 10–20°, angles). You will find it useful to remember the order of magnitude of these numbers.

### DEGREES AND RADIAN

Remember 10 mrad is 0.573°, i.e., about 0.5°.

We can now generalize from single atoms to planes of atoms. Let's imagine that Figure 11.4 shows two 'planes of atoms,'  $P_1$  and  $P_2$ , and that the points B and C are not necessarily atoms but are simply points on these planes and that  $d$  is the shortest distance between

the two planes. How is the 'in-phase' nature changed if we move atom B but keep it on plane  $P_2$ ?

Consider scattering from a single plane as shown in Figure 11.5. Geometry shows that while ray  $R_1$  travels a distance EJ, ray  $R_2$  travels a distance HF and that these two distances are equal. Thus there is no path difference for scattering from atoms located anywhere on a particular plane. This seemingly trivial result means that we can generalize our conclusions from Figure 11.4.

This result is summarized in Figure 11.6. Rays  $R_1$ ,  $R_2$ , and  $R_3$  all scatter in phase if  $\theta = \theta_B$ .

### SCATTERING FROM A PLANE

It does not matter how the atoms (scattering centers) are distributed on these two planes; the scattering from any two points on planes  $P_1$  and  $P_2$  will produce the same path difference  $2d \sin \theta$ .

Next we extend this analysis to include many parallel planes each a distance  $d$  from its neighbors, as is shown in Figure 11.7.

In the special case of Bragg diffraction, the scattering semiangle between the incident beam and the Bragg-diffracted beam is twice the Bragg angle ( $2\theta_B$ ). See Figure 11.7 and refer back to Section 2.12.

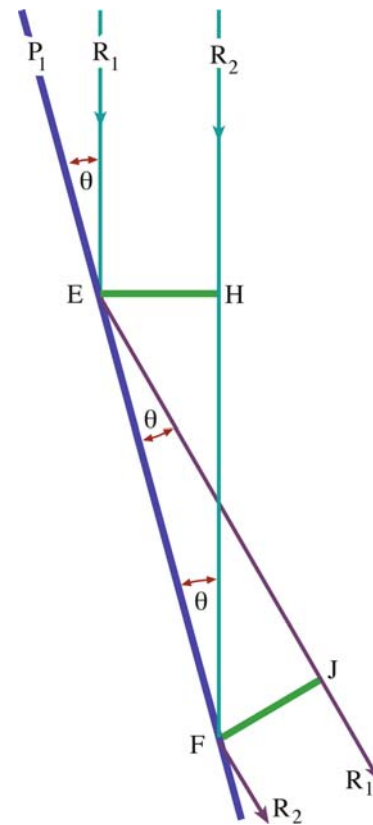
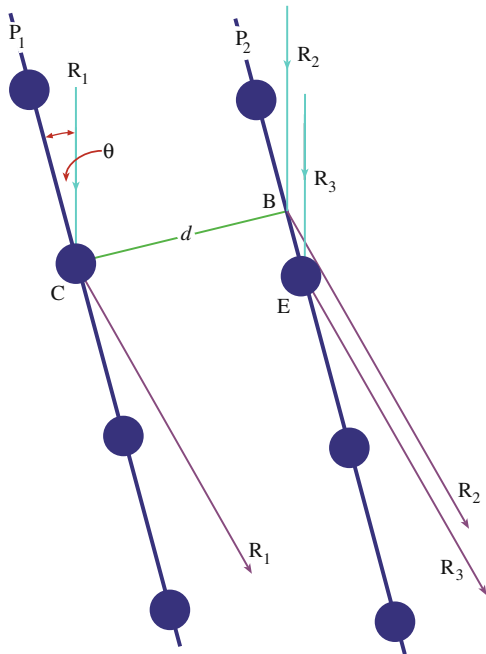
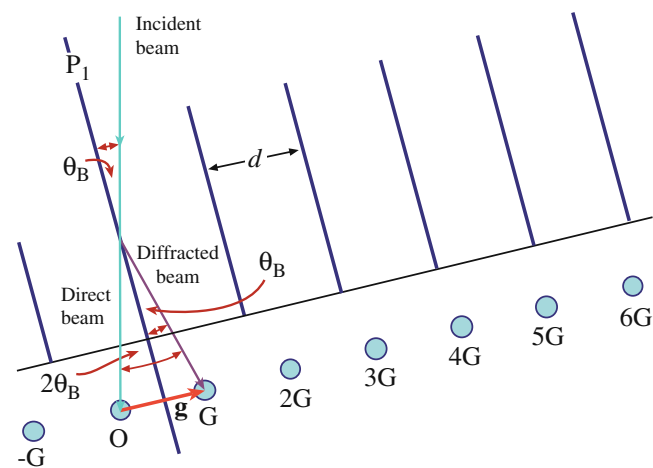


FIGURE 11.5. Two beams are scattered from two points, E and F, which lie on the same plane  $P_1$ . This simple diagram shows that the two beams travel the same distance since triangles EHF and FJE are congruent.



**FIGURE 11.6.** Scattering from three points on two planes. The path difference for scattering from points B and C is  $2d \sin \theta$ , so the path difference for scattering from points C and E is also  $2d \sin \theta$ . Hence, scattering in the direction of the diffracted beam from all points shown will be in phase if  $2d \sin \theta = n\lambda$ .

The Bragg reflection,  $\mathbf{g}$ , is then perpendicular to the set of planes. Clearly this is just another way of expressing equation 11.11. Figures 11.2 and 11.7 remind us that Bragg diffraction occurs when  $\mathbf{K}$  has the value  $\mathbf{g}$ .



**FIGURE 11.7.** Diffraction from a set of planes a distance  $d$  apart. The planes have been oriented to be in the Bragg diffracting condition ( $\theta_B$  is the incident angle). Note that the planes are not parallel to the incident beam. The resultant diffraction spots (reciprocal-lattice points) are labeled  $G$ ,  $2G$ , etc. The vector  $\mathbf{g}$  from the origin ( $O$ ) to the first diffraction spot  $G$  is normal to the diffracting plane.

## THE BRAGG ANGLE

Be very careful with this definition; it is too easy to assume that the Bragg angle,  $\theta_B$ , is the scattering semiangle: it is not! In all other cases,  $\theta$  really is the semiangle.

## 11.5 MEANING OF $n$ IN BRAGG'S LAW

As is shown in Figure 11.7, and in the DP in Figure 11.1, in practice there will not just be one Bragg reflection but a series of reflections which are periodically spaced along a line; these are known as a *systematic row* of reflections,  $-G, 0, G, 2G, 3G$ , etc., with corresponding diffraction vectors,  $\bar{\mathbf{g}}, \mathbf{0}, \mathbf{g}, 2\mathbf{g}, 3\mathbf{g}$ , etc.

*Notation:* When discussing beams in diffraction patterns, the letter  $O$  will refer to the 'direct' beam which is present even when there is no specimen; the letter  $G$  (not bold—it's not a vector) will refer to any single diffracted beam; the number  $\mathbf{0}$  (bold) will refer to the diffraction vector for beam  $O$  (it is a vector of zero length) and the letter  $\mathbf{g}$  (always bold to remind us that it is a vector) will denote the diffraction vector (in the DP) for beam  $G$ . Having said that, many microscopists use  $G$  and  $\mathbf{g}$  interchangeably, so beware.

## BAR $\mathbf{g}$

The vector  $\bar{\mathbf{g}}$  is pronounced "bar  $\mathbf{g}$ " and connects  $O$  to  $-G$ , which is pronounced "minus  $\mathbf{g}$ "! You will also hear  $\bar{\mathbf{g}}$  pronounced "g bar."

These other reflections ( $n\mathbf{g}$ , where  $n \neq 1$ ), called higher-order reflections, are particularly important in TEM. Pictorially, you can imagine them as arising from the interference of electrons scattered from planes which are a distance  $nd$  apart, where  $n$  is a rational fraction. To understand the physical meaning of this statement, put a plane  $P_3$  half way between  $P_1$ , and  $P_2$  as shown in Figure 11.8.

Now planes  $P_1, P_2$ , and  $P_3$  will scatter in phase when

$$2 \left( \frac{d}{2} \right) \sin \theta = \lambda \quad (11.12)$$

because the new 'd' is  $d/2$ . Thus coherent scattering will occur when

$$|\mathbf{g}_2| = \frac{2}{d} \quad (11.13)$$

i.e., when

$$|\mathbf{g}_2| = 2|\mathbf{g}| \quad (11.14)$$

## 11.6 A PICTORIAL INTRODUCTION TO DYNAMICAL EFFECTS

Dynamical diffraction traditionally strikes fear into the heart of the non-mathematician. Unfortunately, in TEM most practical imaging situations involve dynamical scattering. The terminology derives from X-ray theory (where it is not nearly so important). The reason it is very important in electron diffraction is that the electron beam interacts so strongly with the atoms in the crystal. For most purposes, dynamical diffraction can be thought of in quite a simple manner, as you can see in Figure 11.9.

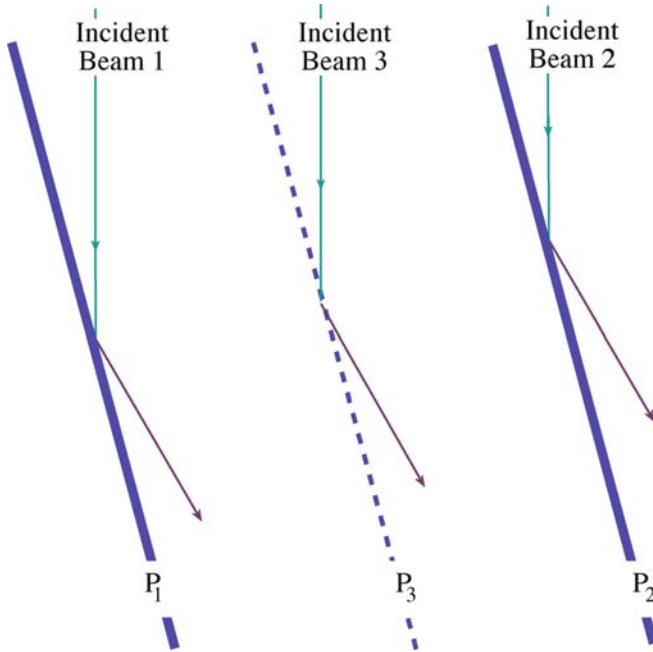


FIGURE 11.8. Scattering from three planes with plane  $P_3$  positioned exactly half way between planes  $P_1$  and  $P_2$ .

As we noted in the discussion of Figure 11.3, this scattering from plane  $P_3$  will occur no matter how the atoms (scattering centers) are distributed on this plane—even if there are no atoms on the plane! Thus we will always see  $\mathbf{g}_2 = 2\mathbf{g}$  and similarly  $\mathbf{g}_3 = 3\mathbf{g}$ , etc. So we can generalize equation 11.12 to be

$$2\left(\frac{d}{n}\right) \sin \theta = \lambda \quad (11.15)$$

or rewrite this as

$$2d \sin \theta = n\lambda \quad (11.16)$$

which gives a physical explanation for the  $n$  in equation 11.7.

To summarize: electrons are diffracting from a set of planes of spacing  $d$  such that we have both constructive and destructive interference. We can consider  $n$  in equation 11.15 as indicating that electrons are diffracting from a set of planes with spacing  $d/n$  rather than  $d$ . This equation can then be applied to planes that are occupied by different atoms. Although this treatment is not rigorous, it will prove to be very useful in practice. The alternative, but equivalent, view is obtained by considering the Laue equations which we will do in Chapter 12. You might consider why we don't have diffraction from planes which are  $nd$  apart instead of  $d/n$ .

**DYNAMICAL DIFFRACTION**  
The beam, which has been strongly Bragg diffracted once, is necessarily in the perfect Bragg orientation to be diffracted back into the direct beam by the same set of planes.

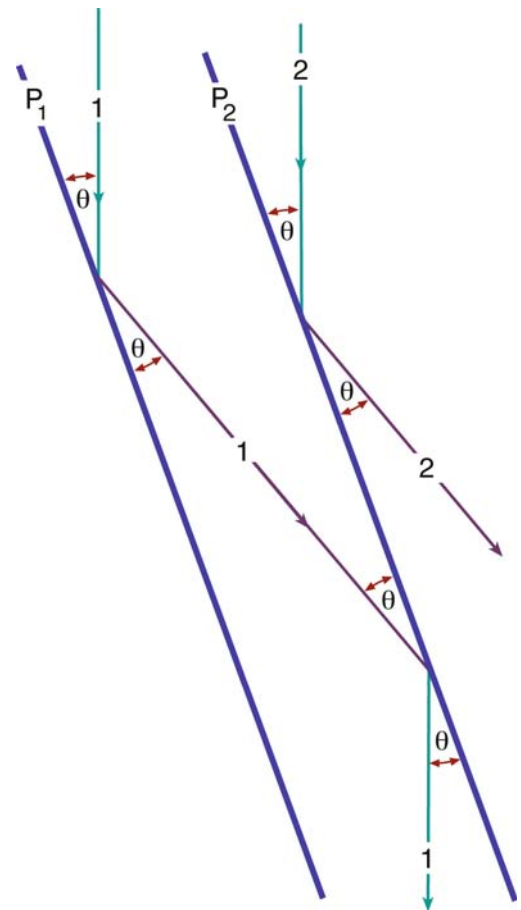


FIGURE 11.9. The beam can be scattered more than once. Any beam which is oriented so as to be Bragg scattered once is automatically in the ideal orientation to be rescattered. This gives rise to the phenomenon of dynamical scattering because the beam can be scattered again and again.

This beam is then said to be a rediffracted beam. The likelihood of this process occurring will increase as the thickness of the specimen increases. Clearly, the rediffracted beam is also perfectly oriented to be diffracted again, and so on. The two beams in Figure 11.9 are said to be dynamically coupled.

## 11.7 USE OF INDICES IN DIFFRACTION PATTERNS

In Chapter 18 we'll teach you how to index DPs, i.e., how to associate a spot in the DP with a diffracting plane in the specimen. For the time being it will be useful if we just introduce the conventions, rather than the methods, of indexing patterns.

First remember that a particular crystal plane is defined by the Miller indices ( $hkl$ ); crystallographically equivalent ( $hkl$ ) planes are denoted as the  $\{hkl\}$  planes. We define the direct beam as the 000 reflection and each diffracted beam as a reflection with different  $hkl$  indices. It is a crystallographic convention to refer to the diffraction spot from a specific ( $hkl$ ) plane, as  $hkl$ , i.e., without the parentheses. If we assign  $hkl$  to  $\mathbf{g}$ , then the second order ( $2\mathbf{g}$ ) spot is  $2h\ 2k\ 2l$ , the  $3\mathbf{g}$  spot is  $3h\ 3k\ 3l$ , etc. Similarly, the  $-\mathbf{g}$  reflection is  $\overline{hkl}$ . We'll discuss these points further in Section 12.3.

Now we can explain why we see so many spots in the DP. If we look along a zone axis in a crystal, we will see sets of planes in the edge-on orientation. Remember that a zone axis is the direction along the intersection of two or more planes.

*Notation:* The zone axis,  $[UVW]$ , is a direction which is common to all the planes of the zone. So  $[UVW]$  is perpendicular to the normal to the plane ( $hkl$ ) if the plane is in the  $[UVW]$  zone. Later, we will see that  $[UVW]$  is defined as the incident beam direction. This result applies to all crystal systems and gives the Weiss zone law  $hU + kV + lW = 0$ .

If there are many planes close to the Bragg orientation, then we will see spots from many different planes. We still have not explained why we can see the 200 spot and the 400 spot in the same pattern: they clearly can't both satisfy the Bragg condition at the same time. We see both spots because of the physical shape of the TEM specimen, as we'll discuss in Chapters 12 and 17.

## 11.8 PRACTICAL ASPECTS OF DIFFRACTION-PATTERN FORMATION

Remember from Chapter 9, we can form diffraction patterns in the TEM in two complementary ways, SAD and CBED patterns.

SADPs are sharply focused spot patterns that we use to select reflections for all imaging modes. We can easily associate the sharp spots with our diffraction vectors,  $\mathbf{g}$ .

CBDPs are arrays of disks. We can associate a  $\mathbf{g}$  vector with each disk but the location of  $\mathbf{g}$  requires more extensive consideration. For this reason, we'll delay more detailed discussion of CBDPs while we develop diffraction theory and then devote Chapters 20 and 21 to the topic, because it is very important.

## 11.9 MORE ON SELECTED-AREA DIFFRACTION PATTERNS

We discussed how you form a DP in the SAD mode in Chapter 9. Now we will discuss some of the practical implications and drawbacks of the method.

Why do we want to select a specific area to contribute to the DP? All foils are distorted to some extent so that diffraction conditions change as we move around the specimen; hence we need to select areas of constant orientation. Also, we may wish to determine the orientation relationship between two different crystals, which we can do by selecting the interfacial region. Alternatively, we

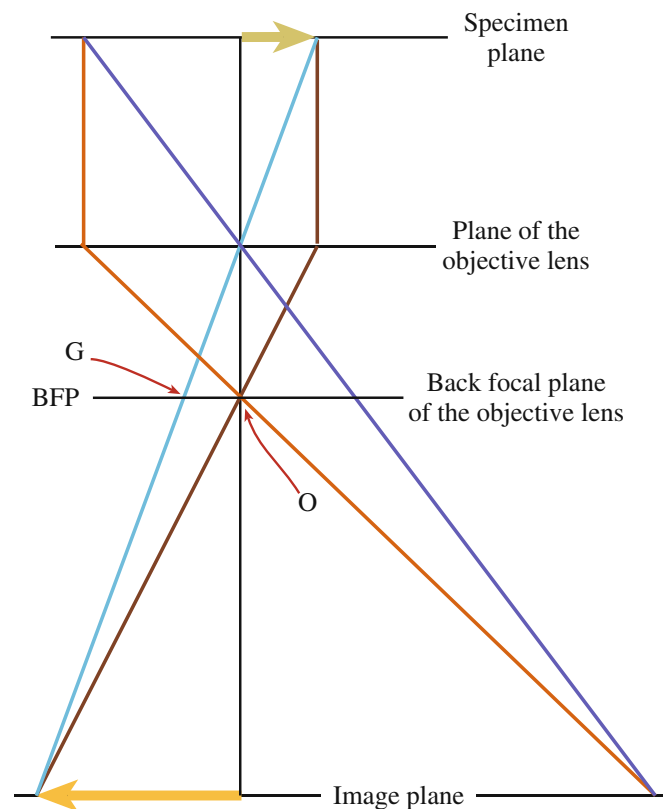


**FIGURE 11.10.** The diffraction pattern is formed at or close to the back focal plane of the objective lens. O is the direct beam and G is the diffracted beam.



may want to study the DP from a small particle within the foil. Figure 11.10 is a reminder that the DP is formed at the back focal plane (BFP) of the objective lens. A similar diagram was shown in Figure 9.13.

The SAD method for selecting an area is to place an aperture in the first image plane below the objective lens. In this case we really are selecting an area, which is the area in an image, but we always refer back to the volume of the diffracting specimen. Since we are working at an image plane we do not need to focus the condenser lens, in fact we generally weaken (underfocus) this lens to give more parallel illumination so that all the rays are focused at the same plane, i.e., the BFP. The spots in the DP then become sharper. In practice, you will generally need to 'fine-tune' the focus of the DP since its focus depends on the excitation of the condenser lens.

The key practical steps in forming an SAD pattern were described in procedure #4 in Section 9.3.A. The two key points to remember are (i) be sure that you are at the eucentric focus position, with an image of the area of interest focused on the screen and (ii) remember to focus the DP with the intermediate lens (diffraction focus).

Remember that using an aperture to select an area in the image plane gives an additional advantage: the area has already been magnified, typically 25×. Thus a 50-μm diameter aperture will select a 2-μm diameter area on the specimen.

You might ask: why can't we just use a smaller SAD aperture to select a smaller area? We can provide the answer by looking at Figure 11.11: the objective lens is not perfect. As we saw in Chapter 6, the beams which are farther away from the optic axis are bent more strongly as they pass through the objective lens. For rays entering the objective lens at an angle β to the optic axis, the image formed at magnification *M* is translated a distance *r<sub>M</sub>* given by

$$r_M = MC_s\beta^3 \quad (11.17)$$

So the area we select using the SAD aperture corresponds to the area *PP<sub>1</sub>* in the object plane *only* for the direct beam. The error increases as β increases, so that it's larger for a larger Bragg angle or for a larger *g*. The result is illustrated schematically in Figure 11.12 with values given in Table 11.1. (Note that we divide *r<sub>M</sub>* by *M* to give the distance at the specimen.) The values in the middle column were calculated for a *C<sub>s</sub>* of 3.3 mm and 100-keV electrons. If you use a smaller aperture, selecting an area of less than 1-μm diameter, even the fourth-order 111 reflection, i.e., the 444 reflection, from this area would not contribute to the SADP. Instead, a different area, possibly even an adjacent crystal, would contribute.

We will produce another selection error if the aperture is not located at the image plane. This effect can be

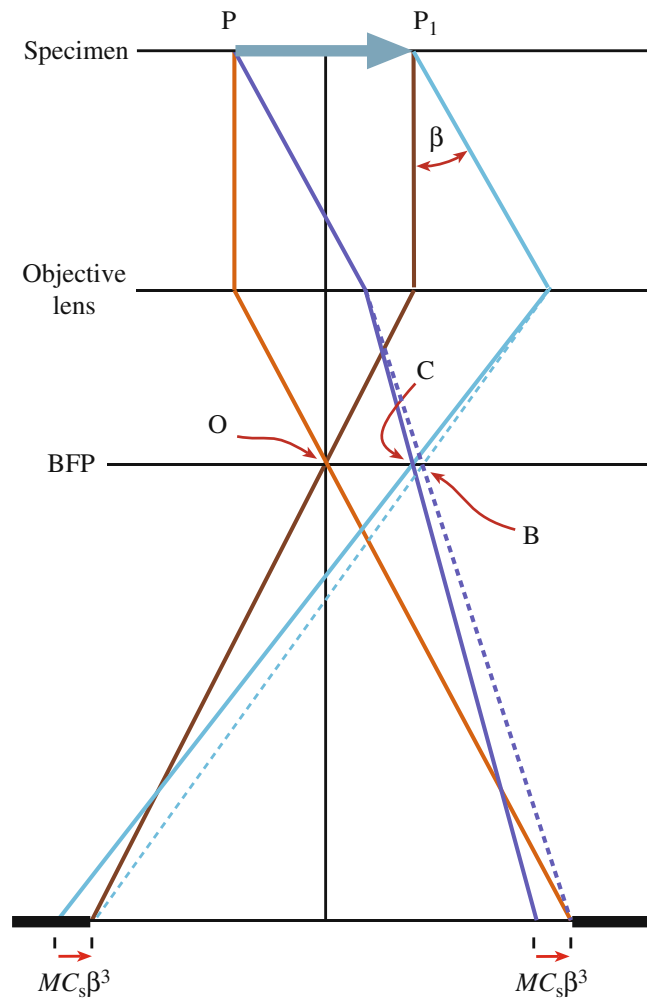


**FIGURE 11.11.** Formation of an SAD pattern showing that there is an error in selecting the area if the beams do not travel at the same angle to the optic axis. This difference is due to spherical aberration in the objective lens. *B* is the diffraction spot position for a perfect lens and *C* is the spot position with spherical aberration.

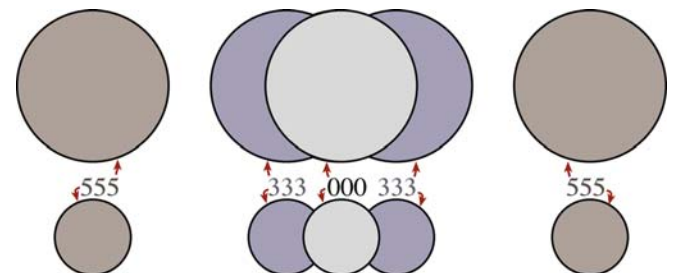


**FIGURE 11.12.** Schematic diagram showing the effective error in area selection, due to spherical aberration, for different reflections in the 111 systematic row for Al (*a<sub>0</sub>* = 0.404 nm) assuming 100-keV electrons and *C<sub>s</sub>* = 3 mm. The 000 and 111 disks almost exactly overlap (the translation is 13 nm). The diameter of each disk in the top row is 1 μm, and the diameter of each disk in the bottom row is 0.5 μm.



**TABLE 11.1 The Displacement Distance of the Image Formed by ‘Reflection G’ Due to Spherical Aberration**

Reflection in SAD pattern	$C_s\beta^3$ (nm) old TEM	$C_s\beta^3$ (nm) now IVEM
111	13	1.2
222	100	9.1
333	350	31.9
444	760	69.3
555	1620	150
666	2800	250

seen clearly in Figure 11.13 where the objective lens is focused on plane  $P_f$  rather than on the specimen. The effect is seen by simple geometry if you extend the diffracted rays back to the specimen plane. The displacement at the first image plane (where the SAD aperture is located) corresponds to a distance  $y$  at the specimen plane where  $y$  is given by

$$y = D\beta \quad (11.18)$$

On some older machines, a ‘click’ on the medium image focus control (i.e., of the objective lens) corresponded to a change in focus,  $D$  of  $\sim 3 \mu\text{m}$ . You will still find on many TEMs that the aperture in the SAD plane is not always in focus when the DP is in focus. You might also consider the implications when we study very thick specimens. Remember that these two sources of error may be additive and therefore quite substantial.

You may still sometimes want to use an aperture which conventional wisdom tells you is ‘too small for SAD.’ Perhaps the best advice when this is the case is, if possible, use CBED. However, you should remember that ‘conventional wisdom’ is often based on Table 11.1, which was first calculated by Hirsch et al. in  $\sim 1963$  and applied to a machine built in the 1950s! A modern 300-kV machine may have a  $C_s$  of  $\sim 1 \text{ mm}$  and a  $\lambda$  (at 300 kV) of 1.968 pm. The values for  $C_s\beta^3$  then become much smaller as shown in the right-hand column of Table 11.1. Clearly you could now use a much smaller SAD aperture, but  $10 \mu\text{m}$  is about the smallest that can be manufactured.

One question which is often asked is: if the SAD aperture is placed at the first image plane, how can it affect the DP which is formed above it? The relationship between the SAD pattern and the image(s) can be illustrated by forming a multiple dark-field image of the type illustrated in Figure 11.14A. To do this, you must first form the SAD pattern in the usual way. Then increase the strength of the intermediate lens so that it’s focused below the BFP in Figure 11.14B. Instead of a point we then see a disk, because the beam is convergent at the BFP. To understand what is

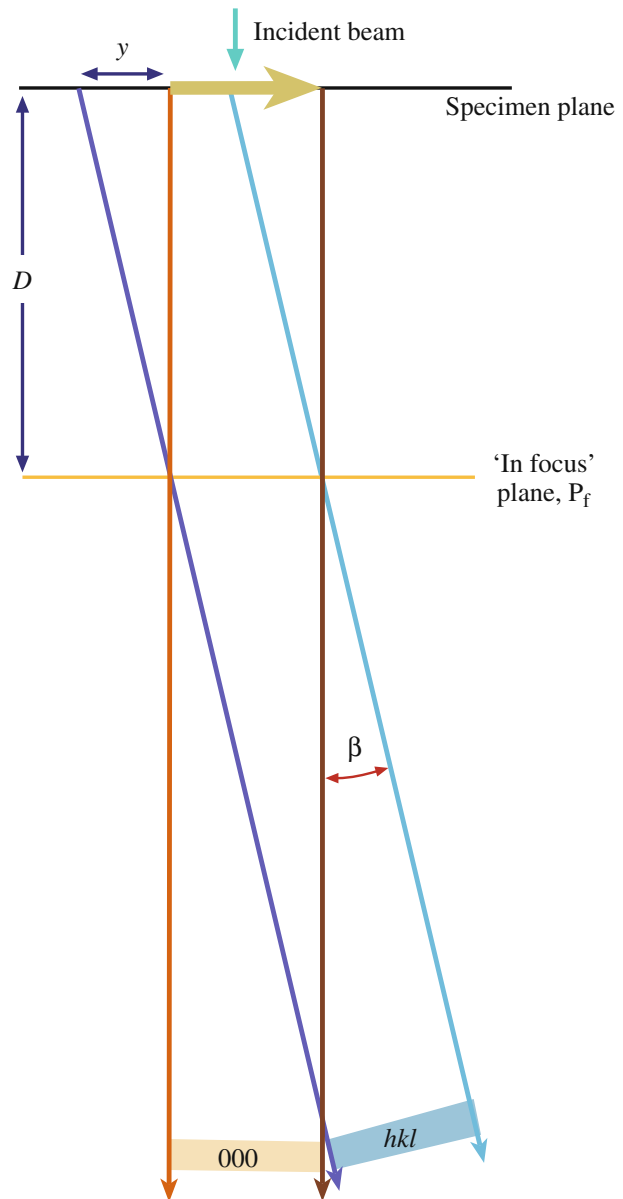
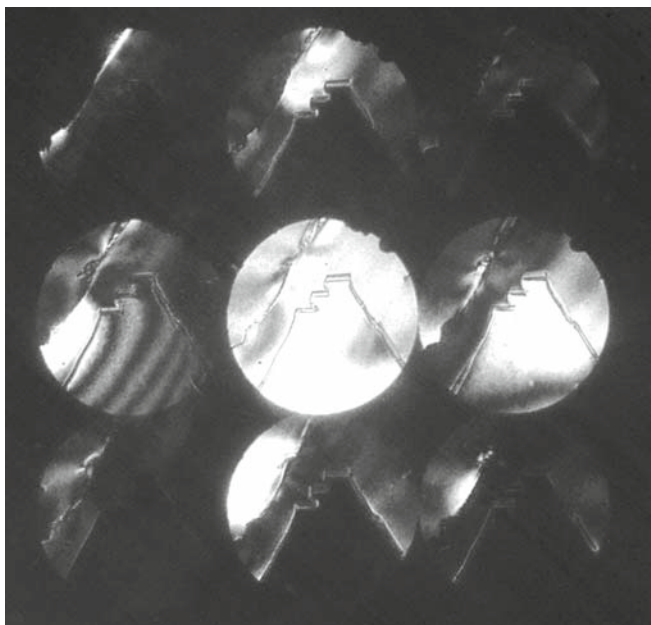


**FIGURE 11.13.** If the lens is not focused on the SAD plane, images associated with the different  $\mathbf{g}$  vectors will be shifted with respect to one another.  $D$  is the defocus. The shift in the selected area is given by  $y = D\beta$ .

happening we must realize that the magnification of the specimen at the BFP is zero (i.e., when ‘X’ in Figure 11.14B is in the BFP plane)! As we increase the strength of the intermediate lens, staying in diffraction mode, we increase the magnification of these images (one bright-field image and many dark-field images). Of course, these images are not in focus but this can be corrected by adjusting the strength of the objective lens, which is just conventional focusing.

Now you can appreciate directly that each disk corresponds to a reflection in the SADP. The reflections that were bright now correspond to bright disks; the

(A)



(B)

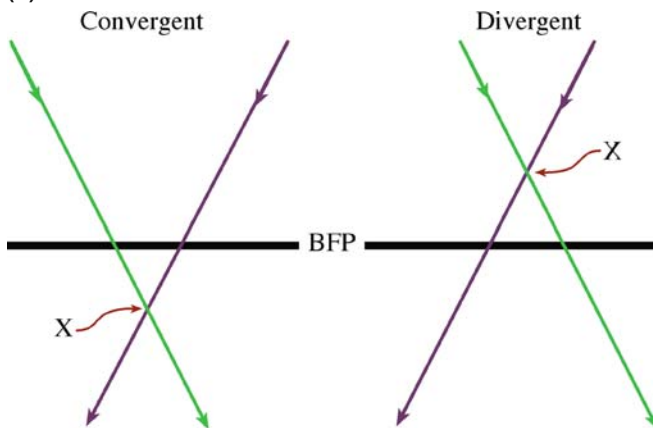


**FIGURE 11.14.** (A) Multiple dark-field images formed by defocusing the SADP revealing dark-field images in each diffraction disk defined by the objective aperture. Close inspection reveals that each image (of a twin boundary) is slightly shifted from the adjacent images, reflecting the increased error in area selection for higher-order reflections; (B) formation of a disk occurs because a defocused beam is either convergent or divergent at the BFP. An underfocused convergent beam is preferred, since it is more parallel than an overfocused divergent beam (see Figure 6.5).

area was close to the Bragg condition for that reflection. It is at first surprising to realize that none of the disks is uniformly bright. Conversely most of the disks are partly bright! We'll examine the reasons for this variation in Chapter 13.

This uncertainty in the area selected to form the SADPs is one reason that CBDPs can have some

advantage whenever you want to get crystallographic information about specific regions of your specimen.

We'll end with some more practical points.

You can change the detail present in your DP simply by changing the C2 lens setting and the exposure time.

To record the SADP you should never use an exposure of <10 seconds (but you will). You don't need to use a 1-second exposure to limit drift! If you're interested in the details in the diffraction pattern you should take as many as three exposures; on film, you might use 10, 30 and 100 seconds. So spread the beam with C2 and remove that beam stop (better still, don't use it; you're damaging your specimen if the beam is that intense). Correct the astigmatism in the intermediate lens after you've spread the beam; this astigmatism becomes noticeable when your spots are small (not all microscopes allow you to do this). Focus the spots to sharp points with the diffraction (intermediate) lens; now you've focused the DP. Just for the exercise, focus the spots in the SADP as you generally view it with the beam condensed down to a minimum diameter. Now spread the beam with C2 and refocus the spots; you will see quite a difference in how sharp the spots are. Use the binoculars for focusing the spots after you've spread the beam. Unless the pattern is well focused, you will miss many of the fine details that make SAD so useful.

Deciding which pattern is best really depends on what information you require. If you would like to see fine detail in your SADP, you will probably need to underfocus the beam using C2. If the beam of interest is of low intensity, you may need to increase the exposure time at the risk of broadening the more intense spots, hence the need to record patterns with a range of exposures. DPs can be recorded on video or sent directly to the computer using a video camera. The use of a CCD camera can give a much greater range of intensities than the photographic film; this will become the preferred method of recording DPs in the future. However, you may have no alternative (i.e., no darkroom).

Cooling your specimen can reduce the thermal-diffuse scattering and thus reduce the background intensity considerably. Changes in the lattice parameter will not usually be a problem in SAD since we are not looking for that level of accuracy, but they will be noticeable in the HOLZ CBDPs (see Chapter 21).

Finally, if your specimen charges, you'll probably have to coat it with a thin film of carbon. Do practice this. Repeat several thin coatings if necessary and be sure that the charging is not due to your specimen not contacting the specimen holder or the holder not contacting the ground.

## CHAPTER SUMMARY

DPs are the basis of all image formation in the TEM as well as all crystallographic analysis and defect characterization. We can understand DPs in terms of Bragg reflection from planes of atoms in the specimen and we can define the diffraction vector  $\mathbf{g}$  associated with each Bragg reflection and associate each  $\mathbf{g}$  with a crystal plane  $hkl$ . The diffracting planes are all in a specific zone axis  $UVW$ , which we can define as parallel to the incident beam direction.

### DIFFRACTION AND OPTICS

Bragg, WL 1965 *The Crystalline State I* Ed. WL Bragg Cornell University Press Ithaca NY (first published in 1933). Find it in your library and browse.

Hecht, E 2001 *Optics* 4th Ed. Addison-Wesley Reading MA. Very readable and current.

James, RW 1965 *The Optical Principles of the Diffraction of X-Rays, The Crystalline State II* Ed. WL Bragg Ed. Cornell University Press Ithaca NY (first published in 1948). Ditto.

Schwartz, LH and Cohen, JB 1987 *Diffraction from Materials* 2nd Ed. Springer New York. One of the two standard texts.

### THE COMPANION TEXT

We'll use this theory throughout the companion text but won't refer to it specifically.

### SELF-ASSESSMENT QUESTIONS

- Q11.1 List the three major differences between electron diffraction and X-ray diffraction.
- Q11.2 If TEM imaging, coupled with electron diffraction, is so wonderful, why do some researchers use X-rays instead for both purposes?
- Q11.3 Why do we usually not measure intensities of spots in TEM DPs?
- Q11.4 Why do we need to specify planes in a lattice?
- Q11.5 What are the major differences between SADPs and CBDPs?
- Q11.6 Formation of an SADP shows that there are errors in selecting the area. Why do the errors occur?
- Q11.7 Why do the spots in the DP vary as we move across the specimen?
- Q11.8 Why do we need to change the C2 setting and exposure time as we change location on the specimen?
- Q11.9 How can we limit thermal-diffuse scattering and thus reduce background intensity?
- Q11.10 Summarize the advantages of TEM over SEM and visible-light microscopes.
- Q11.11 What is necessary for constructive interference to occur?
- Q11.12 Write down Bragg's law.
- Q11.13 How does the specimen thickness affect dynamical scattering?
- Q11.14 Why do you underfocus the condenser lens when obtaining SAD patterns?
- Q11.15 Why don't you always use the smallest selected-area aperture possible when obtaining an SADP?
- Q11.16 When recording an SADP pattern, how long should the exposure time be?
- Q11.17 How does the SAD approach work if the aperture is not actually in the specimen plane?
- Q11.18 What critical information can you readily obtain from a TEM DP?
- Q11.19 In the case of Bragg diffraction, how is the semiangle between the incident beam and the Bragg-diffracted beam related to the Bragg angle?
- Q11.20 What is a 'zone axis'?
- Q11.21 Give a pictorial explanation for the meaning of  $n$  in Bragg's law.
- Q11.22 What is the most basic characteristic of your specimen indicated by the presence of spots in a DP?
- Q11.23 Prove that there is no path difference for scattering from atoms located on the same plane.

### TEXT-SPECIFIC QUESTIONS

These questions are not difficult since we are just introducing DPs.

- T11.1 Using equations in the book, deduce Table 11.1. Summarize all the parameters you use in making an extended version of the table.
- T11.2 Examine Figure 11.14. If the specimen is Si, index the DP. If it's a 300-kV TEM, deduce the camera length.
- T11.3 Explain why Figure 11.14 could not be from Cu.

- T11.4 Consider Figure 11.10. There are five rays and four planes. Number them in the order in which you would draw these lines. Discuss how you would modify this figure so as to draw it to scale.
- T11.5 The DP in Figure 11.1 was obtained from a polycrystalline sample. Identify the single-crystal DPs in this figure.
- T11.6 In Figure 11.14, the disks all appear to show the same area of the specimen. Do you expect this to be exactly the same area? Discuss.
- T11.7 Consider Figure 11.14. Using a reasonable value for the beam divergence, estimate the value for  $\Delta f$  using information in the figure.
- T11.8 Consider Figure 11.12. Assess the accuracy of this drawing. Do a similar drawing for a value of  $C_s = 0.7$  mm with everything else being the same.
- T11.9 We will see later that a critical challenge for high-resolution imaging is image delocalization (MS Word suggests demoralization is a better word). How has this concept been introduced in Chapter 11? If we could correct  $C_s$ , how would SAD in the TEM be improved?
- T11.10 Deduce the Weiss zone law using vector multiplication.

# Thinking in Reciprocal Space

## CHAPTER PREVIEW

In the previous chapter, you've already encountered vectors  $\mathbf{k}$  and  $\mathbf{g}$  and seen that they have lengths with units of  $\text{nm}^{-1}$ . These vectors are referred to as reciprocal-lattice vectors. Now we are going to discuss what this reciprocal lattice is. The reciprocal lattice is simply a lattice in reciprocal space. Note that this lattice is just as real as the 'real lattice' in 'real' space. It's like a new world in *Gulliver's Travels* but the relationship to 'our' world is not a linear scaling factor but a reciprocal one. If something (an object or a length) is large in real space, then it's small in reciprocal space.

When you see an object in real space you need to think, "What would it look like in reciprocal space?"

The reciprocal lattice is a purely geometrical construction. We'll separate the discussion into two parts: (i) the math and (ii) the properties of this lattice. The first is the same as you will meet in any text on condensed-matter physics; the second relates to how we use this construction in TEM. What we will find is that the lattice gives us a method for picturing the geometry of diffraction; it gives us a 'pictorial representation' of diffraction. It helps us to visualize how DPs will vary as the orientation and physical characteristics of the specimen vary.

### 12.1 WHY INTRODUCE ANOTHER LATTICE?

If you're new to the field of diffraction, the concept of reciprocal space may seem a daunting theoretical proposal. You must persevere. This model gives a physical picture of diffraction geometries that is extremely helpful to you, the experimentalist. The best approach is to think of any crystal as having two lattices. The first describes the arrangement of the unit cells of atoms in the crystal (your specimen). The second is an array of points which is uniquely defined for any given crystal but does not correspond to arrays of atoms; instead, each point is associated with a particular set of planes in the crystal. Of course, the reciprocal lattice is just as real as the 'real' lattice; both are simply geometrical constructions. We'll use the reciprocal lattice to give a physical picture of what happens when a crystal diffracts.

#### HISTORICAL NOTE

The reciprocal lattice was rediscovered independently by Ewald and Laue in 1911–1914, but it had been described by Gibbs in 1881 and by Bravais (in a somewhat less useful form) in 1850! The discussion in 1962 of Ewald's contribution to the subject is recommended reading.

In Chapter 11 we showed that Bragg diffraction of electrons by crystals occurs when  $\mathbf{K}$  is equal to  $\mathbf{g}$ . The reciprocal-lattice concept allows us to define a lattice where all the lattice points correspond to the possible  $\mathbf{g}$  vectors.

#### RECIPROCAL

Think of any crystal as having two lattices, one real and the other reciprocal. In the reciprocal lattice, sets of parallel  $(hkl)$  atomic planes are represented by a single point located a distance  $1/d_{hkl}$  from the lattice origin.

To understand why we use the reciprocal lattice, remember that we can always write Bragg's law (equations 11.2 and 11.3) as

$$\frac{2 \sin \theta_B}{\lambda} = \frac{n}{d} = |\mathbf{K}| \quad (12.1)$$

Thus the vector  $\mathbf{K}$  is reciprocally related to  $d$  and vice versa. Before using this new lattice, however, we must work through its formal definition.

## 12.2 MATHEMATICAL DEFINITION OF THE RECIPROCAL LATTICE

In this section we will go through the definition of the reciprocal-lattice as a mathematical construction and prove some of the special mathematical properties of the vector,  $\mathbf{g}$ . You don't need to learn the proofs but you will need to know these equations.

The mathematics of the reciprocal-lattice construction is simple vector algebra.

In real space, we can define any lattice vector,  $\mathbf{r}_n$ , by the equation

$$\mathbf{r}_n = n_1 \mathbf{a} + n_2 \mathbf{b} + n_3 \mathbf{c} \quad (12.2)$$

where the vectors  $\mathbf{a}$ ,  $\mathbf{b}$ , and  $\mathbf{c}$  are the unit-cell translations in real space and  $n_1$ ,  $n_2$ , and  $n_3$  are all integers.

Any reciprocal-lattice vector,  $\mathbf{r}^*$ , can be defined in a similar manner

$$\mathbf{r}^* = m_1 \mathbf{a}^* + m_2 \mathbf{b}^* + m_3 \mathbf{c}^* \quad (12.3)$$

where  $\mathbf{a}^*$ ,  $\mathbf{b}^*$ , and  $\mathbf{c}^*$  are the unit-cell translations in reciprocal space and  $m_1$ ,  $m_2$ , and  $m_3$  are all integers. The directions of these new vectors are defined by the relations

$$\mathbf{a}^* \cdot \mathbf{b} = \mathbf{a}^* \cdot \mathbf{c} = \mathbf{b}^* \cdot \mathbf{c} = \mathbf{b}^* \cdot \mathbf{a} = \mathbf{c}^* \cdot \mathbf{a} = \mathbf{c}^* \cdot \mathbf{b} = 0 \quad (12.4)$$

In words,  $\mathbf{a}^*$  is normal to both  $\mathbf{b}$  and  $\mathbf{c}$ , etc.

We define the lengths of these vectors by another set of relations

$$\mathbf{a}^* \cdot \mathbf{a} = 1; \mathbf{b}^* \cdot \mathbf{b} = 1; \mathbf{c}^* \cdot \mathbf{c} = 1 \quad (12.5)$$

Equation 12.5 then uniquely defines the length of the vector  $\mathbf{a}^*$  in terms of the length of the vector  $\mathbf{a}$ . Therefore, these equations give the scale or dimension of the reciprocal lattice. The product of the projection of  $\mathbf{a}^*$  on the vector  $\mathbf{a}$  multiplied by the length of  $\mathbf{a}$  is unity. Be careful; this result does not mean that  $\mathbf{a}^*$  is parallel to  $\mathbf{a}$  (think about this!). The direction of  $\mathbf{a}^*$  is actually completely defined by equation 12.4. It is perpendicular to both  $\mathbf{b}$  and  $\mathbf{c}$  and must therefore be the normal to the plane containing  $\mathbf{b}$  and  $\mathbf{c}$ .

The vector,  $\mathbf{a}^*$ , is always perpendicular to the plane (100) even when  $\mathbf{a}$  is not.

We can see that if  $\mathbf{a}$ ,  $\mathbf{b}$ , and  $\mathbf{c}$  are large, then the corresponding reciprocal-lattice vectors will be small if we choose conventionally shaped unit cells.

Since  $V_c$ , the volume of the unit cell, is given by  $\mathbf{a} \cdot \mathbf{b} \wedge \mathbf{c}$ , then from equation 12.5 we can write  $\mathbf{a}^*$  as

$$\mathbf{a}^* = \frac{\mathbf{b} \wedge \mathbf{c}}{V_c} \quad (12.6)$$

This definition emphasizes that the vector  $\mathbf{a}^*$  is orthogonal to the vectors  $\mathbf{b}$  and  $\mathbf{c}$ . However, just as  $\mathbf{a}$ ,  $\mathbf{b}$  and  $\mathbf{c}$  need not be normal to one another,  $\mathbf{a}^*$ ,  $\mathbf{b}^*$ , and  $\mathbf{c}^*$  are also not necessarily normal to one another. We use the usual clockwise convention in defining the vector product in equation 12.6.

## 12.3 THE VECTOR $\mathbf{g}$

We can generalize our definition of  $\mathbf{g}$  a little more. Any vector in reciprocal space can be defined as a combination of the vectors  $\mathbf{a}^*$ ,  $\mathbf{b}^*$ , and  $\mathbf{c}^*$ . In particular, we can write  $\mathbf{K}$  in a form for use later

$$\mathbf{K} = \xi \mathbf{a}^* + \eta \mathbf{b}^* + \zeta \mathbf{c}^* \quad (12.7)$$

Here  $\xi$ ,  $\eta$ , and  $\zeta$  are any three numbers, not necessarily integers. A particularly important reciprocal-lattice vector is the vector  $\mathbf{g}_{hkl}$  which is defined as

$$\mathbf{g}_{hkl} = h\mathbf{a}^* + k\mathbf{b}^* + l\mathbf{c}^* \quad (12.8)$$

where  $h$ ,  $k$ , and  $l$  are all now integers and together define the plane  $(hkl)$ .

The definition of the plane  $(hkl)$  is that it cuts the  $a$ ,  $b$ , and  $c$  axes at  $1/h$ ,  $1/k$ , and  $1/l$ , respectively. If you look at Figure 12.1, you'll see that the vector  $\mathbf{AB}$  can be written as  $\mathbf{b}/k - \mathbf{a}/h$ . This vector and all vectors in the  $(hkl)$  plane

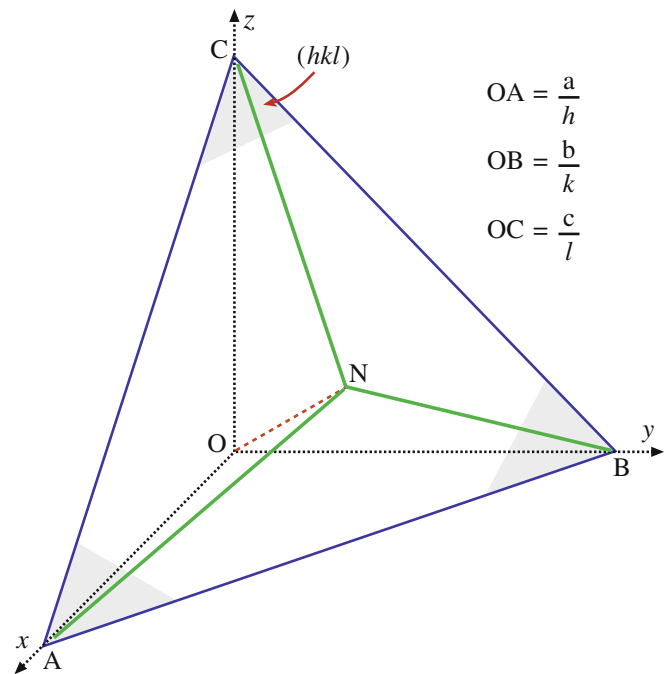


FIGURE 12.1. The plane ABC has Miller indices  $(hkl)$ . The vectors  $\mathbf{OA}$ ,  $\mathbf{OB}$ , and  $\mathbf{OC}$  have lengths  $a/h$ ,  $b/k$ , and  $c/l$ . The vector  $\mathbf{ON}$ , which may be written as  $\mathbf{n}$ , is normal to the plane  $(hkl)$ . In the text we see that the reflection,  $\mathbf{g}$ , which is associated with diffraction from the  $(hkl)$  planes, is parallel to  $\mathbf{n}$  and normal to all vectors in  $(hkl)$ .



are normal to the vector  $\mathbf{g}_{hkl}$  defined in equation 12.8. You can prove this by taking the dot product of  $\mathbf{AB}$  and  $\mathbf{g}$  and using equations 12.4 and 12.5. Therefore, the vector  $\mathbf{g}_{hkl}$  must be *normal* to the plane  $(hkl)$

$$\left(\frac{\mathbf{b}}{k} - \frac{\mathbf{a}}{h}\right) \cdot (h\mathbf{a}^* + k\mathbf{b}^* + l\mathbf{c}^*) = 0 \quad (12.9)$$

The vectors  $\mathbf{AB}$ ,  $\mathbf{BC}$ , and  $\mathbf{CA}$  all lie in the plane  $(hkl)$  and each is normal to  $\mathbf{g}_{hkl}$ . All that we now have to prove is that the length of the vector,  $|\mathbf{g}_{hkl}|$ , is given by  $(d_{hkl})^{-1}$ . To show this relationship, consider a unit vector,  $\mathbf{n}$ , normal to the plane (i.e., parallel to  $\mathbf{g}_{hkl}$ ) and take the dot product with any unit vector inclined to this plane (e.g.,  $\mathbf{a}/h$  or  $\mathbf{b}/k$ ).

The unit vector,  $\mathbf{n}$ , parallel to  $\mathbf{g}$  is simply  $\mathbf{g}/|\mathbf{g}|$ . Therefore, the shortest distance from the origin  $O$  to the plane is the dot product of  $\mathbf{n}$  with vector  $\mathbf{OB}$  (or  $\mathbf{OC}$ , etc.)

$$\mathbf{n} \cdot \frac{\mathbf{a}}{h} = \frac{\mathbf{g}}{|\mathbf{g}|} \cdot \frac{\mathbf{a}}{h} = \frac{(h\mathbf{a}^* + k\mathbf{b}^* + l\mathbf{c}^*) \cdot \mathbf{a}}{|\mathbf{g}|} \cdot \frac{1}{h} = \frac{1}{|\mathbf{g}|} \quad (12.10)$$

where we again used equations 12.4 and 12.5. Since the origin,  $O$ , by definition lies on a plane in this family of planes, equation 12.10 gives the distance between parallel  $(hkl)$  planes, so that

$$d_{hkl} = \frac{1}{|\mathbf{g}|} \quad (12.11)$$

as we required.

- The definition of the  $(hkl)$  indices is  $OA = a/h$ ;  $OB = b/k$ ;  $OC = c/l$ .
- The plane  $ABC$  can then be represented as  $(hkl)$ .

We should emphasize a few points before moving on.

- Remember: the reciprocal lattice is so called because all lengths are in reciprocal units.
- If you are familiar with the derivation of band-gap concepts in elementary solid-state physics, you will have already used these ideas. The difference is that the energies of the electrons being produced in the microscope are  $\geq 100$  keV, whereas those in solids are  $\sim 1$  eV. This will affect the magnitudes of  $\mathbf{k}$  but the  $\mathbf{a}^*$ , etc., will not change with kV.
- Reciprocal-space notation. We introduced the use of brackets in Section 11.7. Now we'll extend this notation to the reciprocal lattice:  $(hkl)$  is shorthand notation for a particular vector in reciprocal space because it is normal to the  $(hkl)$  plane in real space;  $\{hkl\}$  is then the general form for these reciprocal-lattice vectors.  $[UVW]$  is a particular plane in reciprocal space, e.g., it may contain many  $\{hkl\}$  points so that in real space it would be a direction—the zone axis for the  $\{hkl\}$  real-space planes (see Table 12.1).

**TABLE 12.1. Notation for Planes, Directions, and Reflections**

Real space	Reciprocal space	
Particular direction	Particular plane	$[UVW]$
General direction	General plane	$\langle UVW \rangle$
Particular plane	Particular direction	$(hkl)$
General plane	General direction	$\{hkl\}$
Diffraction plane	Indexed reflection	$hkl$

When indexing diffraction spots, you will often find that the brackets have been entirely omitted; this is a sort of convention. You should use brackets if there is any ambiguity or for emphasis.

- In non-cubic material, some special vectors may be parallel to one another, but most pairs will not be parallel. This difference can surprise even the experienced microscopist, particularly if you're used to studying cubic metals. For example, if you orient the electron beam to be along the  $[123]$  zone axis in an orthorhombic crystal such as olivine, the beam will *not* be normal to the  $(123)$  plane.

**WARNING**

Real-lattice vectors and reciprocal-lattice vectors with the same indices (e.g.,  $[123]$  and plane normals  $(123)$ ) are parallel *only* in the case of cubic materials.

**12.4 THE LAUE EQUATIONS AND THEIR RELATION TO BRAGG'S LAW**

To understand the value of the reciprocal lattice, we will now reconsider some of the terms we discussed previously. We use Bragg's law (Section 11.5) because it is so useful. It gives us a physical picture of the constructive-interference phenomenon, but it does not really correspond to the actual situation in TEM. Our justification in using Bragg's law is that we can derive it as a special form of the Laue equations, which really do describe diffraction in the TEM.

So we'll now derive Bragg's law from the Laue equations using simple vector algebra. For much of our discussion we assume that the crystal is infinitely large; we can always take the reciprocal lattice to be infinite. We can then use intuition to see that constructive interference will only occur when

$$\mathbf{K} = \mathbf{g} \quad (12.12)$$

From Figure 12.2 we can see that the magnitude of  $\mathbf{K}$  is always  $(2 \sin \theta)/\lambda$ . At the Bragg condition it is also

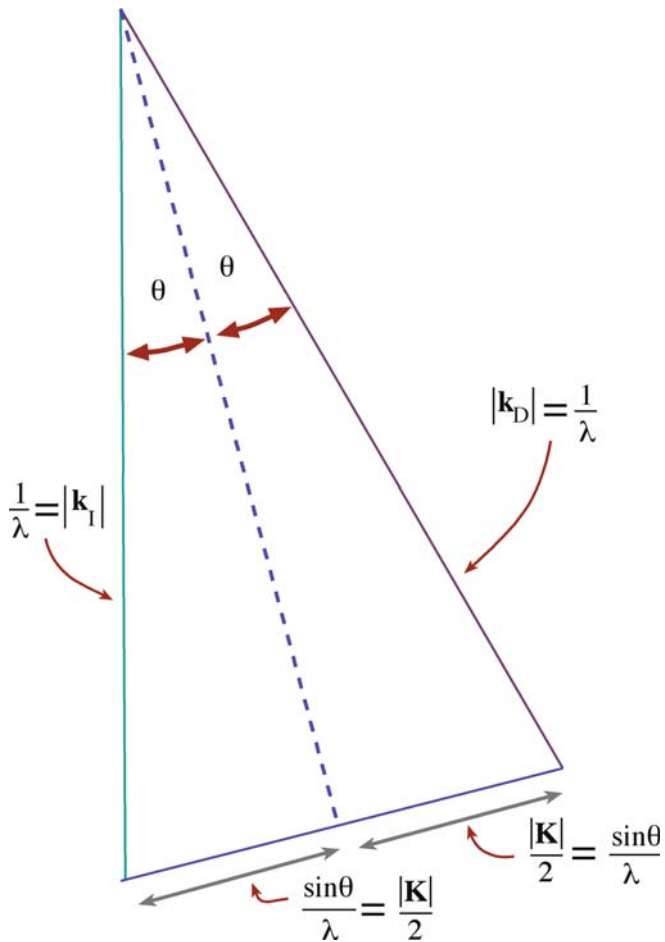


FIGURE 12.2. The geometric relationship between  $\mathbf{k}_I$ ,  $\mathbf{k}_D$ ,  $\mathbf{K}$ ,  $\theta$ , and  $\lambda$ .

equal to the magnitude of  $\mathbf{g}$ , i.e.,  $1/d$ . Therefore, at the Bragg condition we can write

$$\frac{2 \sin \theta}{\lambda} = \frac{1}{d_{hkl}} \quad (12.13)$$

Hence we can write

$$\lambda = 2d \sin \theta \quad (12.14)$$

which is Bragg's law.

Equation 12.12 represents the Laue conditions for constructive interference; so we will refer to this as the condition for Laue, or Bragg, diffraction. Prove for yourself that  $\mathbf{g} \cdot \mathbf{r}_n$  is always an integer,  $N$ . Then we can use equation 12.2 to write the Laue conditions

$$\mathbf{K} \cdot \mathbf{r}_n = N \quad (12.15)$$

This equation tells us that we must satisfy certain conditions on  $\mathbf{K}$  in order to have Bragg (or Laue) diffraction.

Using equation 12.7 and multiplying this dot product we can see that this equation only holds when

$\{n_1 \xi + n_2 \eta + n_3 \zeta\}$  is an integer;  $\mathbf{K} \cdot \mathbf{r}_n = N$  when  $\xi$ ,  $\eta$ , and  $\zeta$  are the integers  $h$ ,  $k$ , and  $l$ .

Note: this is a very special case. By setting  $\mathbf{r}_n$  equal to the three unit vectors in turn, equation 12.15 gives three relationships

$$\mathbf{K} \cdot \mathbf{a} = h \quad (12.16)$$

$$\mathbf{K} \cdot \mathbf{b} = k \quad (12.17)$$

$$\mathbf{K} \cdot \mathbf{c} = l \quad (12.18)$$

Of course, these equations are the same Laue diffraction conditions which we introduced back in Section 3.10.B, as given in equation 12.15. In Section 11.5 we quoted Bragg's law, with an ' $n$ ,' as

$$n\lambda = 2d \sin \theta \quad (12.19)$$

We also discussed the physical reason for  $n$ . We can now treat the same situation mathematically. If the integers  $h$ ,  $k$ , and  $l$  have a common factor then we can write

$$nd_{nh,nk,nl} = d_{hkl} \quad (12.20)$$

So the  $n$  is implicit in the  $d$  used in equation 12.14. You will find that there are many other methods for treating this problem. We have chosen this approach to emphasize the underlying geometric principles.

## 12.5 THE EWALD SPHERE OF REFLECTION

The reciprocal lattice is a 3D array of points, each of which we will now associate with a reciprocal-lattice rod, or relrod for short, which is centered on the point. Furthermore, we will arrange each relrod to be normal to the thin foil, but to have a finite thickness parallel to this foil normal. This geometry of the relrods holds even when we tilt the specimen. The fact that we have rods is the result of the shape of our TEM specimen. At this stage this is purely an empirical construction to allow us to explain why we see spots in the DP even when the Bragg condition is not exactly satisfied. We will examine the shape of these rods and their origin in Chapter 16.

We now construct a sphere of radius  $1/\lambda$ . The sphere is known as the sphere of reflection or generally, and more simply, the 'Ewald sphere' in honor of its inventor P.P. Ewald. Due to Ewald's German origins, Ewald is pronounced 'A. Valt' rather than 'E. Walled.' Ewald's paper which first described the sphere was published in 1913 and was entitled 'Contributions to the Theory of Interferences of X-rays in Crystals.' It appears, in translation, in the monograph edited by Cruickshank et al., along with several of his other papers; the articles collected in this review

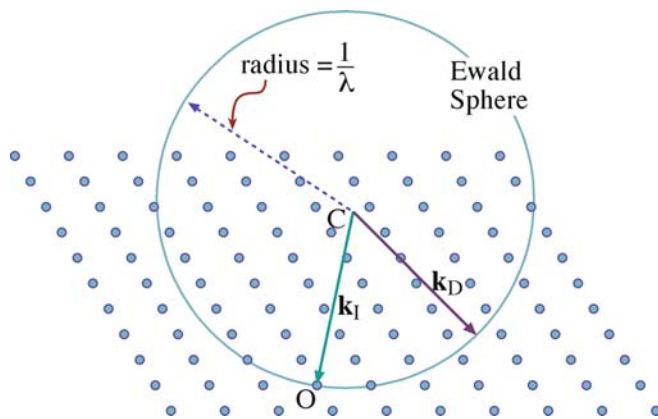


**FIGURE 12.3.** The Ewald sphere of reflection is shown intersecting a non-cubic array of reciprocal-lattice points. The vector  $\mathbf{CO}$  represents  $\mathbf{k}_i$ , the wave vector of the incident wave, and  $O$  is the origin of the reciprocal lattice.  $\mathbf{k}_D$  is any radius vector. When the radius of the sphere is similar to the spacing between the points in the reciprocal lattice, as is the case for X-rays, the sphere can only intersect a few points. When  $\lambda$  is much smaller, as for 100-keV electrons, the radius is much larger, the sphere is flatter, and it intersects many more points.

give a wonderful insight into the whole development of the theory of diffraction.

The sphere is usually represented in two dimensions by a circle and in most figures is drawn together with a two-dimensional section through the reciprocal lattice as shown in Figure 12.3.

The key point is that when the sphere cuts through the reciprocal-lattice point the Bragg condition is satisfied. When it cuts through a rod you still see a diffraction spot, even though the Bragg condition is not satisfied.

We combine the concept of the reciprocal lattice, the relrods, and the Ewald-sphere construction to picture how the intensity of each diffracted beam varies as we tilt the specimen or the electron beam. You may see the position of a spot in the DP move when the Ewald sphere is moved relative to the reciprocal lattice.

We can draw a sphere of radius  $1/\lambda$  in reciprocal space so that it passes through the origin of the reciprocal lattice, point  $O$ , as defined in Chapter 11. If any point in the reciprocal lattice intersects the surface of the sphere, the set of planes corresponding to that point must satisfy the Bragg equation and hence the planes will diffract strongly. Equation 12.11 suggests that we define a vector  $\mathbf{g}$  which can represent the quantity  $d^{-1}$ . The vector has a length and a direction. We choose the obvious length for  $\mathbf{g}$  to be  $d^{-1}$  and make  $\mathbf{g}$  the only unique vector for the plane  $(hkl)$ , i.e., parallel to the normal to this plane.

Of course, the diagram drawn in Figure 12.3 shows a cut through the Ewald sphere. We usually draw such a diagram to include the vector describing the incident beam  $\mathbf{CO}$  but this is not a requirement; in fact it is the exception, since our diagram is a two-dimensional cut through a 3D sphere. When we draw such a diagram we usually choose the plane of the diagram to contain the

## INTENSITY AND RECIPROCAL SPACE

We can associate an ‘intensity’ with any position in reciprocal space, and in particular with any position along one of these rods.

The value for this intensity is such that if the Ewald sphere cuts through that point in reciprocal space, then the diffracted beam,  $\mathbf{g}$ , will have that intensity.

In general, if the Ewald sphere moves, the intensity will change. The important idea to keep in mind is that the reciprocal lattice is just a construction we use to give us a pictorial way of looking at diffraction.

point  $O$ , since this point represents the direct beam. A common cause for confusion concerns the location of the center of the Ewald sphere,  $C$ . The point  $C$  is not the origin; the origin is the point  $O$ . In fact  $C$  will probably not coincide with a reciprocal-lattice point.

## WHERE IS C?

The vector  $\mathbf{CO}$  is  $\mathbf{k}_i$  and has length  $1/\lambda$ ; this defines where  $C$  is located, i.e., we start with  $O$  and measure back to  $C$ .

Now you can appreciate that it is only when the incident beam lies in our chosen plane that the vector  $\mathbf{CO}$  will lie in that plane. For example, we may choose the plane to be parallel to the optic axis of the microscope but tilt the incident beam off this axis; in such cases we will still often be interested in the plane containing both the optic axis and the incident beam. Also notice that  $\mathbf{k}_D$  could be any vector which begins at  $C$  and ends on the sphere.

Consider the relative dimensions of  $d_{hkl}$  and  $\lambda$ . We can see that for X-rays where  $\lambda$  is  $\sim 0.2$  nm and  $1/\lambda$  is  $\sim 5$  nm $^{-1}$ , the Ewald sphere can only intersect a small number of relrods because  $1/d$  is only  $\sim 3$  nm $^{-1}$ . This explains why it is necessary in X-ray diffraction to use white radiation (giving a wide range of  $\lambda$ ) or to oscillate, rotate, or powder the specimen (thus producing many variations of  $d$  and  $\theta$ ) in order to produce enough diffraction spots to analyze the structure. For 100-keV electrons, however,  $\lambda$  is 3.7 pm and  $1/\lambda$  is 270 nm $^{-1}$ . So the surface of the Ewald sphere is almost planar (but fortunately, as we will see in Section 12.6, not quite) in comparison with the array of reciprocal-lattice spots. Therefore, in a TEM, the Bragg condition is nearly satisfied for many planes and, as we saw in Figure 11.1, many diffraction spots are observed from a thin specimen corresponding to a section through the reciprocal lattice.

Rather than carry out the exercise of identifying arrays of spots for every orientation of the specimen, it is common practice to orient the specimen such that

the beam is incident almost parallel to a low-index zone ( $U$ ,  $V$ , and  $W$  are all small numbers), and then to compare the observed zone-axis pattern (ZAP) with standard ones. We'll show you some standard patterns in Chapter 18. This approach is fine if you already know the crystal structure of your material. However, you'll need to know the full procedure if you have a material whose structure you don't know or if you are not able to rotate it to a low-index zone axis. This situation might arise, for example, when you are characterizing a grain boundary.

## 12.6 THE EXCITATION ERROR

We'll now introduce a new quantity,  $\mathbf{s}$ , known as the excitation error or the deviation parameter. Always use these terms carefully! If the beam is exactly parallel to any zone axis then, according to the Laue conditions, there should be no spots in the DP. Clearly there are many spots (e.g., see Figures 1.6 and 2.13B), so there is intensity in the diffracted beams even when the Bragg condition is not exactly satisfied. The actual intensity will depend on how far we are away from the Bragg condition. This distance is measured by a vector,  $\mathbf{s}$ , in reciprocal space such that

$$\mathbf{K} = \mathbf{g} + \mathbf{s} \quad (12.21)$$

The Ewald sphere intersects the reciprocal-lattice point at the center of a rod when  $\mathbf{s} = 0$ . Equation 12.21 is very imprecise! Although  $\mathbf{g}$  is well defined,  $\mathbf{K}$  is not, because it depends on  $\mathbf{k}_D$ , which could be any vector terminating on the Ewald sphere. In Figure 12.4, we show two special values of  $\mathbf{s}$  by choosing two special values of  $\mathbf{k}_D$ . In one,  $\mathbf{k}_D$  lies along the vector  $\mathbf{CG}$  so  $\mathbf{s}_c$  is also parallel to  $\mathbf{CD}$ ; in the second,  $\mathbf{s}_z$  is chosen to be parallel to vector  $\mathbf{CO}$ , the incident-wave vector. A third special situation would be to define  $\mathbf{s}_m$  as being perpendicular to the surface of the specimen, but we don't know where that is. Actually, we will often assume that  $\mathbf{s}_m$  is perpendicular to  $\mathbf{OG}$ , but this need not be the case. We will refer to  $\mathbf{s}$  in several ways:  $\mathbf{s}_g$  will emphasize that  $\mathbf{s}$  is defined for a particular  $\mathbf{g}$  while  $\mathbf{s}_z$  will emphasize that  $\mathbf{s}$  lies along the  $z$ -axis, which often corresponds to the incident-beam direction and the foil normal. We write  $\mathbf{s}$  when we are not being specific.

### THE VECTOR $\mathbf{s}$

This vector,  $\mathbf{s}$ , is a measure of how far we deviate from the exact Bragg condition.

When we drew Figure 12.4, you noticed that we placed the point  $G$  outside the Ewald sphere. Note that we are using  $G$  to emphasize that we are referring to the point, not the vector,  $\mathbf{g}$ , from the origin to the point. In

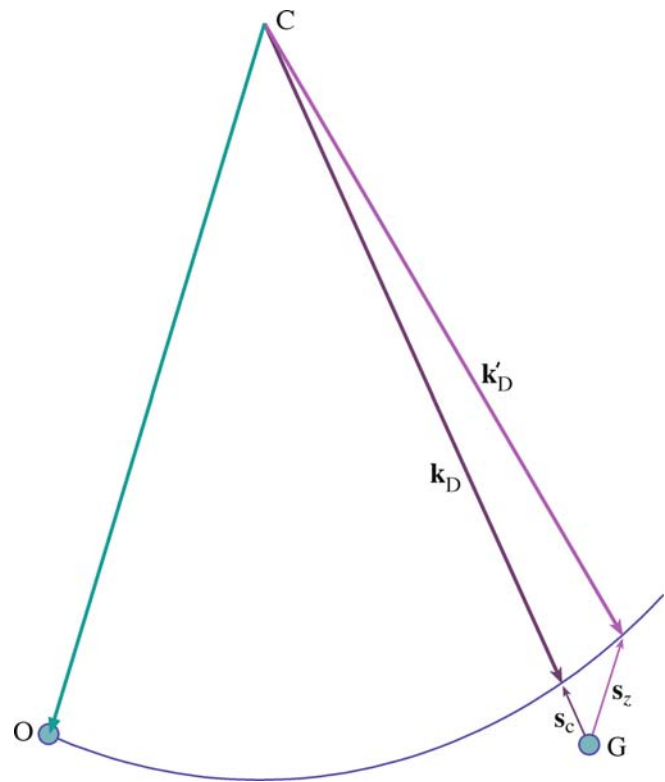


**FIGURE 12.4.** Two special values of  $\mathbf{s}$  are illustrated. When  $\mathbf{k}_D$  lies along  $\mathbf{CG}$  then  $\mathbf{s}_c$  is parallel to  $\mathbf{CD}$ . Alternatively, we can choose  $\mathbf{s}$  to be parallel to the incident beam direction  $\mathbf{CO}$ ; then  $\mathbf{s} = \mathbf{s}_z$  and  $\mathbf{k}_D$  becomes  $\mathbf{k}'_D$ . In each case,  $\mathbf{k}_D$  ends on the Ewald sphere.

Figure 12.4, the row of reciprocal-lattice points is essentially at  $90^\circ$  to the incident beam. If we take all such rows, we define a plane of points (only  $G$  is shown) which are all at  $90^\circ$  to the incident beam. This plane of points is called the zero-order Laue zone (ZOLZ). We can now number all the planes of points which are parallel to the ZOLZ but do not contain the point  $O$ , and call these the higher-order Laue zones or HOLZ. The first of these (going toward  $C$ ) is the FOLZ, the second is the SOLZ, and the rest are just HOLZ.

### SIGN CONVENTION

We define the sign of  $\mathbf{s}$  to be negative when  $G$  is outside the sphere, while  $\mathbf{s}$  is positive when  $G$  is inside the Ewald sphere.

If we now draw the Ewald sphere as shown in Figure 12.5, you can see that it will intersect points in the FOLZ and other HOLZ. We'll see examples of these kinds of DPs in Chapters 20 and 21.

We can change the value of  $\mathbf{s}$  in two ways.

- First, if we tilt the specimen, the row of spots moves but the Ewald sphere does not.
- Second, if we tilt the beam above the specimen, the Ewald sphere moves, because  $\mathbf{k}_I$  tilts, because  $C$  moves!



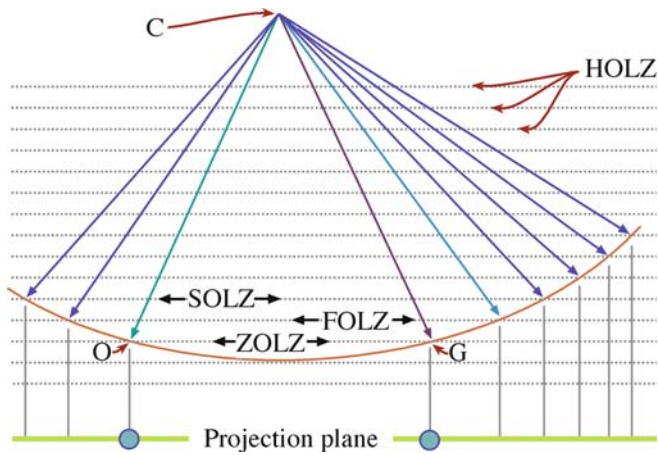


**FIGURE 12.5.** The Ewald sphere intercepts points in higher-order Laue zones (HOLZ) at large angles to the incident-beam direction. If the radius of the sphere increases (higher kV beam) then the sphere flattens and the HOLZ interception is at still larger angles.

Convince yourself of this. The DPs with different values of  $s_z$  may appear identical, but be cautious (more about this in the next chapter). The difference between these two processes is shown in Figure 12.6.

We'll conclude this section by giving you an experimental DP to think about. Figure 12.7 is from a slightly misoriented twin boundary: all you need to know is that different grains are diffracting to give two different DPs.

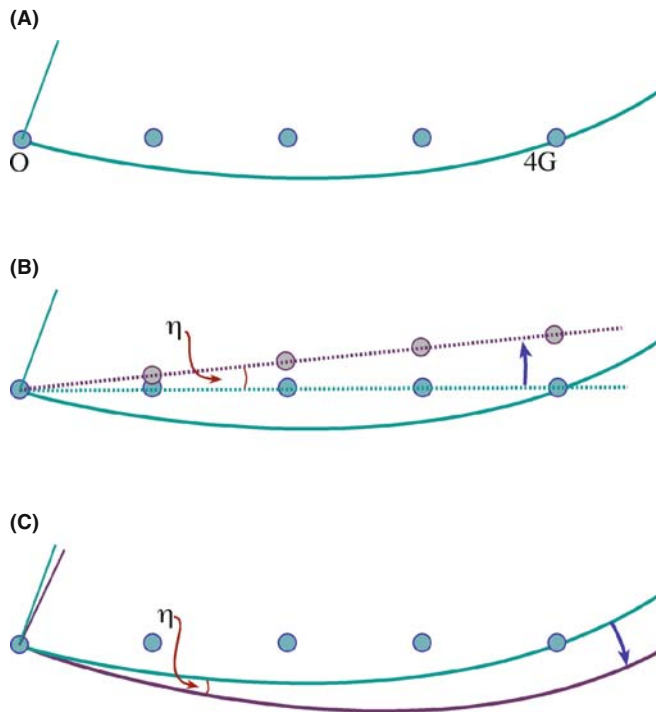


**FIGURE 12.6.** In (A)  $s_z = 0$  for  $4G$ . We can change  $s_z$  in two ways; (B) if we tilt the specimen through angle  $\eta$ , the row of spots moves inside the sphere; (C) if we tilt the beam through  $\eta$  above the specimen, in the opposite direction, the sphere moves outside the row of spots.

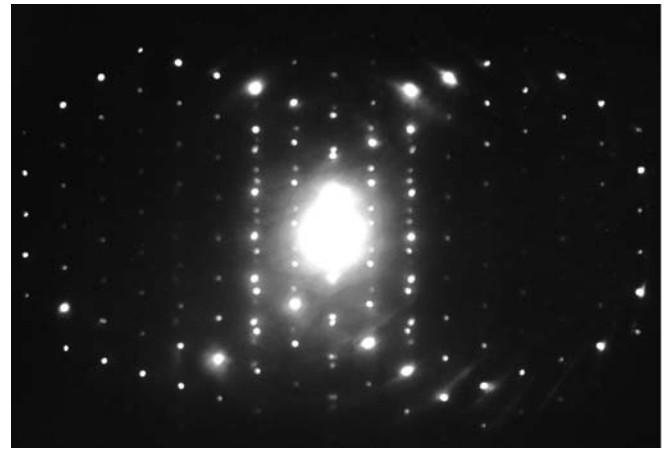


**FIGURE 12.7.** DP taken across a near-twin boundary in  $MgAl_2O_4$  spinel. The rings of bright spots show where the Ewald sphere intercepts the reciprocal lattice of the crystals on either side of the twin boundary.

You can identify a ring of bright spots from each crystal. The question is: why are the rings displaced from one another? Yes, you're right, there is much more to this pattern than first meets the eye, as we'll see in Section 17.3.

## 12.7 THIN-FOIL EFFECT AND THE EFFECT OF ACCELERATING VOLTAGE

We will return to this topic in detail in Chapter 17 after we've examined a little more of the underlying theory. Here, we will briefly remind you that the radius of the Ewald sphere changes as we change kV. As the kV increases, the surface of the sphere becomes flatter. In a way, we were lucky with the initial choice of 100-keV electrons for TEMs since the sphere for 100-keV electrons has a very useful curvature. How does this curvature affect the DP? Well, we know that  $\mathbf{k}_I - \mathbf{k}_D = \mathbf{K} = \mathbf{g}$  where  $|\mathbf{g}|$  is  $d^{-1}$ . Therefore,  $\mathbf{g}$  does not change as we change  $\lambda$ . Since  $d$  does not change but  $\lambda$  does, then Bragg's law tells us that  $\theta$  must decrease as the kV increases. Therefore, if you keep the camera length constant, it will appear that the length of  $\mathbf{g}$  in the DP decreases as  $\lambda$  decreases. Notice that the key word here is 'appear.' If you look back at

**TABLE 12.2. Particular Values of  $\lambda$  and  $\lambda^{-1}$  as a Function of Beam Energy**

$E$	$\lambda$ (pm)	Radius, $\lambda^{-1}$ ( $\text{nm}^{-1}$ )	$(v/c)^2$
100 keV	3.701	270.2	0.3005
120 keV	3.349	298.6	0.3441
200 keV	2.508	398.7	0.4834
300 keV	1.969	508.0	0.6030
400 keV	1.644	608.3	0.6853
1 MeV	0.8719	1147.	0.8856

Section 9.6.B, you'll realize that the problem is that you must recalibrate the camera length for the new accelerating voltage.

The specimen is unchanged so the reciprocal lattice is the same. However, as the kV increases, the radius of the Ewald sphere increases and the diffraction spots appear to move closer together.

What is very important for TEM is that because  $\lambda$  is small, the radius of the Ewald sphere,  $\lambda^{-1}$ , is large and

hence the Ewald sphere is quite flat. Note that this is very different from what we find in LEED or a typical back-reflection Laue X-ray pattern. The result is that we see many spots in the DP. Some values of the radius of the Ewald sphere are given in Table 12.2. You'll find it a useful exercise to generate this table yourself using a spreadsheet. Use the values from Chapter 1:  $m_0 = 9.109 \times 10^{-31}$  kg,  $c = 2.998 \times 10^8$  m/s,  $h = 6.626 \times 10^{-34}$  Nm s and  $1 \text{ eV} = 1.602 \times 10^{-19}$  N m.

## CHAPTER SUMMARY

When combined with the Ewald-sphere construction, the reciprocal lattice gives us a very simple way of thinking about diffraction. When the sphere exactly cuts through a point, Bragg's law or the Laue equations are exactly satisfied. When the sphere just misses a point, we define a distance  $s$  to quantify this excitation error. In other words,  $s$  is a measure of where we cut the rod. Ideally you will become as familiar with tilting reciprocal lattices in space as you are with tilting real lattices in your specimen holder. Remember that the lattices are rigidly connected to one another: when one turns the other does by exactly the same amount. Although Lilliput does not exist, reciprocal space does—at least for the electron microscopist!

Keep in mind the geometry and the dimensions.

- The Ewald sphere has a radius of  $1/\lambda$  and always passes through the point O in the reciprocal lattice.
- Reciprocal-lattice dimensions are  $\text{nm}^{-1}$  although you'll still see  $\text{\AA}^{-1}$ . You know  $10 \text{ \AA} = 1 \text{ nm}$ ; it's not as easy to remember that  $1 \text{ \AA}^{-1} = 10 \text{ nm}^{-1}$ .

## HISTORY

Cruickshank, DWJ, Juretschke, HJ, and Kato, N (Eds.) 1992 *PP Ewald and His Dynamical Theory of X-ray Diffraction* Oxford University Press New York. When you have time.

Ewald, PP 1962 *Fifty Years of X-ray Diffraction* NVA Oosthoek's Uitgeversmaatschappij Utrecht Netherlands. Includes a description of how Ewald developed his description of reciprocal space. PP Ewald was Hans Bethe's father-in-law.

## RECIPROCAL SPACE

Cullity, BD and Stock, SR 2001 *Elements of X-Ray Diffraction* 3rd Ed. Addison-Wesley Reading MA. The latest edition of the standard known simply as 'Cullity.'

James, RW 1965 *The Optical Principles of the Diffraction of X-Rays, The Crystalline State II* Ed. WL Bragg Cornell University Press Ithaca NY (first published in 1948). Special.

Schwartz, LH and Cohen, JB 1987 *Diffraction from Materials*, 2nd Ed. Springer New York. An alternative to Cullity.

Suryanarayana, C and Norton, MG 1998 *X-Ray Diffraction: A Practical Approach* Springer New York. Practical and different.

## THE COMPANION TEXT

The contents of this chapter are used throughout the companion text but not explicitly.

## SELF-ASSESSMENT QUESTIONS

- Q12.1 How does the size of an object in real space relate to its size in reciprocal space?
- Q12.2 When are  $(hkl)$  and  $[hkl]$  parallel for all values of  $h$ ,  $k$ , and  $l$ ?
- Q12.3 Why does the incident-beam direction always point toward the 000 reflection of reciprocal lattice in the Ewald-sphere construction?
- Q12.4 Why does electron diffraction in the TEM show planes of the reciprocal lattice?
- Q12.5 Define excitation error and explain why we want to change its value.
- Q12.6 How are the radius and the surface of the Ewald sphere affected if kV increases?



- Q12.7 What happens to the diffraction spots and the reciprocal lattice when kV increases?
- Q12.8 How are the higher-order Laue (HOLZ) lines affected by increasing the kV?
- Q12.9 Define what we mean by ‘reciprocal lattice.’
- Q12.10 Define the vector  $\mathbf{g}$ .
- Q12.11 What is the sphere of reflection and where is its center?
- Q12.12 Define what we mean by ‘zero-order Laue zone.’
- Q12.13 What is the simple relationship between  $\mathbf{K}$  and  $\mathbf{g}$  that represents the Laue conditions for constructive interference and how does it relate to Bragg’s law?
- Q12.14 How is  $d_{nh, nk, nl}$  related to  $d_{hkl}$ ?
- Q12.15 Is  $d_{123}$  the same as  $d_{321}$  for an orthorhombic crystal?
- Q12.16 What happens to the Ewald sphere when the specimen is tilted?
- Q12.17 What happens to the Ewald sphere when the incident beam is tilted?
- Q12.18 In real space, the following notation  $[UVW]$  and  $(hkl)$  signifies a particular crystalline direction and a particular plane, respectively. What does the same notation mean in reciprocal space?
- Q12.19 Define the reciprocal vector  $\mathbf{a}$ .
- Q12.20 What is the sign convention for the deviation parameter?

### TEXT-SPECIFIC QUESTIONS

- T12.1 Consider Figure 12.7. Determine the angle of misorientation between the two grains and the axis of rotation. Take the perfect twin alignment to be zero misorientation.
- T12.2 Consider Figure 12.6A. If G is the 220 reflection for Ge and you are using a 200-kV TEM, what is the value of  $\mathbf{s}$  for the O, G, 2G, and 3G reflections. Repeat the question for 400-kV electrons and comment on the difference.
- T12.3 For question 12.2, what is the Bragg angle for the excited reflection? (Give your answer in degrees and radians.)
- T12.4 Consider Figure 12.4. The two values of  $\mathbf{s}$  differ significantly and the vectors are inclined to one another. Choosing the 220 reflection in Cu and 100-keV electrons, which effect (magnitude or direction) is likely to be more important?
- T12.5 Consider Figure 12.5. How has this figure been exaggerated? Describe a material which could give the geometry shown here.
- T12.6 Generate Table 12.2 given the data in the text.
- T12.7 If G in Figure 12.6 is Cu 220, estimate  $\lambda$  (ignoring relativistic effects) and hence suggest the kV.
- T12.8 Assuming two major grains give rise to the DP in Figure 12.7, identify them (a tracing is fine). Then explain why there are two different rings of bright spots.
- T12.9 More challenging and specialized. Use historical sources to describe the relationship between Laue, Ewald, and the Braggs and to explain their interactions.

# Diffracted Beams

## CHAPTER PREVIEW

In Chapter 11 we discussed why diffraction occurs; in this chapter we give a more detailed mathematical treatment. It may be more detailed than you need at this stage. Diffraction is one of those phenomena that lends itself directly to a detailed mathematical modeling, but there is a danger: *don't become so engrossed in the math that you miss the principles involved; conversely, don't ignore the subject because it is mathematically daunting!* The topic of this chapter is one which causes major problems for many microscopists. The treatment we will follow is known as the 'dynamical theory.' Later we will make some gross simplifications, partly because this is instructive and partly because these simplifications do apply to some important special cases; the kinematical approximation is one such simplification. Many other texts begin with the so-called 'kinematical' treatment and then advance to the more realistic, more general dynamical case. We will not do this but we will introduce the words and assumptions in Chapter 27.

The main principle of dynamical scattering was discussed in Chapter 11: an electron beam can be strongly scattered by a set of planes of atoms. When these planes are suitably oriented with respect to the beam, they produce a diffracted beam. This diffracted beam can then be rediffracted by a second set of planes in the same specimen, and so on. The physical reason for this repeated, or dynamical, diffraction, is that the electron beam and the atoms in the crystal interact strongly due to Coulomb forces. (X-rays are much less strongly affected by atoms and are thus more likely to be only scattered once, i.e., kinematical scattering.) This repeated scattering between the diffracted beams and the direct beam is the persistent topic of this chapter.

If you have a strong background in physics, you may find the simplifications used in this treatment somewhat unsatisfactory because we should be considering Bloch waves in a periodic object (our crystalline sample). We will discuss the analysis of Bloch waves in Chapter 14. Remember that *experimentally* we will associate arrays of spots in DPs with Bragg beams. Then we will relate these beams to images. We see both images and 'beams' on the screen of the TEM.

In future chapters, we will always discuss the thickness of the specimen in terms of the *extinction distance*. This is a term which we introduce here as a *characteristic length* for a *particular diffracted beam*. So, even in a rigorous Bloch-wave analysis, it is still important to understand the origin of the terminology introduced here (Table 13.1). Remember that the reason for looking at these equations is that they are directly useful to you when you are using the microscope, because they *describe* both the intensity of the electron beam in DPs and the contrast seen in TEM images of crystalline materials.

### 13.1 WHY CALCULATE INTENSITIES?

In this chapter, we will consider only scattering from perfect, defect-free, crystalline materials.

Ultimately we want to understand the images we see in the microscope. The detail we see in these images is determined by the intensity of the electron beam or beams and this varies for different positions in the

image. Our motivation for calculating the intensity of diffracted beams is, therefore, to understand contrast features in TEM images.

In general, the analysis of the intensity of diffracted beams in the TEM is not simple because a beam which is diffracted once will easily be rediffracted. We call this repeated diffraction 'dynamical diffraction.' In a perfect crystal, imagine dividing the crystal into two halves, one

**TABLE 13.1 Terminology and Notation**

$\Psi^T$ at P	The <i>total</i> wave function of the electron beam as measured at a point P at the bottom of the specimen. This wave function is a solution to the Schrödinger equation both inside and outside the specimen. What interests us is not $\Psi^T$ but $\phi_{\mathbf{g}}$ and $\phi_0$
$\phi_{\mathbf{g}}$	The amplitude of the <i>diffracted</i> beam for reflection G. The intensity is $ \phi_{\mathbf{g}} ^2$
$\phi_0$	The amplitude of the <i>direct</i> beam. Don't use the term 'transmitted' beam; all the beams we are studying are transmitted. Don't call it the 'forward-scattered' beam; diffracted beams can also be forward scattered. $\phi_0$ is a special value of $\phi_{\mathbf{g}}$ for the case where $\mathbf{g} = \mathbf{0}$
$\theta$	The angle between a particular set of lattice planes and the direction of the beam scattered constructively by those planes
$\theta_B$	The Bragg angle; a specific value of $\theta$ when $\mathbf{s} = \mathbf{0}$
$dz$	The thickness of a diffracting slice. This thickness can be as small as we wish to make it; it is not limited to atomic planes
$\xi_{\mathbf{g}}$	A characteristic length for reflection $\mathbf{g}$ ; it is called the <i>extinction distance</i>
D, G	D is a diffracted beam; G is a special D and indicates that it is a Bragg-diffracted beam (neither is bold) (see Section 11.5)
$\chi$	The electron wave vector in a vacuum
$\mathbf{k}$	The electron wave vector in the specimen

above the other. The upper half diffracts the direct beam. The lower half further diffracts the direct beam but also rediffracts the diffracted beam. Don't confuse this rediffraction with the term 'double diffraction,' which has a special meaning, described in Chapter 23. If instead of cutting the specimen into two, you cut the specimen into many thin slices, you have multiple, instead of just double, diffraction. We call this effect dynamical diffraction.

Because of dynamical diffraction, we cannot use the intensities of spots in electron DPs (except under very special conditions such as CBED) for structure determination, in the way that we use intensities in X-ray patterns. Actually, a more important practical consideration is that the intensity of the electron beam varies strongly as the thickness of the specimen changes; the thickness may change across distances which are much smaller (as small as 1.5 nm or less) than the lateral dimensions of the electron beam (typically  $>1 \mu\text{m}$  in the TEM imaging mode). As we will see in Chapters 24–27 when we discuss images, the beam intensity also changes when lattice defects are present which is why we can 'see' defects in the TEM.

### 13.2 THE APPROACH

The approach we take here is to develop the basic equations describing the diffraction process and to identify parameters which will be important in understanding the contrast in the image. The different images will then be discussed in Part 3.

*Inside* a crystalline material, we should think in terms of Bloch waves because only certain wave-propagation vectors are allowed in infinite periodic structures: fortunately you don't need to have a thorough understanding of Bloch waves to understand contrast features in the microscope. However, we will consider them in Chapter 14, because a full understanding of the fundamental principles of diffraction from crystals will require this knowledge. What we 'see' in a DP relates directly to 'beams' because the DP, whether in the microscope or on a print, is *outside* the crystal. In this chapter, we will follow the analysis of

Chapter 11, considering the amplitudes of beams simply because this gives a good intuitive understanding of the images—what we *see* in the TEM is the intensity, which is directly related to the amplitude ( $I \propto |\phi|^2$ ).

#### A NOTE ON TERMINOLOGY

In Figure 13.1 we have labeled both the diffracted beams and the spot in the DP,  $G_i$  ( $i = 1, 2, \text{etc.}$ ). When discussing images we will often refer to  $\mathbf{g}_1$ , the diffraction vector for the beam  $G_1$ . Then colloquially we will call  $\mathbf{g}$  the 'reflection  $\mathbf{g}$ '; the origin for this terminology goes back to the diagram for Bragg diffraction: geometrically it looks like 'reflection.'

So, what do we need to calculate? We need to calculate the intensity of the beam at the exit surface of the specimen, e.g., at all points, such as P in Figure 13.1, because this becomes the 'image' after suitable magnification.

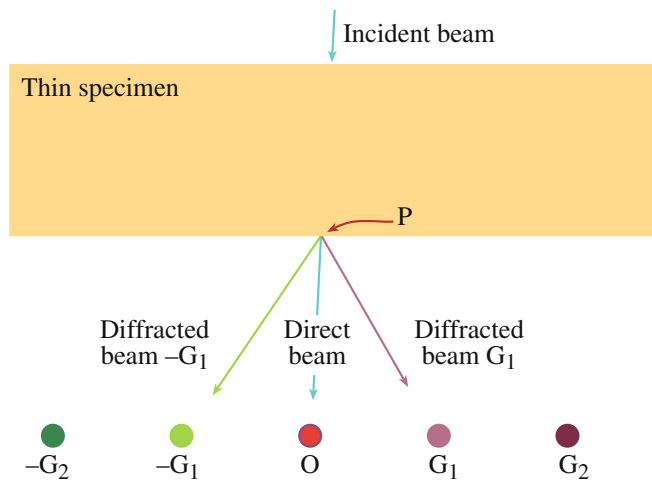


**FIGURE 13.1.** Defining the point P. The incident beam is scattered inside the thin sample. We want to know the intensities of the direct beam (O) and the diffracted ( $G_i$ ) beams for each point P at the bottom surface of the specimen (the exit surface).

Before concluding this topic, we will briefly discuss the approximations we are making. One of the most important of these is the column approximation, which is introduced almost without being noticed. It is not a necessary assumption but it simplifies calculations and again aids intuitive understanding. You will also recognize many similarities to visible-light microscopy, but be wary, there are also many differences.

### 13.3 THE AMPLITUDE OF A DIFFRACTED BEAM

In the analysis of diffracted beams we will consider only crystalline materials. Since any crystal can be constructed by stacking unit cells, we begin by remembering the amplitude scattered by a single unit cell. We can rewrite equation 3.18 so that the amplitude of the electron beam scattered from a unit cell is

$$A_{\text{cell}} = \frac{e^{2\pi i k r}}{r} \sum_i f_i(\theta) e^{2\pi i \mathbf{K} \cdot \mathbf{r}} \quad (13.1)$$

where the summation is over all  $i$  atoms in the unit cell and  $\theta$  is the angle at which the diffracted beam is traveling relative to the incident beam. We have included the term outside the summation because of how the wave propagates; the  $r^{-1}$  term is present because we have a constant flux of electrons traveling through an expanding spherical surface, radius  $r$ . The quantities  $\mathbf{k}$ ,  $\mathbf{K}$ , and  $\mathbf{r}$  were defined in Chapter 11 and  $f(\theta)$  is the atomic-scattering factor. You will often see the sign of the exponent after  $f(\theta)$  reversed. Unfortunately, there are two conventions! These conventions are discussed in Section 13.12; we will use the positive convention to be consistent with most materials-science texts.

Figure 13.2 reminds us that  $\mathbf{K} = \mathbf{k}_D - \mathbf{k}_I$ . The vectors  $\mathbf{r}$  and  $\mathbf{r}_i$  are different:  $\mathbf{r}$  is the distance from a point P

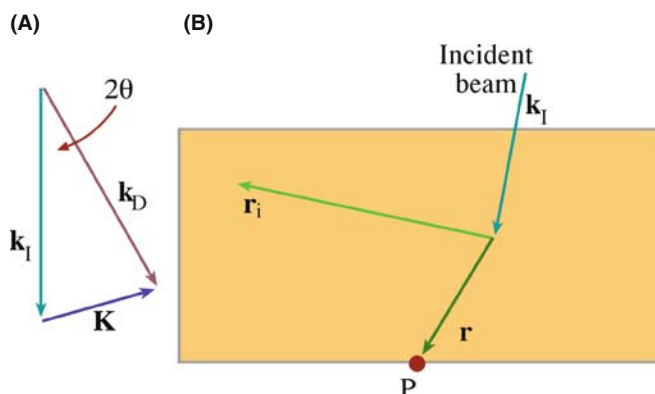


**FIGURE 13.2.** (A) A reminder that  $\mathbf{K} = \mathbf{k}_D - \mathbf{k}_I$ . The vector  $\mathbf{k}_D$  represents the propagation vector for *any* wave. It does not have to be a diffracted beam but it will only give a spot in the DP when it does correspond to a diffracted beam. (B) shows the relation between the radius of the spherical wavefront,  $r$ , the position vector of the  $i^{\text{th}}$  atom,  $\mathbf{r}_i$ , and the point where the intensity is calculated, P.

on the bottom of the specimen to the scattering center and  $\mathbf{r}_i$  defines the position of an atom in the unit cell. Remember that  $f_i(\theta)$  is the *scattering strength* for the ' $i$ ' atom ( $f_i(\theta)$  is greater for Au than for Al, etc., as we saw in Figure 3.5). Since we are summing over all the atoms in the unit cell, we can rename this sum as  $F(\theta)$ , the *structure factor* of the unit cell. (It's just the scattering factor of the unit cell.) Notice that  $F(\theta)$  depends on the nature of all the atoms in the unit cell, their positions, and the direction in which the beam is propagating (related to  $\mathbf{K}$  and hence  $\theta$ ). Go back and check Section 3.9.

Therefore, expression 13.1 can be rewritten as

$$A_{\text{cell}} = \frac{e^{2\pi i \mathbf{k} \cdot \mathbf{r}}}{r} F(\theta) \quad (13.2)$$

To find the intensity at some point P, we then sum over all the unit cells in the specimen. For simplicity, we will not solve this problem mathematically here but simply quote the result and discuss its meaning. Let's say we have  $n$  unit cells per unit area on a plane parallel to the crystal surface and  $a$  is the distance between these planes. The volume of a unit cell,  $V_c$ , is simply  $a/n$ . The amplitude in a *diffracted beam* (in the direction identified by  $\theta$ ) is denoted as  $\phi_g$  and is given by

$$\phi_g = \frac{\pi a i}{\xi_g} \sum_n e^{-2\pi i \mathbf{K} \cdot \mathbf{r}_n} e^{-2\pi i \mathbf{k}_D \cdot \mathbf{r}} \quad (13.3)$$

Here  $\mathbf{r}_n$  denotes the position of each unit cell. (Think about the signs in this equation.) In this analysis, the quantities  $f(\theta)$  and  $F(\theta)$  both have dimensions of length. We'll now explain what the length  $\xi_g$  means in equation 13.3; it is a length because  $\phi_g$ , the scattering amplitude, is dimensionless ( $\xi$  is pronounced 'ksi,' rhyming with 'sigh').

The derivation of these equations involves some tricky manipulation which we will return to later. Some analyses actually make the unrealistic assumption that the intensity of the direct beam,  $|\phi_0|^2$ , remains unchanged. This assumption is usually not justified, especially when the specimen has a finite thickness! If  $|\phi_g|^2$  is not zero then  $|\phi_0|^2$  cannot still be 1.

### 13.4 THE CHARACTERISTIC LENGTH $\xi_g$

At this stage in our analysis it is best to think of the quantity  $\xi_g$  as a 'characteristic length' for the diffraction vector  $\mathbf{g}$  so as not to have any preconceived ideas of what it represents. A detailed analysis shows that the magnitude of  $\xi_g$  can be expressed as

$$\xi_g = \frac{\pi V_c \cos \theta_B}{\lambda F_g} \quad (13.4)$$

where  $F_g$  is the  $F(\theta)$  for reflection  $\mathbf{g}$  (i.e.,  $F_g$  is a special value of  $F(\theta)$  when  $\theta$  is the Bragg angle).

The quantity  $\xi_{\mathbf{g}}$  is an extremely important one; it gives us a way of thinking about nearly all diffraction-contrast phenomena. It is measured in nanometers (or Å) and is known as the ‘extinction distance’ for reasons that will become obvious.

From equation 13.4, you can see that the magnitude of  $\xi_{\mathbf{g}}$  is related to  $F_{\mathbf{g}}$  (and through  $V_c$  to the lattice parameter) and the wavelength of the electrons,  $\lambda$ . If the structure factor ( $F_{\mathbf{g}}$ ) is large,  $\xi_{\mathbf{g}}$  will be small. Therefore,  $\xi_{\mathbf{g}}$  will be small for Au but large for Si.  $F_{\mathbf{g}}$  is large when the atomic number is large, because the Coulomb interactions are larger and  $f(\theta)$  is large. Similarly, as the accelerating voltage is increased,  $\xi_{\mathbf{g}}$ , for a particular material, will increase because the wavelength of the electrons decreases. Table 13.2 lists some useful extinction distances (all for 100-keV electrons).

### SUMMARIZE $\xi_{\mathbf{g}}$

$\xi_{\mathbf{g}}$  is the characteristic length for the diffraction vector  $\mathbf{g}$ . We call it the **extinction distance** because of a property we’ll discover later.

Note that  $\xi_{\mathbf{g}}$  is a scalar quantity.  $\xi_{\mathbf{g}}$  depends on the lattice parameters (through  $V_c$ ), the atomic number (through  $F_{\mathbf{g}}$ ), and the kV used (through  $\lambda$ ).

The effect of the lattice parameter on  $\xi_{\mathbf{g}}$  is illustrated nicely by comparing values of  $\xi_{111}$  for diamond, Si, and Ge: the value for Si is larger than for Ge, as expected, because of the smaller atomic number but note that  $\xi_{\mathbf{g}}$  for Si is also larger than that for diamond, which has a lower atomic number! Diamond has a particularly small lattice parameter, hence there are more atoms in a given volume.

## 13.5 THE HOWIE-WHELAN EQUATIONS

The direct and diffracted beams are detected outside the crystal and we see them on the viewing screen. Now we can think of the wave function inside the crystal as being

TABLE 13.2 Examples of Extinction Distances (in nm)\*

Material	110	111	200	220	400
$hkl =$	110	111	200	220	400
Al	–	56.3	68.5	114.4	202.4
Cu	–	28.6	32.6	47.3	76.4
Au	–	18.3	20.2	27.8	43.5
MgO	–	272.6	46.1	66.2	103.3
Fe	28.6	–	41.2	65.8	116.2
W	18.0	–	24.5	35.5	55.6
Diamond		47.6	–	66.5	121.5
Si		60.2	–	75.7	126.8
Ge		43.0	–	45.2	65.9

\*For two-beam condition at 100 kV.

the sum of the beams passing through the crystal. The direct beam has amplitude  $\phi_0$  (bold  $\mathbf{0}$  to emphasize that the diffraction vector has zero length) and the amplitudes of the diffracted beams can be written as  $\phi_{\mathbf{g}_1}$ ,  $\phi_{\mathbf{g}_2}$ , etc. Each beam has an appropriate phase factor. We write  $\psi^T$ , the total wave function, as a series

$$\psi^T = \phi_0 e^{2\pi i \chi_0 \cdot \mathbf{r}} + \phi_{\mathbf{g}_1} e^{2\pi i \chi_{G_1} \cdot \mathbf{r}} + \phi_{\mathbf{g}_2} e^{2\pi i \chi_{G_2} \cdot \mathbf{r}} + \dots \quad (13.5)$$

where the wave vectors are  $\chi_0$  and  $\chi_D$  ( $\chi$  (chi) is pronounced ‘kai’ and rhymes with sky);  $\chi_0$  is often written simply as  $\chi$ . We use  $\chi_0$  here to emphasize that it is a vector which terminates on the point O in reciprocal space;  $\chi_{G_1}$  terminates on the ‘point’  $G_1$ , etc. At this stage, we are using wave vectors  $\chi_0$  and  $\chi_D$  which describe the wave in the vacuum rather than in the crystal. We will change to being inside the crystal shortly. Most of the time, you could write  $\chi$  as  $\mathbf{k}$ , but there are occasions when the difference is important so we start with  $\chi$  and then change over.

First, we simplify equation 13.5 by considering only one diffracted beam  $\mathbf{G}$ , i.e., we make a ‘two-beam approximation’ (O is the other beam). This is a very important approximation, which we’ll use often. Two-beam conditions mean that we tilt the crystal so there is only one strong diffracted beam (with  $\mathbf{s} = 0$ ). All other diffracted beams are weak ( $\mathbf{s} \gg$  or  $\ll 0$ ), and we ignore their contribution to  $\phi_{\mathbf{g}}$ . Then if the amplitude  $\phi_{\mathbf{g}}$  changes by a small increment as the beam passes through a thin slice of material which is  $dz$  thick we can write down expressions for the *changes* in  $\phi_{\mathbf{g}}$  and  $\phi_0$  by using the concept introduced in equation 13.3 but replacing  $a$  by the short distance  $dz$

$$d\phi_{\mathbf{g}} = \left\{ \frac{\pi i}{\xi_{\mathbf{g}}} \phi_0 e^{2\pi i (\chi_0 - \chi_D) \cdot \mathbf{r}} + \frac{\pi i}{\xi_0} \phi_{\mathbf{g}} \right\} dz \quad (13.6)$$

$$d\phi_0 = \left\{ \frac{\pi i}{\xi_0} \phi_0 + \frac{\pi i}{\xi_{\mathbf{g}}} \phi_{\mathbf{g}} e^{2\pi i (\chi_D - \chi_0) \cdot \mathbf{r}} \right\} dz \quad (13.7)$$

Here  $\chi_0 - \chi_D$  is the change in wave vector as the  $\phi_{\mathbf{g}}$  beam scatters into the  $\phi_0$  beam. Similarly  $\chi_D - \chi_0$  is the change in wave vector as the  $\phi_0$  beam scatters into the  $\phi_{\mathbf{g}}$  beam. Now the *difference*  $\chi_0 - \chi_D$  is identical to  $\mathbf{k}_O - \mathbf{k}_D$  although the individual terms are not equal. Then remember that  $\mathbf{k}_D - \mathbf{k}_O (= \mathbf{K})$  is  $\mathbf{g} + \mathbf{s}$  for the perfect crystal.

You might wonder why we have introduced the wave vector  $\chi$  when it appears to be the same as the  $\mathbf{k}$  we used in equation 13.1. The reason is that equation 13.1 is a very general equation describing scattering from any group of atoms, but we are now going to consider two special cases, namely, an electron in the vacuum (wave vector  $\chi$ ) and one in a crystal (wave vector  $\mathbf{k}$ ). Incidentally, the excitation error,  $\mathbf{s}$ , should really be written as  $\mathbf{s}_{\mathbf{g}}$ , since it refers to a particular  $\mathbf{g}$  vector. You can think



of the parameter  $\xi_0$  as the characteristic length for forward scattering, i.e., scattering from any beam into itself, whereas  $\xi_g$  corresponds to scattering through an angle corresponding to a diffraction vector  $\mathbf{g}$ .

The change in  $\phi_g$  depends on the magnitude of **both**  $\phi_g$  and  $\phi_0$ .

These two equations (13.6 and 13.7) can then be rearranged to give a pair of coupled differential equations. We say that  $\phi_0$  and  $\phi_g$  are ‘dynamically coupled.’ The term *dynamical diffraction* thus means that the amplitudes (and therefore the intensities) of the direct and diffracted beams are constantly changing, i.e., they are dynamic

$$\frac{d\phi_g}{dz} = \frac{\pi i}{\xi_g} \phi_0 e^{-2\pi i s z} + \frac{\pi i}{\xi_0} \phi_g \quad (13.8)$$

and

$$\frac{d\phi_0}{dz} = \frac{\pi i}{\xi_0} \phi_0 + \frac{\pi i}{\xi_g} \phi_g e^{2\pi i s z} \quad (13.9)$$

Microscopists usually refer to this pair of equations as the ‘*Howie-Whelan*’ equations after Howie and Whelan (1961), who laid the foundations for understanding diffraction contrast in the TEM; you may also see them referred to as the ‘Darwin-Howie-Whelan equations’ since Darwin (1914) developed the dynamical theory for X-rays! Note that we are further simplifying the expression by writing

$$e^{-2\pi i \mathbf{s} \cdot \mathbf{r}} = e^{-2\pi i s z} \quad (13.10)$$

In doing so, we are making the approximation that  $\mathbf{s}$  and  $\mathbf{r}$  are both parallel to  $z$ , i.e., at this time, we ignore components of  $\mathbf{s}$  that are not parallel to the electron beam. The approximation may be written as

$$|\mathbf{s}_g| = s_z \quad (13.11)$$

We then drop the  $z$  subscript; just remember it is still there. There are situations where the difference can become important.

Although this approach is totally phenomenological (i.e., we haven’t really given any physical justification for the assumptions we have made and actually we know we should use Bloch waves), you will see that it provides enormous insight into the interpretation of your images and DPs. In Chapter 25, we will use these ideas to understand why we see defects in the TEM.

The fundamental idea is that, at any given position in the specimen, the change in the amplitudes of *both* the direct beam and the diffracted beam depends on the amplitude of *both* beams. The fact that part of the change in  $\phi_0$  is due to the magnitude of  $\phi_0$  itself, gives rise to the term *forward scattering*; remember the origin of scattering from Section 2.2. Note that scattering from

$\phi_g$  to  $\phi_g$  is also forward scattering, although it takes place in a different forward direction (i.e.,  $\theta = \theta_B$  and scattering is parallel to  $\mathbf{k}_D$  rather than  $\mathbf{k}_O$ ). So forward scattering does occur but it does not change the direction of the beam. However, it does have a characteristic length,  $\xi_0$ ; this length is another way of saying we have a refractive-index effect for electrons which we’ll address later in Section 14.4.

### DIRECT

Remember: don’t refer to the direct beam as the unscattered or the transmitted beam!

## 13.6 REFORMULATING THE HOWIE-WHELAN EQUATIONS

From here on, the math is quite straightforward. What we are going to do may seem like a lot of work to derive one equation (13.48) but the result will allow you to picture more clearly what is happening. If you don’t want to bother with the math, you can skip to equations 13.47 and 13.48 but you must not miss those two equations; they are essential for understanding images of crystalline materials.

The pair of equations, 13.8 and 13.9, can be simplified by making the substitutions (i.e., a transformation of variables)

$$\phi_{0(\text{sub})} = \phi_0 e^{-\frac{\pi i z}{\xi_0}} \quad (13.12)$$

and

$$\phi_{g(\text{sub})} = \phi_g e^{2\pi i s z - \frac{\pi i z}{\xi_0}} \quad (13.13)$$

Then equations 13.8 and 13.9 become

$$\frac{d\phi_{g(\text{sub})}}{dz} = \frac{\pi i}{\xi_g} \phi_{0(\text{sub})} + 2\pi i s \phi_{g(\text{sub})} \quad (13.14)$$

and

$$\frac{d\phi_{0(\text{sub})}}{dz} = \frac{\pi i}{\xi_g} \phi_{g(\text{sub})} \quad (13.15)$$

Since  $\phi_0$  and  $\phi_{0(\text{sub})}$  only differ by a phase factor, we will ignore the difference in calculating intensities since only the amplitude is then important; similarly for  $\phi_g$  and  $\phi_{g(\text{sub})}$ . The result of our substitution is that we have removed the phase factor involving  $\xi_0$ , i.e., we’ve removed the refractive-index effect. Equations 13.14 and 13.15 can be combined to give the second-order differential equation for  $\phi_0$



$$\frac{d^2\phi_0}{dz^2} - 2\pi i s \frac{d\phi_0}{dz} + \frac{\pi^2}{\xi_g^2} \phi_0 = 0 \quad (13.16)$$

We can obtain a similar equation for  $\phi_g$  and then obtain solutions for these reformulated expressions.

Note that the only other quantities appearing in this equation for  $\phi_0$  are  $z$ ,  $s$ , and  $\xi_g$ :  $z$  and  $s$  are geometric parameters; the nature of the material only enters through  $\xi_g$ .

### 13.7 SOLVING THE HOWIE-WHELAN EQUATIONS

If we can solve the Howie-Whelan equations, then we can predict the intensities in the direct and diffracted beams (i.e.,  $|\phi_0|^2$  and  $|\phi_g|^2$  in the two-beam case). If we take it step by step, then we know that solutions to equation 13.16 (a second-order differential equation in one variable,  $\phi_0$ ) must have the form

$$\phi_0 = C_0 e^{2\pi i \gamma z} \quad (13.17a)$$

So we can write that

$$\frac{d\phi_0}{dz} = 2\pi i \gamma C_0 e^{2\pi i \gamma z} \quad (13.17b)$$

and

$$\frac{d^2\phi_0}{dz^2} = -4\pi^2 \gamma^2 C_0 e^{2\pi i \gamma z} \quad (13.17c)$$

What we need to determine is the phase  $\gamma$  and the amplitude  $C_0$ . Note that since  $z$  is a distance in real space, then  $\gamma$  must be a distance in reciprocal space. Substituting this expression into equation 13.16 shows that  $\gamma$  must be a solution to the algebraic equation

$$\gamma^2 - s\gamma - \frac{\xi_g^{-2}}{4} = 0 \quad (13.18)$$

Now  $\phi_g$  is related to  $\phi_0$  through equation 13.15. By substituting equation 13.17a into equation 13.15 we find that for each  $\phi_0$ , we also have a  $\phi_g$  given by

$$\phi_g = 2\xi_g \gamma C_0 e^{2\pi i \gamma z} \quad (13.19)$$

To emphasize the similarity to equation 13.17a we can define

$$\phi_g = C_g e^{2\pi i \gamma z} \quad (13.20)$$

Then we can see directly that

$$\frac{C_g}{C_0} = 2\xi_g \gamma \quad (13.21)$$

We've actually got this far without solving any equation! There are two solutions to the quadratic equation (13.18), using the standard formula

$$x = \frac{-b \pm \sqrt{b^2 - 4ac}}{2a} \quad (13.22)$$

to give

$$\gamma^{(1)} = \frac{\left(s - \sqrt{s^2 + \frac{1}{\xi_g^2}}\right)}{2} \quad (13.23a)$$

and

$$\gamma^{(2)} = \frac{\left(s + \sqrt{s^2 + \frac{1}{\xi_g^2}}\right)}{2} \quad (13.23b)$$

We have now found two solutions to the Howie-Whelan equations.

There are two different values for  $\phi_0$  and two corresponding values for  $\phi_g$ .

Now we need to understand what these solutions mean physically. Specifically, what can we learn about  $\gamma^{(1)}$  and  $\gamma^{(2)}$ ? Note that they are always real but may be positive or negative depending on the sign and size of  $s$  and that they are *independent* of  $z$ .

### 13.8 THE IMPORTANCE OF $\gamma^{(1)}$ AND $\gamma^{(2)}$

Since  $\gamma^{(1)}$  and  $\gamma^{(2)}$  are solutions of equation 13.18 from the properties of quadratic equations or by combining equations 13.23a and b, we know that

$$\gamma^{(1)} + \gamma^{(2)} = s \quad (13.24)$$

which is a purely geometric quantity, and

$$\gamma^{(1)} \times \gamma^{(2)} = -\frac{1}{4\xi_g^2} \quad (13.25)$$

which is a property of the material. Remember that  $\gamma$  is a length in reciprocal space.

In order to make the equations easier to work with, it is useful to define another quantity,  $w$ , which is *dimensionless* but has the same sign as  $s$ .

$$w = s\xi_g \quad (13.26)$$

In practical situations  $w$  may vary from 0 to  $\pm 10$ . We can then express the two forms of equation 13.21 (because there are *two* values of  $\gamma$ ) in terms of  $\gamma$  or, more conveniently, in terms of  $w$

$$\frac{C_g^{(1)}}{C_0^{(1)}} = 2\xi_g \gamma^{(1)} = w - \sqrt{w^2 + 1} \quad (13.27)$$

and

$$\frac{C_{\mathbf{g}}^{(2)}}{C_{\mathbf{0}}^{(2)}} = 2\xi_{\mathbf{g}}\gamma^{(2)} = w + \sqrt{w^2 + 1} \quad (13.28)$$

(the superscripts on  $C_{\mathbf{g}}^{(1)}$ , etc., correspond to the superscripts on  $\gamma^{(1)}$  and  $\gamma^{(2)}$ , i.e., the two solutions to the original quadratic equation). Now it is useful to make another substitution (or transformation) to simplify these relationships. We define  $\beta$  by

$$w = \cot \beta \quad (13.29)$$

Now we can impose a restriction on the absolute magnitudes of  $\phi_{\mathbf{0}}$  and  $\phi_{\mathbf{g}}$  so that they satisfy the relations

$$C_{\mathbf{0}}^{(1)2} + C_{\mathbf{g}}^{(1)2} = 1 = C_{\mathbf{0}}^{(2)2} + C_{\mathbf{g}}^{(2)2} \quad (13.30)$$

By normalizing these values for  $C$  separately for each value of  $\gamma$ , we are restricting the intensity of the beam to values between 0 and 1 (see below). Then if we substitute equation 13.29 into equation 13.27 and then into equation 13.28 we find (using  $1 - \cos \beta = 2 \sin^2(\beta/2)$  and  $\sin \beta = 2 \sin(\beta/2) \cos(\beta/2)$ ) that the  $C$  values have the following simple forms

$$\begin{aligned} C_{\mathbf{0}}^{(1)} &= \cos \frac{\beta}{2} & C_{\mathbf{g}}^{(1)} &= -\sin \frac{\beta}{2} \\ C_{\mathbf{0}}^{(2)} &= \sin \frac{\beta}{2} & C_{\mathbf{g}}^{(2)} &= \cos \frac{\beta}{2} \end{aligned} \quad (13.31)$$

Now you can understand why we introduced  $\beta$  in equation 13.29. The two independent solutions to the reformulated Howie-Whelan equation for  $\phi_{\mathbf{0}}$  (13.16) are then  $\phi_{\mathbf{0}} = C_{\mathbf{0}}^{(1)} \exp(2\pi i \gamma^{(1)} z)$  and  $\phi_{\mathbf{0}} = C_{\mathbf{0}}^{(2)} \exp(2\pi i \gamma^{(2)} z)$  and *each value* has a corresponding value for  $\phi_{\mathbf{g}}$ .

We can already see that the ratio of the amplitudes of the diffracted and direct beams,  $C_{\mathbf{g}}$  to  $C_{\mathbf{0}}$  (and therefore the intensities), in equation 13.21 depends on  $\gamma$ , the phase of the wave, and hence on  $s$ , the excitation error. Hence the ratios in equations 13.27 and 13.28 depend on how close the specimen is to the Bragg orientation. We are particularly concerned about *the* Bragg condition because we have chosen a two-beam situation.

### THE SUBSTITUTION

Because of this simple substitution you can easily confirm that, for this two-beam situation, the probability of finding the electron in one beam or the other remains unity ( $|\psi^T|^2 = 1$ ). Hence the reason we use a normalized intensity in equation 13.30.

In the two-beam approximation, equation 13.5 is expressed in terms of  $\phi_{\mathbf{0}}$  and  $\phi_{\mathbf{g}}$ , both of which depend on  $\gamma$  (equation 13.17), so equation 13.5 can then be written in terms of both values of  $\gamma$  (and hence  $C_{\mathbf{0}}^{(1)}$ ,  $C_{\mathbf{0}}^{(2)}$ , etc.), giving two independent quantities  $b^{(1)}$  and  $b^{(2)}$ . Either of these two functions could be  $\psi^T$ , the total wave function. Alternatively, the total wave function could be some combination of them, i.e., part  $b^{(1)}$  plus part  $b^{(2)}$ . Both of these wave functions are dependent on  $\mathbf{r}$  and have their own values of  $\mathbf{k}$  that we identify as  $\mathbf{k}^{(j)}$ .

Each value of  $\gamma$  gives a different value of  $\mathbf{k}$  that we call  $\mathbf{k}^{(j)}$ .

Thus we can write expressions for  $b^{(1)}$  and  $b^{(2)}$ .

$$b^{(1)}(\mathbf{k}^{(1)}, \mathbf{r}) = C_{\mathbf{0}}^{(1)} e^{2\pi i \mathbf{k}^{(1)} \cdot \mathbf{r}} + C_{\mathbf{g}}^{(1)} e^{2\pi i (\mathbf{k}^{(1)} + \mathbf{g}) \cdot \mathbf{r}} \quad (13.32)$$

and

$$b^{(2)}(\mathbf{k}^{(2)}, \mathbf{r}) = C_{\mathbf{0}}^{(2)} e^{2\pi i \mathbf{k}^{(2)} \cdot \mathbf{r}} + C_{\mathbf{g}}^{(2)} e^{2\pi i (\mathbf{k}^{(2)} + \mathbf{g}) \cdot \mathbf{r}} \quad (13.33)$$

*Remember:* each of these Bloch-wave functions could be a wave in the crystal—each one depends on only one of the  $\mathbf{k}$  values. In general, the total wave function will be a combination of these two waves. We'll return to the important relationship between  $\mathbf{k}$  and  $\gamma$  in Section 13.9. We use the letter 'b' here because we've actually obtained expressions for the Bloch waves mentioned in Section 13.2, which we'll discuss in the next chapter.

## 13.9 THE TOTAL WAVE AMPLITUDE

We have now found two different wave functions which can both propagate in the crystal. We still have to determine what  $\phi_{\mathbf{0}}$  and  $\phi_{\mathbf{g}}$  are. The total wave vector,  $\psi^T$ , is a combination of the two (Bloch) waves,  $b^{(1)}$  and  $b^{(2)}$

$$\psi^T = \mathcal{A}^{(1)} b^{(1)} + \mathcal{A}^{(2)} b^{(2)} \quad (13.34)$$

where the constants  $\mathcal{A}^{(1)}$  and  $\mathcal{A}^{(2)}$  determine the relative contribution of each (Bloch) wave. We can now combine the last few equations (13.31–13.33 and 13.34) to give

$$\begin{aligned} \psi^T &= \mathcal{A}^{(1)} \left\{ \cos \frac{\beta}{2} e^{2\pi i \mathbf{k}^{(1)} \cdot \mathbf{r}} - \sin \frac{\beta}{2} e^{2\pi i (\mathbf{k}^{(1)} + \mathbf{g}) \cdot \mathbf{r}} \right\} \\ &+ \mathcal{A}^{(2)} \left\{ \sin \frac{\beta}{2} e^{2\pi i \mathbf{k}^{(2)} \cdot \mathbf{r}} - \cos \frac{\beta}{2} e^{2\pi i (\mathbf{k}^{(2)} + \mathbf{g}) \cdot \mathbf{r}} \right\} \end{aligned} \quad (13.35)$$

All that now remains is to determine the magnitudes of  $\mathcal{A}^{(1)}$  and  $\mathcal{A}^{(2)}$  which we can do by remembering that we have a thin TEM specimen. In mathematical terminology the constants  $\mathcal{A}^{(1)}$  and  $\mathcal{A}^{(2)}$  must now be determined using the boundary conditions.

It is helpful to rearrange equation 13.35 first

$$\begin{aligned} \psi^T = & \{ \mathcal{A}^{(2)} \sin \frac{\beta}{2} e^{2\pi i \mathbf{k}^{(2)} \cdot \mathbf{r}} - \mathcal{A}^{(1)} \cos \frac{\beta}{2} e^{2\pi i \mathbf{k}^{(1)} \cdot \mathbf{r}} \} \\ & + \{ \mathcal{A}^{(2)} \cos \frac{\beta}{2} e^{2\pi i \mathbf{k}^{(2)} \cdot \mathbf{r}} - \mathcal{A}^{(1)} \sin \frac{\beta}{2} e^{2\pi i \mathbf{k}^{(1)} \cdot \mathbf{r}} \} e^{2\pi i \mathbf{g} \cdot \mathbf{r}} \end{aligned} \quad (13.36)$$

Only the second term depends on  $\mathbf{g}$ , so this must be the  $\phi_{\mathbf{g}}$  term. We know that at the top of the specimen ( $\mathbf{r} = 0$ ),  $\phi_0$  is unity and  $\phi_{\mathbf{g}}$  is zero (independent of  $\gamma$ )—the amplitude of the diffracted beam is zero before it's diffracted! It follows directly that

$$\mathcal{A}^{(1)} = \cos \frac{\beta}{2} \quad (13.37)$$

$$\mathcal{A}^{(2)} = \sin \frac{\beta}{2} \quad (13.38)$$

These equations (13.37 and 13.38) tell us that  $\mathcal{A}$  in equation 13.34 is just determined by the value of  $\mathbf{s}$ , i.e., the deviation from the Bragg condition. So you can adjust the values of  $\mathcal{A}$  by changing  $\mathbf{s}$ , which we now know just involves tilting the specimen.

Now, finally, we can write down the general expressions for  $\phi_0$  and  $\phi_{\mathbf{g}}$ , each as a function of  $z$ . First we need to modify equation 13.5 by using the substitution of equations 13.12 and 13.13, so it becomes

$$\psi^T = \phi_0 e^{2\pi i \mathbf{k} \cdot \mathbf{r}} + \phi_{\mathbf{g}} e^{2\pi i (\mathbf{k} + \mathbf{g}) \cdot \mathbf{r}} \quad (13.39)$$

(Remember that  $\chi_D = \chi_O + \mathbf{g} + \mathbf{s}$  (or  $\mathbf{k}_D = \mathbf{k}_O + \mathbf{g} + \mathbf{s}$ ), where  $\mathbf{k}_O$  is written as  $\mathbf{k}$  and  $D$  is  $G_1$  in equation 13.5; then you'll see that the term containing  $\mathbf{s}$  in equation 13.13 drops out.) The  $\phi_0$  and  $\phi_{\mathbf{g}}$  components in equation 13.36 are easily recognized by the presence of  $\exp(2\pi i \mathbf{g} \cdot \mathbf{r})$ . Comparing equations 13.36 and 13.39 (having replaced  $\mathcal{A}$  using equations 13.37 and 13.38) we see that

$$\phi_{\mathbf{g}} = \sin \frac{\beta}{2} \cos \frac{\beta}{2} \left\{ e^{2\pi i (\mathbf{k}^{(2)} - \mathbf{K}) \cdot \mathbf{r}} - e^{2\pi i (\mathbf{k}^{(1)} - \mathbf{K}) \cdot \mathbf{r}} \right\} \quad (13.40)$$

Since we are only considering the  $z$  component, we know, from equations 13.17 and 13.19, that the exponential term must have the phase  $2\pi i \gamma z$ , i.e.,

$$(\mathbf{k}^{(2)} - \mathbf{K})_z = \gamma^{(2)} \text{ and } (\mathbf{k}^{(1)} - \mathbf{K})_z = \gamma^{(1)} \quad (13.41)$$

What we are interested in is the magnitude of  $\gamma^{(1)}$  and  $\gamma^{(2)}$ .

We can now manipulate equation 13.40 using equation 13.41 and the expression  $e^{i\theta} = \cos \theta + i \sin \theta$  to give

$$\phi_0 = \{ \cos(\pi z \Delta \mathbf{k}) - i \cos \beta \cdot \sin(\pi z \Delta \mathbf{k}) \} e^{\pi i s z} \quad (13.42)$$

and

$$\phi_{\mathbf{g}} = +i \sin \beta \cdot \sin(\pi z \Delta \mathbf{k}) \cdot e^{\pi i s z} \quad (13.43)$$

In these equations  $\Delta k$  is simply  $|\mathbf{k}^{(2)} - \mathbf{k}^{(1)}|$ . Leaving the term  $e^{\pi i s z}$  in these equations does not affect the

amplitudes of  $\phi_0$  and  $\phi_{\mathbf{g}}$  or the beam intensities but it will make it easier for you to check that these expressions satisfy, for example, equation 13.16.

### A KEY RESULT

We have shown directly that  $\phi_0$  in equation 13.39 is a mixture of terms containing  $\mathbf{k}^{(1)}$  and  $\mathbf{k}^{(2)}$ . This is why  $\phi_{\mathbf{g}}$  depends on  $\Delta k$ .

## 13.10 THE EFFECTIVE EXCITATION ERROR

We can now write down the intensity at the bottom (exit surface) of the specimen ( $z = t$ ) and manipulate the equations by substituting for  $\Delta k$  and  $w$ . The term  $\Delta k$  in equations 13.42 and 13.43 is the same as  $\Delta \gamma$ , i.e.,  $\gamma^{(2)} - \gamma^{(1)}$  (see equation 13.41). We can therefore write down  $\Delta k$  by considering equations 13.27 and 13.28

$$\Delta k = \frac{\sqrt{w^2 + 1}}{\xi_{\mathbf{g}}} \quad (13.44)$$

The intensity in the diffracted beam,  $|\phi_{\mathbf{g}}|^2 = \phi_{\mathbf{g}} \phi_{\mathbf{g}}^*$ , is obtained from equation 13.43

$$I_{\mathbf{g}} = |\phi_{\mathbf{g}}|^2 = \sin^2 \beta \cdot \sin^2(\pi t \Delta k) \quad (13.45)$$

$$I_{\mathbf{g}} = |\phi_{\mathbf{g}}|^2 = \frac{1}{w^2 + 1} \sin^2 \frac{\pi t \sqrt{w^2 + 1}}{\xi_{\mathbf{g}}} \quad (13.46)$$

We can make this equation look more familiar by defining an effective excitation error,  $s_{\text{eff}}$

$$s_{\text{eff}} = \sqrt{s^2 + \frac{1}{\xi_{\mathbf{g}}^2}} = \frac{\sqrt{w^2 + 1}}{\xi_{\mathbf{g}}} \quad (13.47)$$

Now the equation becomes

$$|\phi_{\mathbf{g}}|^2 = \left( \frac{\pi t}{\xi_{\mathbf{g}}} \right)^2 \cdot \frac{\sin^2(\pi t s_{\text{eff}})}{(\pi t s_{\text{eff}})^2} \quad (13.48)$$

This equation gives us the intensity in the Bragg-diffracted beam. In writing down equation 13.47, we have defined another important new quantity  $s_{\text{eff}}$ , so labeled because it's the *effective* excitation error.

### THE REALLY IMPORTANT EQUATION

It's so important, we'll repeat it

$$|\phi_{\mathbf{g}}|^2 = \left( \frac{\pi t}{\xi_{\mathbf{g}}} \right)^2 \cdot \frac{\sin^2(\pi t s_{\text{eff}})}{(\pi t s_{\text{eff}})^2}$$

One important result shown directly by equation 13.45 is that the intensity,  $I_g$ , in the diffracted beam emerging from the specimen is proportional to  $\sin^2(\pi t \Delta k)$  and thus  $I_0$  is proportional to  $\cos^2(\pi t \Delta k)$ .  $I_g$  and  $I_0$  are both periodic in both  $t$  and  $s_{\text{eff}}$ . As  $\phi_g$  increases and decreases,  $\phi_0$  behaves in a complementary manner so that

$$I_0 = 1 - I_g \quad (13.49)$$

Remember when testing this formula that  $I = \phi \phi^*$  ( $\phi^*$  is the complex conjugate of  $\phi$ ).

The effective excitation error,  $s_{\text{eff}}$ , is a very important quantity. We can summarize some important properties

- The quantity  $s_{\text{eff}}$  is never zero.
- When  $s$  is zero,  $s_{\text{eff}}$  is  $\xi_g^{-1}$ .
- When  $s$  is very large, then  $s_{\text{eff}}$  becomes essentially the same as  $s$ .

### 13.11 THE COLUMN APPROXIMATION

When we form an image, we try to focus the objective lens on a plane in or below the specimen (remember that here, below means underfocus). One special plane we can choose is the plane which corresponds to the bottom of the specimen, assuming that this plane is perpendicular to the direction of the propagating beam. Whatever plane we choose, what we see depends on the beams that finally leave the bottom of the specimen, so let's concentrate on this one plane. Look at Figure 13.3A; P is the point at the bottom of the specimen, and we are calculating the values of  $\phi_0$  and  $\phi_g$  at this point to construct our image. Where do the electrons come from in order to contribute to  $\phi_0$  and  $\phi_g$ ? The answer is the cone APB where the angle APB is  $\sim 2\theta_B$ . In other words, we don't just have a diffracted beam which

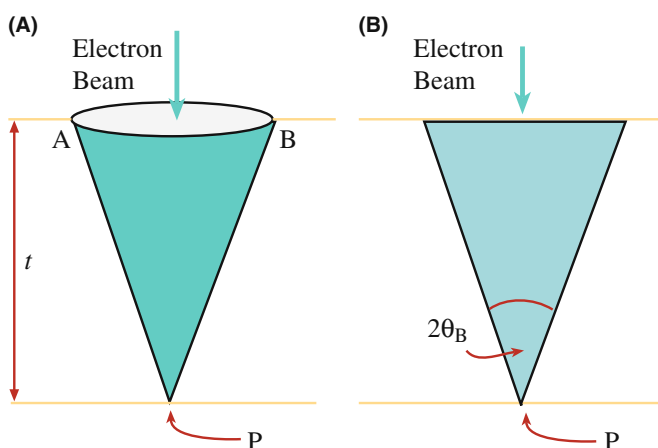


**FIGURE 13.3.** (A) The intensity of the beams at point P at the bottom of the specimen is influenced by all the scattering within a cone of material. The solid angle of the cone is determined by the diameter of the Fresnel zones which, in turn, are principally determined by  $\lambda$ . The cross section (B) is the more typical view of the cone.

propagates through the specimen from the top to point P. There is actually a cone of material which contributes to the intensity at point P. The shape of the cone can be calculated using the Fresnel-zone construction, which was actually developed nearly 200 years ago for visible-light optics. Figure 13.3B, which is how the cone is usually drawn, summarizes the relevant parameters; don't forget that a cone, not a triangle, of material contributes to the intensity at P. A clear derivation is given by Hecht. Why is it a Fresnel diffraction? The answer is that we form an image, i.e., look at a plane, which is very close to where the diffraction 'event' occurred, we are in the near-field, or Fresnel, regime (see Section 2.9).

#### FOCUSING

As usual, we should focus only by moving the specimen up and down, but we don't.

Let's consider some actual numbers: At 100 kV,  $\lambda = 3.7$  pm,  $\theta_B \sim 0.01$  radians or  $\sim 0.5^\circ$ . So if the thickness of the specimen is 100 nm, then AB is  $\sim 2$  nm. If we increase the  $t$ , then the width of the column will also increase. However, if we increase the accelerating voltage so as to increase the thickness we can penetrate, the wavelength decreases causing the Bragg angle also to decrease. This allows us to make the approximation shown in Figure 13.4A and B when calculating  $\phi_0$  and  $\phi_g$ . This model is known as the column approximation.

The great advantage of this approximation is that it allows us to calculate the scattering from slices which have a constant width as we pass down the column, which itself lies in a well-defined direction (generally parallel to  $\mathbf{k}_D$ ). We might anticipate problems with very small defects on a very

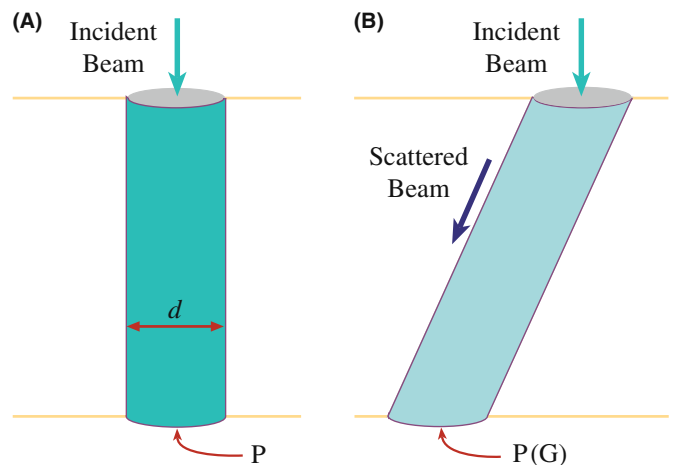


**FIGURE 13.4.** The column approximation for (A) the direct beam and (B) a diffracted beam. A column replaces the cone. The diameter of the column ( $d$ ) should be the average diameter of the cone it replaces ( $AB/2$  in Figure 13.3). (B) This value will depend on the thickness of the sample. In practice it is usually taken to be  $\sim 2$  nm.

fine detail, especially when these features can vary their positions in the foil. The more correct, non-column treatment was introduced by Takagi; the analysis by Howie and Basinski is what we use in computer programs.

### COLUMN APPROXIMATION

The column approximation often hides itself very well, but it is actually used in many calculations of images.

## 13.12 THE APPROXIMATIONS AND SIMPLIFICATIONS

In order to minimize the mathematics and to emphasize the underlying physical principles involved in the analysis of diffracted beams, we have made a number of assumptions, simplifications, and approximations. Although we are not going to cover all of these points, you should be aware of some of them

- We have completely neglected any effects due to backscattering of the electrons. This approximation is reasonable since we are dealing with electrons which have very high energies. However, if you are familiar with SEM, you will have encountered back-scattered electron (BSE) imaging and possibly, rocking-beam channeling patterns (RCPs) or electron backscattered diffraction (EBSD) patterns. So some electrons must be backscattered.
- In some parts of the discussion, it is an implicit assumption that the crystal has a center of symmetry. This assumption is hidden in our use of  $\xi_g$ . If the material is non-centrosymmetric, then the BF image and images formed using only a systematic row of reflections will not be affected. Differences will occur in some DF images or when non-systematic reflections contribute to the image. In these cases, you will need to use a computer program to predict or interpret the contrast.

### TWO OPPOSITE CONVENTIONS

Two conventions are used to describe the exponential dependence on  $\mathbf{k}$  and  $\mathbf{r}$ ; both are commonly used.

$$e^{2\pi i \mathbf{k} \cdot \mathbf{r}} \quad \text{or} \quad e^{-2\pi i \mathbf{k} \cdot \mathbf{r}}$$

These conventions have been discussed by Spence. In our analysis, we have chosen to use  $e^{2\pi i \mathbf{k} \cdot \mathbf{r}}$  which Spence has termed the ‘quantum-mechanical’ convention.

Note that Spence uses the alternative ‘crystallographic’ convention, except when he discusses Bloch waves.

- From Chapter 11, you know that it is impossible to set up a true two-beam condition for a thin TEM specimen. There will always be more than one diffracted spot visible. So how do we measure  $\xi_g$  exactly? The answer is that we don’t, but we can make a very good estimate.
- Remember the use of  $z$  and  $t$ . When we consider the diffracted beam, then  $z$  and  $t$  are measured along the direction of the diffracted beam. In general, this distance will be different for each beam. The saving feature is that we are usually concerned with small Bragg angles. As a thought exercise, you might consider the effect of having a steeply inclined wedge or a specimen which, although parallel sided, is steeply inclined to the electron beam.
- The full analysis of scattering includes a term in  $r^{-1}$  which says that the intensity falls off as  $r^{-2}$ . This is just the standard flux relation—the number of electrons passing through a spherical surface around the scattering point is constant. (The surface area of a sphere is proportional to  $r^2$ .) This term has been omitted throughout our discussion since it only affects the absolute intensity. A practical lesson from this is that you should use the lowest magnification that will give you the desired resolution; remember that the highest useful magnification in a TEM image is about  $10^6$  (see Section 6.6.B).

In the quantum mechanical convention, the time-dependent Schrödinger equation is written as

$$\frac{\hbar^2}{8\pi^2 m} \nabla^2 \psi = -i \frac{\hbar}{2\pi} \frac{d\psi}{dt} \quad (13.51)$$

with the full solution being

$$\psi(\mathbf{r}, t) = A e^{+i(\mathbf{k} \cdot \mathbf{r} - \omega t)} \quad (13.52)$$

- The concept of a refractive-index effect for electron waves is directly analogous to that for visible-light waves, or any other electromagnetic radiation, in that the potential of the crystal causes a change in the kinetic energy of the electrons (because their total energy is unchanged) and therefore, their velocity is changed. Normally, of course, we think of this as a change in the wavelength of the electrons. The magnitude of  $\mathbf{k}$  will always be larger than that of  $\chi$ .
- We have not mentioned the absorption of Bragg beams, yet we know that this must occur since we can only examine thin specimens in the TEM. Absorption of beams is considered in Section 14.6 and Section 23.8.



### 13.13 THE COUPLED HARMONIC OSCILLATOR ANALOG

The expression for the intensity of the diffracted beam is particularly simple when  $s = 0$ . Then from equation 13.48 we can write

$$|\phi_g|^2 = \sin^2\left(\frac{\pi t}{\xi_g}\right) \quad (13.53)$$

and similarly

$$|\phi_0|^2 = 1 - \sin^2\left(\frac{\pi t}{\xi_g}\right) \quad (13.54)$$

Both equations now only have one variable, the thickness of the specimen. We will refer to these equations when we discuss images in Chapter 23, but we can note immediately that  $I_g$  is zero at  $t = 0$  and again at  $t = \xi_g$  (or in general at  $t = n\xi_g$ , where  $n$  is an integer). This is the reason we call  $\xi_g$  the extinction distance. This situation corresponds to two coupled simple-harmonic oscillators with energy (i.e., intensity,  $I_0$  and  $I_g$ ) being continuously transferred from one to the other and back again. Notice that  $I_g$  can only increase to unity when  $s = 0$ .

### CHAPTER SUMMARY

In this chapter, we have derived equations and introduced terminology that will form the basis for our discussion of diffraction-contrast images. It is not necessary for you to be able to reproduce the mathematical derivations but equations 13.47 and 13.48 are crucial and must be understood. Our analysis was quickly limited to two beams, the direct beam and one Bragg-diffracted beam. In deriving the Howie-Whelan equations, we must consider both forward scattering and Bragg diffraction. We introduced a new parameter, the critical length  $\xi_g$ , and explained why this parameter is called the extinction distance. This length was defined in equation 13.4 which shows that  $\xi_g$  depends on the *material*, the *reflection*, and the *wavelength of the electrons*. Two particular points you need to remember are

- If the voltage increases then  $\lambda$  decreases and  $\xi_g$  increases.
- The contribution of each Bloch wave is determined by  $s$ .

In Section 24.3, we'll show how the two-beam analysis can be extended using the concept of the scattering matrix.

### REFERENCES

This treatment of diffracted beams follows that given by Hirsch and Whelan and the textbook by Hirsch et al. that built on Darwin's treatment of X-ray diffraction.

### HISTORY

Darwin, CG 1914 *Röntgen-Ray Reflection I;II* Phil. Mag. **27** 315–333 and 675-690. Charles Galton Darwin was a grandson of Charles Robert Darwin and, like (*the*) Darwin (and Hirsch), became a Fellow of Christ's College.

Hecht, E 1987 *Optics*, 4th ed., Addison-Wesley, Reading MA.

Howie, A and Whelan, MJ 1961 *Diffraction Contrast of Electron Microscope Images of Crystal Lattice Defects. II The Development of a Dynamical Theory* Proc. Roy. Soc. **A263** 217–237.

### THE COLUMN APPROXIMATION

Howie, A and Basinski, ZS 1968 *Approximations of the Dynamical Theory of Diffraction Contrast* Phil. Mag. **17** 1039–1063.

Takagi, S. 1962 *Dynamical Theory of Diffraction Applicable to Crystals with Any Kind of Small Distortion* Acta Cryst. **15** 1311–1312.

## NOTATION

Spence, JCH 2003 *Experimental High-Resolution Electron Microscopy* 3rd Ed. Oxford University Press New York. Uses the quantum-mechanical convention rather than the crystallographic one.

## THE COMPANION TEXT

The H-W equations are the basis of many home-written programs including those available in the text by Head et al. If you are taking the time to simulate diffraction-contrast images, you might as well use a package which will allow you at least to assess the influence of beams in the systematic row and then see how such multi-beam images compare to those predicted by this analytical treatment. A complete chapter is devoted to this topic in the companion text.

## SELF-ASSESSMENT QUESTIONS

- Q13.1 What does  $\xi_g$ , the characteristic length, depend on?
- Q13.2 How is the structure factor related to the characteristic length,  $\xi_g$ ?
- Q13.3 What do we mean by the phrase *two-beam condition* and when is it satisfied?
- Q13.4 Can forward scattering change the direction of the beam?
- Q13.5 What does dynamical diffraction mean in the two-beam case?
- Q13.6 What is the difference relationship between the constant  $\mathcal{A}^{(1)}$  and  $\mathcal{A}^{(2)}$  and  $\mathbf{s}$ ?
- Q13.7 How can we change the value of the constants  $\mathcal{A}$ ?
- Q13.8 Explain in words how changing the accelerating voltage affects the characteristic length,  $\xi_g$ ?
- Q13.9 Why do we use the column approximation?
- Q13.10 What will happen to the width of the column if the thickness of the specimen increases. How can we change the width of the column?
- Q13.11 How does dynamical diffraction affect the interpretation of DPs?
- Q13.12 What is the structure factor and what does it depend on?
- Q13.13 Why is  $\xi_g$ , the characteristic length, better known as the extinction distance?
- Q13.14 What is the total wave function and why should we really be talking about Bloch waves?
- Q13.15 What is the relationship between the intensity of the incident beam and the intensity of the diffracted beam? Give the equations and the name they go by.
- Q13.16 Write down an expression for the effective excitation error.
- Q13.17 Give an equation for the intensity in the Bragg-diffracted beam using the effective excitation error  $s_{\text{eff}}$  for a specimen thickness  $t$ .
- Q13.18 What happens to the effective excitation error when  $s = 0$ ? Can the effective excitation error ever equal zero? (Explain your reasoning.)
- Q13.19 What value does the effective excitation error approach as the excitation error,  $s$ , becomes large?
- Q13.20 Define what  $\phi_g$  and  $\phi_0$  mean in the context of this chapter and how they relate to the beam intensities  $I_g$  and  $I_0$ ?
- Q13.21 In principle, could the intensities predicted by the Howie-Whelan equations affect what you see in DPs? Is this likely to occur in practice?

## TEXT-SPECIFIC QUESTIONS

- T13.1 Examine Table 13.2. (a) Discuss why MgO, 111 looks odd. (b) Explain why  $\xi_{220}$  for diamond is less than  $\xi_{220}$  for Si and why this appears unexpected at first.
- T13.2 Taking reasonable values for the different parameters:  $V_c$ ,  $\theta_B$ ,  $\lambda$ , and  $F$ , deduce  $\xi_{111}$  for Cu and W using equation 13.4.
- T13.3 Starting with equations 13.6 and 13.7, deduce equations 13.8 and 13.9 showing where we make the approximations.
- T13.4 We state that we know we should use Bloch waves. Why is this so? Would this be true if the specimen were amorphous? If not, what would you recommend (assuming that you have to work with amorphous materials)?
- T13.5 Derive equation 13.18.
- T13.6 We show that there are two solutions to the Howie-Whelan equations. Explain in words why this is so. What is the physical significance of this result?
- T13.7 Show that equations 13.42 and 13.43 do satisfy equation 13.16.
- T13.8 Consider the Cu<sub>220</sub> reflection in a 200-kV TEM. Increase  $s$  in six equal increments to a value of  $2 \times 10^{-3} \text{ \AA}^{-1}$  (six values excluding 0 but including  $2 \times 10^{-3} \text{ \AA}^{-1}$ ). Construct a table to show how  $s_{\text{eff}}$  varies. Give your results in  $\text{ \AA}^{-1}$  and  $\text{ nm}^{-1}$ .

- T13.9 In Figure 13.4  $d$  is said to be  $\sim 2$  nm. Consider five samples of Si with thickness 20, 50, 100, 200 nm, and  $1 \mu\text{m}$  in a 200-eV TEM with 220 excited. What value should we use for  $d$  in each case?
- T13.10 Repeat question 13.9 for Cu and 111.
- T13.11 We state that the highest useful magnification in a TEM is about  $10^6$ . How is this changed if we add a CCD camera? What is the lowest useful magnification with and without a CCD camera (excluding the DP)? How is this changed if you use a FEGTEM?
- T13.12 For the perfect crystal situation, what is the ratio of  $|\phi_{\mathbf{g}}|^2$  to  $|\phi_0|^2$  when  $s$  is  $10^{-1} \text{ \AA}^{-1}$  and  $10^{-2} \text{ \AA}^{-1}$  for the 220 reflection in Cu and Si at 100 kV. Explain any assumptions you make.
- T13.13 Do you think Darwin's papers are really relevant to the Howie-Whelan equations?
- T13.14 Using reasonable values for  $f$ , deduce values for  $\xi_{\mathbf{g}}$  for
- Cu with 220 and 100 keV
  - Si with 111 and 200 keV
  - W with 100 and 300 keV.
- What assumptions have been made in applying this formula?
- T13.15 Are the values given in Table 13.2 for Al, Fe, and Ge consistent?
- T13.16 We differentiate between  $\chi$  and  $\mathbf{k}$ . Do you expect there is a significant difference? Discuss the magnitude of this difference, how it varies with kV and how you might assess this magnitude.
- T13.17 Using earlier equations, deduce equations 13.8 and 13.9.
- T13.18 How will dynamical scattering of X-rays compare to that for electrons?
- T13.19 After equation 13.16 we state that the nature of the material only enters through  $\xi_{\mathbf{g}}$ . Argue against this statement.
- T13.20 Consider Figure 12.6A for Cu  $G=220$  and 100-keV electrons. Deduce  $w$  in equation 13.26. Hence, determine  $\beta$  in equation 13.2.
- T13.21 Use the results of the previous question to deduce  $C_0^{(1)}$ , etc., in equation 13.31.

# Bloch Waves

## CHAPTER PREVIEW

This topic is rather mathematical, with long sequences of differential equations. The discussion of Bloch waves given here follows the treatment of Hirsch et al. which, in turn, was based on the original analysis of electron diffraction by Bethe (1928). The notation we will use closely follows that used by Bethe. Remember that  $\mathbf{g}$  can be any reciprocal-lattice vector, although we will also use it to represent a specific vector.

This analysis leads directly to one of the most important concepts used to understand images of defects in thin foils: it explains the physical origin of the *extinction distance*,  $\xi_{\mathbf{g}}$ , and thus shows why it is so important. So again it is worth persevering. However, many successful microscopists have skipped this topic. We suggest you first skim through this chapter. Then, when you've recognized its importance and seen the key equations, go back to the beginning and work your way through.

We make certain assumptions about the materials we are considering and what voltages are used. You must keep these assumptions in mind when applying these concepts. The most important point is that, within the limits of our approximations, the analysis is rigorous and we can really understand the meaning of  $\xi_{\mathbf{g}}$ . If you've previously come across the idea of kinematical diffraction, this chapter will make it clear why this theory is, at best, only an approximation to reality.

We start by considering the property of a crystal which we know quite well, namely, the inner potential. You should remember that, strictly speaking, everything we are about to go through in this section applies only to perfect crystals; crystals with surfaces are not 'perfect.' The periodic nature of the crystal potential leads to the concepts of Bloch functions and Bloch waves.

We include a discussion of the two-beam case, since this can easily be solved analytically and can be related directly to the results discussed in Chapter 13 on diffracted beams. In Chapter 15 we will discuss a graphical representation of the equations we are deriving here. As with the Ewald sphere and reciprocal lattice, the diagrams make for an easier understanding and give a useful guide when you are actually using the TEM. We will consider absorption of Bloch waves here but when we use it in, e.g., Section 24.7, the physical significance will be more obvious.

### 14.1 WAVE EQUATION IN TEM

We are going to modify the Schrödinger equation for use in TEM to explain why the Bloch waves have the form they do. We are not going to try to be mathematically rigorous in deriving this modified equation; reference texts for this purpose are listed at the end of the chapter. Let's start with the time-independent Schrödinger equation

$$\left[ -\frac{\hbar^2}{8\pi^2m} \nabla^2 + V(\mathbf{r}) \right] \psi(\mathbf{r}) = E \psi(\mathbf{r}) \quad (14.1)$$

The first term (in  $\nabla^2$ ) represents the kinetic energy and the second term, the potential energy;  $E$  represents the total energy. In TEM we usually talk in terms of the accelerating voltage and the crystal potential and, therefore, we rearrange this equation in terms of voltages. In doing so, we have to be careful about signs since the charge on the electron is negative and the applied electric field (associated with the accelerating voltage) points toward the gun! All that equation 14.1 says is that the electron has a kinetic energy due to the acceleration it is given in the gun. Initially, this is the total energy of the electron. When the electron passes

through the crystal, it will have a potential energy due to the periodic potential associated with the atoms in the crystal.

### THE SIGNS

- The charge on the electron,  $q$ , is a negative number,  $-e$ , where  $e$  is a positive number.
- The accelerating voltage,  $-V$  (usually between 100 kV and 1 MV), is negative for a positive charge leaving the gun. This quantity,  $-V$ , is really the ‘electric-field potential.’
- The initial energy given to the electron is a positive number,  $E$  (in eV); it is just the charge times the accelerating voltage. We can write this as  $eV$  where both  $e$  and  $V$  are positive numbers.
- The potential inside the crystal,  $V(\mathbf{r})$ , is a positive number reaching a local maximum at the nucleus of an atom; the nucleus is positive.
- The potential energy,  $\mathcal{V}$ , of the electron outside the crystal is zero; it decreases when the electron is inside the crystal ( $\mathcal{V}$  is  $q$  times  $V(\mathbf{r})$ , i.e.,  $-eV(\mathbf{r})$ ) and is therefore always a negative number.

Now we can rearrange equation 14.1 in terms of the accelerating voltage and the crystal potential

$$\nabla^2 \psi(\mathbf{r}) + \frac{8\pi^2 m e}{h^2} [V + V(\mathbf{r})] \psi(\mathbf{r}) = 0 \quad (14.2)$$

The task before us is obvious: we have to solve equation 14.2. In general, however, this is a difficult problem! What makes it possible for us is that  $V(\mathbf{r})$  has special properties because we are only considering crystalline materials.

## 14.2 THE CRYSTAL

The basic property of a crystal is that its inner potential,  $V(\mathbf{r})$ , is *periodic*. We can therefore express this property as

$$V(\mathbf{r}) = V(\mathbf{r} + \mathbf{R}) \quad (14.3)$$

where  $\mathbf{R}$  represents any lattice vector of the crystal and, as usual,  $\mathbf{r}$  represents any real-space vector. Equation 14.3 is the fundamental definition of a perfect crystal: the environment at point  $\mathbf{r}$  is identical to that at point  $\mathbf{r} + \mathbf{R}$ . We can draw this inner potential as shown in Figure 14.1 for the one-dimensional case and you can imagine it in 3D. The atomic nuclei are positively charged; the surrounding electrons gradually screen this charge and the atom appears neutral from the outside. In a crystal, a nucleus is never far away, so an electron which we ‘shoot’ through the crystal will always

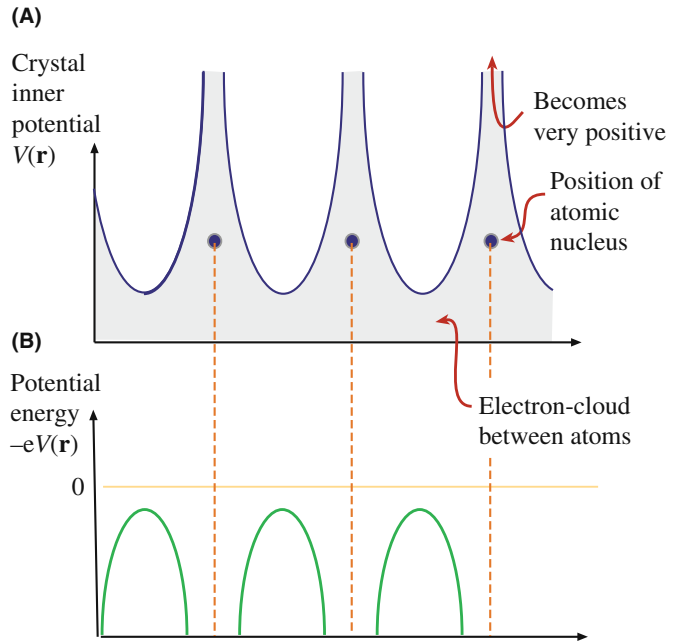


**FIGURE 14.1.** (A) The local charge sensed by the beam electron as it passes through a metal, represented as a row of ‘ion’ cores (black circles) in a sea of electrons. The local charge is very large and positive in the vicinity of the ion and becomes small, but not zero between the ions. The difference between the minimum charge and zero corresponds to the mean inner potential of the crystal, which is a few eV (positive). So the beam electron experiences a small positive attraction as it enters the crystal, hence its kinetic energy (velocity) increases. (B)  $V(\mathbf{r})$  is the potential of the electrons, so their potential energy is negative and becomes more so, the closer they pass by the ions.

see a positive potential; hence  $V(\mathbf{r})$  is always positive as noted in Section 14.1 and in Figure 3.1.

The electron beam can be described by its total wave function  $\psi^{\text{tot}}$  which must always be a solution of the Schrödinger equation; i.e., this equation describes how an electron behaves both inside and outside the crystal.

In the discussion which follows, we will use potentials so the units will be volts. You can always change to the energy formalism, but remember that the charge on the electron is a negative number.

We know that for any crystal the inner potential must be real, i.e., the potential energy must be real, so that  $V(\mathbf{r})$  and its complex conjugate, which we denote as  $V^*(\mathbf{r})$ , are identical

$$V(\mathbf{r}) = V^*(\mathbf{r}) \quad (14.4a)$$

Now to make the treatment simple, we consider the case of crystals with a *center of symmetry*

$$V(\mathbf{r}) = V(-\mathbf{r}) \quad (14.4b)$$

The case of non-centrosymmetric crystals, such as GaAs, could be considered, but the equations would



become much more complicated. Since  $V(\mathbf{r})$  is periodic, we can express it as a Fourier series in which we sum over all the lattice points in reciprocal space

$$V(\mathbf{r}) = \sum_{\mathbf{g}} V_{\mathbf{g}} e^{2\pi i \mathbf{g} \cdot \mathbf{r}} \quad (14.5)$$

Here  $V_{\mathbf{g}}$  is, by definition, the  $\mathbf{g}$  component of  $V$  in the Fourier series. Now, in order to make future equations simpler we define a parameter  $U_{\mathbf{g}}$  related to  $V_{\mathbf{g}}$  by

$$V_{\mathbf{g}} = \frac{\hbar^2}{2m_e} U_{\mathbf{g}} \quad (14.6)$$

In the Fourier series given in equation 14.5 and modified by equation 14.6,  $V_{\mathbf{g}}$  and  $U_{\mathbf{g}}$  are referred to as the Fourier coefficients. Equation 14.5 becomes

$$V(\mathbf{r}) = \frac{\hbar^2}{2m_e} \sum_{\mathbf{g}} U_{\mathbf{g}} e^{2\pi i \mathbf{g} \cdot \mathbf{r}} \quad (14.7)$$

Now  $V(\mathbf{r})$  has been expanded as a Fourier sum; all the conditions on  $V_{\mathbf{g}}$  also apply to each  $U_{\mathbf{g}}$  so that

$$U_{\mathbf{g}} = U_{\mathbf{g}}^* = U_{-\mathbf{g}} \quad (14.8)$$

You can check these relationships by just replacing  $\mathbf{r}$  by  $-\mathbf{r}$ , etc. Before continuing, however, you may find it useful to review the relative magnitudes of the energies which are summarized in Table 14.1.

Much of what we are now discussing is mathematically the same as you may have seen in condensed-matter physics. The big difference is that we are injecting electrons with kinetic energies which are 5–6 orders of magnitude greater than the band gap of Si. Notice that the mean inner potential energy is  $V$  in equation 14.1. The actual value of  $V$  is not as precise as it might sometimes appear. You should remember that it is the average background potential energy and is directly related to the characteristic length  $\xi_0$  that we introduced in Chapter 13. More values of  $V$  are given in Table 14.2. One interesting feature of this table is that the magnitude of  $V$  only varies by a factor of 3 when the atomic number changes from 4 to 74.

**TABLE 14.1 A Comparison of the Orders of Magnitudes of the Energies Being Discussed in This Chapter**

Quantity	Energy (eV)
$kT$ (room temp.: $T = 293\text{ K}$ )	0.025
Band gap of Si	1.1
Mean inner potential energy for Si	$\sim 11$
Energy of electrons in TEM	$\geq 100,000$

**TABLE 14.2 Comparison of Mean Inner Potential Energies for Different Elements**

Element	Inner Potential Energy (eV)
Be	$7.8 \pm 0.4$
C	$7.8 \pm 0.6$
Al	$12.4 \pm 1$
Cu	$23.5 \pm 0.6$
Ag	$20.7 \pm 2$
Au	$21.1 \pm 2$
Si	11.5
Ge	$15.6 \pm 0.8$
W	23.4
ZnS	$10.2 \pm 1$

## 14.3 BLOCH FUNCTIONS

Since the electron is in a periodic potential its wave function must have the symmetry of the crystal. The solutions to the Schrödinger equation which always have the required translation property are known as Bloch waves. Since these wave functions,  $\psi^{(j)}(\mathbf{r})$ , are special, we'll define them as

$$\psi^{(j)}(\mathbf{r}) = b(\mathbf{k}^{(j)}, \mathbf{r}) = b^{(j)}(\mathbf{r}) \quad (14.9)$$

The reason for the 'j' is that each Bloch wave has a single value of  $\mathbf{k}$  (each Bloch wave is a plane wave) which we can denote as  $\mathbf{k}^{(j)}$ ; in general, there will be more than one Bloch wave for a particular physical situation. The notation we will use is such that, whenever we have  $\mathbf{k}^{(j)}$  in an expression, we will identify this by the superscript which implies that the function varies with  $\mathbf{k}^{(j)}$ . Bloch's theorem states that this wave function in a periodic potential can be written as

$$b^{(j)}(\mathbf{r}) = b(\mathbf{k}^{(j)}, \mathbf{r}) = \mu(\mathbf{k}^{(j)}, \mathbf{r}) e^{2\pi i \mathbf{k}^{(j)} \cdot \mathbf{r}} = \mu^{(j)}(\mathbf{r}) e^{2\pi i \mathbf{k}^{(j)} \cdot \mathbf{r}} \quad (14.10)$$

such that the Bloch function,  $\mu^{(j)}(\mathbf{r})$ , can itself be expressed as a Fourier series since  $\mu(\mathbf{r})$  is also a periodic function of  $\mathbf{r}$

$$\mu^{(j)}(\mathbf{r}) = \sum_{\mathbf{g}} C_{\mathbf{g}}^{(j)}(\mathbf{k}^{(j)}) e^{2\pi i \mathbf{g} \cdot \mathbf{r}} \quad (14.11)$$

We'll call  $C_{\mathbf{g}}^{(j)}$  the  $j$ -sub- $\mathbf{g}$  plane-wave amplitude and generally refer to the  $C$  values as the plane-wave amplitudes; they depend on which  $\mathbf{k}^{(j)}$  we are considering, but not on  $\mathbf{r}$ . We combine these definitions to give  $b$  which is itself dependent on  $j$

$$b^{(j)}(\mathbf{r}) = \sum_{\mathbf{g}} C_{\mathbf{g}}^{(j)} e^{2\pi i (\mathbf{k}^{(j)} + \mathbf{g}) \cdot \mathbf{r}} \quad (14.12)$$

Using our notation, the superscript on  $C$  indicates that  $C^{(j)}$  depends on  $j$  because it is associated with  $\mathbf{k}^{(j)}$ . We can now write the expanded expression for  $b^{(j)}(\mathbf{r})$ , which is a solution to the Schrödinger equation

$$b^{(j)}(\mathbf{r}) = C_0^{(j)} e^{2\pi i \mathbf{k}^{(j)} \cdot \mathbf{r}} + C_{\mathbf{g}}^{(j)} e^{2\pi i (\mathbf{k}^{(j)} + \mathbf{g}) \cdot \mathbf{r}} + \dots \quad (14.13)$$

The first term in this series is  $C_0$ ; the subscript zero is because the length of this  $\mathbf{g}$  vector is 0. Much of the following analysis is exactly the same as you may have encountered in studying semiconductor band-gap theory. The difference will be that we can make certain approximations which are only valid because the electrons used in TEM have much higher energies (100 keV to 1 MeV) than the inner potential of the crystal ( $\sim 7\text{--}24\text{ eV}$ ). It is always important to keep in mind the magnitude of the quantities we are considering and remember that the Bloch function has the periodicity of the lattice. When you are reading other texts, you'll see that physics textbooks will tend to omit the term  $2\pi$  in such expressions so that  $|\mathbf{k}|$  becomes  $2\pi/\lambda$  instead of  $1/\lambda$ .

### EACH BLOCH WAVE

The main point to remember is that each Bloch wave is associated with just one  $\mathbf{k}^{(j)}$  but it is a continuously varying function of  $\mathbf{r}$ . Each Bloch wave is a sum over all the points in reciprocal space. In other words, each Bloch wave depends on every  $\mathbf{g}$ , and conversely, each  $\mathbf{g}$  beam depends on every Bloch wave!

We haven't done anything yet, just restated the problem and remembered Bloch's theorem. The analysis we've just completed follows the original treatment of Bethe (1928). We can now express  $\psi^{\text{tot}}$  using equation 14.9 to give

$$\psi^{\text{tot}} = \sum_{j=1}^n \mathcal{A}^{(j)} \psi^{(j)} = \sum_{j=1}^n \mathcal{A}^{(j)} b(\mathbf{k}^{(j)}, \mathbf{r}) \quad (14.14)$$

In this equation,  $\mathcal{A}^{(j)}$  will be determined by the specimen type, the specimen orientation, etc., i.e., the boundary conditions. The  $\mathcal{A}$ s are known as the Bloch-wave excitation coefficients, since they tell us the relative contributions of each Bloch wave, i.e., how strongly each Bloch wave is excited.

## 14.4 SCHRÖDINGER'S EQUATION FOR BLOCH WAVES

What we are now going to do is to rewrite the Schrödinger equation to incorporate the properties of Bloch waves automatically. If you wish, you can skip this section and just accept the result given in equation 14.27. The way we include the periodicity is to express the inner potential in equation 14.2 as the Fourier series given in equation 14.7

$$\nabla^2 \psi(\mathbf{r}) + \frac{8\pi^2 m e}{h^2} \left( E + \frac{h^2}{2m e} \sum_{\mathbf{g}} U_{\mathbf{g}} e^{2\pi i \mathbf{g} \cdot \mathbf{r}} \right) \psi(\mathbf{r}) = 0 \quad (14.15)$$

Now we simplify the algebra to give

$$\nabla^2 \psi(\mathbf{r}) + 4\pi^2 \left( \frac{2m e}{h^2} E + \sum_{\mathbf{g}} U_{\mathbf{g}} e^{2\pi i \mathbf{g} \cdot \mathbf{r}} \right) \psi(\mathbf{r}) = 0 \quad (14.16)$$

and hence

$$\frac{1}{4\pi^2} \nabla^2 \psi(\mathbf{r}) + \left( \frac{2m e}{h^2} E + \sum_{\mathbf{g}} U_{\mathbf{g}} e^{2\pi i \mathbf{g} \cdot \mathbf{r}} \right) \psi(\mathbf{r}) = 0 \quad (14.17)$$

Next, we can introduce a new quantity  $K$  which is defined by the equation

$$K^2 = \frac{2m e E}{h^2} + U_0 = \chi^2 + U_0 \quad (14.18)$$

With this definition we have removed the  $U_0$  term from the sum over all  $\mathbf{g}$ , so that equation 14.15 is now

$$\frac{1}{4\pi^2} \nabla^2 \psi(\mathbf{r}) + K^2 \psi(\mathbf{r}) + \sum_{\mathbf{g} \neq 0} U_{\mathbf{g}} e^{2\pi i \mathbf{g} \cdot \mathbf{r}} \psi(\mathbf{r}) = 0 \quad (14.19)$$

The reason for doing this is that we are going to be concerned with different diffraction vectors,  $\mathbf{g}$ . The  $U_0$  term does not depend on  $\mathbf{g}$ . We call  $U_0$  the (scaled) mean inner potential of the crystal; this potential is thus a 'background' or continuum property of the crystal; it does not directly depend on the crystal structure. (You may recognize this manipulation as the refractive-index idea reappearing.)

When  $V(\mathbf{r})$  is 0, then  $U_0$  is 0 so that  $K^2$  takes on a special value which we have already called  $\chi^2$

$$\chi^2 = \frac{2m e E}{h^2} \quad (14.20)$$

The mass,  $m$ , is actually the relativistic mass, not the rest mass;  $eE$  is the kinetic energy of the electron (in the vacuum between the gun and the specimen). We know that

$$\frac{1}{2} m v^2 = \frac{(m v)^2}{2m} = \frac{p^2}{2m} = \frac{(h k)^2}{2m} \quad (14.21)$$

where  $v$  is the velocity,  $\mathbf{p}$  the momentum, and  $\mathbf{k}$  a wave vector. Thus  $\chi$  is the wave vector of the electron outside the crystal as we had in Chapter 13.

The meaning of  $K$  is now clear:  $\mathbf{K}$  is the wave vector of the electron *inside* the specimen, i.e., after correcting for the refractive-index effect. Since  $U_0$  is a positive number,  $K$  is always larger than  $\chi$ . Hence the kinetic energy of the electrons in the crystal is greater than in the vacuum. The potential energy inside the crystal is negative so, even

though it may be counterintuitive, you now know that electrons travel faster in the crystal! The wavelength of the electrons in the crystal is therefore smaller than the wavelength outside ( $\lambda$  is the reciprocal of  $k$ ).

### ELECTRON SPEED IN A CRYSTAL

Electrons travel faster in the crystal. Light slows down in a crystal.

Remember that light is electromagnetic radiation. The refractive index for light is  $n = c/v$  and is always  $\geq 1$ ;  $c$  is the velocity of light in a vacuum and  $v$  is the velocity in any other material. This is one of those cases where we have to be wary when applying ideas derived for light waves to electron waves.

### DISPERSION

When discussing light, the word dispersion means *separation of electromagnetic radiation into constituents of different wavelength*. In electron optics, the meaning is exactly the same but we emphasize different  $\mathbf{k}$  vectors or different energy.

Equations 14.18 and 14.20 are *dispersion relations*. Such equations relate the magnitude of the wave vector,  $K$  or  $\chi$ , to the energy of the electron.

We want to simplify equation 14.19. We know that  $\psi(\mathbf{r})$  is a Bloch wave (given by equation 14.12) so we can obtain an expression for  $\nabla^2\psi(\mathbf{r})$  by differentiating  $b^{(j)}(\mathbf{r})$ . Remember that  $C_{\mathbf{g}}^{(j)}$  does not depend on  $\mathbf{r}$

$$\nabla^2\psi(\mathbf{r}) = \sum_{\mathbf{g}} C_{\mathbf{g}}^{(j)} \nabla^2 \left( e^{2\pi i(\mathbf{k}^{(j)} + \mathbf{g}) \cdot \mathbf{r}} \right) \quad (14.22)$$

Thus we can write

$$\nabla^2\psi(\mathbf{r}) = -(2\pi)^2 \sum_{\mathbf{g}} |\mathbf{k}^{(j)} + \mathbf{g}|^2 C_{\mathbf{g}}^{(j)} e^{2\pi i(\mathbf{k}^{(j)} + \mathbf{g}) \cdot \mathbf{r}} \quad (14.23)$$

Now we insert this expression in equation 14.19

$$\frac{1}{4\pi^2} \left( -4\pi^2 \sum_{\mathbf{g}} |\mathbf{k}^{(j)} + \mathbf{g}|^2 C_{\mathbf{g}}^{(j)} e^{2\pi i(\mathbf{k}^{(j)} + \mathbf{g}) \cdot \mathbf{r}} \right) + K^2 \sum_{\mathbf{g}} C_{\mathbf{g}}^{(j)} e^{2\pi i(\mathbf{k}^{(j)} + \mathbf{g}) \cdot \mathbf{r}} + \sum_{\mathbf{h} \neq 0} U_{\mathbf{h}} e^{2\pi i\mathbf{h} \cdot \mathbf{r}} \sum_{\mathbf{g}} C_{\mathbf{g}}^{(j)} e^{2\pi i(\mathbf{k}^{(j)} + \mathbf{g}) \cdot \mathbf{r}} = 0 \quad (14.24)$$

In doing so we replace the  $\mathbf{g}$  in the summation in equation 14.19 by  $\mathbf{h}$  just for clarity (!); both are called ‘dummy’ variables. If we sum over all the values of a variable we can ‘center’ the variable wherever we wish. We can further simplify the third term in equation 14.24 by combining the exponential terms and renaming  $\mathbf{g}$

$$\begin{aligned} & \sum_{\mathbf{g}} \sum_{\mathbf{h} \neq 0} U_{\mathbf{h}} C_{\mathbf{g}}^{(j)} e^{2\pi i(\mathbf{k}^{(j)} + \mathbf{g} + \mathbf{h}) \cdot \mathbf{r}} \\ &= \sum_{\mathbf{g} - \mathbf{h}} \sum_{\mathbf{h} \neq 0} U_{\mathbf{h}} C_{\mathbf{g} - \mathbf{h}}^{(j)} e^{2\pi i(\mathbf{k}^{(j)} + \mathbf{g}) \cdot \mathbf{r}} \end{aligned} \quad (14.25)$$

Now the sum over all  $\mathbf{g} - \mathbf{h}$  vectors is the same as the sum over all  $\mathbf{g}$  vectors so we replace  $\mathbf{g} - \mathbf{h}$  by  $\mathbf{g}$ . (Remember, all we are doing is renaming these dummy variables in a consistent way.) Then equation 14.24, and hence 14.19, becomes much simpler

$$\sum_{\mathbf{g}} \left( \left\{ -|\mathbf{k}^{(j)} + \mathbf{g}|^2 + K^2 \right\} C_{\mathbf{g}}^{(j)} + \sum_{\mathbf{h} \neq 0} U_{\mathbf{h}} C_{\mathbf{g} - \mathbf{h}}^{(j)} \right) e^{2\pi i(\mathbf{k}^{(j)} + \mathbf{g}) \cdot \mathbf{r}} = 0 \quad (14.26)$$

We can obtain a useful relation by noting that the coefficients of each term in  $\exp(2\pi i\mathbf{g} \cdot \mathbf{r})$  must separately be equal to zero. The only way that equation 14.26 can be true is if the term inside the bracket is always zero. The result is a series of equations (one for each value of  $\mathbf{g}$ )

$$\left\{ -|\mathbf{k}^{(j)} + \mathbf{g}|^2 + K^2 \right\} C_{\mathbf{g}}^{(j)} + \sum_{\mathbf{h} \neq 0} U_{\mathbf{h}} C_{\mathbf{g} - \mathbf{h}}^{(j)} = 0 \quad (14.27)$$

This is another really important set of equations; they restate the Bloch-wave expression of the Schrödinger equation.

Notice that we are not summing over  $\mathbf{g}$  in equation 14.27. The reason for excluding  $\mathbf{h} = 0$  from the sum is that we have already included it in the first term.

## 14.5 THE PLANE-WAVE AMPLITUDES

We can rewrite and reorder equation 14.27 by, yet again, renaming the variable  $\mathbf{h}$  as  $\mathbf{g} - \mathbf{h}$ . When we do this, we must exclude  $\mathbf{h} = \mathbf{g}$  in the sum

$$\left\{ K^2 - |\mathbf{k}^{(j)} + \mathbf{g}|^2 \right\} C_{\mathbf{g}}^{(j)} + \sum_{\mathbf{h} \neq \mathbf{g}} U_{\mathbf{g} - \mathbf{h}} C_{\mathbf{h}}^{(j)} = 0 \quad (14.28)$$

The reason for making this change is that it emphasizes that the ‘ $U$ ’ terms are the features which couple together the ‘ $C$ ’ terms. In other words, this equation tells us how the potential of the crystal, the  $U$  terms, mixes the different Bloch waves. The  $C$  terms are the Bloch-wave amplitudes. This is the *dynamical coupling* concept.

This equation represents a set of equations which are the fundamental equations of the dynamical theory. (They are called the secular equations in condensed-matter physics texts.) This equation also links the concepts of Bragg beams and Bloch waves.

$U_{\mathbf{g} - \mathbf{h}}$  is the component of the inner potential which couples the Bragg beams with reciprocal-lattice vectors  $\mathbf{g}$  and  $\mathbf{h}$  to one another.

Now we again simplify the situation by limiting the treatment to two beams,  $O$  and  $P$ ; i.e., we consider the case where the only values of  $C_{\mathbf{g}}$  which are *non-zero* are  $C_0^{(j)}$  and  $C_P^{(j)}$  but  $U_P$  and  $U_{-P}$  are both allowed.

Remember that the superscript on  $C$  indicates that  $\mathbf{k}^{(j)}$  is a variable. Note that  $\mathbf{P}$  could be any diffracted beam. Letting  $\mathbf{g} = \mathbf{0}$  in equation 14.27 gives

$$\left(K^2 - |\mathbf{k}^{(j)}|^2\right) C_0^{(j)} + U_{-\mathbf{p}} C_{\mathbf{p}}^{(j)} = 0 \quad (14.29)$$

In deriving this and the following equation, we consider all the possible values of  $\mathbf{h}$  which would give us  $C_0^{(j)}$  or  $C_{\mathbf{p}}^{(j)}$ .

Next let  $\mathbf{g} = \mathbf{p}$  in equation 14.28 and reverse the order of terms to emphasize that we have two equations in  $C_0$  and  $C_{\mathbf{p}}$

$$U_{\mathbf{p}} C_0^{(j)} + \left(K^2 - |\mathbf{k}^{(j)} + \mathbf{p}|^2\right) C_{\mathbf{p}}^{(j)} = 0 \quad (14.30)$$

There are no other possible equations, so to solve these two equations we set the determinant of the coefficients equal to zero

$$\begin{vmatrix} K^2 - |\mathbf{k}^{(j)}|^2 & U_{-\mathbf{p}} \\ U_{\mathbf{p}} & K^2 - |\mathbf{k}^{(j)} + \mathbf{p}|^2 \end{vmatrix} \\ = \left(K^2 - |\mathbf{k}^{(j)}|^2\right) \left(K^2 - |\mathbf{k}^{(j)} + \mathbf{p}|^2\right) - U_{\mathbf{p}} U_{-\mathbf{p}} = 0 \quad (14.31)$$

The mean inner potential of the crystal is usually  $\leq 20$  V while the energy of the electrons is  $\geq 100,000$  eV. Because  $|\mathbf{k}^{(j)} + \mathbf{p}|$  and  $|\mathbf{k}^{(j)}|$  are both very close to  $K$ , it's the difference that is important. Since  $\mathbf{P}$  could be any diffracted beam, we can rename it  $\mathbf{G}$  to make it look more familiar!

$$\begin{vmatrix} K^2 - |\mathbf{k}^{(j)}|^2 & U_{-\mathbf{g}} \\ U_{\mathbf{g}} & K^2 - |\mathbf{k}^{(j)} + \mathbf{g}|^2 \end{vmatrix} \\ = \left(K^2 - |\mathbf{k}^{(j)}|^2\right) \left(K^2 - |\mathbf{k}^{(j)} + \mathbf{g}|^2\right) - U_{\mathbf{g}} U_{-\mathbf{g}} = 0 \quad (14.32)$$

Now we can use the simple algebraic relation

$$x^2 - y^2 = (x - y)(x + y) \quad (14.33)$$

and make the high-energy approximation that  $|\mathbf{k}^{(j)}|$ ,  $|\mathbf{k}^{(j)} + \mathbf{g}|$ , and  $K$  are all similar in magnitude. Then equation 14.32 becomes

$$\left(|\mathbf{k}^{(j)}| - K\right) \left(|\mathbf{k}^{(j)} + \mathbf{g}| - K\right) = \frac{U_{\mathbf{g}} U_{-\mathbf{g}}}{4K^2} = \frac{|U_{\mathbf{g}}|^2}{4K^2} \quad (14.34)$$

It is important not to confuse  $\mathbf{k}^{(j)}$  with  $\mathbf{k}_I$  or  $\mathbf{k}_D$  and to remember that  $|\mathbf{K}| (= |\mathbf{k}_D - \mathbf{k}_I|)$  is not  $K$ . Incidentally, it is not until we write this equation that we use the assumption that the crystal has a center of symmetry (see equation 14.4b).

Equation 14.34 is a more complex dispersion relation than equations 14.18 and 14.20. Since  $\mathbf{k}^{(j)}$  can point in any direction, this dispersion relation defines a surface, known as the dispersion surface, which is just the locus of all allowed  $\mathbf{k}^{(j)}$  vectors for a particular fixed energy. (See Chapter 15.) The simpler relations given in

equations 14.18 and 14.20 each defined a sphere; the vectors  $\mathbf{K}$  and  $\chi$  can point in any direction.

From equation 14.29 (renaming  $\mathbf{p}$  as  $\mathbf{g}$ ), we have

$$\frac{C_{\mathbf{g}}^{(j)}}{C_0^{(j)}} = \frac{|\mathbf{k}^{(j)}|^2 - K^2}{U_{-\mathbf{g}}} \quad (14.35)$$

which we can rewrite as

$$\frac{C_{\mathbf{g}}^{(j)}}{C_0^{(j)}} = \frac{(|\mathbf{k}^{(j)}| - K)(|\mathbf{k}^{(j)}| + K)}{U_{-\mathbf{g}}} \approx \frac{2K(|\mathbf{k}^{(j)}| - K)}{U_{-\mathbf{g}}} \quad (14.36)$$

Thus we can, in principle, say how  $C_0^{(j)}$  and  $C_{\mathbf{g}}^{(j)}$  are related.

Now we could extend this analysis to show how all the values of  $C$  are related in a many-beam situation. If we did that we could write a new expression

$$\mathcal{A}^{(j)} \{C_{\mathbf{g}}^{(j)}\} = \mathbf{0} \quad (14.37)$$

where  $\{C_{\mathbf{g}}^{(j)}\}$  now denotes a column vector with elements  $C_{\mathbf{g}}^{(j)}$ .  $\mathcal{A}^{(j)}$  is a matrix defined by

$$a_{gg} = K^2 - |\mathbf{k}^{(j)} + \mathbf{g}|^2 \quad (14.38)$$

with the off-diagonal elements given by the Fourier coefficients of the crystal potential

$$a_{gh} = U_{g-h} \quad (14.39)$$

Here,  $g$  refers to rows and  $h$  to columns in the  $\mathbf{A}$  matrix. Except in special cases, such as the two-beam case in equation 14.31, you'll only encounter this formalism in computer programs! A particularly clear case is given by Metherell and is adapted here for five beams, comprising  $\mathbf{g}$ ,  $\mathbf{0}$ ,  $\mathbf{g}$ ,  $2\mathbf{g}$ , and  $3\mathbf{g}$  beams. The  $5 \times 5$  matrix can be written out (using  $g$  and  $h$  rather than  $\mathbf{g}$  and  $\mathbf{h}$ ) as

$$\mathbf{A} = \begin{pmatrix} a_{-g-g} & U_{-g-0} & U_{-g-g} & U_{-g-2g} & U_{-g-3g} \\ U_{0-(-g)} & a_{00} & U_{0-g} & U_{0-2g} & U_{0-3g} \\ U_{g-(-g)} & U_{g-0} & a_{gg} & U_{g-2g} & U_{g-3g} \\ U_{2g-(-g)} & U_{2g-0} & U_{2g-g} & a_{2g2g} & U_{2g-3g} \\ U_{3g-(-g)} & U_{3g-0} & U_{3g-g} & U_{3g-2g} & a_{3g3g} \end{pmatrix} \quad (14.40)$$

In the first column  $h$  is  $-g$ ; in the second,  $h$  is zero, etc. In the first row ' $g$ ' is  $-g$ ; in the second, ' $g$ ' is zero. So we can simplify this matrix as

$$\mathbf{A} = \begin{pmatrix} a_{-g} & U_{-g} & U_{-2g} & U_{-3g} & U_{-4g} \\ U_g & a_0 & U_{-g} & U_{-2g} & U_{3g} \\ U_{2g} & U_g & a_g & U_{-g} & U_{-2g} \\ U_{3g} & U_{2g} & U_g & a_{2g} & U_{-g} \\ U_{4g} & U_{3g} & U_{2g} & U_g & a_{3g} \end{pmatrix} \quad (14.41)$$

Some points to notice are

- The terms  $U_{\mathbf{g}}$ ,  $C_{\mathbf{g}}^{(j)}$ , and  $a_{\mathbf{g}}$  are related by a set of linear equations (the matrix in 14.37).
- We can't solve for actual values of the  $C_{\mathbf{g}}^{(j)}$  terms, but we can find the ratios  $C_{\mathbf{g}}^{(j)}/C_{\mathbf{0}}^{(j)}$ .

We won't take this topic much further here but refer you again to the excellent article by Metherell who shows that equation 14.37 can be expressed as an eigenvalue equation where  $\{C_{\mathbf{g}}^{(j)}\}$  appears as the eigenvectors and the wave vectors  $\mathbf{k}^{(j)}$  appear as the eigenvalues. He expresses this equation as

$$\mathbf{M}\{C_{\mathbf{g}}^{(j)}\} = \gamma^{(j)}\{C_{\mathbf{g}}^{(j)}\} \quad (14.42)$$

where the matrix  $\mathbf{M}$  has diagonal elements  $m_{gg}$  and off-diagonal elements  $m_{gh}$ . The reason we mention this fact here is that the  $m_{gg}$  terms correspond to the excitation errors,  $s_{\mathbf{g}}$ , and the  $m_{gh}$  terms correspond to the extinction distance  $\xi_{\mathbf{g}-\mathbf{h}}$ . Remember that  $h$  is the column and notice that the subscript here is  $\mathbf{g}-\mathbf{h}$ ; this extinction distance is related to the interference between the  $\mathbf{g}$  beam and the  $\mathbf{h}$  beam. Now if you're intrigued and your math is strong, see Metherell's article.

If you're familiar with this math approach, you'll recognize that eigenvectors must satisfy certain relations for normalization and orthogonality. If you look back to Chapter 13, you'll see that we normalized  $C_{\mathbf{g}}^{(j)}$  in writing equation 13.30.

As you can see, the math is beginning to become tricky! In the next chapter, we will derive explicit expressions for  $\xi_{\mathbf{0}}$  and  $\xi_{\mathbf{g}}$  in the two-beam case, namely

$$\xi_{\mathbf{0}} = \frac{2K \cos \theta_B}{U_{\mathbf{0}}} \quad (14.43)$$

and

$$\xi_{\mathbf{0}} = \frac{2K \cos \theta_B}{U_{\mathbf{g}}} = \frac{1}{\Delta \mathbf{k}} \quad (14.44)$$

In our derivation we will use a graphical representation of the dispersion equations. This approach has much in common with the Ewald-sphere/reciprocal-lattice approach to understanding diffraction. It's particularly useful since it gives you, the microscopist, another picture, this time related to imaging.

## 14.6 ABSORPTION OF BLOCH WAVES

When we have just two beams excited, O and G, we showed in Section 13.9 that we can express the wave function  $\psi$  as

$$\psi(\mathbf{r}) = \mathcal{A}^{(1)}b^{(1)}(\mathbf{r}) + \mathcal{A}^{(2)}b^{(2)}(\mathbf{r}) \quad (14.45)$$

where

$$\mathcal{A}^{(1)} = \cos \frac{\beta}{2}; \mathcal{A}^{(2)} = \sin \frac{\beta}{2} \quad (14.46)$$

We can plot these curves for  $\mathcal{A}^{(1)}$  and  $\mathcal{A}^{(2)}$  in relation to the positions of the atoms in a simple-cubic crystal where the electron beam is close to the [001] zone axis. Figure 14.2 shows that the intensity in Bloch wave 1 is centered on the column of atoms (Figure 14.2A) while that in Bloch wave 2 is centered between the atoms (Figure 14.2B). (If you read Hirsch et al., you should note that they have 1 and 2 reversed.) Therefore Bloch wave 1 interacts more strongly with the column of atoms and will be 'absorbed' preferentially. Conversely, Bloch wave 2 will be channeled through the specimen. The intensity in the  $\mathbf{g}$  beam depends on the thickness of the specimen because of the interference between these two Bloch waves. This preferential absorption means that we may expect to 'lose' this thickness dependence even though we can still 'see' through the specimen. We'll return to this topic in Chapter 24.

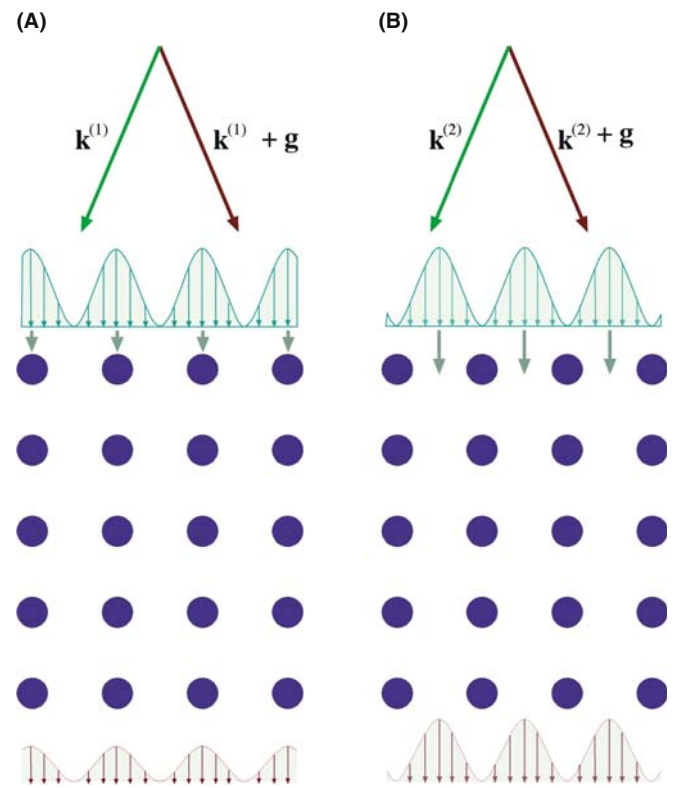


**FIGURE 14.2.** The two types of Bloch wave in the crystal aligned at the Bragg condition: (A) the maximum lies along the ion cores and Bloch wave 1 interacts strongly; (B) the maximum lies between the ions so that the interactions are weaker.



## CHAPTER SUMMARY

We told you at the beginning of the chapter that this discussion would seem to be just theory or manipulating equations. There are, however, some really important ideas

- A basic property of a crystal is that its inner potential,  $V(\mathbf{r})$ , is periodic and positive.
- An electron in a crystal can be described by a sum of Bloch waves which themselves are solutions to the Schrödinger equation.
- The wave functions  $\phi_0$  and  $\phi_{\mathbf{g}}$  are not solutions to this equation and therefore don't actually exist as waves in the crystal.
- All Bloch waves have the same total energy.

Therefore, if we really want to understand what goes on in the crystal, we must be able to understand the concept of Bloch waves. However, you can understand how to relate images to the structure of the specimen without considering Bloch waves. You just have to accept that the analysis using beams (hence  $\phi_0$  and  $\phi_{\mathbf{g}}$ ) is phenomenological. Equations 14.27 and 14.28 give you the essential clue to what really happens: each set of equations tells us how the Bloch waves are coupled. When you've worked through this chapter, go through Sections 13.8 and 13.9 again.

There are many possible solutions to the Schrödinger equation, and each Bloch wave is a plane wave; that is, it can be associated with well-defined propagation vector  $\mathbf{k}^{(j)}$  as shown in equation 14.9.

The Bloch waves are generally different because the  $U_{\mathbf{g}}$  terms are different, i.e., they have different potential energies. Therefore, they have different kinetic energies and different wave vectors.

Finally, a word on relativity. We've kept our treatment as simple as possible, but you should remember that the equations should be relativistically corrected; most texts have ignored relativistic effects when discussing this topic.

## REFERENCES

This chapter follows the treatment given by Hirsch et al. in Chapter 9 of their classic text; the details are provided by Metherell.

## BLOCH WAVES

Ashcroft, NW and Mermin, ND 1976 *Solid State Physics* W.B. Saunders Co. Philadelphia PA. Chapter 8 ( $2\pi/\lambda$  is used).

Bethe, HA 1928 *Theorie der Beugung von Elektronen an Kristallen* Ann. Phys. Lpz. **87** 55–129. Another classic reference (in German).

Howie, A 1971 in *Electron Microscopy in Materials Science* 275–305 Ed. U Valdré Academic Press New York.

Kittel, CJ 2004 *Solid-State Physics* 8th Ed. John Wiley & Sons New York. For the physicists.

Metherell, AJF 1975 in *Electron Microscopy in Materials Science II* 397–552 Eds. U Valdré and E Ruedl CEC, Brussels. This is perhaps the clearest and most comprehensive article available on this subject (over 150 pages long). It is strongly recommended reading if you've made it through this chapter and want to begin programming.

## THE COMPANION TEXT

EMS can be used to simulate HRTEM images using the Bloch-wave approach.

## SELF-ASSESSMENT QUESTIONS

- Q14.1 Summarize the reasons for assigning the sign we do to the accelerating voltage, the sign of the energy of the electron, the sign of the potential, and the sign of the potential energy.
- Q14.2 Even when the atomic number varies from 4 to 74, the inner potential energy only changes by a factor of  $\sim 3$ . Why?
- Q14.3 You're told that the inner potential energy of W is 23.4. Comment on this value.
- Q14.4 What is a Bloch wave?
- Q14.5 What is a Bloch function?

- Q14.6 What is the Bloch theorem?
- Q14.7 Why are we talking about plane waves throughout this chapter?
- Q14.8 Write down an equation relating  $K$  and  $\chi$ .
- Q14.9 Write down an expression relating  $K$  to  $E$  outside the crystal.
- Q14.10 Write down the Bloch-wave expression for the Schrödinger equation. What does this equation tell you?
- Q14.11 Explain in words the meaning of the term  $U_{\mathbf{g}-\mathbf{h}}$ .
- Q14.12 In a crystal, light slows down but electrons speed up. What is the fundamental difference between these two phenomena?
- Q14.13 The terms  $U_{\mathbf{g}}$ ,  $C_{\mathbf{g}}^{(j)}$  and  $a_{\mathbf{g}}$  are related by a set of linear equations through the matrix  $\mathbf{A}$ . Write down the matrix  $\mathbf{A}$  for the situation where only  $\bar{\mathbf{g}}$ ,  $0$ ,  $\mathbf{g}$ ,  $2\mathbf{g}$ , and  $3\mathbf{g}$  are important.
- Q14.14 In the two-beam diffraction situation, how many Bloch waves are important?
- Q14.15 The ‘ $U$ ’ terms are the features which couple together the ‘ $C$ ’ terms. What does this mean?
- Q14.16  $U_{\mathbf{g}-\mathbf{h}}$  is the component of the inner potential which couples together the Bragg beams with reciprocal-lattice vectors  $\mathbf{g}$  and  $\mathbf{h}$ . We don’t really have Bragg beams in a crystal. Explain this apparent inconsistency.
- Q14.17 How is it possible for all Bloch waves to have the same energy?
- Q14.18 In the TEM image, we lose thickness dependence even though we can still see through the specimen. How does Bloch wave theory explain this effect?
- Q14.19 If your sample is YAG (bcc with  $a = \sim 1$  nm) rather than a model, mono-atomic, simple-cubic crystal, how will your Bloch wave analysis be affected?
- Q14.20 If you have a Si/SiO<sub>2</sub>/Si sandwich of equally thick (20 nm) layers such that the beam passes through the layers in succession, how will this affect your discussion of Bloch waves?

### TEXT-SPECIFIC QUESTIONS

- T14.1 For discussion, compare how the velocity of electrons and light change when they enter a crystal. Consider (i) how this will be affected if the specimen is amorphous; (ii) if the accelerating voltage is increased from 100 kV to 1 MV; (iii) if the microscope were a TPM (p: positron) instead.
- T14.2 Consider equation 14.44. Calculate a value for  $\Delta\mathbf{k}$  when  $s = 0$  for 100 kV, Cu 220. How does this value compare to  $\mathbf{g}$  and  $\lambda^{-1}$  and why do we ask?
- T14.3 Evaluate equation 14.20 for 100-kV electrons.
- T14.4 How does Figure 14.1A differ for [001], [110], and [111] in Si and Cu?
- T14.5 How would you modify Figure 14.1B to explain the values of Table 14.2 more clearly?
- T14.6 Consider Figure 14.2. Imagine that the crystal is an extinction distance thick. Draw the intensity plots for the Bloch waves at depth  $\xi/4$ ,  $\xi/2$ ,  $3\xi/4$ , and  $\xi$ .
- T14.7 Excluding the other III–V compounds which are closely related to GaAs, list five other crystal types that do not have a center of symmetry.
- T14.8 Consider equations 14.1 and 14.2. Where does the relativistic correction enter?
- T14.9 In equations 14.45 and 14.46,  $\mathcal{A}^{(1)^2} + \mathcal{A}^{(2)^2}$  is 1. Why is this?
- T14.10 The vectors  $\mathbf{k}$  and  $\boldsymbol{\chi}$  differ because of the refractive-index effect. How large is the refractive index and how does this quantity relate to (if it does) the refractive index for light?
- T14.11 (Challenging) If the extinction distance depends on  $U_{\mathbf{g}}$  for a crystal, can amorphous specimens show thickness fringes?
- T14.12 (Challenging) Why does  $\xi_{\mathbf{g}}$  decrease when both 220 and  $2\bar{2}0$  are excited?

# Dispersion Surfaces

## CHAPTER PREVIEW

The analysis of Bloch waves given in the previous chapter is closely related to the classic analysis of waves that you've seen in condensed-matter physics or semiconductor theory. In semiconductors in particular, we often talk of band diagrams and indirect or direct band gaps. We use terms like conduction bands, valence bands, and Brillouin-zone boundaries (BZBs). We visualize these quantities by drawing diagrams of  $E(\mathbf{k})$ , the electron energy (which is a function of  $\mathbf{k}$ ) versus  $\mathbf{k}$ , the wave vector. This plot of  $E(\mathbf{k})$  versus  $\mathbf{k}$  is known as a dispersion diagram. To remind you of the magnitudes involved, the band gap in Si is 1.1 eV and that of Ge is 0.7 eV. In a good insulator, it can be 10 eV. We now follow the same approach to represent pictorially what we described in equations in Chapters 13 and 14. Remember that the big difference from the solid-state physics approach is that the energy of the electrons in the beam in the TEM is  $\geq 100$  keV.

In this chapter we will see the real origin of the extinction distance  $\xi_{\mathbf{g}}$ , which we introduced in equation 13.4. We will discuss how it relates to particular materials and why it varies with the diffraction vector being used. We will then discuss the physical origin of the concept of the effective extinction distance: i.e., the value which the extinction distance appears to have when  $s \neq 0$ . This discussion of dispersion surfaces is included as a separate chapter, so that you can omit it without affecting your understanding of the rest of the text. We should give you a warning: this is a subject which has probably turned off many potential microscopists. It can be very mathematical, pure theoretical physics, or it can provide many useful insights into image formation. We are trying for the latter. If we aren't completely successful, take heart; nearly every established microscopist has survived without completely mastering this concept!

## 15.1 INTRODUCTION

The analysis of Bloch waves as they apply to electrons in solids is well documented in the condensed-matter physics literature. However, what we want from the theory is different from what an electrical engineer might want: we want to understand how it applies to the formation of contrast in TEM images and DPs. With this aim in mind, we will again follow the treatment given in Metherell's classic and well-hidden article, already referenced in Chapters 13 and 14. In Chapter 14, we derived equations relating  $\mathbf{k}$  to  $U_{\mathbf{g}}$ . (See Section 14.2 for the definition of  $U_{\mathbf{g}}$ .) Specifically, we found that there are two Bloch waves if there are two Bragg beams,  $\mathbf{0}$  and  $\mathbf{g}$ . We can rewrite equation 14.35 incorporating equation 14.32 as

$$\frac{C_{\mathbf{g}}^{(j)}}{C_{\mathbf{0}}^{(j)}} = \frac{(\mathbf{k}^{(j)})^2 - K^2}{U_{-\mathbf{g}}} = \frac{U_{\mathbf{g}}}{(\mathbf{k}^{(j)} + \mathbf{g})^2 - K^2} \quad (15.1)$$

where  $C_{\mathbf{0}}^{(j)}$  is the amplitude of the plane wave with wave vector  $\mathbf{k}^{(j)}$ , and  $C_{\mathbf{g}}^{(j)}$  is the amplitude of the plane wave with wave vector  $\mathbf{k}^{(j)} + \mathbf{g}$ . The Bloch wave was given in equation 14.12 as

$$b^{(j)}(\mathbf{r}) = \sum_{\mathbf{g}} C_{\mathbf{g}}^{(j)} e^{2\pi i(\mathbf{k}^{(j)} + \mathbf{g}) \cdot \mathbf{r}} \quad (15.2)$$

Equation 15.1 says that the values of  $C_{\mathbf{g}}^{(j)}$  and  $C_{\mathbf{0}}^{(j)}$  are directly related to  $k^{(j)2} - K^2$  and thus to  $k^{(j)} - K$ .

In the general many-beam case (actually, in any situation where we have more than two beams), the situation is more complicated. However, we can separate the problem into two parts

- Determine all the allowed wave vectors  $\mathbf{k}^{(j)}$  in a crystal, including all possible orientations of the crystal.
- Determine which set of the allowed  $\mathbf{k}^{(j)}$  wave vectors is actually present when you fix the orientation of your crystal.

The first statement fixes the total energy of the electron and selects the crystal. The second statement applies the boundary conditions for the particular situation you are considering, as we'll illustrate in Sections 15.5 and 15.6.

The solution to the first part of the problem is found by setting  $|\mathcal{A}^{(j)}| = 0$ . (We defined  $\mathcal{A}^{(j)}$  in Section 14.3 and gave an expression for it in Section 14.5.) If you multiply the determinant, you get a polynomial to the power  $2n$  in  $\mathbf{k}^{(j)}$

$$\mathcal{A}_{2n}(\mathbf{k}^{(j)})^{2n} + \mathcal{A}_{2n-1}(\mathbf{k}^{(j)})^{2n-1} + \mathbf{K} = 0 \quad (15.3)$$

The coefficient  $\mathcal{A}_n$  depends on  $K^2$  (i.e., the energy) and  $\mathbf{g}$  (i.e., the crystal).

So, the polynomial in  $\mathbf{k}^{(j)}$  relates  $\mathbf{k}^{(j)}$  to the total energy. This is a dispersion relation as we defined the term in Section 14.4. The equation has  $2n$  roots and some might be complex. To quote Metherell, "at first sight therefore, the situation appears to be a complicated one!" So in following Metherell we make two simplifications

- We consider only the high-energy case.
- We assume that we only excite reflections in the ZOLZ.

There are three reasons for reminding you of these simplifications

- If you want to make a Bloch-wave calculation where you include more than two Bragg beams, then you will need a computer.
- The diagrams we're considering in this chapter are a pictorial representation. The diagrams help us think about what is actually happening to the Bloch waves. If we just did the calculation, we would lose the physical 'feel' for the problem.
- None of the diagrams we will draw will consider HOLZ reflections; if we make the beam energy high enough, we don't need to consider them. However, the energy is not really that high and HOLZ reflections are not only seen experimentally, but can also provide valuable information, as we'll see in Chapters 20 and 21. The saving factor is that modern computers have no problems in handling these equations, especially since they are so amenable to matrix manipulation.

### THE DISPERSION SURFACE

...is a pictorial representation of the relationship between  $\mathbf{k}$  and energy.

## 15.2 THE DISPERSION DIAGRAM WHEN $U_g = 0$

We start with equation 14.34, namely

$$\left(|\mathbf{k}^{(j)}| - K\right)\left(|\mathbf{k}^{(j)} + \mathbf{g}| - K\right) = \frac{|U_g|^2}{4K^2} \quad (15.4)$$

Remember that this equation was derived for the two-beam case. When the electrons are in the vacuum, i.e., outside the specimen, the Fourier coefficients  $U_g$  are 0. When  $U_g = 0$ , the left side of this equation is zero and the equation has two solutions.

$$K = |\mathbf{k}^{(j)}| \text{ or } K = |\mathbf{k}^{(j)} + \mathbf{g}| \quad (15.5)$$

where  $j$  is 1 or 2. If we plot out these two solutions we find, as shown in Figure 15.1, that we have two interpenetrating spheres, since both  $\mathbf{k}_I$  and  $\mathbf{k}_D$  can lie in any direction. Since these two  $\mathbf{k}$  vectors have the same length, the two spheres represent surfaces of constant energy, called dispersion surfaces, one centered on  $O$  and the other centered on  $G$ .

Of course, we already know that the energy of the electron in a vacuum is related to its wave vector by

$$E = \frac{p^2}{2m} = \frac{\hbar^2 \chi^2}{2m} \quad (15.6)$$

where  $\mathbf{p}$ , the momentum, is related to the wave vector in a vacuum,  $\chi$ , by  $\mathbf{p} = \hbar\chi$ . Here,  $\chi$  is the  $K$  when the electron is in a vacuum.

Rearranging, we have

$$\chi = \left\{ \frac{2m}{\hbar^2} E \right\}^{\frac{1}{2}} \quad (15.7)$$

The dotted line drawn in Figure 15.1 represents a plane that is defined by the circle created by the intersecting spheres. You will probably be very familiar with the BZB from condensed-matter physics.

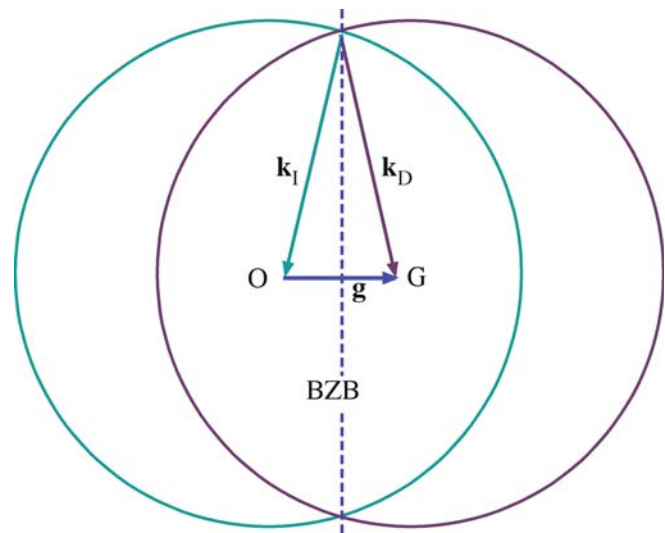


**FIGURE 15.1.** Cross section through two spheres of radii  $\mathbf{k}_I$  and  $\mathbf{k}_D$  centered on  $O$  and  $G$ , respectively. The spheres represent surfaces of constant energy and the dotted line is the trace of the diffracting plane (and is also equivalent to the BZB).

While you work through the diagrams in this chapter, you must remember that for high-energy electrons the scattering angles, e.g.,  $2\theta_B$ , are usually small and the region of interest in reciprocal space is, therefore, close to the BZB. We can redraw part of Figure 15.1 to show an enlarged view of the region close to the BZB in Figure 15.2. At high energies, we approximate the surfaces as a pair of straight lines because  $\lambda$  is very small.

### 15.3 THE DISPERSION DIAGRAM WHEN $U_g \neq 0$

When  $U_g \neq 0$  we know from equation 15.4 that  $K$  can never be equal to  $|\mathbf{k}_I|$  or  $|\mathbf{k}_D|$ . Since equation 15.4 is quadratic we must have two values for  $|\mathbf{k}|$ . So, the two 'spheres' can't intersect if  $U_g \neq 0$ . You noticed that equation 15.4 resembles that for a hyperbola,  $xy = a$ , where the  $x$  and the  $y$  axes are shown in Figure 15.2. We can draw these two hyperbolae with their asymptotes as

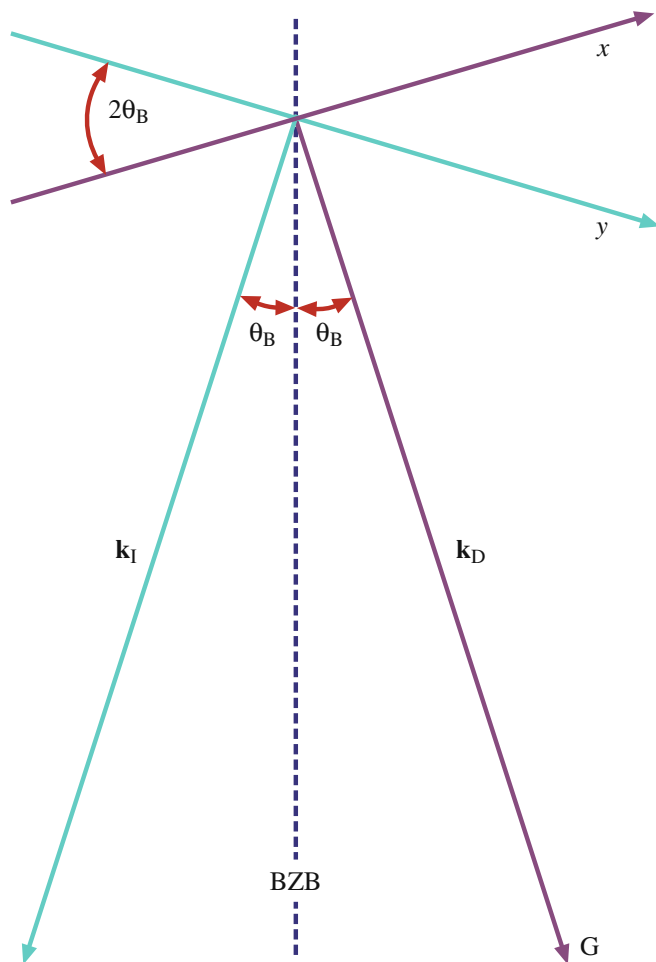


**FIGURE 15.2.** An enlarged view of the interception of the two dispersion spheres at the BZB. The projections of the two dispersion surfaces approximate to straight lines  $x$  and  $y$  which are normal to  $\mathbf{k}_D$  and  $\mathbf{k}_I$ , respectively.

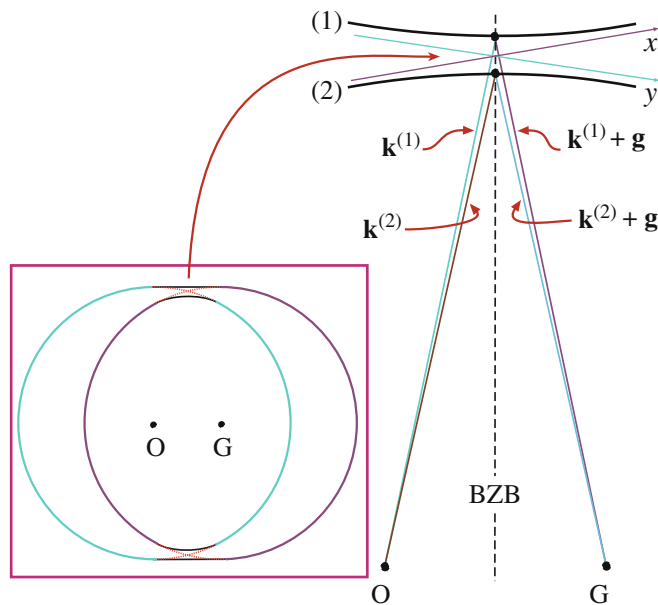


**FIGURE 15.3.** When the electron is inside the specimen (i.e.,  $U_g \neq 0$ ) there are two values of  $\mathbf{k}$ . The two dispersion spheres can't intersect and two branches of the dispersion surface (1) and (2) are created. The enlarged view of the 'non-intersection' shows the vectors,  $\mathbf{k}^{(1)}$  and  $\mathbf{k}^{(2)}$ , and  $\mathbf{k}^{(1)} + \mathbf{g}$  and  $\mathbf{k}^{(2)} + \mathbf{g}$ .

shown in Figure 15.3. These surfaces (remember we are in three dimensions) are known as *branches* of the dispersion surface. The upper branch (identified here by the '1') corresponds to  $\mathbf{k}^{(1)}$  and the lower (identified by the '2') to  $\mathbf{k}^{(2)}$ . We now have vectors  $\mathbf{k}^{(1)}$  and  $\mathbf{k}^{(2)}$  where we used to just have  $\mathbf{K}_I$ . There are some critical points to remember in this discussion from Chapters 13 and 14

- The Bloch wave  $b^{(1)}(\mathbf{k}^{(1)}, \mathbf{r})$  is associated with  $\mathbf{k}^{(1)}$ .
- The Bloch wave  $b^{(2)}(\mathbf{k}^{(2)}, \mathbf{r})$  is associated with  $\mathbf{k}^{(2)}$ .
- The intensity of the Bragg beam is a function of thickness  $|\phi_g(t)|^2 \propto \sin^2(\pi t \Delta k)$  (from equation 13.45).

The difference between Figures 15.1 and 15.3 is the gap between the two branches in Figure 15.3. This gap is present because  $U_g$  is not zero;  $U_g$  is not zero because we have a periodic array of atoms, i.e., a crystal. This gap is directly analogous to the band gap in semiconductor theory where there are forbidden electron energies within the crystal.

### 15.4 RELATING DISPERSION SURFACES AND DIFFRACTION PATTERNS

We can gain a lot of physical insight into Bloch waves using the dispersion-surface construction rather than solving the Bloch-wave equations on the computer. Our approach is relatively simple.



- We start with the dispersion surface shown in Figure 15.4A and draw an initial line to represent the incoming beam traversing the thin foil. We assume an idealized thin specimen with parallel surfaces that are perpendicular to the vertical, optic axis of our TEM and we choose  $\mathbf{g}$  to be parallel to the surface. The incident beam is allowed to be inclined to the surface of the specimen.
- We then draw a line normal to any surface that the initial line encounters. This allows us to match the components of wave vectors parallel to that surface. This is the wave-matching construction.

- We then extend the points  $M_1$  and  $M_2$  back to the ' $\chi$ ' spheres in Figure 15.4B; these spheres are the  $\chi$  spheres when we are in the crystal.
- The last part of the process is always to relate the waves in the crystal to the beams in the vacuum since our recording film, CCD camera, etc., is always outside the crystal.

That's the plan—now we go through it step by step. As shown on the enlarged view in Figure 15.5, each of the  $\mathbf{k}$  vectors has an associated wave amplitude  $C_{\mathbf{g}}^{(j)}$  associated with it.

In this discussion, we will limit ourselves to the two beams, O and G. As we know from Section 13.8, the only values of  $C$  (the coefficients of the Bloch waves) that will then be non-zero are  $C_0^{(1)}$ ,  $C_0^{(2)}$ ,  $C_{\mathbf{g}}^{(1)}$ , and  $C_{\mathbf{g}}^{(2)}$ .

**WAVE MATCHING**

If we were doing this mathematically, this matching would be the boundary condition.

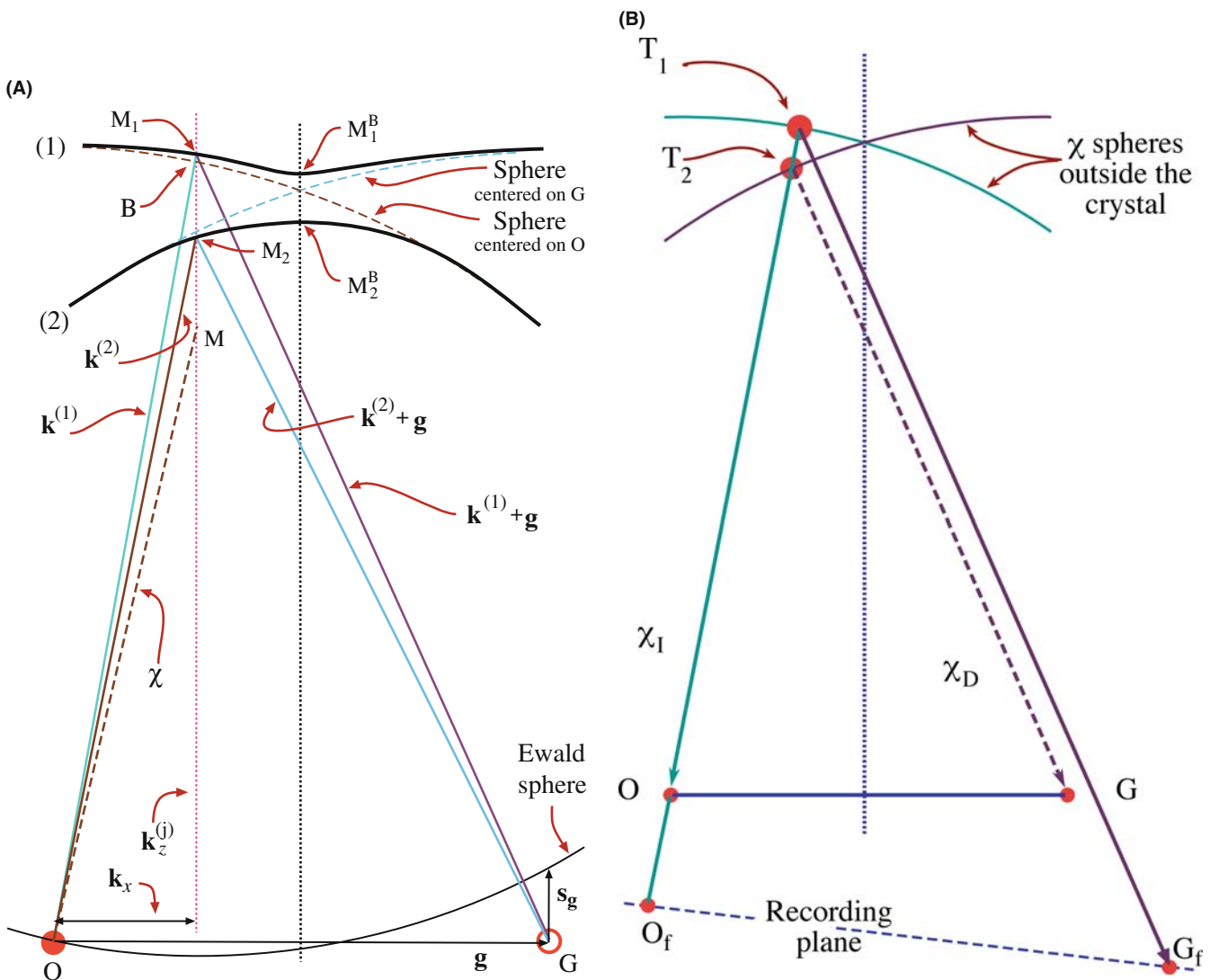


**FIGURE 15.4.** (A) Combination of the dispersion surfaces (1) and (2), centered on O and G, with the Ewald sphere construction. The surface of the specimen has been set to be parallel to  $\mathbf{g}$ , so points  $M_1^B$  and  $M_2^B$  on the branches (1) and (2) are excited. The incident beam direction is then parallel given by the vector  $\mathbf{MO}$ . If we tilt the beam so  $\chi$  (as shown) becomes more vertical, the excited points move to  $M_1$  and  $M_2$  giving the tie line  $M_1M_2$ . The vectors  $\mathbf{k}^{(1)}$  and  $\mathbf{k}^{(2)}$  start at  $M_1$  and  $M_2$ , respectively, and end on O. (B) Extension of the lines  $OM_1$  and  $OM_2$  in (A) back to the  $\chi$  spheres at  $T_1$  and  $T_2$ , respectively, relates the waves in the crystal to the beams outside. The points  $O_f$  and  $G_f$  are what you record on the photographic film.

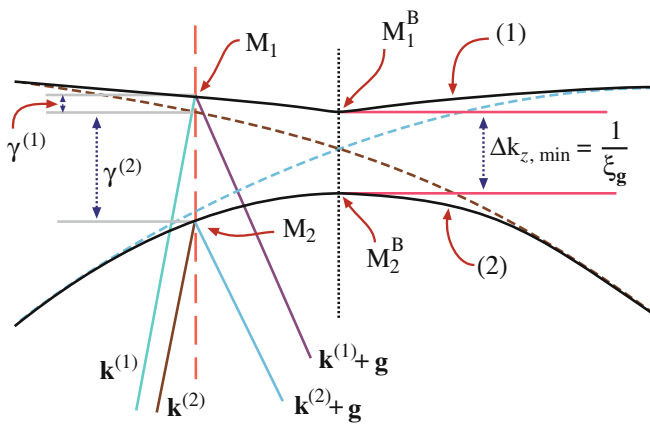


FIGURE 15.5. An enlarged region of Figure 15.4A showing how the vectors  $\mathbf{k}^{(1)}$  and  $\mathbf{k}^{(2)}$  are related to the quantities  $\gamma^{(1)}$  and  $\gamma^{(2)}$  and the distance  $\Delta k_z$ .

First, we need to know which points on the dispersion surface will actually correspond to the diffraction condition we have chosen. We also need to know the orientation of the specimen relative to the beam and the orientation of the Bragg planes (which is why we start by fixing this).

*To begin.* We consider the case where the surface of the specimen is parallel to  $\mathbf{g}$ ; we will explain why we are so specific on this point in a moment.

Now we have fixed the specimen and  $\mathbf{g}$  relative to the optic axis. Next we orient the incident beam. Note that the beam is not parallel to the  $(hkl)$  planes; its  $\mathbf{k}_i$  is determined by  $\chi$  but isn't shown in the figure. We will excite points  $M_1^B$  and  $M_2^B$  on separate branches of the dispersion surface because this is where the dotted line cuts the two surfaces. The extinction distance will then correspond to  $\Delta k^{-1}$  for  $s=0$  as in Section 13.10. If we now tilt the incident beam so that  $\chi$  moves closer to the vertical (keeping the specimen fixed), then the excited points become  $M_1$  and  $M_2$  and, as we see in Figure 15.4,  $s$  becomes negative.

We define the lines  $M_1^B M_2^B$  and  $M_1 M_2$  to be *tie lines* because they tie together points on the different branches of the dispersion surface. Both tie lines are parallel to the BZB because we chose the top surface of the specimen to be parallel to  $\mathbf{g}$ .

Each of these tie lines is normal to the surface that produces it.

The diagrams of the dispersion surface in Figures 15.4 and 15.5 contain lots of reminders

- For this orientation,  $\mathbf{k}_x$  is the same for all  $\mathbf{k}$  vectors ending on O.
- You can recognize  $\gamma^{(1)}$  and  $\gamma^{(2)}$  from Section 13.7.
- The vacuum wave vector  $\chi$  is always shorter than  $\mathbf{K}$  or  $\mathbf{k}$ .

We can understand these changes from the following argument. The O beam is always excited so  $C_0^{(1)}$  and

$C_0^{(j)}$  will always be relatively large. Which other values of  $C$  are large will depend on where the Ewald sphere cuts the systematic row of rods.

Now we can consider what happens when the surface of the specimen is *not* parallel to  $\mathbf{g}$ . Here, the normal to the surface,  $\mathbf{n}$ , is not parallel to the BZB (since the BZB is normal to  $\mathbf{g}$ ). However, the tie line is always parallel to  $\mathbf{n}$  so the tie line is no longer parallel to the BZB. Remember: this construction is graphically matching the components of the  $\mathbf{k}$  vector which are parallel to the surface of the specimen. We saw this clearly in Figure 15.4 where we commented that  $\mathbf{k}_x$  is the same for all the vectors ending on O because we chose  $\mathbf{g}$  to be parallel to the surface and the surface to be normal to the optic axis in that case.

We don't need tie lines in solid-state physics if the electrons are always moving in a perfect lattice where we don't consider surfaces.

### TIE LINES

The tie line is a graphical method of satisfying the boundary conditions imposed by the TEM specimen.

We are now ready to consider the more common TEM wedge specimen shown in Figure 15.6A and then we'll see how these excited Bloch waves relate to the DP.

In this figure we have drawn the wedge with the top surface horizontal. Thus we have tie line  $\mathbf{n}_1$  along the optic axis. When the electrons exit the crystal at the inclined bottom surface, we again match components parallel to this surface so we have tie line  $\mathbf{n}_2$ . Notice that we must draw  $\mathbf{n}_2$  through both  $M_1$  and  $M_2$ . These tie lines don't excite extra points on the dispersion surface because we are leaving the crystal.

Once we're outside the crystal, we know that the wave vector must be  $\chi$  and that  $\chi$  defines a pair of spheres centered on O and G. So we extend the  $\mathbf{n}_2$  tie lines until they reach the  $\chi$  spheres. Now we have excited four points, as we see graphically in Figure 15.6A. The points on the O circle are labeled  $O_1$  and  $O_2$ ; those on the G circle are  $D_1$  and  $D_2$ . We have labeled the subscripts this way because they correspond to the plane waves  $\chi_0^{(1)}$ ,  $\chi_0^{(2)}$ , etc., as also shown in Figure 15.6A.

*To conclude.* Now we have reached the final step. We have to relate these beams to the DP. Yes, they are real beams, not Bloch waves, because we are now outside the specimen and in a vacuum. We show this in Figure 15.6B. All of the  $\chi$  beams have been related to point  $O_1$  because  $\chi_0^{(1)}$  is the incident beam. Remember:  $\chi_0^{(1)}$  is not vertical because we made  $\mathbf{g}$  horizontal and tilted the incident beam. The vectors  $\chi_0^{(1)}$  and  $\chi_0^{(2)}$  are not quite parallel because although they are both radii of the same sphere of radius  $\chi$ , they actually originate at different points on the circle (see Figure 15.6A).

The conclusion is that we will have two spots at O and two spots at G. In other words, the fact that we have

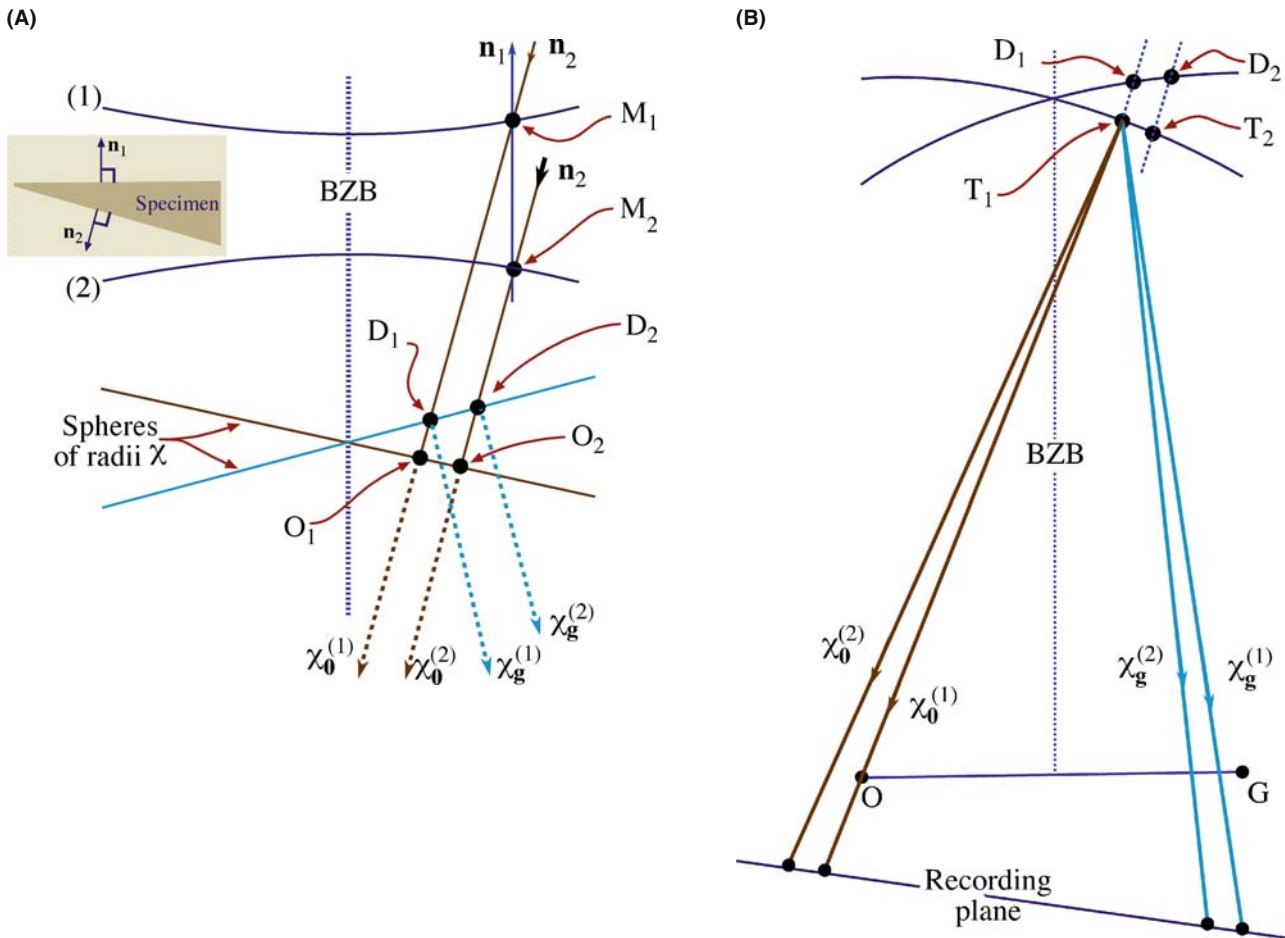


**FIGURE 15.6.** (A) The same diagram as Figure 15.4B, but for a wedge specimen with the top surface parallel to  $\mathbf{g}$  (normal  $\mathbf{n}_1$ ) and the bottom surface normal  $\mathbf{n}_2$ . Instead of exciting two points,  $O_1$  and  $O_2$ , we excite two more,  $D_1$  and  $D_2$ , which correspond to the plane waves  $\chi_0^{(1)}$ ,  $\chi_0^{(2)}$ , outside the crystal. In (B) we relate all the beams to the point  $O_1$  and we produce two beams at  $O$  and two at  $G$ . Thus we can predict that a wedge foil will give doublets at  $O$  and  $G$ .

a wedge specimen has split the spots at  $G$ . We will see these split spots in Chapter 18 and we will return to this topic in Chapter 23 when we discuss images.

It can be useful to extend the wedge case to the double wedge. For example, imagine an inclined planar defect in a parallel-sided slab with  $\mathbf{g}$  parallel to the slab surface as shown in Figure 15.7. Everything is as before at the top surface. At the inclined interface then, tie lines do create new excited points  $B_1$  and  $B_2$  on the 1 and 2 branches of the dispersion surface.

Now,  $\mathbf{n}_3$  is the tie line due to the bottom surface and  $\mathbf{n}_3$  is parallel to  $\mathbf{n}_1$ . We extend the  $\mathbf{n}_3$  tie lines to the  $\chi$  spheres and find that now we have three  $\chi_0$  vectors and three  $\chi_D$  vectors. Translating these  $\chi$  vectors to  $O_1$  as the common origin produces the beam diagram shown in Figure 15.7B. Now we have three spots at  $O$  and three spots at  $G$ . We will return to this topic in Chapter 24 when we discuss images of planar defects, but here let's summarize the new concepts they give us

- The dispersion surface is a graphical approach to thinking about Bloch waves.

- We have to match the components of any wave entering and leaving any surface, internal or external.
- We use the exit-surface tie line to link to the  $\chi$  spheres.
- Having two inclined surfaces causes a splitting of the Bragg beams.
- An internal interface, such as a stacking fault, increases the number of points excited on the dispersion surfaces and the number of spots at reflection  $G$ !

To understand the importance of these ideas, try to imagine what will happen when a defect, which is not abrupt, is present in the crystal (more on this in Section 15.8).

### 15.5 THE RELATION BETWEEN $U_g$ , $\xi_g$ , AND $s_g$

We can best appreciate the importance of the dispersion-surface construction by looking at Figure 15.4. This figure shows the original spheres as dashed lines: they are nearly flat close to the BZB. The electron beam is

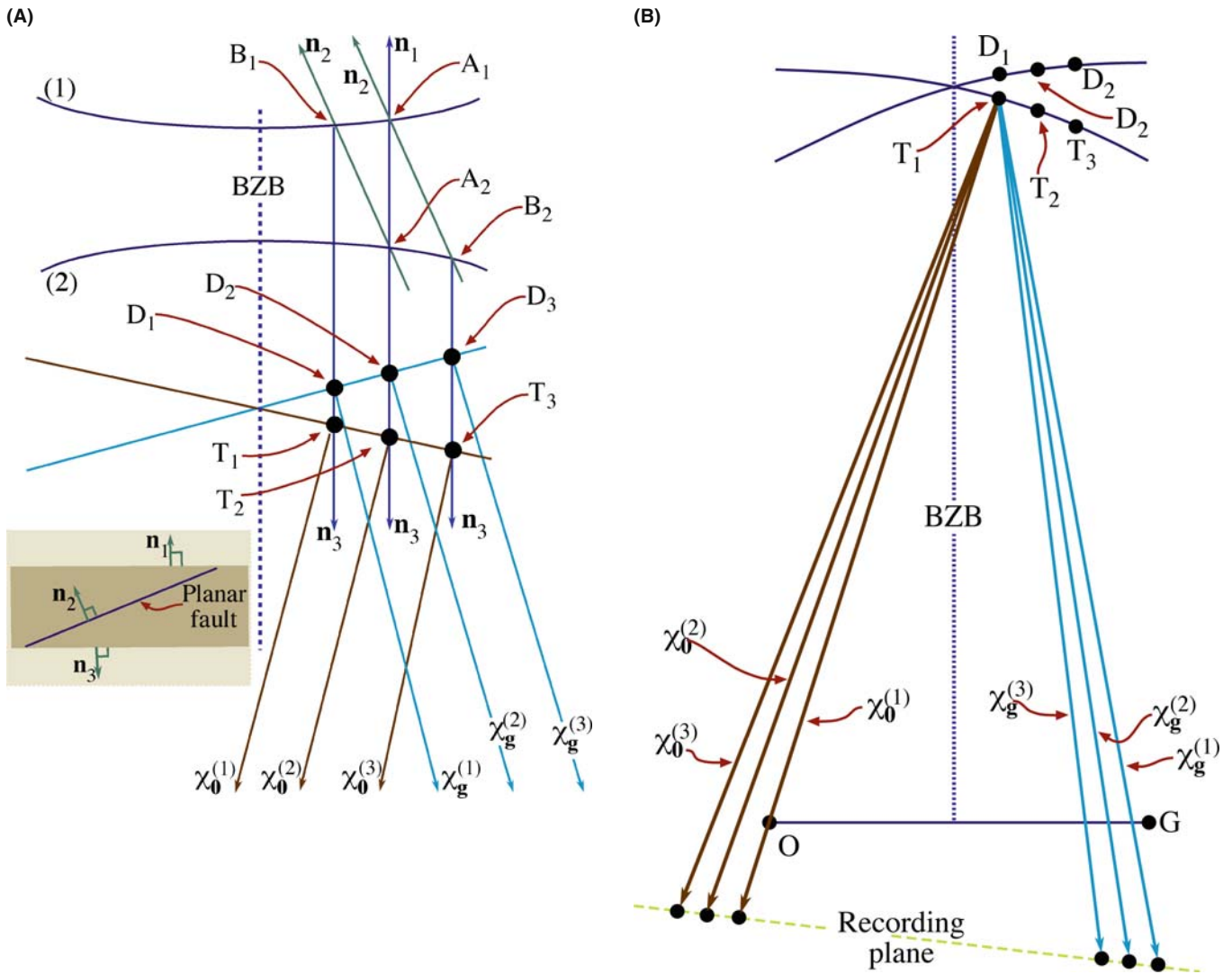


**FIGURE 15.7.** (A) An enlarged view of the dispersion surface in Figure 15.6 close to the BZB, but this time for a specimen in which both surfaces are parallel to  $\mathbf{g}$  but there is an inclined fault which produces a third wave  $\chi_0^{(3)}$  and  $\chi_g^{(3)}$ . If we then move all the vectors to  $O_1$  again, we predict there will be three spots at  $O$  and three at  $G$ .

initially traveling with wave vector  $\chi$  outside the crystal. When the beam enters the crystal the  $z$  component of this wave vector changes (this is the refraction effect we saw in Chapters 11 and 13), but the  $xy$  component is unchanged. Therefore, the allowed  $\mathbf{k}$  vectors in the crystal are  $\mathbf{k}^{(1)}$  and  $\mathbf{k}^{(2)}$ . One  $\mathbf{k}$  vector begins on branch 1 and ends at  $O$ , while the other begins at branch 2 and ends at  $O$ .

### BRANCHES AND BEAMS

There are only two  $\mathbf{k}$  vectors because there are only two branches of the dispersion surface. There are two branches of the dispersion surface because we have a crystal potential (hence  $U_g$ ). There are only two branches because we are considering only two beams.

Clearly we can draw in  $\mathbf{k}_g^{(2)}$  and  $\mathbf{k}_g^{(1)}$  by adding  $\mathbf{g}$ . Now, how does  $\mathbf{k}_0^{(1)}$ , say, relate to  $\mathbf{K}$ ? The point  $\mathbf{K}$  is also determined by the tie line through  $\chi$ , and lies on the circle centered on  $O$ . Most importantly, neither  $\mathbf{k}_1$  nor  $\mathbf{k}_2$  is equal to  $\mathbf{K}$ . If you look back at equation 13.41 you can see that

$$k_z^{(i)} - K_z = \gamma^{(i)} \quad (15.8)$$

So  $\gamma^{(i)}$  is simply the distance of the point  $M_j$  from the  $K$  sphere centered on  $O$ . We can write this relationship explicitly

$$\mathbf{k}^{(i)} = \mathbf{k}_z^{(i)} + \mathbf{k}_x^{(i)} \quad (15.9)$$

$$= (K + \gamma^{(i)})\mathbf{u}_z + k_x\mathbf{u}_x \quad (15.10)$$



Notice that the last term here is independent of  $i$ . Look again at Figure 15.4. We can see that  $\Delta k_z$  is a minimum when  $M_1$  and  $M_2$  lie on the BZB. In that situation

$$\Delta k_{z_{\min}} = \gamma^{(1)} - \gamma^{(2)} \quad (15.11)$$

Simply by looking at the diagram, and as expected from Chapter 13, you also know that

$$\gamma^{(1)} - \gamma^{(2)} = \frac{U_g}{k} = \frac{1}{\xi_g} \quad (15.12)$$

So

$$\Delta k_z = \frac{1}{\xi_g} \quad (15.13)$$

The origin of the thickness oscillations that we will see in the two-beam TEM image is the difference in wavelength of the two Bloch waves. It's the beating between the two Bloch waves.

Thus we see that the gap  $\Delta k_z$  at the BZB is given by the reciprocal of the extinction distance. We'll summarize again to be quite sure that it is clear!

- We have a crystal, therefore  $U_g \neq 0$ .
- Since  $U_g \neq 0$  we have two branches to the dispersion surface and hence a band gap.
- The bandgap is  $\Delta k_z$ .
- Hence we have a finite extinction distance (i.e.,  $\xi_g$  is not infinite).

An aside: think how  $s_{\text{eff}}$  and  $s$  would be related if  $\xi_g$  were infinite. (Go back to equation 13.47.)

If the tie line  $M_1M_2$  does not lie on the BZB then when we draw the Ewald sphere centered just below  $M_1$  (with radius of length  $1/\lambda$  or  $|K|$ ) we see that  $s_g$  is non-zero. We can easily see from the equations in Section 13.10 that, in general,  $\Delta k_z$  is given by

$$\Delta k_z = s_{\text{eff}} = \frac{1}{\xi_{\text{eff}}} \quad (15.14)$$

This equation is the key to understanding the origins of the extinction distance and why the effective extinction distance depends on the size of the excitation error,  $s$ . It says that the band gap increases as we increase  $s$ . Looking at it another way, as we move the tie line off the BZB, the band gap  $\Delta k$  increases.

Some questions raised here are

- What is the physical reason that  $\Delta k_z$  is related to  $s$ ?
- What happens if  $\mathbf{g}$  is not parallel to the foil surface or, indeed, if the foil surfaces are not parallel to one another?

You can also appreciate why we had a problem defining  $s$  when we first encountered it!

## 15.6 THE AMPLITUDES OF BLOCH WAVES

In Section 13.9, we found that the total wave function for the two-beam case can be expressed as the sum of two Bloch waves

$$\psi(\mathbf{r}) = \mathcal{A}^{(1)}b^{(1)} + \mathcal{A}^{(2)}b^{(2)} \quad (15.15)$$

We showed that the relative contributions of the two Bloch waves  $\mathcal{A}^{(1)}$  and  $\mathcal{A}^{(2)}$  are  $\cos \beta/2$  and  $\sin \beta/2$ , respectively; in addition,  $w = \cot \beta = s\xi_g$ .

We also showed in Section 13.8 that

$$b^{(1)}(\mathbf{k}^{(1)}, \mathbf{r}) = C_0^{(1)} e^{2\pi i \mathbf{k}^{(1)} \cdot \mathbf{r}} + C_g^{(1)} e^{2\pi i (\mathbf{k}^{(1)} + \mathbf{g}) \cdot \mathbf{r}} \quad (15.16)$$

and

$$b^{(2)}(\mathbf{k}^{(2)}, \mathbf{r}) = C_0^{(2)} e^{2\pi i \mathbf{k}^{(2)} \cdot \mathbf{r}} + C_g^{(2)} e^{2\pi i (\mathbf{k}^{(2)} + \mathbf{g}) \cdot \mathbf{r}} \quad (15.17)$$

The Bloch wave coefficients were given by equation set 13.31

$$\begin{array}{cccc} C_0^{(1)} & C_0^{(2)} & C_g^{(1)} & C_g^{(2)} \\ \cos \beta/2 & \sin \beta/2 & -\sin \beta/2 & \cos \beta/2 \end{array}$$

Now we can consider some special cases and examine the actual values for  $C_0^{(1)}$ ,  $\mathcal{A}^{(1)}$ , etc. (Table 15.1).

For the Bragg case,  $s_g = 0$ ,  $\mathbf{g}$  is exactly excited and  $\mathcal{A}^{(1)}$  and  $\mathcal{A}^{(2)}$  are both equal to  $1/\sqrt{2}$ . In other words, the two Bloch waves are equally excited.

For the case where  $s_g < 0$ , we now have  $\cos(\beta/2) > \sin(\beta/2)$  so that  $\mathcal{A}^{(1)}$  is greater than  $\mathcal{A}^{(2)}$ . If we reverse the sign of  $s$ ,  $\cos(\beta/2) < \sin(\beta/2)$  and  $\mathcal{A}^{(1)}$  is less than  $\mathcal{A}^{(2)}$ .

TABLE 15.1 Values of Bloch Wave Variables

$s$	$w$	$\beta$	$\beta/2$	$\cos(\beta/2)$	$\sin(\beta/2)$
0	0	$\pi/2$	$\pi/4$	$1/\sqrt{2}$	$1/\sqrt{2}$
+0.01	$+\Delta$	$(\pi/2) - \delta$	$(\pi/4) - (\delta/2)$	$(1/\sqrt{2}) + \epsilon$	$(1/\sqrt{2}) - \epsilon$
-0.01	$-\Delta$	$(\pi/2) + \delta$	$(\pi/4) + (\delta/4)$	$(1/\sqrt{2}) - \epsilon$	$(1/\sqrt{2}) + \epsilon$

### AMPLITUDE OF BLOCH WAVE

Whether Bloch wave 1 or Bloch wave 2 has the largest amplitude depends on the sign of  $s$ .

Now, let's relate this information to the dispersion surface shown in Figure 15.4. When  $s_g < 0$ , as shown here, the  $M_1M_2$  tie line is to the left of the BZB, which



is associated with reflection  $G$ . When the tie line is closer to  $O$  than  $G$ , Bloch wave 1 is more strongly excited; the reverse is true when the tie line crosses the BZB. We should remember that the analysis in Chapter 13 was for a two-beam case, where we were close to the Bragg condition. So this discussion of  $\mathcal{A}^{(1)}$  and  $\mathcal{A}^{(2)}$  only applies to small values of  $s$ .

### 15.7 EXTENDING TO MORE BEAMS

If we allow more beams to contribute to the image, we can imagine the dispersion surface for the case where  $U_g = 0$  by constructing more spheres, shown in Figure 15.8. If we have  $n$  beams then we will have  $n$  spheres. Note that each sphere is centered on its corresponding reciprocal-lattice point and neighboring spheres intersect periodically spaced BZBs. The gap in Figure 15.3 always occurs at the BZB. The BZB itself always corresponds to a plane which is the perpendicular bisector of a  $\mathbf{g}$  vector. Thus the diagram for  $>2$  beams shown in Figure 15.8 will become more complicated with many band gaps and many branches as shown in Figure 15.9. The magnitude of the band gap does decrease as the rank of the neighboring branches increases.

In Chapter 27, we'll discuss what happens in images when  $3\mathbf{g}$  is excited. We will actually consider the two-beam condition where  $\mathbf{0}$  and  $3\mathbf{g}$  are the two beams.

We follow the convention used by Metherell and number the branches of the dispersion surface from top down.

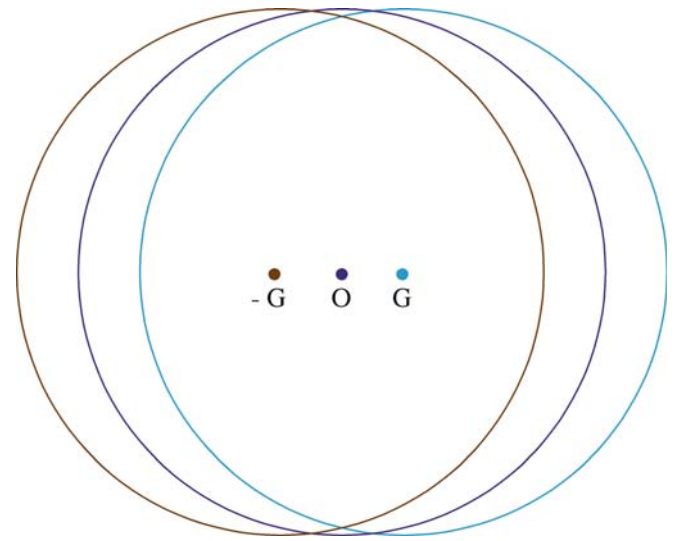


FIGURE 15.8. Three dispersion spheres due to three reflections,  $-G$ ,  $O$ , and  $G$ . If we had  $n$  spots we would have  $n$  spheres.

Then  $i = 1$  corresponds to the branch with the highest kinetic energy. Remember that all the electrons have the same total energy in this treatment. You must also be aware that some earlier texts number the top branch two and the second branch one, following Hirsch et al. This was fine when only two branches were considered.

We can still associate the amplitudes  $C_0$ ,  $C_g$ , etc., with the sphere centered on  $\mathbf{0}$ ,  $\mathbf{g}$ , etc. The result is shown by the labels  $C_0$ ,  $C_g$ , etc., in Figure 15.9. For

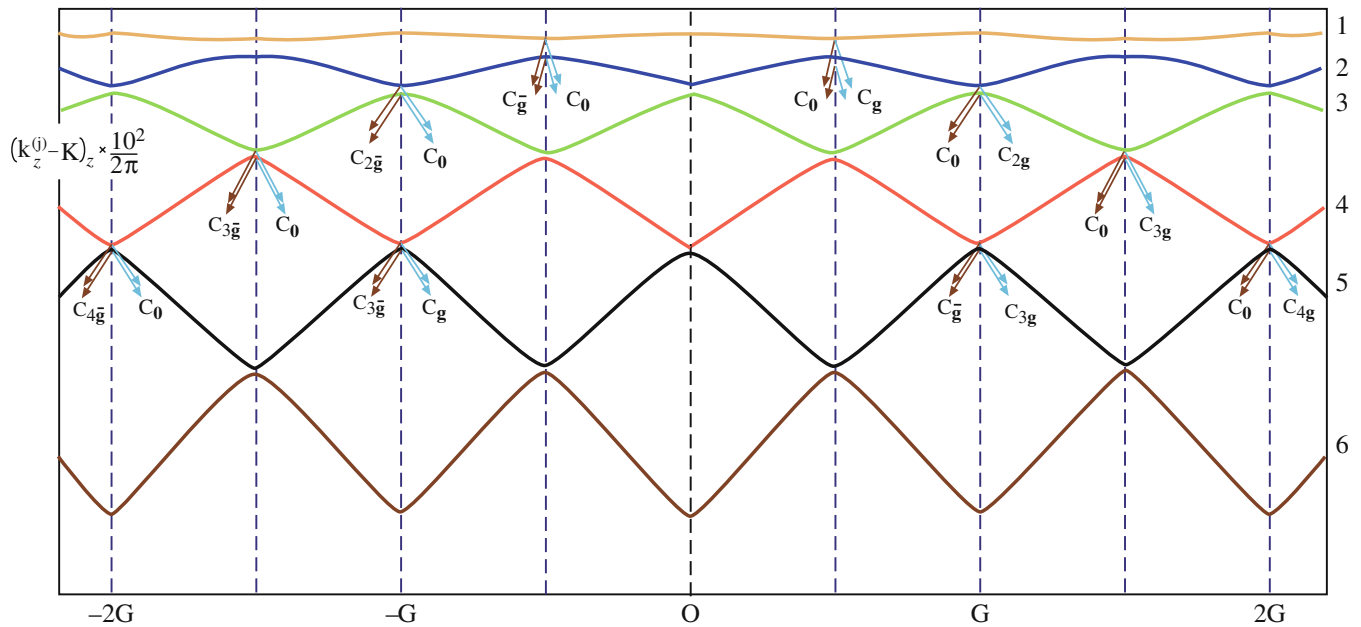


FIGURE 15.9. Six branches of the dispersion surfaces. The two branches  $i = 1$  and  $i = 2$  have the highest energy and give the largest band gap; notice that these branches give the terms in  $C_0$  and  $C_g$ ; smaller gaps occur between branches with lower energy. The diagram can be approximated to a set of spheres centered on  $O$ ,  $\pm G$  and  $\pm 2G$ , etc.;  $C_0$  is 'normal' to the sphere centered on  $O$ , while  $C_g$  is 'normal' to the sphere centered on  $\mathbf{g}$ , etc.

example, imagine the original spheres centered on  $\mathbf{0}$  and  $\mathbf{g}$ ; they intersect on the BZB which passes through  $\mathbf{g}/2$  so the  $C_0, C_g$  are labeled as shown.

Similarly, the spheres centered on  $\mathbf{0}$  and  $3\mathbf{g}$  intersect on the BZB which passes through  $3\mathbf{g}/2$  so  $C_0, C_{3g}$  are labeled. As a general rule,  $C_{ng}$  will be largest for the pair of reflections which are excited, i.e.,  $\mathbf{0}$  and  $n\mathbf{g}$  and will be related by the  $ng/2$  BZB.

We now extend these arguments to the situation where many beams are excited. Values of  $C$  other than  $C_0$  and  $C_{ng}$  will be non-zero since it's no longer a two-beam case. So the tie line  $M_1M_2$  will then intersect many branches of the dispersion surface. The reason these contributions are smaller when  $\mathbf{g}$  is excited is that they do not intersect the  $\mathbf{0}$  circle. However, they can contribute to the image. Figure 15.9 shows how this can be visualized. (Remember the dispersion surface is a way of visualizing Bloch wave coefficients.) If we satisfy reflection  $2G$ , then  $C_0^{(1)}, C_0^{(2)}, C_{2g}^{(1)},$  and  $C_{2g}^{(2)}$  are all large. The gap  $\Delta k_{4,5}$  between branch 4 and branch 5 at  $G$  (on the BZB) is small; the 'circles' would have intersected in the vacuum. If we think about the Ewald sphere we can show that the  $s$  values for  $\bar{\mathbf{g}}$  and  $3\mathbf{g}$  are identical. We'll see later (Chapter 26) that these reflections will actually couple strongly, although both are weakly excited and the extinction distance is large (because the gap  $\Delta k_{4,5}$  is small). The extinction distance for the coupling of  $\bar{\mathbf{g}}$  and  $3\mathbf{g}$  when  $2\mathbf{g}$  is strongly excited is  $\xi_{4g} (\xi_{3g-\bar{g}})$ . We can see this is true by looking at the branch  $4/5$  gap on the BZB for  $G$ .

## 15.8 DISPERSION SURFACES AND DEFECTS

The original reason for introducing the concept of Bloch waves was that only Bloch waves can exist in a periodic potential, i.e., there are no beams in the crystal. So what happens when a defect is present? We'll discuss this situation in some detail in Chapters 23–26 but will mention the basic ideas here, emphasizing the Bloch waves rather than the defects.

In Section 15.4, we discussed the effect that a planar fault can have on the Bloch waves using the dispersion-surface representation. What we were actually doing was matching the components parallel to the planar defect, so the effect of the planar fault was to create new tie lines  $\mathbf{n}_2$ . The general result is that, when a defect is present, energy is transferred from one Bloch wave to the other along the tie line; this is known as *interband scattering*. This concept is not only important for our understanding of images of planar defects but also illustrates a general principle for defects.

The difficulty with non-planar defects is that the tie lines are not so well defined. You can, however, imagine the result: instead of having points on the dispersion surface, we will have a distribution of points. We then relate this distribution to the DP. We do this with the tie lines normal to the exit surface and then translate to  $O_1$  in the usual way. So, our distribution of points on the dispersion surface will become a distribution of spots in the DP; this distribution is what we will call a streak in Chapter 17.

### CHAPTER SUMMARY

Dispersion surfaces allow us to draw diagrams to represent the equations given in Chapter 14. These surfaces are essentially plots of the  $\mathbf{k}$  vector of the Bloch waves (which is directly related to the energy) versus the  $\mathbf{K}$  vector. They correspond directly to the band diagrams, which are used extensively to represent energy levels in semiconductors; the difference is that in semiconductors, we emphasize energy by plotting energy versus reciprocal-lattice vector (our  $\mathbf{K}$  vector). The  $\mathbf{k}$  vectors themselves vary because, although the total energy of each electron is a constant, the potential energy decreases when the electron is close to the nucleus, causing the kinetic energy to increase.

The most important equation for imaging theory is 15.14, which relates  $\Delta k_z, s_{\text{eff}}$ , and  $\xi_{\text{eff}}$ . Notice that  $\Delta k_z$  is defined for two Bloch waves but is only small when the Bragg equation is nearly satisfied. This relationship links Bloch waves and Bragg beams.  $\Delta k$  is non-zero because we have a crystal which produces a periodic potential.  $\Delta k$  gives rise to thickness fringes and all thickness effects. Thus we see that thickness variations are due to the interference, or beating, of pairs of Bloch waves. As we increase  $n$ ,  $\xi_g$  increases because the gap between the two relevant branches of the dispersion surface becomes narrower. Defects present in the crystal cause a mixing or coupling of the Bloch waves: they 'tie' the branches of the dispersion surface and cause interband scattering.

We've emphasized throughout this chapter that the dispersion surface is a pictorial representation of the  $\mathbf{k}$  versus  $K$  relationship. We'll close by quoting the result derived by Kato.

In any wave field, the direction of energy flow is along the normal to the surface of the dispersion surface. This result is equally valid for 'electron wave packets' and other waves. The physicist might say that the Poynting vector is normal to the dispersion surface.

Although there are many texts that discuss dispersion surfaces and band gaps in semiconductors, beware of the  $2\pi/\lambda$  versus  $1/\lambda$  problem since many of the texts are written by, and for, physicists. Defect analysis using Bloch waves has generally been the preserve of the physicist. However, there are some excellent programs available which use a Bloch-wave approach analysis.

We give the usual caveat: beware of black boxes. Metherell's article goes to greater depth than covered here. However, it has been an inspiration for much of this chapter and is highly recommended for advanced study. It is beautifully written and explained, but is certainly more advanced than our text. If you want to delve deeper into this topic, this is *the* article. Note that Metherell uses the  $e^{ikr}$  notation.

## REFERENCES

As in Chapter 14 we follow the treatment of Hirsch et al. as extended and illustrated by Metherell. For anyone familiar with Mathematica™ (or the corresponding) MatLab it would be an interesting challenge to construct (and share) notebooks for these diagrams.

## BLOCH WAVES

Ashcroft, NW and Mermin, ND 1976 *Solid State Physics* W.B. Saunders Co. Philadelphia. Chapter 8 ( $2\pi/\lambda$  is used).

Kato, N 1957 *The Flow of X-rays and Materials Waves in Ideally Perfect Single Crystals* Acta Cryst. **11** 885–887.

Kittel, CJ 2004 *Solid-State Physics* 8th Ed. John Wiley & Sons New York.

Metherell, AJF 1975 in *Electron Microscopy in Materials Science II* 397–552 Eds. U Valdré and E Ruedl CEC Brussels. *The reference.*

## THE COMPANION TEXT

The companion text doesn't extend this topic much, but there is hope to have a discussion of the use of Mathematica™ notebooks in the future.

## SELF-ASSESSMENT QUESTIONS

- Q15.1 What does the word dispersion mean in the context of this chapter?
- Q15.2 Write down an expression for  $b^{(j)}(\mathbf{r})$  in terms of  $\mathbf{k}^{(j)}$  and  $C_{\mathbf{g}}^{(j)}$ .
- Q15.3 We restrict our discussion to the case where only reflections in the ZOLZ are excited. What is the simple physical reason for doing this?
- Q15.4 Draw the dispersion surface diagram for the two-beam case where the crystal has zero inner potential; then explain the term 'dispersion surface.'
- Q15.5 The vectors  $\mathbf{k}^{(1)}$  and  $\mathbf{k}^{(2)}$  are not parallel to one another. What is the physical reason for this and does it have any implications?
- Q15.6 Why do  $\mathbf{k}^{(1)}$  and  $\mathbf{k}^{(2)}$  end (or begin) on branches (1) and (2) and not on the 'curves' x and y?
- Q15.7 We used to have  $\mathbf{K}_D$ . Now we have  $\mathbf{k}^{(1)} + \mathbf{g}$  and  $\mathbf{k}^{(2)} + \mathbf{g}$ . Why don't we have  $\mathbf{K}_D$ ? Does  $\mathbf{K}_D$  still exist?
- Q15.8 What is a BZB? Write out the name and explain what causes it.
- Q15.9 Draw the dispersion surface for two beams where  $\mathbf{g}$  is not satisfied. (Draw Figure 15.4 without looking at it).
- Q15.10 Consider Figure 15.4 when the incident beam,  $\chi_1$ , is parallel to the diffracting planes. Why is this not a good example of two-beam diffraction?
- Q15.11 In Figure 15.4, M is 'below' the dispersion surface. Can it be above this surface? Justify your answer.
- Q15.12 In Figure 15.4,  $\mathbf{k}^{(2)} + \mathbf{g}$  is longer than  $\mathbf{k}^{(2)} + \mathbf{g}$ . Does this mean that  $\lambda$  has changed?
- Q15.13 In Figure 15.4, why is the tie line  $M_1M_2$  normal to  $\mathbf{g}$ ?
- Q15.14 The wave vector  $\chi$  is always shorter than  $\mathbf{K}$  or  $\mathbf{k}$ . Explain why this is so.
- Q15.15 The tie line is a graphical method of satisfying the boundary conditions imposed by the specimen. Explain why this is so.
- Q15.16 In Figure 15.6, are points  $O_1$ ,  $O_2$ ,  $D_1$ , and  $D_2$  really relevant since they don't lie on the dispersion surface for the crystal?
- Q15.17 Explain in words why there are three  $\chi_0$  vectors ( $\chi_0^{(1)}$ ,  $\chi_0^{(2)}$ , and  $\chi_0^{(3)}$ ) in Figure 15.7.
- Q15.18 In the two-beam case when  $G$  is on the Ewald sphere, what are the magnitudes of the Bloch wave coefficients?
- Q15.19 If  $s_{\mathbf{g}} < 0$ , we can show that  $\mathcal{A}^{(1)} > \mathcal{A}^{(2)}$ . What does this mean physically?

## TEXT-SPECIFIC QUESTIONS

The following questions contain the manufacturers' warning label.

- T15.1 Why are there two expressions for  $C_{\mathbf{g}}^{(j)}/C_{\mathbf{0}}^{(j)}$  in equation 15.1?
- T15.2 What is the physical reason that  $\Delta k_z$  is related to  $s$ ?
- T15.3 If  $\mathbf{g}$  is not parallel to the foil surface, how will the Bloch-wave construction change?
- T15.4 If the two surfaces of the specimen are not parallel to one another, how will the Bloch-wave construction change?
- T15.5 When the specimen is oriented so that  $\mathbf{G}$  is on the Ewald sphere, we again have a situation like that shown in Figure 15.9; many beams are excited but one does have  $s_{\mathbf{g}} = 0$ . You form a BF image. How does the periodicity of the thickness fringes relate to this diagram? In particular, how is the extinction distance related to the two-beam value?
- T15.6 When the specimen is oriented with the beam parallel to the diffracting planes, we have a situation like that shown in Figure 15.9; many beams are excited but none have  $s_{\mathbf{g}} = 0$ . You form a BF image. How does the periodicity of the thickness fringes relate to this diagram?
- T15.7 We initially follow Metherell's simplification of assuming that only reflections in the ZOLZ are excited. Discuss what complications might arise if we did not make this assumption. Are we likely to encounter this in practice, and if so, under what conditions?
- T15.8 We also made the approximation that the accelerating voltage is high. Discuss when this approximation might break down.
- T15.9 In Figure 15.4, we draw  $\mathbf{OG}$  so that it is not parallel to  $\mathbf{O}_r\mathbf{G}_r$ . Could this really happen? Discuss why  $\mathbf{T}_1\mathbf{G}_r$  is parallel to  $\mathbf{T}_2\mathbf{G}$  and should this be so?
- T15.10 In Figure 15.6B, why is  $\chi_0^{(2)}$  not parallel to  $\chi_0^{(1)}$  and why are there two such vectors when we are outside the crystal? What is the relevance of  $\mathbf{D}_2$  and  $\mathbf{T}_3$  in this figure?

# Diffraction from Crystals

## CHAPTER PREVIEW

Since our emphasis is on crystalline materials, we will first discuss how the details of the crystal symmetry affect the DPs we expect to see. What we're doing here is taking the concepts of the reciprocal lattice and applying it to particular examples. There are two basic lessons.

- You must learn some of the rules that we will derive for particular crystal structures; one example will be to determine which reflections are allowed for an fcc crystal.
- The other lesson is more general and is really concerned with why we have these rules. Why are certain reflections absent or weak and how can you use this information to learn more about your material?

We can deduce some selection rules for different crystal structures that tell you which reflections are allowed. We suggest you learn the most common ones by heart. Throughout this chapter, we'll assume that the crystal is perfect and infinite, which it never is. In Chapter 17, we will examine what happens when we include defects or allow the diffracting crystal to become relatively small. In Chapter 18, we'll go through the process of indexing experimental DPs.

## 16.1 REVIEW OF DIFFRACTION FROM A PRIMITIVE LATTICE

In Chapters 11–15, we examined diffraction from a regular array of lattice points. We will now define such an array as a primitive lattice where there is only one lattice point in the unit cell. Actually, we did begin to consider the present topic when we discussed the meaning of  $n$  in the Bragg equation  $2d \sin \theta_B = n\lambda$  in Sections 11.5 and 12.4. We showed that the diffraction from the (200) planes would give rise to a 200 reflection even when there were only atoms on the (100) planes.

By combining equations 13.3 and 13.4, we can see that the amplitude of the diffracted beam is given by

$$\phi_{\mathbf{g}} = \frac{a i \lambda F_{\mathbf{g}}}{V_c \cos \theta} \sum_n e^{-2\pi i \mathbf{K} \cdot \mathbf{r}_n} e^{2\pi i \mathbf{K}_D \cdot \mathbf{r}}$$

where  $F_{\mathbf{g}}$  is the structure factor for the material. Since the same type of atom was at each lattice point, we only needed to consider one atomic scattering factor  $f$  in Chapter 13. Now we are going to include different types of atoms as we build up real crystal unit cells. From Section 3.7 we know that  $f$  varies with the

scattering angle. However, in this chapter we are going to restrict ourselves to small values of  $\theta$  (excluding zero) and will assume that we have fixed values of  $f$ ; you can easily extend this analysis to other scattering angles. For convenience, we've summarized some useful values of  $f$  in Table 16.1.

If you study the original paper of Ibers, from which these data were taken, you will appreciate that these numbers are not really well known. This is unfortunate since much of our analysis depends on the values of  $f$ . Furthermore, we have an additional reason for choosing  $\theta$  not to be zero in Table 16.1 because these values are even less reliable. Fortunately, what saves us is that we are only interested in the details of the intensities in some special cases and then the effects are really insensitive to the precise value of  $f$ .

We are just going to take these numbers and move on, but you may want to investigate a little further. Some points you should consider are

- Why are these numbers not better known? We discussed this topic in Chapters 2 and 3. The atomic scattering factor is related to the differential scattering cross section (Section 3.7)



**TABLE 16.1 Selected Values of  $f(\theta)$ , the Atomic Scattering Amplitude at  $\theta = \theta_B$**

Element	$f(\theta)$ (Å)	Element	$f(\theta)$ (Å)
H	0.31	Ca	3.40
Li	0.75	Cr	3.56
Be	1.16	Mn	3.55
B	1.37	Fe	3.54
C	1.43	Co	3.51
N	1.44	Ni	3.48
O	1.42		
		Cu	3.44
Na	1.59	Zn	3.39
Mg	1.95	Ga	3.64
Al	2.30	As	4.07
P	2.59	Ag	5.58
		W	7.43

These are values were derived using a self-consistent field theory ( $\sin \theta/\lambda = 0.2 \text{ \AA}^{-1}$ ) and are based on the rest mass. The  $f(\theta)$  value must be multiplied by  $(1 - (v/c)^2)^{-1/2}$  for electrons with velocity  $v$ .

$$|f(\theta)|^2 = \frac{d\sigma(\theta)}{d\Omega} \quad (16.2)$$

and the cross section is not well known at typical TEM voltages.

- If the crystal is ionic, do we use  $f(\theta)$  for the atom or for the ion?
- If the material is covalently bonded, how can we incorporate the bonds into our scattering model?

How we calculate  $f(\theta)$  depends on the model we use to describe the atom. You can find more details in the references at the end of the chapter, but beware, this is not an easy topic.

The simplest method is just to ignore any ionic character! If you look at Table 16.1, you'll see that if the atomic number is large enough, then the change in  $f$  caused by removing an electron may not be great. In ionic materials, we form ions by removing or adding outer electrons so the interaction of the electron beam with the nucleus is not significantly affected. However, you should remember that this argument applies only to  $f$ . We'll see in Part 4 that we can detect differences between differently bonded atoms using EELS. So, bonding does affect the electron beam.

The overall effect of the covalent, i.e., directional, component of the bonding is usually ignored. However, as you realize, all the bonds in Si, for example, are aligned along one particular type of crystallographic direction so you may indeed be able to detect some special features in the DPs.

## 16.2 STRUCTURE FACTORS: THE IDEA

In this section, we are building on Chapter 12. To keep things simple, we will illustrate the concept of the structure factor for cubic crystals. If we have a simple-cubic

crystal, then all possible values of  $\mathbf{g}$  can give a reflection in the DP. Each reciprocal-lattice point will then correspond to a possible beam. The next step will be to add the basis (i.e., the group of atoms associated with each lattice point) to the primitive lattice. Since we still have the primitive lattice, all of these points will still exist in the reciprocal lattice but the reflections will be weighted. You will find that there are three different ways to look at the situation, which in fact are all equivalent

- *Selection rules:* This is perhaps closest to physics. The structure of the crystal imposes certain selection rules which determine which beams are allowed.
- *Weights (or weighting factors):* We can assign a weight (which may be zero) to each of the points in the reciprocal lattice. This is the terminology used by Ewald. The nice feature about weighting factors is that they are analogous to scattering factors.
- *Structure factors ( $F$ ):* These are the unit-cell equivalents of the atomic-scattering amplitude,  $f(\theta)$ ; they can be thought of as unit-cell scattering amplitudes. This is the terminology favored in materials science.

There are two ways to address this topic:

- We can examine the physical idea of interference as we did in Chapters 2 and 3. This approach can give some useful guidelines to you, the experimentalist. For example, we'll see that the 200 reflection in Si should usually be absent; it should always be present, though weak, in GaAs. Similarly, in  $\text{Ni}_3\text{Al}$ , the 100 reflection is weak, but in Ni it is absent.
- Some materials have a special lattice in real space, for example, fcc or bcc lattices. In these cases, we can describe a corresponding special lattice in reciprocal space. What this means is that certain reflections are always forbidden for these particular structures; these are known as 'kinematically forbidden' reflections. (We'll see, however, that they can be present due to dynamical scattering events, and structure factors do not take any account of dynamical scattering.) The reciprocal lattice (of allowed reflections) of an fcc crystal is bcc, and vice versa.

In equation 13.1 we described the scattering from the unit cell by the expression

$$A_{\text{cell}} = \frac{e^{2\pi i k r}}{\mathbf{r}} \sum_i f_i(\theta) e^{2\pi i \mathbf{K} \cdot \mathbf{r}_i} \quad (16.3)$$

What this equation says is that the atoms within the unit cell all scatter with a phase difference given by  $2\pi i \mathbf{K} \cdot \mathbf{r}_i$  where  $\mathbf{r}_i$  is a vector which defines the location of each atom within the unit cell

$$\mathbf{r}_i = x_i \mathbf{a} + y_i \mathbf{b} + z_i \mathbf{c} \quad (16.4)$$

We'll start by considering only the case where  $\mathbf{K} = \mathbf{g}$  since this is an infinite, perfect crystal

$$\mathbf{K} = h\mathbf{a}^* + k\mathbf{b}^* + l\mathbf{c}^* \quad (16.5)$$

So we can write

$$F_{hkl} = \sum_i f_i e^{2\pi i(hx_i + ky_i + lz_i)} \quad (16.6)$$

This is our key equation; it is completely general.

This equation applies whether there is one atom or one hundred atoms in the unit cell, no matter where they are located, and it applies to all crystal lattices. What we do next is simply insert the atomic coordinates into equation 16.6 and calculate  $F_{hkl}$ .

### 16.3 SOME IMPORTANT STRUCTURES: BCC, FCC AND HCP

We will now calculate the structure factor for bcc and fcc crystals, because they illustrate the points we just made in Section 16.2 and because, as a materials scientist, you must know these results. You can regard the reciprocal lattice in two ways

- The reciprocal lattice for bcc and fcc are themselves special lattices.
- All reciprocal lattices of cubic materials are simple cubic, but some of the lattice points have a zero structure factor.

*Body-centered cubic:* The bcc structure is particularly easy. If we set the origin on one lattice point at  $(0, 0, 0)$ , the other lattice point is at  $(1/2, 1/2, 1/2)$  and we substitute these values of  $(x, y, z)$  into equation 16.6, then

$$F = f \left\{ 1 + e^{\pi i(h+k+l)} \right\} \quad (16.7)$$

Now, since  $h, k, l$  are all integers, if we define the sum  $h + k + l = N$ , then the exponential can take two values:  $+1$ , for  $N$  even, and  $-1$ , for  $N$  odd.

Thus, we can say that

- $F = 2f$  if  $h + k + l$  is even,
- $F = 0$  if  $h + k + l$  is odd.

There are **no** other possibilities. The resulting indexed bcc reciprocal lattice is shown in Figure 16.1. This lattice of allowed reflections is face-centered cubic. The reason it may not look like the familiar fcc lattice in real space is that the indices in reciprocal space must all be integers.

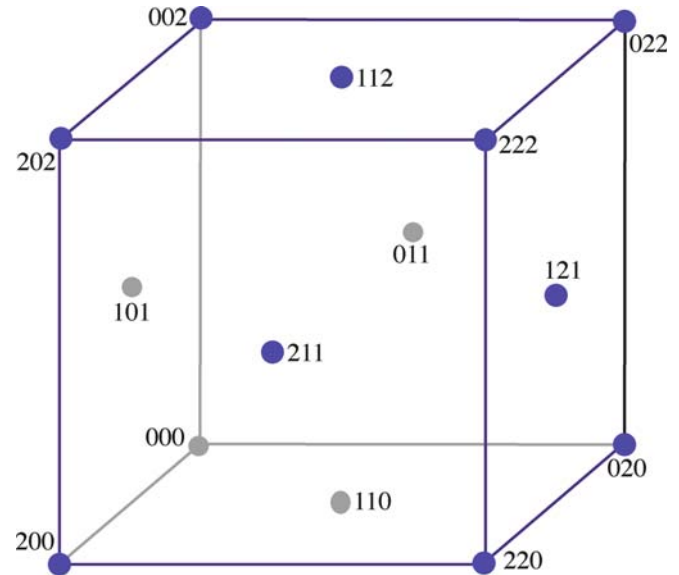


**FIGURE 16.1.** The reciprocal lattice for the bcc crystal structure. The lattice points that correspond to systematic absences have been removed, so the actual arrangement of points is an fcc lattice.

*Face-centered cubic:* If we take the same approach for the fcc structure, we now have to include four atoms in the unit cell. We can view this cell as simple cubic with a four-atom basis. The coordinates of the atoms are

$$(x, y, z) = (0, 0, 0), \left(\frac{1}{2}, \frac{1}{2}, 0\right), \left(\frac{1}{2}, 0, \frac{1}{2}\right), \left(0, \frac{1}{2}, \frac{1}{2}\right) \quad (16.8)$$

Substituting these values for  $\mathbf{r}_i$  into equation 16.6 gives

$$F = f \left\{ 1 + e^{\pi i(h+k)} + e^{\pi i(h+l)} + e^{\pi i(k+l)} \right\} \quad (16.9)$$

Again, we consider the possible values of the integers  $h, k, l$ . If all three are either odd or even, then all of the exponential terms are  $e^{2\pi i}$ . Therefore, all the phases of the diffracted waves are multiples of  $2\pi$  and are in phase. However, if one of  $h, k$ , or  $l$  is odd but the other two even, or vice versa, then two of the three phase factors will be odd multiples of  $\pi$  giving two terms of  $-1$  in equation 16.9. Therefore

- $F = 4f$  if  $h, k, l$  are all even or all odd,
- $F = 0$  if  $h, k, l$  are mixed even and odd.

The resulting lattice is shown in Figure 16.2. This time the reciprocal lattice of allowed reflections is bcc with all the indices being integers.

*Hexagonal close-packed:* Generally DPs from hcp crystals are more difficult to index for two reasons

- Except for  $(0001)$ , the patterns can be different for every material because the  $c/a$  ratio is different.

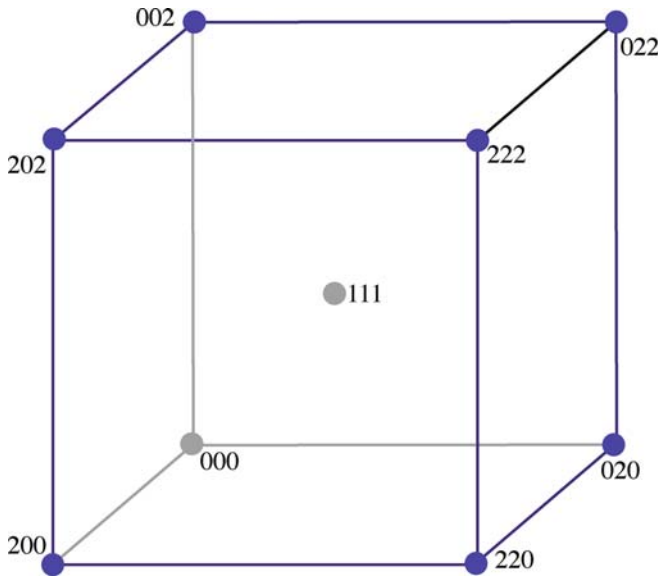


FIGURE 16.2. The reciprocal lattice for the fcc crystal structure. The lattice points that correspond to systematic absences have been removed, so the actual arrangement of points is a bcc lattice.

- We use the three-index notation to derive the structure-factor rules.
- We use the four-index Miller-Bravais notation to index the lattice planes and thus the DPs.

For the hcp structure, we only have to include two atoms in the unit cell. We can view this cell as a simple rhombohedral cell with a two-atom basis. The coordinates of the atoms are

$$(x, y, z) = (0, 0, 0), \left(\frac{1}{3}, \frac{2}{3}, \frac{1}{2}\right) \quad (16.10)$$

Substituting these values for  $\mathbf{r}_i$  into equation 16.7 gives

$$F = f \left\{ 1 + e^{2\pi i \left(\frac{h}{3} + \frac{2k}{3} + \frac{l}{2}\right)} \right\} \quad (16.11)$$

We simplify the notation by setting  $h/3 + 2k/3 + l/2 = X$ ; the complication is simply that  $X$  may be a fraction. The analysis is quite straightforward if we consider  $|F|^2$ , which is what we need in the expression for intensities. Then we can rearrange as follows.

$$|F|^2 = f^2 (1 + e^{2\pi i X})(1 + e^{-2\pi i X}) = f^2 (2 + e^{2\pi i X} + e^{-2\pi i X}) \quad (16.12)$$

$$|F|^2 = f^2 (2 + 2 \cos 2\pi X) = f^2 (4 \cos^2 \pi X) \quad (16.13)$$

Now we can write down the rules for hcp which depend mainly on whether or not  $h + 2k$  is a multiple of 3.

- $|F|^2 = 0$  if  $h + 2k = 3m$  and  $l$  is odd,
- $|F|^2 = 4f^2$  if  $h + 2k = 3m$  and  $l$  is even,
- $|F|^2 = 3f^2$  if  $h + 2k = 3m \pm 1$  and  $l$  is odd,
- $|F|^2 = f^2$  if  $h + 2k = 3m \pm 1$  and  $l$  is even.

Thus the  $11\bar{2}0$  and  $11\bar{2}6$  reflections will be strong but the  $11\bar{2}3$  reflection will be absent. Likewise  $10\bar{1}0$  and  $20\bar{2}0$  are weak but  $30\bar{3}0$  is strong. Most importantly,  $0001$  is absent. You can see that the four-index Miller-Bravais notation takes some time to master. The third index is only included to emphasize the symmetry; if the third index were not included, you might not realize that, e.g., the  $(110)$  and  $(1\bar{2}0)$  are crystallographically equivalent.

You need to know a few other expressions for this system. If you are working with hcp materials, you *must* have a copy of Frank's (1965) paper on indexing this system.

If the direction  $[uvtw]$  lies in the plane  $(hki)$ , then we can show that

$$uh + vk + ti + wl = 0 \quad (16.14)$$

The normal to the plane  $(h,k,i,l)$  is actually the Cartesian vector  $[h,k,i,l/\lambda]$ , and likewise the crystallographic direction  $[u,v,t,w]$  is actually the vector  $[u,v,t,\lambda w]$  in the Cartesian system. So using the four-index Cartesian vector notation, equation 16.14 can be written as

$$[u, v, t, \lambda w][h, k, i, l/\lambda] = 0 \quad (16.15)$$

In cubic crystals, the direction  $[hkl]$  is always normal to the plane  $(hkl)$ , but this is not the case for hcp crystals. You can show using some simple geometry that

$$\lambda^2 = \left(\frac{2}{3}\right) \left(\frac{c}{a}\right)^2 \quad (16.16)$$

Thus the Cartesian vector  $[HKIL]$ , which is normal to the plane  $(hkil)$ , is the vector

$$\left( h, k, i, \left(\frac{3}{2}\right)^{\frac{1}{2}} \left(\frac{a}{c}\right) l \right) \quad (16.17)$$

$[11\bar{2}0]$  is normal to the  $(11\bar{2}0)$  plane because  $l$  is zero but  $[01\bar{1}2]$  is not normal to the  $(01\bar{1}2)$  plane.

We can now write down an expression for the angle,  $\phi$ , between two planes  $(hkil)$  and  $(defg)$ . We use equation 16.17 to deduce the normals to the planes, then take the dot product of these two four-index vectors to deduce  $\cos \phi$  in the form

$$\cos \phi = \frac{hd + ke + \frac{1}{2}(he + kd) + \frac{3}{4}lg\left(\frac{a}{c}\right)^2}{\left\{h^2 + k^2 + hk + \frac{3}{4}l^2\left(\frac{a}{c}\right)^2\right\}^{\frac{1}{2}} \left\{d^2 + e^2 + de + \frac{3}{4}g^2\left(\frac{a}{c}\right)^2\right\}^{\frac{1}{2}}} \quad (16.18)$$

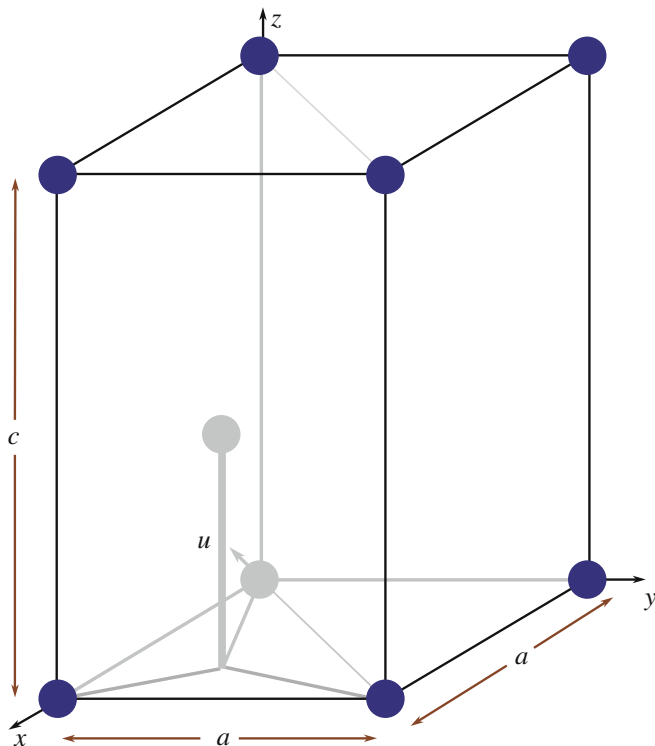


**FIGURE 16.3.** The hcp unit cell showing the four axes used in the Miller-Bravais indexing system. The three axes in the basal plane,  $x$ ,  $y$ , and  $u$ , are all crystallographically equivalent and the  $z$ -axis is normal to the basal plane.

The hcp unit cell is shown in Figure 16.3. Remember that there are three crystallographically equivalent axes  $x$ ,  $y$  and  $u$ , and that the indices of any plane can be written as  $(uviv)$  where  $i = (u + v)$ .

## 16.4 EXTENDING FCC AND HCP TO INCLUDE A BASIS

What we did in the previous section was to calculate the reciprocal lattice of a simple-cubic crystal with a basis of four atoms in fcc and two atoms in bcc. We can take this analysis one step further by starting with fcc and adding a basis. This extension both illustrates the technique and deduces structure-factor rules for three important materials.

*NaCl, GaAs, and Si:* Each of these three crystal structures is an fcc lattice with a basis. In other words, we can separate out the atoms lying on the fcc lattice and those which make up the basis.

*NaCl:* Let's locate each of the Na atoms on an fcc site; although NaCl is ionic, we'll refer to the ions as atoms since we generally do not take account of the charge on the ion.

We usually say that for every Na atom, there is a Cl atom related to it by the vector  $[1/2, 0, 0]$ . However, to emphasize the cubic symmetry, we can choose the alternate basis vector  $[1/2, 1/2, 1/2]$ . The phase factor for the

Cl atom will be the same as for the Na atom, but with an additional phase of  $\pi i(h + k + l)$ . Of course, the atomic scattering amplitudes,  $f$ , are also different for the two atoms. We can write this expression for  $F$  as

$$F = \{f_{\text{Na}} + f_{\text{Cl}}e^{\pi i(h+k+l)}\} \{1 + e^{\pi i(h+k)} + e^{\pi i(h+l)} + e^{\pi i(k+l)}\} \quad (16.19)$$

This again gives rise to some rules:

- $F = 4(f_{\text{Na}} + f_{\text{Cl}})$  if  $h, k, l$  are all even,
- $F = 4(f_{\text{Na}} - f_{\text{Cl}})$  if  $h, k, l$  are all odd,
- $F = 0$  if  $h, k, l$  are mixed.

Clearly, the third condition is the same as for any fcc structure because the factor with four terms is then zero, exactly as we deduced for fcc. You can check this if you imagine that  $f_{\text{Cl}}$  is zero. Whether the sign in  $(f_{\text{Na}} \pm f_{\text{Cl}})$  is positive or negative is the new feature. What this means in practice is that reflections with  $h, k, l$  all even will appear much more intense in the DP than those with  $h, k, l$  all odd. Look at the values given for  $f$  in Table 16.1. LiF, KCl, MgO, NiO, FeO, and ErAs all have the NaCl structure. Since they have different pairs of atomic-scattering amplitudes, the term corresponding to  $4(f_{\text{Na}} - f_{\text{Cl}})$  will be different in each case. Reflections with  $h, k$ , and  $l$  all odd are thus sensitive to the chemistry of the compound and we call them 'chemically sensitive reflections.' We will see further examples in Chapter 29 of how this sensitivity can be used in imaging.

*GaAs:* You should repeat the above exercise with the Ga located on the fcc lattice and the As related to it by the basis vector  $[1/4, 1/4, 1/4]$ . (Crystallographers will immediately note that this puts the As atom in the tetrahedron instead of the octahedron as found in NaCl.) Now the expression for  $F$  becomes (see equation 16.9 for  $F_{\text{fcc}}$ )

$$F = \{f_{\text{Ga}} + f_{\text{As}}e^{\frac{\pi i}{2}(h+k+l)}\}F_{\text{fcc}} \quad (16.20)$$

So the rules are slightly more complicated:

- $F = 0$  if  $h, k, l$  are mixed as always for fcc,
- $F = 4(f_{\text{Ga}} \pm i f_{\text{As}})$  if  $h, k, l$  are all odd,
- $F = 4(f_{\text{Ga}} - f_{\text{As}})$  if  $h, k, l$  are all even and  $h+k+l = 2N$  where  $N$  is odd (e.g., the 200 reflection),
- $F = 4(f_{\text{Ga}} + f_{\text{As}})$  if  $h, k, l$  are all even and  $h+k+l = 2N$  where  $N$  is even (e.g., the 400 reflection).

You can appreciate the difference between the 200 reflection and the 400 reflection by drawing a projection onto the (001) plane and applying the physical ideas we discussed in Chapter 11. The case where all three indices are odd is interesting. However, for this case remember that we only see intensities (i.e.,  $|F|^2$  not  $F$ ) so  $|F|^2$  is  $16(f_{\text{Ga}}^2 + f_{\text{As}}^2)$  and is independent of the

sign initially present. Of course, the structure factor is still different from the others derived here.

*Si:* Now we can easily extend this analysis to Si, Ge, or diamond. Just replace both  $f_{\text{Ga}}$  and  $f_{\text{As}}$  in our results by  $f_{\text{Si}}$ . The major change is that  $F$  is zero when  $h+k+l = 2N$  and  $N$  is odd. The best known example of this is again the 200 reflection. For Si and Ge, it has  $F = 0$ , but  $F$  is finite for GaAs.

Now for ‘hcp.’

*Wurtzite:* The wurtzite structure is to hcp what GaAs (or zinc blende) is to fcc! It is an important structure because it includes BeO, ZnO, AlN, and GaN, all of which have been widely studied. We can think of it as adding a second hcp lattice displaced by  $[1/3, 1/3, 1/8]$  or  $[0, 0, 3/8]$  relative to the first. The problem is that we now have a four-atom basis because the second atom in the hcp cell does not lie at a lattice site. This is a good exercise for Section 16.8, if you look ahead.

## 16.5 APPLYING THE BCC AND FCC ANALYSIS TO SIMPLE CUBIC

*Extending bcc to NiAl (B2):* For this material, we can easily modify the original treatment of the bcc structure, since now the centering atom is different, so NiAl is simple cubic. If we choose to place the Ni atom at  $(0, 0, 0)$  and the Al atoms at  $[1/2, 1/2, 1/2]$ , then

$$F = \left\{ f_{\text{Ni}} + f_{\text{Al}} e^{\pi i(h+k+l)} \right\} \quad (16.21)$$

This leads to two values for  $F$ , neither of which is zero.

- $F = f_{\text{Ni}} + f_{\text{Al}}$  if  $h + k + l$  is even,
- $F = f_{\text{Ni}} - f_{\text{Al}}$  if  $h + k + l$  is odd.

This would, of course, be the bcc result if  $f_{\text{Ni}}$  and  $f_{\text{Al}}$  were the same. The result of this difference is that all of the reflections for NiAl will be present in a DP because  $F$  is never zero. This result is, of course, exactly what we would expect, because NiAl really is simple cubic. Other materials with this structure include CsCl, CoGa, FeAl, and CuZn. Reflections like (100) are chemically sensitive for NiAl.

*The Cu<sub>3</sub>Au (L1<sub>2</sub>) structure:* There are many important ordered intermetallics with this structure such as Al<sub>3</sub>Li and Fe<sub>3</sub>Al. The most important is Ni<sub>3</sub>Al (because of its role in Ni-base superalloys). We can treat Ni<sub>3</sub>Al in a similar manner to NiAl. Here the Al atom sits on the  $(0, 0, 0)$  site and the three Ni atoms center the faces. The expression for  $F$  now becomes

$$F = f_{\text{Al}} + f_{\text{Ni}} \left\{ e^{\pi i(h+k)} + e^{\pi i(h+l)} + e^{\pi i(k+l)} \right\} \quad (16.22)$$

The rules for Ni<sub>3</sub>Al are

- $F = (f_{\text{Al}} + 3f_{\text{Ni}})$  if  $h, k, l$  are all even or all odd.
- $F = (f_{\text{Al}} - f_{\text{Ni}})$  if  $h, k, l$  are mixed.

Again, all of the possible reciprocal-lattice points for Ni<sub>3</sub>Al will give rise to Bragg reflections because the structure is really simple cubic. The mixed  $hkl$  reflections are now the chemically sensitive reflections. This material is particularly interesting since it can be heat-treated so as to randomize the distribution of the two elements; then each site will be occupied by 75% Ni, 25% Al, and  $F$  for mixed  $hkl$  will be zero. For this reason, reflections with mixed  $hkl$  are referred to as superlattice reflections (see Section 16.7).

## 16.6 EXTENDING HCP TO TiAl

The TiAl structure is not as well known as the previous two cases, but illustrates a similar class of materials. We noted in Section 16.4 that the two atoms in the hcp structure are not equivalent. In TiAl, we actually make them chemically distinct too. This means that the rules for hcp will be modified again. Using equation 16.11, we find that

$$F = f_{\text{Ti}} + f_{\text{Al}} e^{2\pi i\left(\frac{h}{3} + \frac{2k}{3} + \frac{l}{2}\right)} \quad (16.23)$$

The most important result is that the (0001) reflection is now allowed since  $F = f_{\text{Ti}} - f_{\text{Al}}$ . TiAl really does have a primitive hexagonal unit cell.

## 16.7 SUPERLATTICE REFLECTIONS AND IMAGING

The reciprocal lattices for Ni<sub>3</sub>Al and NiAl are shown in Figure 16.4; the small circles indicate the chemically sensitive reciprocal-lattice points. The terminology which has developed calls the chemically sensitive reflections *superlattice reflections*; the idea is that the fcc lattice is viewed as the lattice and the chemically sensitive reflections then lie on a lattice with a finer scale in reciprocal space. The chemically sensitive superlattice reflections are all forbidden in the disordered fcc structure.

Superlattice reflections are those present because the material is ordered such that the actual real-space unit cell is larger and thus the reciprocal-space cell is smaller.

For many years, these superlattice reflections were regarded as a special feature in some unusual materials. However, ordered materials, particularly the ordered intermetallics which we mentioned in Section 16.4, are finding increased uses. We will illustrate the wide variety of superlattice effects by selecting some examples.

Figure 16.5 shows an image from Cu<sub>3</sub>Au, the archetypal A<sub>3</sub>B ordered fcc structure. The crystal has been



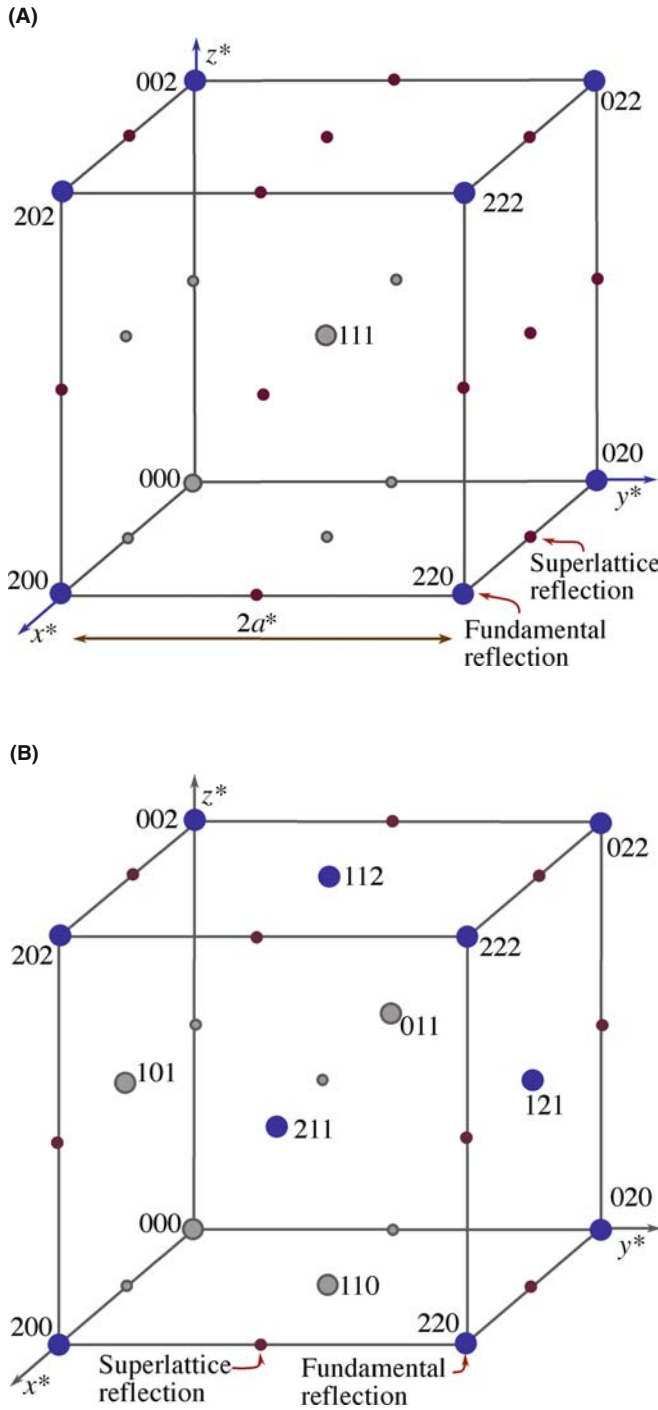


**FIGURE 16.4.** The reciprocal lattices for (A) the  $\text{Ni}_3\text{Al}$  and (B) the  $\text{NiAl}$  structures. In (A)  $\text{Ni}_3\text{Al}$  is fcc, so the fcc-forbidden reflections ( $h, k, l$  mixed even and odd) are allowed and become chemically sensitive (superlattice) reflections. In (B)  $\text{NiAl}$  is bcc, so the bcc-forbidden reflections (if  $h + k + l$  odd) are now allowed superlattice reflections.

irradiated with ions so that small regions known as cascades have been damaged just enough that the Cu and Au have been mixed up, i.e., the ordering has been destroyed locally (Jenkins et al.). The DF image has been formed using the 110 reflection, which we know is a superlattice reflection. By destroying the ordering,

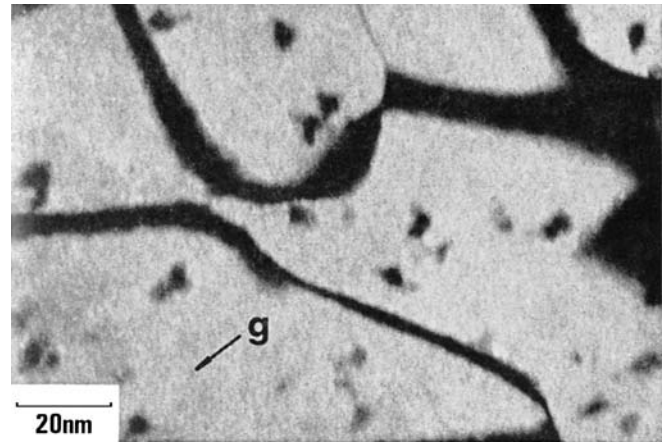


**FIGURE 16.5.** DF image from a chemically sensitive 110 reflection showing bright ordered domains in  $\text{Cu}_3\text{Au}$ . The dark areas in the bright domains are regions of local disorder induced by ion beam damage.

we ‘destroy’ the superlattice reflection for the disordered region, so the disordered region appears black when the ordered matrix appears bright. Thus, we can ‘see’ the disordered region, measure its size, etc., even though it is not diffracting electrons. The dark bands between the domains are inclined anti-phase domain boundaries (APBs), a specific kind of planar defect which we’ll examine in more detail in Section 24.6.

Figure 16.6A and B shows a 002 DF image and the corresponding DP from a  $\text{GaAs}/\text{Al}_x\text{Ga}_{1-x}\text{As}$  quantum-well structure. The  $\text{Al}_x\text{Ga}_{1-x}\text{As}$  appears lighter than the GaAs because the 002 reflection is a superlattice reflection; remember, it would be forbidden for GaAs if  $f_{\text{Ga}}$  and  $f_{\text{As}}$  were equal. The reason the  $\text{Al}_x\text{Ga}_{1-x}\text{As}$  appears lighter is that we have replaced a fraction  $x$  of the Ga atoms with the lighter Al atoms, thus increasing the difference  $f_{\text{III}} - f_{\text{V}}$ . Clearly, this is a classic example of chemically sensitive reflections. At this point we should

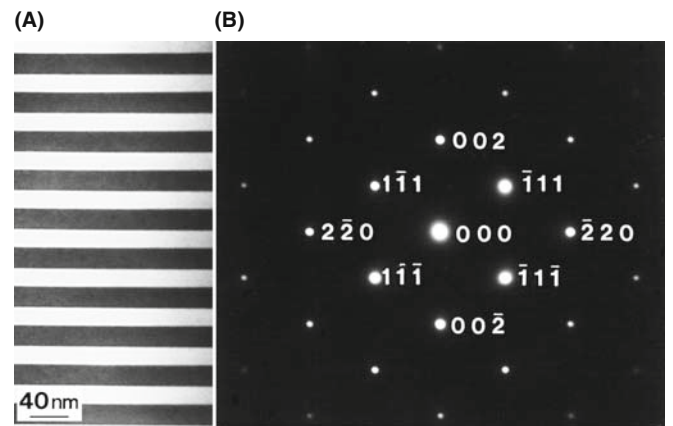


**FIGURE 16.6.** (A) DF image from a 002 chemically sensitive reflection in  $\text{GaAs}/\text{Al}_x\text{Ga}_{1-x}\text{As}$ . The  $\text{Al}_x\text{Ga}_{1-x}\text{As}$  is the lighter region because Al replaced Ga in the GaAs (darker regions). (B) DP showing the less intense 002 and other superlattice reflections.

remind you about intensities in images and DPs. The discussion we have just gone through assumes that we have a thin specimen, so that we are within the first thickness zone (i.e., the specimen is thinner than one extinction distance). In other words, be wary of trying to be quantitative about these intensities since superlattice beams are also dynamically diffracted.

Our third example is from a ceramic, vanadium carbide. The structure of VC is the same as for NaCl so we already have the rules. However, this carbide is usually non-stoichiometric, having the composition  $V_xC_y$ , where  $x > y$ . The two images and DPs shown in Figure 16.7 were taken from well-ordered  $V_6C_5$  and  $V_8C_7$  where  $1/6$  and  $1/8$  of the carbon sites are not occupied by C: we say these sites are occupied by vacancies and the vacancies have formed ordered arrays. Clearly since we only have four atoms of each element in the unit cell, the vacancies must be distributed over more than one cell so the new lattice parameter must be greater than the lattice parameter ( $a$ ) of the VC fcc lattice. So, we expect to see extra spots that are closer to the origin than (001). This is the case in both patterns shown here. The ordering actually destroys the cubic

symmetry, so we have several orientations of the ordered carbides that are related to one another by the way they break the symmetry. By forming DF images, we can identify which region of the specimen corresponds to which variant (Dodsworth et al.).

## 16.8 DIFFRACTION FROM LONG-PERIOD SUPERLATTICES

In the previous section, the atoms or vacancies in the different structures essentially arranged themselves to increase the lattice parameter and therefore give rise to superlattice reflections. In this section, we will discuss several examples where either we (or nature) have arranged the materials to give much larger superlattices. We will begin by considering the image and DP shown in Figure 16.8, which are from an artificial  $GaAs/Al_xGa_{1-x}As$  superlattice. The superlattice is created chemically by changing from four layers of GaAs to four of  $(Al_xGa_{1-x})As$ . So we see a series of three closely spaced extra spots in the DP which correspond to the new long lattice parameter in real space.

Another example is shown in Figure 16.9. This is a very long period ( $\sim 10$  nm) artificial superlattice of alternating layers of Si and Mo. The extra reflections are very close and are not as useful as they were in Figure 16.6, but they do allow us to check the periodicity of the real-space structure very easily and quickly and without needing to use HRTEM (Chapter 28). This can be useful, particularly for artificially grown superlattices, since the superlattice periodicity is ‘internally calibrated’ in the DP by the lattice spacing of the material. (Remember that, for comparison, the magnification of a TEM image is usually subject to a  $\pm 10\%$  uncertainty.)

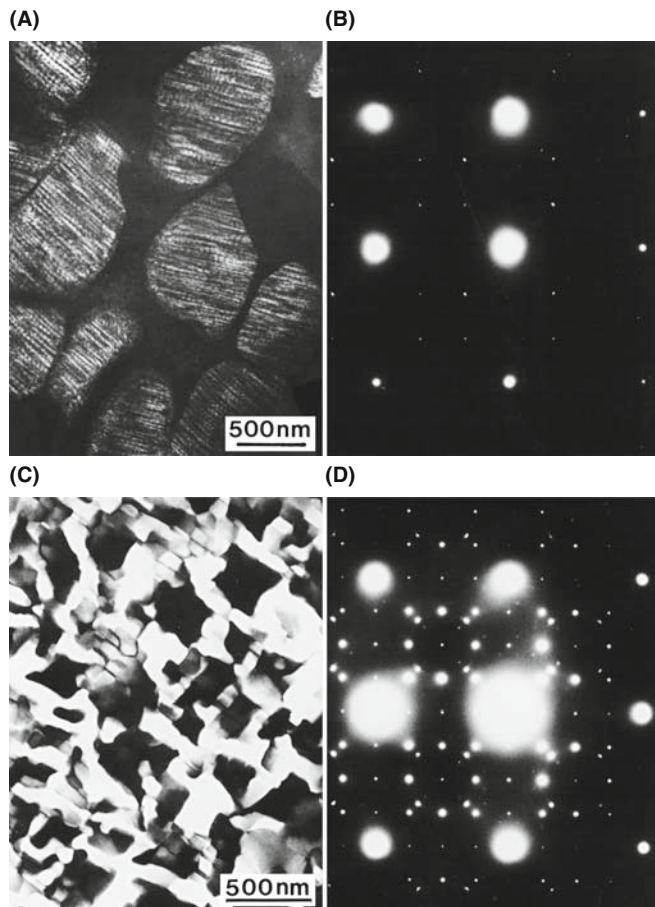


**FIGURE 16.7.** (A) DF image of ordered  $V_6C_5$  and (B) accompanying DP. (C) DF image of  $V_8C_7$  and (D) DP. In both carbides the ordering is due to vacancies on the C sublattice.

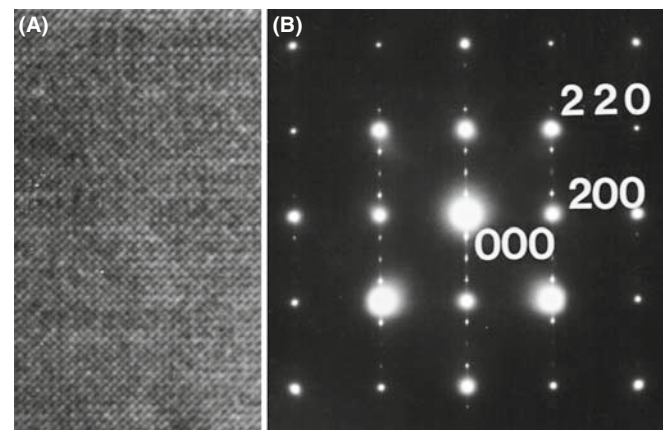


**FIGURE 16.8.** (A)  $GaAs/Al_xGa_{1-x}As$  structure in which order is created by alternating four layers of GaAs and four of  $(Al_xGa_{1-x})As$ . (B) DP showing three superlattice spots between the fundamental reflections in the 020 direction.

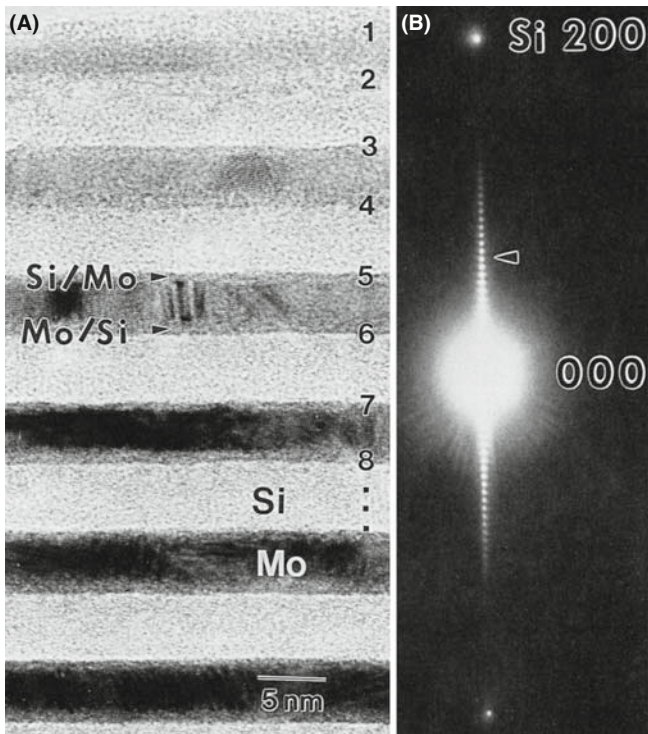


**FIGURE 16.9.** (A) Artificial superlattice of Si and Mo layers ~5 nm thick. (B) Expanded DP around 000 showing many superlattice spots (arrowed). The large spacing of the superlattice in real space results in very small spacing of the superlattice reflections in the DP in reciprocal space. Compare with Figure 16.8.

### 16.9 FORBIDDEN REFLECTIONS

We mentioned in Section 16.2 that certain reflections are always forbidden for some structures because they have  $F = 0$ . They are known as kinematically forbidden reflections, because such reflections can sometimes actually be present due to dynamical scattering events. This process is illustrated in Figure 16.10. The DP is the [011] pattern in Si so that the 200 reflection should be absent according to Section 16.4. The reason it is usually present is that, since we are oriented at the zone axis, the  $11\bar{1}$  beam, which has  $F \neq 0$ , acts like a new incident beam and is rediffracted by the  $(1\bar{1}1)$  plane. The result is that we appear to excite the 200 reflection since

$$(11\bar{1}) + (1\bar{1}1) = (200) \quad (16.24)$$

From this example, you can appreciate the use of the phrase ‘kinematically forbidden.’

### 16.10 USING THE INTERNATIONAL TABLES

As long as you work with fcc or bcc metals or the other special structures listed here, you can use the simple rules derived in this chapter. Once you venture further,

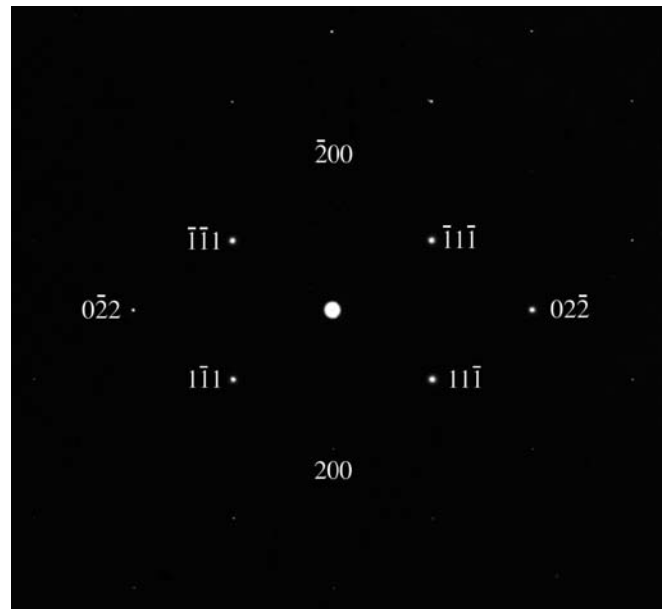


**FIGURE 16.10.** The [011] DP from Si. The 200 reflection is forbidden, but it is present because the allowed  $11\bar{1}$  diffracted beam acts like a new incident beam and is rediffracted by the  $(1\bar{1}1)$  plane. The sum of the two allowed reflections  $(11\bar{1}) + (1\bar{1}1)$  results in a 200 reflection, which is so weak you may not see it.

you should quickly become familiar with the International Tables for Crystallography (Hahn), in particular with the introductory booklet. You must know the crystal structure of your material; if not, you will in principle be able to determine it after studying Chapter 21. If, for example, you were working with  $\alpha\text{-Al}_2\text{O}_3$ , you

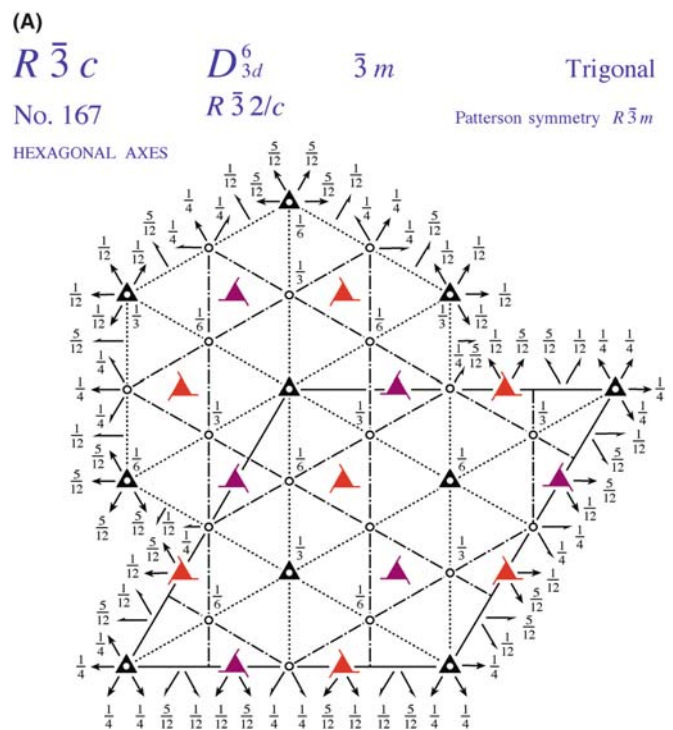


**FIGURE 16.11.** (continued).



would know that the space group is  $R\bar{3}c$  or No. 167. Looking this up in the International Tables, you would find the information shown in Figure 16.11A. In this case, you'd have to decide whether you want to use rhombohedral axes or hexagonal axes; you'll notice that there are three times as many atoms in the hexagonal cell. The tables in Figure 16.11B tell you which

reflections are allowed, although you can work out or look up the values of  $F$  if you want them. You know the chemical formula of your material, but you still need to know which sites are occupied. Look up the positions from X-ray diffraction data. The paper by Lee and Lagerlof summarizes the analysis for this particular example.

(B)

### Positions

Multiplicity,  
Wyckoff letter,  
Site symmetry

### Coordinates

(0,0,0)+       $(\frac{2}{3}, \frac{1}{3}, \frac{1}{3})+$        $(\frac{1}{3}, \frac{2}{3}, \frac{2}{3})+$

36	<i>f</i>	1	(1) $x, y, z$	(2) $\bar{y}, x-y, z$	(3) $\bar{x}+y, \bar{x}, z$
			(4) $y, x, \bar{z}+\frac{1}{2}$	(5) $x-y, \bar{y}, \bar{z}+\frac{1}{2}$	(6) $\bar{x}, \bar{x}+y, \bar{z}+\frac{1}{2}$
			(7) $\bar{x}, \bar{y}, \bar{z}$	(8) $y, \bar{x}+y, \bar{z}$	(9) $x-y, x, \bar{z}$
			(10) $\bar{y}, \bar{x}, z+\frac{1}{2}$	(11) $\bar{x}+y, y, z+\frac{1}{2}$	(12) $x, x-y, z+\frac{1}{2}$

18	<i>e</i>	.2	$x, 0, \frac{1}{4}$	$0, x, \frac{1}{4}$	$\bar{x}, \bar{x}, \frac{1}{4}$	$\bar{x}, 0, \frac{3}{4}$	$0, \bar{x}, \frac{3}{4}$	$x, x, \frac{3}{4}$
18	<i>d</i>	$\bar{1}$	$\frac{1}{2}, 0, 0$	$0, \frac{1}{2}, 0$	$\frac{1}{2}, \frac{1}{2}, 0$	$0, \frac{1}{2}, \frac{1}{2}$	$\frac{1}{2}, 0, \frac{1}{2}$	$\frac{1}{2}, \frac{1}{2}, \frac{1}{2}$
12	<i>c</i>	3.	$0, 0, z$	$0, 0, \bar{z}+\frac{1}{2}$	$0, 0, \bar{z}$	$0, 0, z+\frac{1}{2}$		
6	<i>b</i>	$\bar{3}$ .	$0, 0, 0$	$0, 0, \frac{1}{2}$				
6	<i>a</i>	32	$0, 0, \frac{1}{4}$	$0, 0, \frac{3}{4}$				

### Positions

Multiplicity,  
Wyckoff letter,  
Site symmetry

### Coordinates

12	<i>f</i>	1	(1) $x, y, z$	(2) $z, x, y$	(3) $y, z, x$
			(4) $\bar{y}+\frac{1}{2}, \bar{x}+\frac{1}{2}, \bar{z}+\frac{1}{2}$	(5) $\bar{x}+\frac{1}{2}, \bar{z}+\frac{1}{2}, \bar{y}+\frac{1}{2}$	(6) $\bar{z}+\frac{1}{2}, \bar{y}+\frac{1}{2}, \bar{x}+\frac{1}{2}$
			(7) $\bar{x}, \bar{y}, \bar{z}$	(8) $\bar{z}, \bar{x}, \bar{y}$	(9) $\bar{y}, \bar{z}, \bar{x}$
			(10) $y+\frac{1}{2}, x+\frac{1}{2}, z+\frac{1}{2}$	(11) $x+\frac{1}{2}, z+\frac{1}{2}, y+\frac{1}{2}$	(12) $z+\frac{1}{2}, y+\frac{1}{2}, x+\frac{1}{2}$

6	<i>e</i>	.2	$x, \bar{x}+\frac{1}{2}, \frac{1}{4}$	$\frac{1}{4}, x, \bar{x}+\frac{1}{2}$	$\bar{x}+\frac{1}{2}, \frac{1}{4}, x$
			$\bar{x}, x+\frac{1}{2}, \frac{3}{4}$	$\frac{3}{4}, \bar{x}, x+\frac{1}{2}$	$x+\frac{1}{2}, \frac{3}{4}, \bar{x}$
6	<i>d</i>	$\bar{1}$	$\frac{1}{2}, 0, 0$	$0, \frac{1}{2}, 0$	$0, 0, \frac{1}{2}$
			$\frac{1}{2}, 0, \frac{1}{2}$	$0, \frac{1}{2}, \frac{1}{2}$	$\frac{1}{2}, \frac{1}{2}, 0$
4	<i>c</i>	3.	$x, x, x$	$\bar{x}+\frac{1}{2}, \bar{x}+\frac{1}{2}, \bar{x}+\frac{1}{2}$	$\bar{x}, \bar{x}, \bar{x}$
			$x+\frac{1}{2}, x+\frac{1}{2}, x+\frac{1}{2}$		
2	<i>b</i>	$\bar{3}$ .	$0, 0, 0$	$\frac{1}{2}, \frac{1}{2}, \frac{1}{2}$	
2	<i>a</i>	32	$\frac{1}{4}, \frac{1}{4}, \frac{1}{4}$	$\frac{3}{4}, \frac{3}{4}, \frac{3}{4}$	

### Reflection conditions

#### General:

$$\begin{aligned} hkl : -h+k+l &= 3n \\ hki0 : -h+k &= 3n \\ hh\bar{2}hl : l &= 3n \\ h\bar{h}0l : h+l &= 3n, l = 2n \\ 000l : l &= 6n \\ h\bar{h}00 : h &= 3n \end{aligned}$$

#### Special:

as above, plus  
no extra conditions

$$\begin{aligned} hkil : l &= 2n \\ hkil : l &= 2n \\ hkil : l &= 2n \\ hkil : l &= 2n \end{aligned}$$

### Reflection conditions

#### General:

$$\begin{aligned} hhl : l &= 2n \\ hhh : h &= 2n \end{aligned}$$

#### Special:

as above, plus  
no extra conditions

$$\begin{aligned} hkl : h+k+l &= 2n \\ hkl : h+k+l &= 2n \\ hkl : h+k+l &= 2n \\ hkl : h+k+l &= 2n \end{aligned}$$

FIGURE 16.11. (A) Symmetry information, as given in the International Tables for trigonal  $\alpha$ - $\text{Al}_2\text{O}_3$ , with space group  $R\bar{3}c$  (No. 167), showing the two possible unit cells based on the rhombohedral and hexagonal cells. The symmetry elements at specific lattice points are also indicated. (B) The atomic positions for the two choices of unit cells in (A).

That was the traditional approach. Now, you should have access to EMS or Crystal Kit. Alternatively, use jEMS over the WWW (Section 1.6). In all

these software packages you can just type in your space group or pull down a menu to find the structure-factor information.

## CHAPTER SUMMARY

When we introduced the primitive lattice at the beginning of this chapter, we only considered the lattice sites which actually define the unit cell. If there are other lattice points, these would give us the Bravais lattices. We will conclude by summarizing some of the selection rules for the different structures in Table 16.2

**TABLE 16.2 Examples of Selection Rules for Several Crystal Structures.  $F$  is the Structure Factor**

Crystal type	Reflection present for	$F$	No. of lattice points per cell
Primitive	Any $h, k, l$	$f$	1
Body centered	$(h + k + l) = 2n$	$2f$	2
Face centered including GaAs and NaCl	$h, k$ and $l$ all odd or all even	$4f$	4
Diamond	As fcc but if all even and $h + k + l \neq 4n$ then absent, anyway		
Base centered	$h, k$ and $l$ all odd or all even	$2f$	2
Hexagonal close-packed	$h + 2k = 3n$ with $l$ odd	0	0001
	$h + 2k = 3n$ with $l$ even	$2f$	0002
	$h + 2k = 3n \pm 1$ with $l$ odd	$f3$	0111
	$h + 2k = 3n \pm 1$ with $l$ even	$f$	0110

In practice, it will become important that you simply *know* some of the DPs for your material. You can, however, look up these patterns in some of the textbooks listed in Chapter 1, but the best sources are the texts by Andrews et al. and Edington; we reproduce some of them in Figures 18.17–18.19. Alternatively, software (e.g., jEMS) available on the WWW (Section 1.5) will print out standard spot patterns of most important crystal structures. When you're sitting at the TEM, you don't have time to index a pattern from first principles and then decide whether or not you are at a pole that contains the reflection you want to use. To do this you'll have to be able to index the DPs and determine the beam direction, which we'll describe in detail in Chapter 18.

## REFERENCES

Examples of indexed DPs are given in the texts by Edington and Andrews et al. As usual, we recommend your checking the books by Kelly and Groves, Cullity.

### DPs and Crystal Data

- Andrews, KW, Dyson, DJ and Keown, SR (1971) *Interpretation of Electron Diffraction Patterns* 2nd Ed. Plenum Press New York. Stereographic projections, angles, spacings, and much more.
- Massalski, T, Okamoto, H, Subramanian, PR and Kacprzak, L (Eds.) (1990) *Binary Alloy Phase Diagrams* 2nd Ed. ASM International Materials Park OH. Appendix A1 gives a complete list of the Pearson Symbols ( $L1_2$ , etc.) with their space group and Strukturbericht designation.
- Misell, DL and Brown, EB (1987) *Electron Diffraction: An Introduction for Biologists*, Volume 12 of the series *Practical Methods in Electron Microscopy* Ed. AM Glauert Elsevier New York. Materials science students should not be put off by the title: this is an invaluable practical guide to indexing DPs and more.



## SOME CRYSTALLOGRAPHY

- Dodsworth, J, Kohlstedt, DL and Carter, CB 1983 *Grain Boundaries in Transition Metal Carbides* Adv. Ceram. **6** 102–109.
- Frank, FC 1965 *On Miller-Bravais Indices and Four-Dimensional Vectors* Acta Cryst. **18** 862–866. A favorite.
- Hahn, T 1988 *International Tables for Crystallography. Brief teaching edition of volume A, space-group symmetry*, Kluwer Academic Publishers Dordrecht Netherlands.
- Ibers, JA 1957 *New Atomic Form Factors for Beryllium and Boron* Acta Cryst. **10** 86. One page.
- Jenkins, ML, Katerbau, K-H and Wilkens, M 1976 *Transmission Electron Microscopy Studies of Displacement Cascades in Cu<sub>3</sub>Au* Phil. Mag. **34** 1141–1153.
- Lee, WE and Lagerlof, KPD 1985 *Structural and Electron Diffraction Data for Sapphire ( $\alpha$ -Al<sub>2</sub>O<sub>3</sub>)* J. Electron Microsc. Tech. **2** 247–258.

## THE COMPANION TEXT

You'll find jEMS useful for simulating DPs.

## SELF-ASSESSMENT QUESTIONS

- Q16.1 What is the key assumption that is made in the amplitude calculation in this chapter?
- Q16.2 Give one reason why DP selection rules are sometimes broken.
- Q16.3 In a bcc Fe specimen, will any kinematically forbidden reflections occur in the DP?
- Q16.4 In a bcc specimen, is the 110 reflection allowed?
- Q16.5 In fcc, will you see the 111 and/or 100 reflections?
- Q16.6 In NaCl, which *hkl* reflections are chemically sensitive?
- Q16.7 In GaAs, which reflections are forbidden?
- Q16.8 When determining if a reflection is forbidden or allowed, need we only consider the structure factor, *F*?
- Q16.9 If a material is very well ordered, what does it mean to have formed a superlattice in the DP?
- Q16.10 List some advantages in determining superlattice spacings from a DP rather than an image.
- Q16.11 Why is the 200 reflection of Si seen in Figure 16.9?
- Q16.12 Why are hcp DPs more difficult to index than cubic DPs?
- Q16.13 Explain the concept of structure factor in words?
- Q16.14 What two things should you keep in mind when looking up tabulated values of the atomic scattering factor?
- Q16.15 In Figure 16.8, what is the true periodicity in the [020] direction?
- Q16.16 What do we mean by the term 'chemically sensitive reflection'? Give two examples.
- Q16.17 When is it particularly important to use the International Tables?
- Q16.18 Why does the uncertainty in *f* values not usually affect our analysis of DPs?
- Q16.19 Why are *f* values not precisely known?
- Q16.20 Give the general equation for the structure factor.
- Q16.21 Write down the structure factor rules for a bcc crystal and describe the reciprocal lattice.
- Q16.22 Write down the structure factor rules for an fcc crystal and describe the reciprocal lattice.
- Q16.23 Write down the structure factor rules for an hcp crystal. Can you describe the reciprocal lattice?
- Q16.24 What is the Cartesian vector which is normal to the plane (*hkl*)?
- Q16.25 How many atoms are needed (minimum number) to calculate the structure factor for simple cubic, fcc, bcc and hcp structures?
- Q16.26 How do the structures of NaCl and NiAl differ?
- Q16.27 In Figure 16.5, why can we see the ordered domains but not the disordered domains?
- Q16.28 In Figure 16.6, why is the Al<sub>x</sub>Ga<sub>1-x</sub>As region brighter than the GaAs region?
- Q16.29 In Figure 16.7, why is the symmetry of the two DPs changed?
- Q16.30 In Figure 16.8, why are there rows of fainter spots between bright spots?
- Q16.31 In Figure 16.9, why can we see superlattice reflections even though half the material is amorphous?
- Q16.32 If the crystal is ionic, do we use *f* for the atom or for the ion?
- Q16.33 What is a basis?
- Q16.34 Describe three equivalent descriptions of systematic absences in crystals.
- Q16.35 How can you easily distinguish GaAs from Si given two (001) DPs?
- Q16.36 Why didn't we see superlattice spots in the DP in Figure 16.6B?

## TEXT-SPECIFIC QUESTIONS

- T16.1 Starting with the fcc case, deduce the structure factor rules for NaCl.
- T16.2 Deduce the structure factor rules for NiAl.

- T16.3 Consider Figure 16.6. Draw a schematic of the DP. Index all the remaining reflections. Look at the 002 row of reflections; indicate the location of the extra reflections which should be present due to the superlattice. Justify your answer.
- T16.4 Sketch the DP shown in Figure 16.10 with a box as large as that shown in this figure. Add all the other reflections you would expect to see. Justify your answer.
- T16.5 Look at Figure 16.9. Explain all the contrast features you see in this image (after you've read Part 3).
- T16.6 Using Figure 16.11, explain which positions are occupied in both the rhombohedral and hexagonal cells for  $\text{Al}_2\text{O}_3$ . Neglecting the possibility of dynamical scattering, explain why you will, or will not, see the 0001,  $1\bar{1}00$  and/or  $11\bar{2}0$  reflections. Will you see the 112, 111 and/or 100 reflections?
- T16.7 A simple orthorhombic lattice has the following lattice constants:  $a = 0.30$  nm;  $b = 0.40$  nm;  $c = 0.50$  nm. Draw the DP when a crystal is observed along the [100], [010] and [001] directions, respectively. The DPs should be drawn in the same scale. *NB*: There are no 'forbidden' reflections in this structure. (Courtesy Anders Thølen.)
- T16.8 The alloy  $\text{CuAu}_3$  has an ordered structure. What does the DP look like when the crystal is viewed along the [110] direction? (Courtesy Anders Thølen.)
- T16.9 Electron diffraction from a powder material gives a ring pattern. When the incoming beam is tilted an angle  $\theta$  relative to the optical axis the ring pattern moves. Calculate the angle  $\theta$  the incoming beam has been tilted when the center of the DP is moved so it falls on the {222} ring of the original pattern. The material is Pt (fcc) with a lattice constant 0.392 nm. The acceleration voltage is 100 kV. (Courtesy Anders Thølen.)
- T16.10 What reflections would you expect to observe in an electron DP(s) from a c-centered monoclinic cell? (Courtesy Lucille Giannuzzi.)
- T16.11 The unit cell of a crystal of  $\text{Ti}_2\text{Nb}_{10}\text{O}_{29}$  is orthorhombic (space group *Amma*) with  $a = 28.5$  Å,  $b = 3.8$  Å,  $c = 20.5$  Å. The DP of 1a is from one of the principal axis patterns. Give the Miller indices for this pattern. The pattern 1b is from a slightly tilted crystal. Find the tilt axis, tilt angle and the excitation error from the spot circled. A further tilt of the crystal gave the pattern of 1c printed to the same scale. What is the Miller index of the spot arrowed? ( $\lambda = 0.037$  Å) (See J. Appl. Phys. **42** 5891.) (Courtesy John Spence.)
- T16.12  $\text{LaMnO}_3$  has a perovskite structure shown below. Calculate the structure factors for {110}, {100}, {200} and {220} in terms of the atomic-scattering factors (such as  $f_{\text{La}}$ ,  $f_{\text{Mn}}$ ,  $f_{\text{O}}$ ). (A) Use the size of the spot to represent the intensity, sketch the [001] DP of this structure. (B) Index the first eight diffraction spots. (Courtesy ZL Wang.)
- T16.13 A ternary phase has the following atoms in a cubic unit cell: A at (0,0,0), B at (1/2, 1/2,0) and C at (1/2,0,1/2), (0,1/2,1/2). Calculate the following structure factors in terms of  $f_A$ ,  $f_B$  and  $f_C$ : (a) (001) and (010) and (b) (100) and (200). (Courtesy ZL Wang.)
- T16.14 A ternary alloy ( $\text{A}_2\text{BC}$ ) has the fcc structure shown in (a) below at elevated temperatures. As the temperature is lowered, all the C atoms go to the corners of the lattice while the A and B atoms randomly occupy the face centers, as shown in (b). At still lower temperatures, the B atoms occupy the (1/2,1/2,0) sites, indicated in (c). Sketch the [100] DPs for each of these structures, plotting the positions and relative intensities of the different reflections. (Courtesy ZL Wang.)
- T16.15 Consider a face-centered orthorhombic lattice. By means of the definition of the reciprocal lattice, obtain expressions for the three basic vectors of the reciprocal lattice of this real-space lattice, in terms of the vectors **a**, **b** and **c**. (Courtesy ZL Wang.)
- T16.16 A phase in the Fe-C-Al system has the following structure: Al at (0,0,0), Fe at (1/2,1/2,0), (1/2,0,1/2), (0,1/2,1/2) and C at (1/2, 1/2,1/2). The atomic-scattering factors for the three elements are shown in the plot below. (a) Derive the expression for the structure factor in terms of  $f_{\text{Al}}$ ,  $f_{\text{Fe}}$  and  $f_{\text{C}}$ . (b) Calculate the relative intensity ratios for the following reflection in the DP: (i)  $I_{(001)}/I_{(002)}$  and (ii)  $I_{(011)}/I_{(002)}$ . (c) Sketch and index the [100] DP of this phase. (Courtesy ZL Wang.)

# Diffraction from Small Volumes

## CHAPTER PREVIEW

A very important concept in TEM is that we only ever diffract from small volumes. These volumes are now called nanoparticles, nanograins, nanobelts, etc. By definition, no TEM specimen is infinite in all directions and all defects are small. Of course, the beam is also never infinitely wide! This chapter therefore discusses how the size of what we are examining influences the appearance of the DP. Although we will discuss many different aspects of diffraction, there are three important ideas that underlie all this discussion

- We are diffracting from small volumes.
- We are diffracting from crystals.
- We need to index the DPs we see and relate the patterns to the image.

The fact that it is possible to obtain diffraction from several planes in a zone at the same time is due to the effect of the specimen shape on the diffracted-intensity distribution. The diffraction spot is only a mathematical point if the specimen is perfect and infinite in all directions. For example, a TEM specimen is effectively infinite ( $\sim 3$  mm) relative to the unit-cell dimensions in the plane of the specimen, but very thin ( $< 0.5$   $\mu\text{m}$ ) parallel to the electron beam. This means that the diffracted intensity can be represented in the reciprocal lattice as a relrod (see Chapter 12) stretched parallel to the electron beam in reciprocal space, rather than as a point, and the relrod does have a width. Therefore, over a range of angles, the Ewald sphere will still intercept the relrod and diffracted intensity will still be generated. This is equivalent to saying that the Laue condition is relaxed in one dimension in the TEM owing to the specimen shape. For this reason, accurate structural analysis of unknown specimens is very difficult in conventional TEM diffraction, and X-rays are usually the most accurate method for structure determination if your specimen is large. However, we will reconsider this statement in Chapter 21.

## 17.1 INTRODUCTION

In Chapter 12, we stated that each point in the reciprocal lattice can actually be associated with a rod. This construction allowed us to discuss the geometry of DPs, taking account of the experimental fact that we see spots in the DP even when  $\mathbf{s}$  is not exactly zero. In fact, without this construction, there is no reason to discuss  $\mathbf{s}$ . Now we are going to show quantitatively why we have rods. As we suggested earlier, the reason is that we have a thin specimen: a small thickness in real space gives a large length in reciprocal space. This concept is valid in all directions, not just parallel to the electron beam. Hence, we call this the ‘shape effect.’ The intensity in the diffracted beam is strongest for a given thickness

when  $\mathbf{K} = \mathbf{g}$ , but we still have intensity when  $\mathbf{K}$  is not exactly equal to  $\mathbf{g}$ , or when

$$\mathbf{K} = \mathbf{g} + \mathbf{s} \quad (17.1)$$

Then we can write, from equation 13.48

$$|\phi_{\mathbf{g}}|^2 = \left(\frac{\pi t}{\xi_{\mathbf{g}}}\right)^2 \cdot \frac{\sin^2(\pi t s_{\text{eff}})}{(\pi t s_{\text{eff}})^2} \quad (17.2)$$

We model the specimen as a thin rectangular slab as shown in Figure 17.1. To keep the math simple, we will assume that we have a rectangular unit cell with sides  $a$ ,  $b$ ,  $c$  and that there are  $N_x$  cells in the  $x$  direction,  $N_y$  in

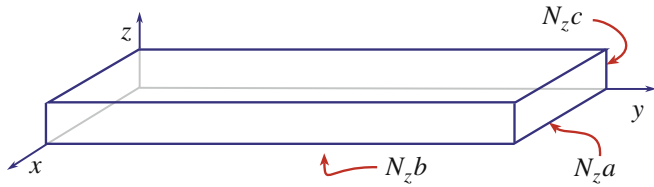


**FIGURE 17.1.** An idealized thin-foil specimen modeled as a rectangular slab made up of rectangular unit cells of sides  $a, b, c$ . There are  $N_x$  cells in the  $x$  direction,  $N_y$  in the  $y$  direction and  $N_z$  in the  $z$  direction.

the  $y$  direction and  $N_z$  in the  $z$  direction. All that we have to do to determine the total diffracted amplitude is to add the amplitudes from each cell, allowing for the phase factor that is present, because the cells are displaced from one another. Each cell has the same structure factor  $F$ .

We can do the addition of amplitudes in two ways. The first way is to do the summation. In the second, we will show how the same result follows if you start with the integral expression for  $\phi_g$ . These expressions lead to the important idea of a relrod and subsidiary maxima; in DPs we can see the effects of the relrods, but you may never see the subsidiary maxima.

What we are going to do is derive equations for the shape of the relrods which were introduced in Section 12.5 and which we used in Chapter 13 to explain why we ‘see’ spots in the DP even when  $s \neq 0$ . This whole approach gives us a pictorial aid to understanding diffraction from small volumes. After developing the theory for the simple case, we will go on to discuss the complications introduced because we look at real materials, and specimens of real materials are usually not flat platelets.

### 17.1.A The Summation Approach

This approach starts with expressing the total amplitude,  $A$ , of the diffracted beam as the sum of contributions from all the individual cells in a parallel-sided specimen. (Note: this is a kinematical approach and ignores dynamical scattering.)

$$A = F \sum_{n_x} e^{i2\pi n_x \mathbf{K} \cdot \mathbf{a}} \sum_{n_y} e^{i2\pi n_y \mathbf{K} \cdot \mathbf{b}} \sum_{n_z} e^{i2\pi n_z \mathbf{K} \cdot \mathbf{c}} \quad (17.3)$$

Here  $n_x, n_y$  and  $n_z$  have their usual meanings and all are integers; we have  $N_x \times N_y \times N_z$  cells in the specimen. As shown in Figure 17.1, we will let  $n_x$  vary from 0 to  $N_x - 1$  and similarly with  $n_y$  and  $n_z$ . The location of each unit cell is then defined by the vector  $\mathbf{r}_n$

$$\mathbf{r}_n = n_x \mathbf{a} + n_y \mathbf{b} + n_z \mathbf{c} \quad (17.4)$$

To simplify the first summation we set  $X$  equal to  $e^{i2\pi \mathbf{K} \cdot \mathbf{a}}$ . Then each separate summation term is a geometric series, so we can sum the  $n_x$  series as

$$\begin{aligned} S &= \sum_{n_x=0}^{n_x=N_x-1} X^n = X^0 + X^1 + \dots + X^{N_x-1} \\ SX &= X^1 + X^2 + \dots + X^{N_x} = X^{N_x} - X^0 + S \\ S &= \frac{1 - X^{N_x}}{1 - X} \end{aligned} \quad (17.5)$$

Now replace  $X$  by  $e^{i2\pi \mathbf{K} \cdot \mathbf{a}}$  to find the sum.

$$\sum_{n_x=0}^{n_x=N_x-1} e^{i2\pi n_x \mathbf{K} \cdot \mathbf{a}} = \frac{1 - e^{i2\pi N_x \mathbf{K} \cdot \mathbf{a}}}{1 - e^{i2\pi \mathbf{K} \cdot \mathbf{a}}} \quad (17.6)$$

Since we are interested in the intensities, we multiply this sum by its complex conjugate. To do this we use some simple trigonometric relationships

$$\begin{aligned} (1 - e^{-i\alpha})(1 - e^{i\alpha}) &= (1 - \cos\alpha + i\sin\alpha)(1 - \cos\alpha - i\sin\alpha) \\ &= (1 - 2\cos\alpha + \cos^2\alpha) + \sin^2\alpha = 2(1 - \cos\alpha) = 4\sin^2\frac{\alpha}{2} \end{aligned} \quad (17.7a)$$

or

$$(1 - e^{-i\alpha})(1 - e^{i\alpha}) = 4 \left( \frac{e^{i\frac{\alpha}{2}} - e^{-i\frac{\alpha}{2}}}{2} \right) \left( \frac{e^{-i\frac{\alpha}{2}} - e^{i\frac{\alpha}{2}}}{2} \right) \quad (17.7b)$$

The intensity is then related to

$$\left| \sum_{n_x=0}^{n_x=N_x-1} e^{i2\pi n_x \mathbf{K} \cdot \mathbf{a}} \right|^2 = \frac{(1 - e^{-i2\pi N_x \mathbf{K} \cdot \mathbf{a}})(1 - e^{i2\pi N_x \mathbf{K} \cdot \mathbf{a}})}{(1 - e^{-i2\pi \mathbf{K} \cdot \mathbf{a}})(1 - e^{i2\pi \mathbf{K} \cdot \mathbf{a}})} \quad (17.8a)$$

or

$$\left| \sum_{n_x=0}^{n_x=N_x-1} e^{i2\pi n_x \mathbf{K} \cdot \mathbf{a}} \right|^2 = \frac{4 \sin^2(\pi N_x \mathbf{K} \cdot \mathbf{a})}{4 \sin^2(\pi \mathbf{K} \cdot \mathbf{a})} \quad (17.8b)$$

Then we can write

$$\begin{aligned} I &= |A|^2 = |F|^2 \left( \frac{\sin^2(\pi N_x \mathbf{K} \cdot \mathbf{a})}{\sin^2(\pi \mathbf{K} \cdot \mathbf{a})} \right) \\ &\quad \left( \frac{\sin^2(\pi N_y \mathbf{K} \cdot \mathbf{b})}{\sin^2(\pi \mathbf{K} \cdot \mathbf{b})} \right) \left( \frac{\sin^2(\pi N_z \mathbf{K} \cdot \mathbf{c})}{\sin^2(\pi \mathbf{K} \cdot \mathbf{c})} \right) \end{aligned} \quad (17.9)$$

If the dot product  $\mathbf{K} \cdot \mathbf{a}$  is an integer, then the first of these terms is unity. This is, of course, the Bragg condition and the intensity is then a maximum. There are also subsidiary maxima or minima when

$$\pi N_x \mathbf{K} \cdot \mathbf{a} = \frac{\pi}{2} C \quad (17.10)$$

where  $C =$  an integer. Reordering this equation, we have

$$\mathbf{K} \cdot \mathbf{a} = \frac{C}{2N_x} \quad (17.11)$$

Equation 17.9 is the basis of the shape effect and leads to the idea of the relrod, which you recall is the name we give to a reciprocal-lattice rod (look back at Section 12.5).

### 17.1.B The Integration Approach

If we take equation 13.2, which is the amplitude diffracted by a single unit cell, and sum this over all the cells in the specimen, the amplitude of the diffracted beam can be written as

$$\phi_{\mathbf{g}} = \frac{e^{2\pi i \mathbf{k} \cdot \mathbf{r}}}{r} \sum_n F_n e^{(-2\pi i \mathbf{K} \cdot \mathbf{r}_n)} \quad (17.12)$$

Since we have defined  $\mathbf{K}$  to be  $\mathbf{g} + \mathbf{s}$ , we can rewrite this equation as

$$\phi_{\mathbf{g}} = \frac{e^{2\pi i \mathbf{k} \cdot \mathbf{r}}}{r} \sum_n F_{\mathbf{g}} e^{(-2\pi i (\mathbf{g} + \mathbf{s}_g) \cdot \mathbf{r}_n)} \quad (17.13)$$

Now we know that  $\mathbf{g} \cdot \mathbf{r}_n$  is an integer by the definition of  $\mathbf{g}$  and  $\mathbf{r}_n$  and we will refer to  $\mathbf{s}_g$  as  $\mathbf{s}$ . Hence we can write equation 17.13 as

$$\phi_{\mathbf{g}} = \frac{e^{2\pi i \mathbf{k} \cdot \mathbf{r}}}{r} \sum_n F_{\mathbf{g}} e^{(-2\pi i \mathbf{s} \cdot \mathbf{r}_n)} \quad (17.14)$$

where  $\mathbf{s}$  is the deviation parameter for reflection  $\mathbf{g}$ . If we make the approximation that the crystal contains many unit cells, we can replace this sum by an integral to give

$$\phi_{\mathbf{g}} = \frac{e^{2\pi i \mathbf{k} \cdot \mathbf{r}}}{r V_c} F_{\mathbf{g}} \int_{\text{crystal}} e^{(-2\pi i \mathbf{s} \cdot \mathbf{r}_n)} dV \quad (17.15)$$

This is where the present treatment differs from the first. If we now express  $\mathbf{s}$  and  $\mathbf{r}_n$  as the vectors

$$\mathbf{s} = u\mathbf{a}^* + v\mathbf{b}^* + w\mathbf{c}^* \quad (17.16)$$

and

$$\mathbf{r}_n = h\mathbf{a} + k\mathbf{b} + l\mathbf{c} \quad (17.17)$$

then we can write

$$\phi_{\mathbf{g}} = \frac{e^{2\pi i \mathbf{k} \cdot \mathbf{r}}}{r V_c} F_{\mathbf{g}} \int_0^C \int_0^B \int_0^A e^{-2\pi i (ux + vy + wz)} dx dy dz \quad (17.18)$$

where  $A = N_x a$ , etc. This integral is straightforward.

$$\begin{aligned} \int_0^A e^{-2\pi i u x} dx &= \frac{e^{-2\pi i u A} - 1}{-2\pi i u} = \left( \frac{e^{-\pi i u A}}{\pi i u} \right) \left( \frac{e^{\pi i u A} - e^{-\pi i u A}}{2i} \right) \\ &= \frac{e^{-\pi i u A}}{\pi i u} \sin(\pi u A) \end{aligned} \quad (17.19)$$

$$\phi_{\mathbf{g}} = \frac{e^{2\pi i \mathbf{k} \cdot \mathbf{r}}}{r V_c} F_{\mathbf{g}} \frac{(\sin \pi A u)}{(\pi u)} \frac{(\sin \pi B v)}{(\pi v)} \frac{(\sin \pi C w)}{(\pi w)} e^{iD} \quad (17.20)$$

( $D$  is an unimportant phase factor.) The intensity is then as given by equation 17.9, but we have explicitly kept the  $r^{-2}$  and  $V_c^{-2}$  dependence for the intensities.

You should recognize the form of equations 17.9 and 17.20. These equations have the same form as that given back in equation 2.12 for diffraction from a diffraction grating. The corresponding diffraction grating has  $N_x$  lines which are spaced a distance  $a$  apart. The physical similarity is that the grating, just like our crystal, has a finite size.

## 17.2 THE THIN-FOIL EFFECT

Equation 17.9 is very important for TEM. It tells us why the relrods we introduced in Chapter 12 have a finite length if we measure them to the first minimum. It also tells us that the diffracted intensity does depend on the value of  $\mathbf{s}$ ; it is not a constant for any position along the rod.

### RELRODS AND INTENSITY

Just remember that when we said “the intensity” we meant “the intensity which the diffracted beam will have if  $\mathbf{s}$  takes a particular value; i.e., if the Ewald sphere cuts the relrod at that point.”

We can better appreciate this variation along the rod if we plot the intensity and draw the Ewald sphere, as shown in Figure 17.2. We only draw the intensity plot for one direction at a time. This diagram shows the Ewald sphere cutting the relrod on one side while showing the intensity along the relrod on the right-hand plot.

Figure 17.2 is an extension of Ewald’s ‘pictorial representation’ of diffraction. We can now draw the reciprocal lattice as shown for a simple-cubic crystal in Figure 17.3, such that every point is replaced by a relrod and every relrod is described by equation 17.9. If the surface of the crystal is exactly parallel to the (112) plane, but we orient the specimen slightly off the [001] pole, then the Ewald sphere cuts the relrod as different positions relative to the square array of spots, which is the projection of the spots at zero tilt (Figure 17.3B). The DP will appear as shown in Figure 17.3C. In Figure 17.3C, C is the projected position of the center of the



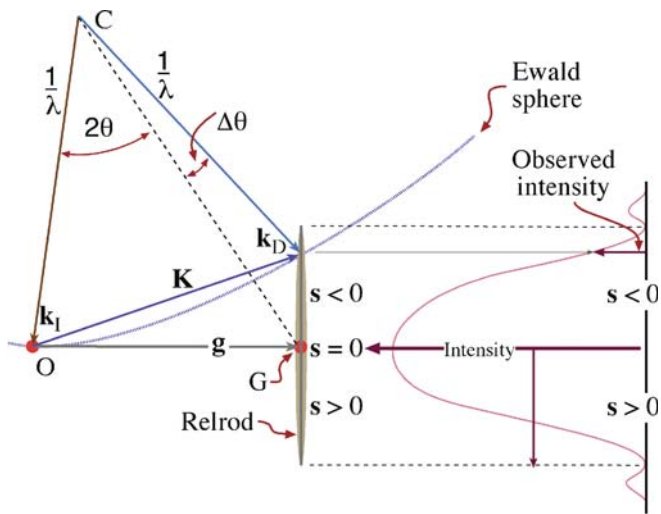


**FIGURE 17.2.** The relrod at  $g_{hkl}$  when the beam is  $\Delta\theta$  away from the exact Bragg condition. The Ewald sphere intercepts the relrod at a negative value of  $s$  which defines the vector  $\mathbf{K} = \mathbf{g} + \mathbf{s}$ . The intensity of the diffracted beam as a function of where the Ewald sphere cuts the relrod is shown on the right of the diagram. In this case the intensity has fallen to almost zero.

Ewald sphere. As an exercise, consider whether the pattern would differ if the surface were cut slightly off (001) but oriented at the [001] pole. Then repeat the first exercise but instead of tilting the specimen, tilt the electron beam through the same small angle.

Remember that we deduced equation 17.9 by simply adding the amplitudes from all the unit cells, taking the position of the cells into account.

We calculated a 'structure factor' for the whole volume which contributes to  $\phi_g$ ; we call this calculated factor the shape factor.

We should then use this shape factor rather than the structure factor (since  $F$  is included in equation 17.9) in our dynamical calculations of  $\phi_g$ . The problem is, of course, that the shape factor can be different for every specimen we examine.

We have just deduced a method for picturing how the shape of a perfect parallelepiped (of sides  $N_x a$ ,  $N_y b$  and  $N_z c$ ) affects the DP. Now for the next step, we will use this concept of the shape factor to examine how the DPs will be affected by more complex shapes, such as the wedge shape of many real TEM specimens or the perfect parallelepiped of the stacking fault. Then we will consider defects which themselves do not have sharp boundaries; the dislocation is a perfect example of such an imperfection.

### 17.3 DIFFRACTION FROM WEDGE-SHAPED SPECIMENS

Most TEM specimens do not have parallel surfaces but are wedge-shaped. In drawing the relrods for such a wedge-shaped specimen, we extend the results of Section 17.2

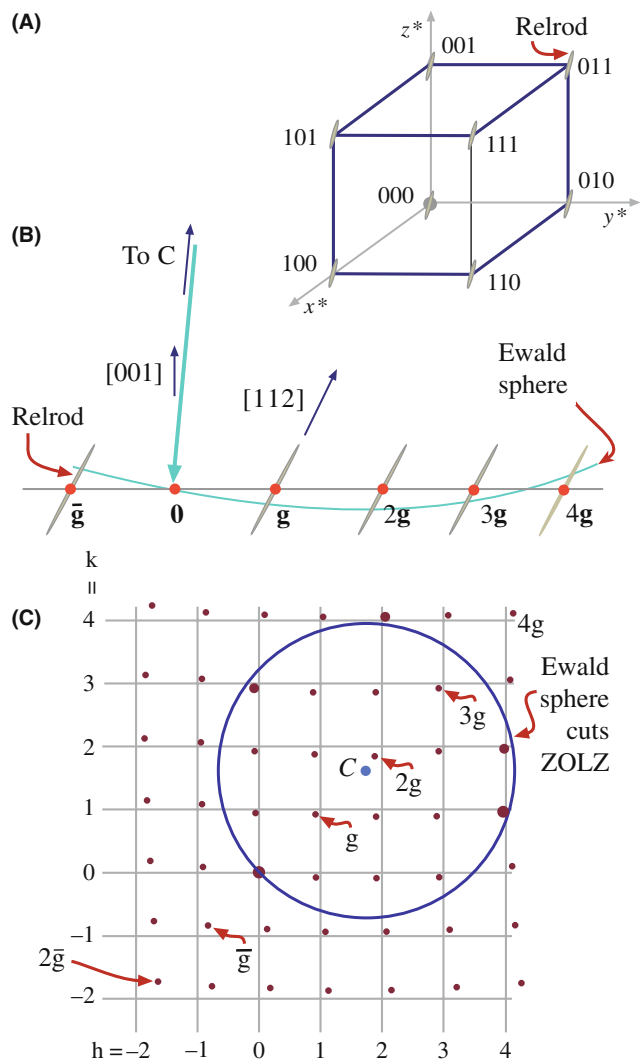


**FIGURE 17.3.** (A) For a thin specimen, every point is replaced by a relrod. (B) The Ewald sphere cutting the relrods in (A) when the crystal is tilted slightly off the (001) axis. (C) The effect of the tilt in (B) on the DP. Notice that all of the spots in the DP are displaced relative to their positions on the square grid (the projection of the spots at zero tilt), but that the magnitude of the displacement varies depending on the sign and size of  $s$ . Of course, spots on the Ewald sphere must be the 'correct' distance from 000.

by saying that the relrod will always be normal to the surface. So, for a wedge-shaped specimen (Figure 17.4A) we must have two relrods as shown in Figure 17.4B. What we see in the DP is determined by how the Ewald sphere cuts these two relrods. As shown in Figure 17.4C and D, we will see two spots which lie along a line which is normal to the edge of the wedge. Notice that all the pairs of spots are aligned in the same direction as we expected and that their separation is larger for larger values of  $s$ . This simple relrod model predicts that we would see only one spot if  $s = 0$ . In fact, we should see two or more spots because the relrod model fails when we are in a strongly dynamical diffraction condition. We will return to this point in the next section and again in Chapter 24.

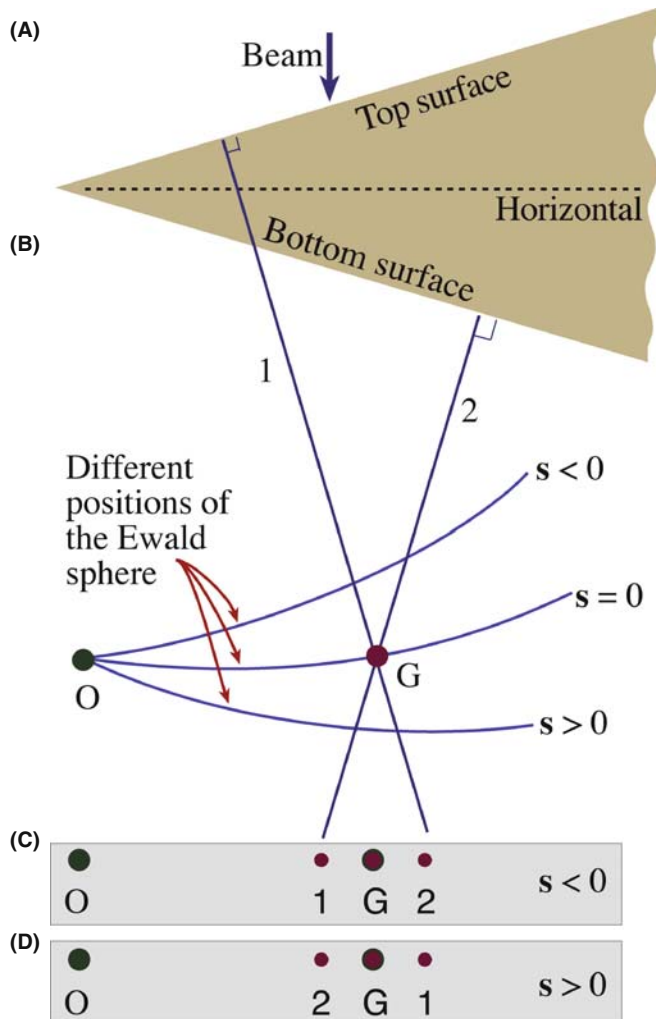


**FIGURE 17.4.** (A) Diffraction from a wedge-shaped crystal. (B) Notice that when  $s < 0$ , relrod 1 is on the left of relrod 2 but the order reverses when  $s$  becomes  $> 0$ . The effect of this pair of relrods is to create a doublet shown in (C) and (D). The middle spot is the matrix relrod for a parallel-sided thin foil and is absent for the wedge in A.

### 17.4 DIFFRACTION FROM PLANAR DEFECTS

The shape factor concept can be readily applied to understand diffraction from a flat platelet or planar fault. The geometry is shown in Figure 17.5. The idea is that the platelet is itself a thin parallelepiped which is inclined to the specimen parallelepiped (Figure 17.5A). The result is that we have two relrods, one normal to the specimen surface and a much longer one normal to the thin platelet (Figure 17.5B and C). When we cut these relrods with the Ewald sphere we produce two spots in the DP and, as for the wedge specimen, the separation of the spots increases with increasing  $s$ . The line MN lies normal to the trace of the platelet. There are, however, some differences in this case. Although the  $m$  and  $n$  relrods are very different in length and actual intensity,

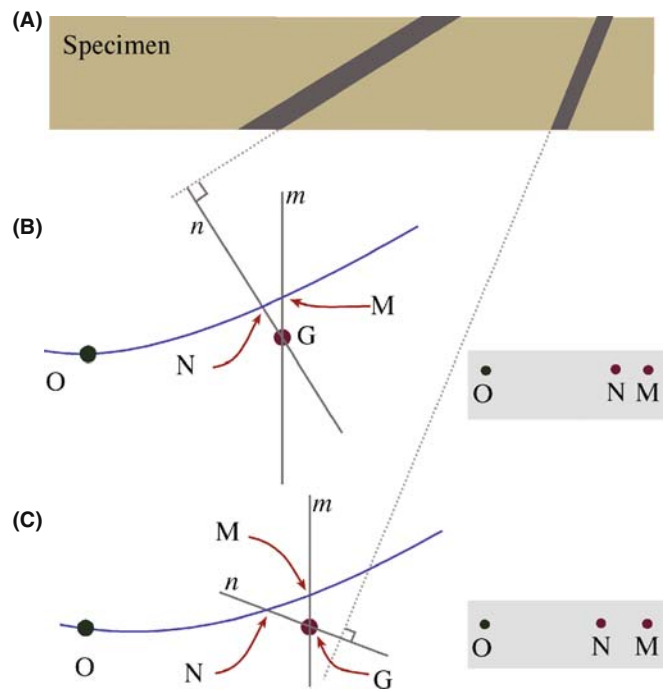


**FIGURE 17.5.** The effect of a thin inclined plate in a thin specimen. (A) Two plates are shown to illustrate the effect of changing the inclination of the plate relative to the foil surface. When  $s \neq 0$  we see two spots in the DP because there are two relrods for the two different planar-defect inclinations in (B) and (C).

the diffracting volume is much greater for the specimen than for the platelet. Thus, we can usually distinguish reflections M and N.

Providing we know the orientation of the specimen relative to the DP, we can tell whether the inclination angle is less than or greater than  $90^\circ$ ; i.e., we can determine the inclination of the planar defect without moving the specimen or using any theory of image contrast (see Chapter 24). As in Section 17.3, we would actually see two spots when  $s = 0$  if we could make the spots small enough. We'll return to this topic in Section 17.7.

A stacking fault in an fcc crystal can be thought of as a very thin platelet of hcp material as shown in Figure 17.6; so it really is a platelet with perfect lattice matching parallel to its surface.

We can understand diffraction effects from other planar interfaces by considering two cases

- If the grains on either side of the interface contain a common reflection, then the diffraction effects can be modeled by the thin platelet.
- In the case where a reflection is not common to the two grains, then for that reflection the diffracting crystal behaves like a wedge specimen with one surface parallel to the planar defect. We can ignore the crystal that is not diffracting.

The two DPs in Figure 17.7 show that you really do see pairs of spots for these two types of boundary. As

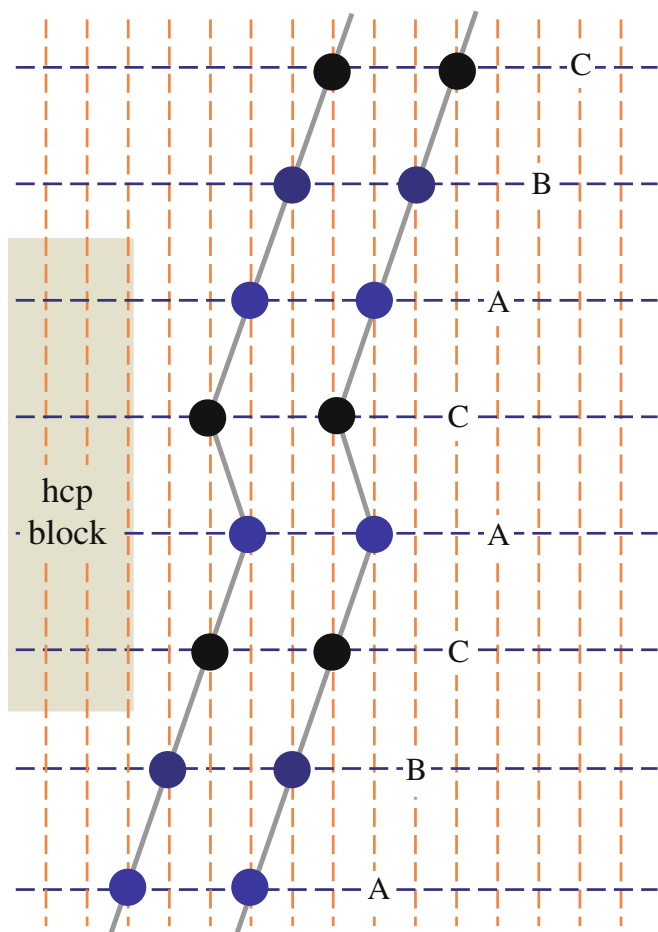


FIGURE 17.6. Schematic of the stacking sequence of close-packed planes A, B, C, in an fcc crystal showing that the SF is similar to a thin layer of hcp material, stacking ACAC.

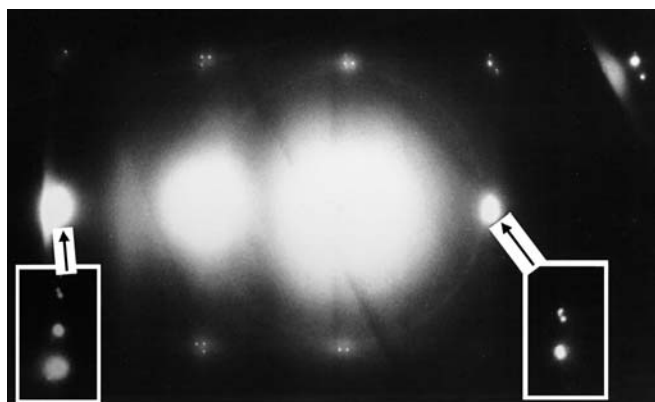


FIGURE 17.7. Pairs of spots in a DP from a grain boundary.

before, the two spots lie normal to the boundary traces, i.e., the intersection of the boundary with the surface of the specimen.

There are two reasons for emphasizing the extra spots which are present because of the interface

- You should always check that any extra spots you see cannot be explained in this way.

- You must be careful when determining spot spacing (as when estimating lattice parameters). You must set  $s$  to zero for this purpose and that can usually only be done for a few reflections at any time (one reflection always being O, not D, of course).

Twin boundaries are often found to consist of flat segments in particular orientations. The first-order twin boundary in fcc crystals tends to facet parallel to the common  $\{111\}$  plane as shown schematically in Figure 17.8A. This means that if we orient the specimen so that this common plane is nearly parallel to the beam, we will excite the common  $\{111\}$  reflection. Now our platelet is parallel to the beam so that its relrod is normal to the beam. If the specimen is also thin, we can arrange that the Ewald sphere cuts along the length of the relrod. Now, as we can see in Figure 17.8B, we see a 'streak' in the DP rather than a spot. The streak actually extends from in the  $[111]$  direction because, as you can appreciate from Figure 17.8A, the twin is a *very* thin platelet.

### FROM NANOPARTICLES

Since we'll only detect any effect when the particle is  $\leq 100$  nm, these particles could be called nanoparticles. Anyone working with such particles must understand this effect which is closely related to Debye-Scherrer analysis in XRD.

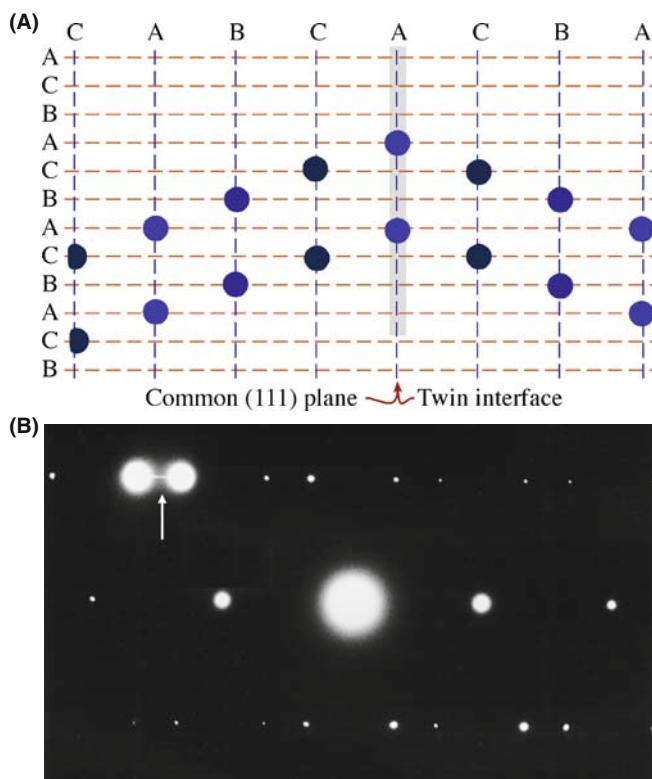


FIGURE 17.8. (A) Schematic of twin and (B) DP with a streak (arrowed) normal to the twin plane. Note that  $s=0$  for the two bright diffracted spots.

If we regard the surface as a planar defect, we can also observe extra spots in the DP due to a reconstruction of the surface. One factor to be cautious about is that the apparent reconstruction might be influenced by contamination since the TEM is not generally a UHV system.

## 17.5 DIFFRACTION FROM PARTICLES

Particles come in all shapes and sizes, so we will not try to be exhaustive. Actually, the principle involved in determining the shape factor in reciprocal space is simply ‘small becomes large’ and vice versa. The shape factors are shown schematically for several particles in Figure 17.9. You should be aware that you will probably never see the subsidiary minima shown in these diagrams.

One example which is common is the platelet shown in Figure 17.10; these can occur as GP zones or other

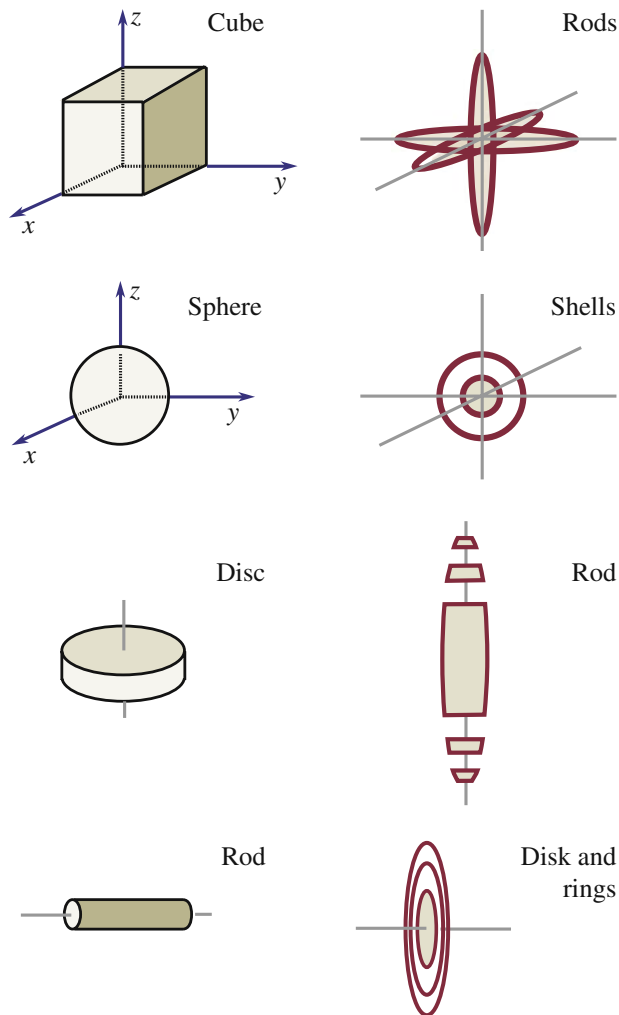


FIGURE 17.9. Examples of how spots in reciprocal space have different shapes depending on the shape of the particles which are diffracting.

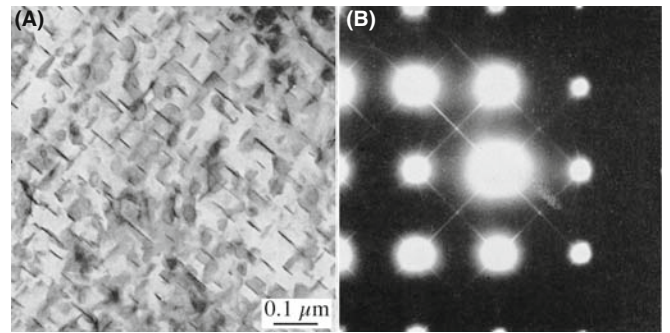


FIGURE 17.10. Very thin plate-like precipitates (A) cause long streaks in the DP (B). In this example, the precipitates are GP zones in an Fe-2.9 at.% Mo alloy.

thin disk-shaped precipitates. When the platelets are oriented parallel to the beam, we see streaks in the DP just as we saw them in Figure 17.8B. The difference in this figure is that the platelets can lie on all the crystallographically equivalent planes in the crystal. For these GP zones they lie on  $\{001\}$  planes so the streaks run in  $\langle 001 \rangle$  directions for the cubic crystal connecting, for example, 000 and 200. You should notice that these spots would still be connected if the crystal were not cubic. You'll also see that there is a sharp point at the 100 position even though 100 is not an allowed reflection for bcc crystals. The reason we see this spot is that we are cutting the rod which runs parallel to the electron beam in the  $[001]$  direction.

The smallest ‘particle’ can be thought of as a vacancy, a substitutional atom or an interstitial atom. We will not expect to see any clear effect of a single point defect but, as we saw in Section 16.7, these point defects can order to give a clear superlattice, and therefore extra spots.

As you might expect then, if we have many point defects but not enough to give long-range order, we might expect short-range ordering. Perhaps the clearest example of this phenomenon again occurs in the metal carbides. The effect is shown in Figure 17.11. The short-range ordering gives rise to diffuse scattering in the DP which at first appears quite random, sometimes as circles around the spots and appearing at other times as circles between spots or not circles at all! By combining many different patterns, Sauvage and Parthé proposed that the diffuse scattering could be mapped out as shown in Figure 17.11D. This figure strongly resembles a Fermi surface diagram which you may have encountered in condensed-matter physics. We will discuss some aspects of imaging using diffusely scattered electrons in Section 29.4, but the important points to recognize are

- Point defects really can cause diffraction effects, especially if they interact with one another.
- Diffuse scattering can still be interpreted by the Ewald-sphere construction.



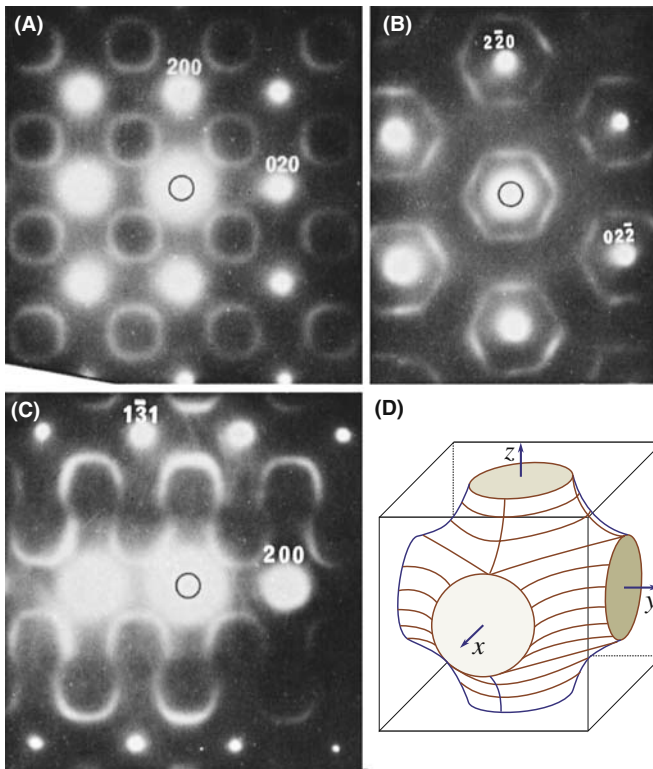


**FIGURE 17.11.** Short-range ordering can cause diffuse scattering in the DP (A–C). The DPs in this example were obtained from a vanadium carbide. In this case, the 3D map of diffuse intensity has a shape which strongly resembles a Fermi surface shown in (D).

If you are intrigued by this topic, you will find the literature on discommensurate structures in intercalated material a complementary challenge. A library/web search on ‘discommensurate’ and ‘intercalated’ will quickly net more recent papers.

## 17.6 DIFFRACTION FROM DISLOCATIONS, INDIVIDUALLY AND COLLECTIVELY

In Chapter 25 we will discuss images of dislocations. A dislocation is a line defect that is characterized by its line direction and its Burgers vector. The crystal around the defect is distorted or strained.

For a single dislocation, this strain is not expected to cause new spots in the DP, but we do expect diffuse scattering since the dislocation is a line defect. If a region from 0.2 to 1 nm around the core is greatly distorted (we’ll see the effect of this strain in Chapter 25), then the diffuse scattering will extend from  $1 \text{ nm}^{-1}$  to perhaps  $5 \text{ nm}^{-1}$  from the reciprocal-lattice points, giving a diffuse disk (the reciprocal shape of a long needle). Some planes are essentially unaffected by the dislocations, so we might expect the diffuse scattering to vary in magnitude for the different reciprocal-lattice points. (We’ll examine this  $\mathbf{g} \cdot \mathbf{b} = 0$  effect in Chapter 24.)

With this simple discussion and without ever seeing this diffuse scattering, we can draw an important conclusion: if we want to learn about the structure of a dislocation core, we must include the diffuse scattering in the image-formation process. We must include that intensity in the objective aperture and the corresponding image calculations.

### DIFFUSE SCATTERING

The diffuse intensity from a dislocation is *not* located at the reciprocal-lattice point.

Because the distorted volume associated with a single dislocation is so small, we do not expect to see this intensity in the DP unless we have many dislocations in an ordered array (just like the point defects in Section 17.5). We can demonstrate that this intensity is present by diffracting from an ordered array of dislocations as shown in Figure 17.12. The specimen used to form this image was rather special. Dislocations are present in region A, but not in region B. The array actually forms a structured grain boundary in A, but a layer of glass is present in B. The insets show the same part of the SADPs from the two regions. In B, you can see three spots. The top two are from one grain, the bottom one is from the other grain. The reason for the pair is that  $s$  is

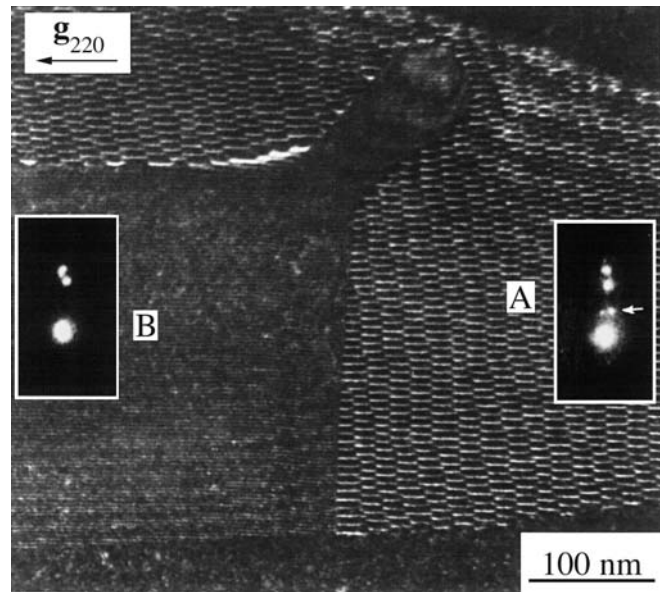


**FIGURE 17.12.** Diffraction from an ordered array of dislocations. Dislocations are present in region A, but not in region B. The insets show a small part of the DP from the two regions. The extra spots present in A are caused by the visible array of dislocations; these spots are a doublet because there is also a second, nearly orthogonal, set of dislocations present which acts as a separate grating. The other pair is due to the wedge shape and so is common to both DPs.



large for that grain, but almost zero for the other. This is an example of the application of Section 17.3.

In A you see the same three spots (because the two grains are still present) but now there are two extra spots. The reason we see two extra spots is that we have two arrays of dislocations. You are seeing the scattering from the dislocations because they have formed an array with long-range ordering, just like the vacancies in  $V_8C_7$  in Chapter 16.

If you look at the DP when the array of dislocations lies parallel to the beam, you may be able to see a set of streaks as shown in Figure 17.13. The separation of the streaks is the inverse of the actual separation of the dislocations. You see streaks because you have relrods in reciprocal space and we are cutting along these rods with the Ewald sphere. The length of the relrods gives you a measure of how far the strain field of the dislocations extends out into the two grains. In other words, we are seeing a thickness of the strain-field regions. The object of this discussion is not to examine grain boundaries, but to show that the strain field from an array of dislocations causes scattering in the DP and thus to infer that one dislocation will also cause scattering, but it will just be much more diffuse (and very weak).

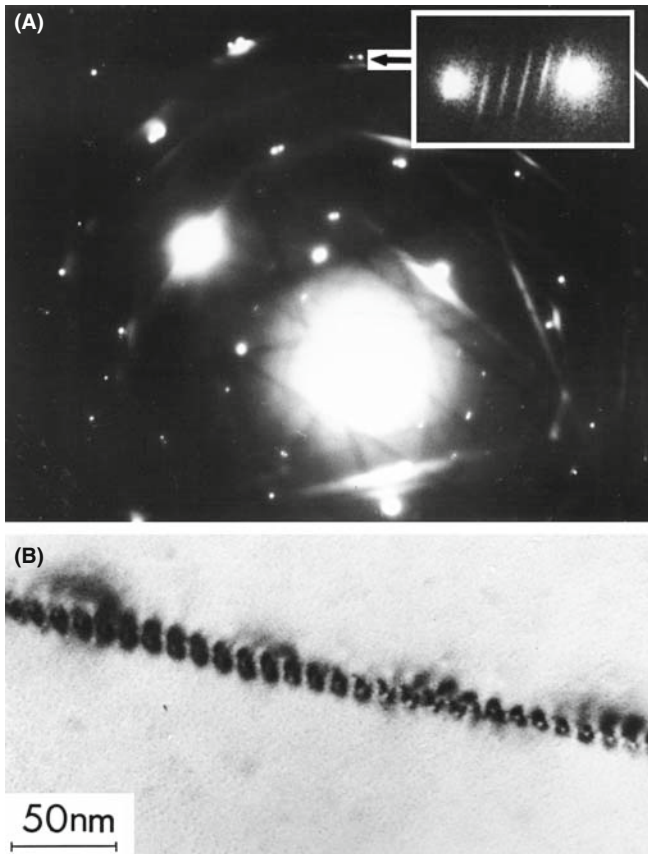


**FIGURE 17.13.** (A) The set of streaks from an array of dislocations in  $Al_2O_3$  lying parallel to the electron beam. The distance between the streaks is inversely related to the spacing of the dislocations shown in the image (B).

Before moving on, consider the diffraction spots in Figure 17.12 again. Why are the pairs of dislocation spots (arrowed) located where they are? Put another way: which of the two spots in region B corresponds to the N relrod and which corresponds to the M relrod? (See Figure 17.5 for the definition of M and N.)

### THE PERIODICITY RULE

If there is a structural periodicity in real space, then there will be an array of points or relrods in reciprocal space and an array of spots or streaks in the DP.

We then ask a simple question: how many objects are required in order to produce a detectable effect in the DP? The answer is two! This point is illustrated in Figure 17.14, which shows a DP and an image of two twin boundaries which are  $\sim 15$  nm apart. The spacing of the new spots between the twin spots in the DP (expanded in the inserts) is  $0.067 \text{ nm}^{-1}$ , as expected. Now, why can this occur? The analogy is the Young's slits experiment in visible-light optics. The illustration also reminds us of a special feature of the TEM, namely, that even without a FEG, the electron beam is remarkably coherent.

## 17.7 DIFFRACTION AND THE DISPERSION SURFACE

Several times in this chapter, we have said "actually, we will see two spots when  $s = 0$ ," even though the relrod model says that you will only see one. The origin of two spots from a wedge specimen (there may be more for more complicated defects) is due to the dynamical nature of the scattering process. The theory has been derived by Amelinckx and his co-workers in a series of papers. Unfortunately, this group used a different notation, but they did summarize their results graphically. We will also return to this topic when we discuss images in Chapter 24. As an example, the relrod diagram given for the stacking fault in Figure 17.5 should be drawn so that the relrods are the asymptotic to two straight lines, as shown in Figure 17.15. When the Ewald sphere cuts these curves at  $s = 0$ , we see that there are two spots which move apart as we increase  $s$  (either positive or, as shown here, negative) until they are at the points defined by the straight lines. So, will there not be a vector that exactly corresponds to  $g$ ? The answer, of course, is yes, because of the adjacent perfect crystal so we must have three spots, but these are very difficult to see because  $s$  must be very close to zero. Without going into any theory, we can guess the origin of these curves: they look remarkably like the curves of the dispersion

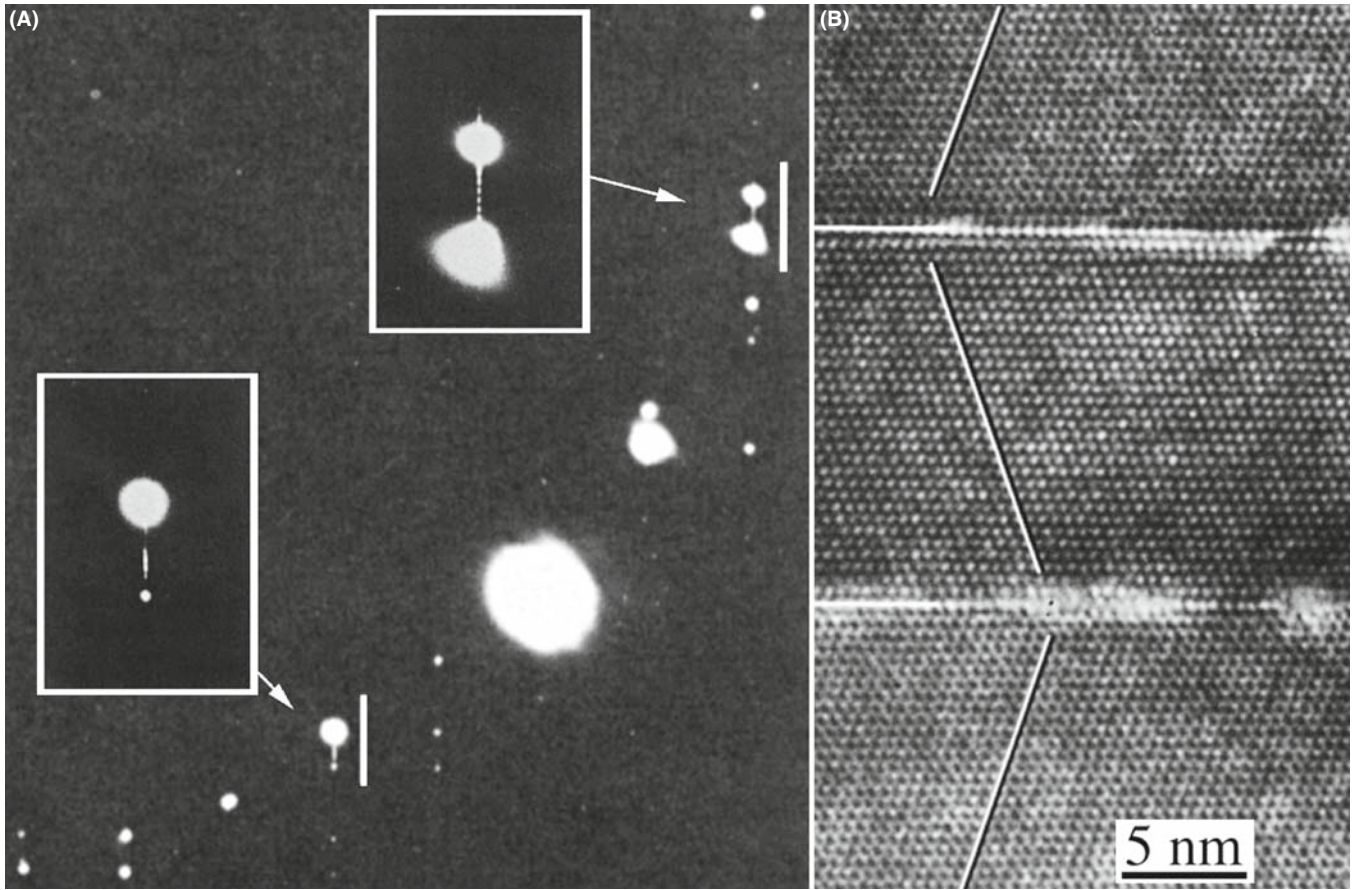


**FIGURE 17.14.** Extra spots can be formed in the DP (A) when only two defects are scattering in phase. The separation of the extra spots is related to the inverse of the separation of the two twin boundaries seen in the image (B).

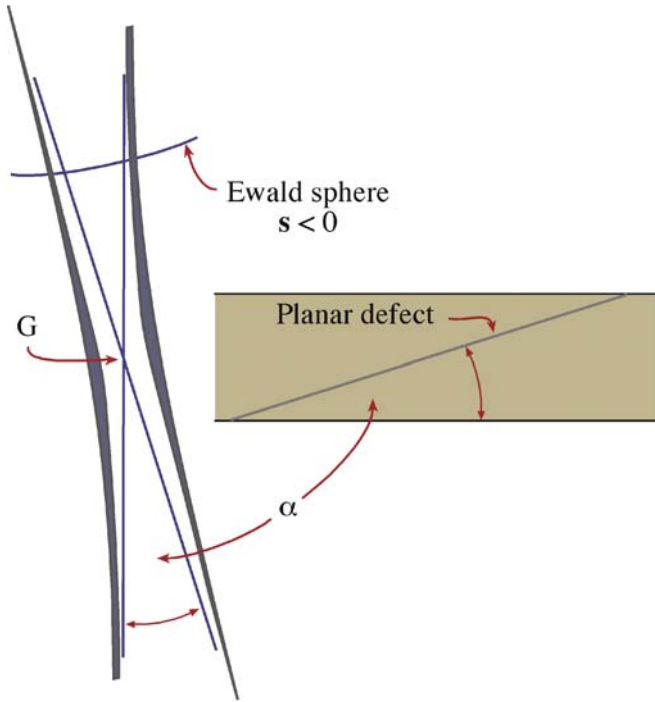


**FIGURE 17.15.** The relrods from two planes inclined at angle  $\alpha$  are actually the asymptotes to two straight lines, so that they don't cross at  $G$ ; when  $s=0$ , the distance between these two curves is  $\xi_g^{-1}$ .

surface which also had asymptotes (see Figure 15.3). These curves are indeed directly related.

When you increase  $s$ , you move out of the dynamical regime and into the kinematical one, where the simple relrod model applies (see Chapter 26). At  $s=0$ , the distance between the curves is inversely proportional to  $\xi_g$ , the extinction distance for reflection  $g$ .

You can understand why this is so in the following pictorial way. What you see in the image will be determined by the DP. What you see in the DP is determined by which relrods, or surfaces, the Ewald sphere intersects. All the information about extinction distances and coupling of diffracted beams is fundamentally contained in the dispersion surface ( $\xi_g$  is just  $\Delta k^{-1}$  at  $s=0$ ). Both the dispersion surface and the reciprocal-lattice/Ewald-sphere models are just pictorial representations of the same diffraction process. So, all the information in the dispersion-surface model should also be present in the reciprocal-lattice/Ewald-sphere model.

The relrods are the asymptotes to these two hyperbolas. Alternatively, we could say that the relrods and the asymptotes are a result of the kinematical diffraction

approximation. There is a one-to-one correlation between what happens at the dispersion surface in the vicinity of the BZB to what happens when the Ewald sphere cuts the relrods in the vicinity of the reciprocal-lattice point, G. Imagine rotating the dispersion-surface diagram through  $90^\circ$ . These ideas have been extensively studied by van Landuyt, de Ridder, Gevers, Amelinckx

et al., as summarized in the general references at the end of this chapter. What Amelinckx's group has done is to give us the rules on how to transfer this information from the dispersion surface to the reciprocal lattice and hence to the DP. In Section 24.9, we'll relate this concept to images. If you thought dispersion surfaces were difficult, make s large and stick to relrods!

## CHAPTER SUMMARY

In this chapter, we have begun to examine the unique features of diffraction in the TEM. These features arise because we are always diffracting from small volumes. The sizes of both our specimen and the special features present in our specimen are always small, so that we must take into account the shape effect. This is particularly important for nanoparticles and nanograins—you must keep this in mind when imaging. Of course, the same considerations will also apply to other forms of diffraction; it's just that only TEM can examine the diffraction information from the vicinity of crystal defects. In other words, the shape effect is not a limitation due to the fact that we are using high-energy electrons. By understanding the concept of the shape effect you can actually learn more about defects in crystals; conversely, you can make some major errors if you do not understand the shape effect. Two points to remember are

- When a platelet is parallel to the beam its relrod is normal to the beam. If the specimen is also thin, we can arrange that the Ewald sphere cuts along the length of the relrod. Now you see a 'streak' in the DP rather than a spot.
- Beam splitting at  $s = 0$  and the dispersion surface both arise because of dynamical scattering.

## DIFFRACTION FROM INTERFACES

The relation between diffraction and images from planar defects has been the subject of a long series of papers from the group led by Prof. Severin Amelinckx. The examples below from Phys. stat. sol. will give you a start to your study.

- Carter, CB (1984) *Electron Diffraction from Microtwins and Long-Period Polytypes* Phil. Mag. A **50** 133–141. The Young's slit experiment in the TEM.
- de Ridder, R, Van Landuyt, J, Gevers, R and Amelinckx, S (1968) *The Fine Structure of Spots in Electron Diffraction Resulting from the Presence of Planar Interfaces and Dislocations. IV. Wedge Crystals* Phys. stat. sol. **30** 797–815; See also: (1970) *ibid.* **38** 747; (1970) *ibid.* **40** 271; (1970) *ibid.* **41** 519; (1970) *ibid.* **42** 645.
- Gevers, R (1971) in *Electron Microscopy in Materials Science* (Ed. U. Valdrè) p302–310, Academic Press, New York. An introduction to the work of Amelinckx' group.
- Gevers, R, Van Landuyt, J and Amelinckx, S (1966) *The Fine Structure of Spots in Electron Diffraction Resulting from the Presence of Planar Interfaces and Dislocations. I. General Theory and Its Application to Stacking Faults and Anti-phase Boundaries* Phys. stat. sol. **18** 343–361; See also (1967) *ibid.* **21** 393; (1967) *ibid.* **23** 549; (1968) *ibid.* **26** 577.
- Van Landuyt, J (1964) *An Electron Microscopic Investigation of Phenomena Associated with Solid Solution of Oxygen in Niobium* Phys. stat. sol. **6** 957–974.
- Van Landuyt, J, Gevers, R and Amelinckx, S (1966) *On the Determination of the Nature of Stacking Faults in fcc Metals from the Bright Field Image* Phys. stat. sol. **18** 167–172.

## DIFFUSE SCATTERING AND INTERCALATION

- Carter, CB and Williams, PM, 1972, *An Electron Microscopy Study of Intercalation in Transition Metal Dichalcogenides* Phil. Mag. **26** (2), 393–398. To encourage new students!
- Sauvage, M and Parthé, E (1972) *Vacancy Short-Range Order in Substoichiometric Transition Metal Carbides and Nitrides with the NaCl structure. II. Numerical Calculation of Vacancy Arrangement* Acta Cryst. **A28** 607–616.
- Wilson, JA, Di Salvo, FJ and Mahajan, S (1975) *Charge-Density Waves and Superlattices in the Metallic Layered Transition Metal Dichalcogenides* Adv. Phys. **24** 117–201. An early review of intercalation.



## THE COMPANION TEXT

Although there is great interest in nanomaterials and XRD is often used to characterize them, diffraction from such materials in the TEM is used much less because imaging is then almost routine. Hence there have not been recent advances in electron diffraction except as CBED, which is treated in the companion text.

## SELF-ASSESSMENT QUESTIONS

- Q17.1 When the Bragg condition is not satisfied exactly, why do spots appear in the DP?  
Q17.2 Reproduce the summation and integral calculations of amplitudes to explain the existence of relrods.  
Q17.3 When the specimen is tilted slightly off a particular zone, why might spots in the DP move away from their ideal positions in the DP?  
Q17.4 Is a relrod a 'real' object?  
Q17.5 In a specimen containing thin platelets, how is it possible to distinguish the DP spots associated with the thinness of the specimen from those due to the platelets?  
Q17.6 If a single dislocation is observed in the specimen, should the DP change?  
Q17.7 When is it possible to view along the entire length of a relrod?  
Q17.8 The spots in the right inset of Figure 17.14 are very clear. Why did we show this region rather than the region between 000 and the common 111?  
Q17.9 What is the definition of a twin boundary?  
Q17.10 For what conditions might you see diffuse circles surround the DP spots?  
Q17.11 How does the thickness of the TEM foil affect how (when) the Laue conditions are satisfied?  
Q17.12 How can the thickness of the specimen affect the accuracy of lattice-parameter determination?  
Q17.13 How can the wedge shape of a specimen influence the appearance of the diffraction spots?  
Q17.14 When  $s = 0$ , the (curved) relrod models predicts two spots will be seen in the DP. Why?  
Q17.15 In Figure 17.8, we can see a streak between two spots in the DP. What does this tell us?  
Q17.16 It is only possible to see a streak in the DP when the specimen is thin. Explain.  
Q17.17 Does short-range ordering give rise to effects in the DP?  
Q17.18 In Figure 17.5, what determines the distance between spots M and N?  
Q17.19 When viewing a twist boundary nearly flat on, we look at the DP and see that there are three spots at  $-2\mathbf{g}$  and two spots at  $+\mathbf{g}$ ? Why is there an extra spot at  $-2\mathbf{g}$ ?  
Q17.20 Why is the  $2\mathbf{g}$  reflection inside the square but  $4\mathbf{g}$  reflection outside for the DP in Figure 17.3C?  
Q17.21 For a wedge specimen, we say we have two sets of relrods because there are two surfaces. How does this fit with our idea of relrods arising from thin plates?  
Q17.22 Can you see an effect in the DP if a twin boundary is viewed flat on?  
Q17.23 Why do we see the (100) reflection in Figure 17.10?  
Q17.24 How many objects are required in order to produce a detectable periodicity in the DP?

## TEXT-SPECIFIC QUESTIONS

- T17.1 Consider Figure 17.13 and the relationship of streak length to defect (interface) width. What is the width of the grain boundary according to the DP?  
T17.2 Examine the extra spots in inset A of Figure 17.12. Compare the spacing of dislocations giving rise to these spots with the periodicity of the spots.  
T17.3 Explain why there are spots in inset B of Figure 17.12.  
T17.4 Consider Figure 17.15. How would this figure change if the top half of the figure (above the planar defect) were removed?  
T17.5 Consider Figure 17.14B. Construct the DP you expect to see, assuming it's Si.  
T17.6 Consider Figure 17.7. If this DP is from an 001 twist boundary, what is the angle of misorientation?  
T17.7 Consider Figure 17.7. How can the lower reflection be the brighter in both insets?  
T17.8 Consider Figure 17.3. Redraw the figure with the Ewald sphere cutting through  $(-2, -2)$  and  $(0, -2)$ .  
T17.9 Fully index the DP in Figure 17.10. Explain why this material must be BCC and not FCC.  
T17.10 Why is the streak seen where it is in Figure 17.8?  
T17.11 Figure 17.8A shows two grains. Which spots in Figure 17.8B correspond to which grains?  
T17.12 Look at Figure 17.14. Is the spacing of the fine spots in the inset consistent with the image? Justify your answer.  
T17.13 Consider Figure 17.14. Why are there several spots in a row rather than just one extra spot?  
T17.14 Why do the streaks in Figure 17.13 shift parallel to their length as we look from one spot to the other in the insert?  
T17.15 A thin Al metal foil contains needle-shaped precipitates which are 2 nm in diameter and 20 nm long. The needle lies in the (001) plane and its axis is parallel to the [110] direction. Sketch the [001] DP of the foil. (Courtesy ZL Wang.)

# Obtaining and Indexing Parallel-Beam Diffraction Patterns

## CHAPTER PREVIEW

The core strength of TEM is that you can obtain both a DP and an image from the same part of your specimen (not to mention various spectra). To obtain the crystallographic data, a method for interpreting and indexing the DP is essential and this aspect is the theme for the next four chapters. We'll start in this chapter by considering classic selected-area diffraction (SAD) patterns (SADPs) and how to index them, but also introduce other related, if less widely used, parallel-beam diffraction methods.

You can proceed to index your pattern in several ways, depending on how much information you already know about your specimen. We will begin the chapter by considering the experimental approach with the aim of being able to identify shortcuts whenever possible. The experienced microscopist will readily identify many patterns just by looking at them, but will still need to index new patterns or to identify unfamiliar ones. The fastest and most efficient experimental approach may take advantage of several concepts covered in the preceding two chapters and the following three. Today, sophisticated computer software is available which takes much of the tedium out of the indexing process.

Most DPs in a TEM are single-crystal (spot) patterns because the area from which we can routinely obtain SADPs ( $< 1 \mu\text{m}$ ) is smaller than typical grain sizes of most engineering materials. However, with increased emphasis on nanocrystalline materials (grain size  $< 0.1 \mu\text{m}$ ), it is more usual for the DPs to contain contributions from many crystals and so ring/textured SADPs are increasingly common. (We'll cover convergent-beam (CBED) and other forms of micro/nanodiffraction patterns, which can come from regions  $< 10 \text{ nm}$ , in Chapters 20 and 21.) Using the DP, we can identify the crystal (which we often already know) and its orientation (which we probably don't) with respect to both the beam and to any adjacent crystals. The positions of the allowed  $hkl$  reflections are characteristic of the crystal system. Indexing associates each spot or ring in the DP with a plane ( $hkl$ ), or set of planes  $\{hkl\}$ , in the crystal. From the indexing of the spots, you can deduce the orientation of the crystal in terms of the zone axis  $[UVW]$  in which the indexed planes lie.

### BEAM DIRECTION

It is convention to define  $[UVW]$  as the beam direction. This direction is *normal* to the plane of the DP and *anti-parallel* to the electron beam.

If you want to know the orientation relationship between two crystals, you need to know more than one  $[UVW]$  for each crystal and, as we'll show, it is the determination of orientation relationships between different phases or differently oriented crystals that is the most useful information to come out of DP indexing. Orientation determination in the TEM is so important that we devote a complete chapter to the topic in the companion text. Now, computer control of both DP formation and DP indexing is very much the norm, but if you don't understand the principles, you shouldn't believe the computer output (GIGO). So we deliberately confine our discussion of computer-assisted indexing to the end of this chapter.



## 18.1 CHOOSING YOUR TECHNIQUE

The technique you choose to study your specimen will depend on what you *want* to learn and what you *can* learn. For example, if you want to learn about the crystal structure of a particular region, diffraction is generally the way to go although you may find moiré fringes (Chapter 23) or HRTEM (Chapter 28) more appropriate. Basically there are three diffraction approaches:

- You can spread the beam to give nearly parallel illumination and then use an aperture to select an area in the first image formed by the objective lens (giving the SADPs of Chapters 9 and 11). We emphasize SAD indexing in this chapter.
- SADPs often contain Kikuchi lines which give more accurate orientation determination (see Chapter 19).
- You can focus the beam on a small area of your specimen to form a CBED pattern (we won't use CBEDP) (see Chapters 20 and 21).

### SAD ACRONYMS

SADP versus SAD pattern, SAED versus SAD and CBEDP versus CBEDP versus CBED pattern. We try to use DP throughout the book but some conventions are very well established!

We can also summarize the possibilities as a function of the grain size of the material. Let's consider this particular specimen characteristic

- The grain size may be very small,  $\ll 10$  nm, typical of many nanocrystalline thin films. This is a problem because it's rare that a single grain will extend through the thickness of your specimen, in which case you can't easily index an individual crystal pattern. (This is the rhino problem (Figure 1.7) for DPs!) However, in this case you probably won't want to know the *orientation* of a particular grain but will instead be interested in knowing the *texture* of the material.
- The grain size is between 10 and  $\sim 100$  nm. Here CBED may be useful because it gives you a small probe. However, much of the benefit of CBED comes from having specimens which are  $> 100$  nm thick; the best thickness depends on the structure factor (atomic number) of your specimen. If you're careful and are using a recent-model TEM in which  $C_s$  and  $\lambda$  are small, you might be able to use SAD in this range of grain size, as we saw in Table 11.1.
- The grain size is in the range 100 nm to  $\sim 2$   $\mu\text{m}$ . In this situation, SAD can be used quite routinely in a modern TEM. You must be aware of the limitations and

be prepared to unravel a complex DP. Because of errors due to  $C_s$  and  $\Delta f$ , the problem will be distinguishing which spots arise from the area you selected and which spots arise from neighboring areas.

- The specimen is uniformly thin with grain size  $> 2$   $\mu\text{m}$ . This type of specimen is just a simpler version of the last case. You should have no problem in applying SAD techniques even at lower voltages and in older microscopes. Now CBED will be very useful in examining local changes *within* a grain.
- The grains of interest are large ( $> 2$   $\mu\text{m}$ , even better if they are  $> 5$   $\mu\text{m}$ ) with both thin areas ( $< 100$ – $300$  nm thick, depending on the material) and areas which are sufficiently thick for Kikuchi lines to be visible (see next chapter). Now you can use any of these techniques, except texture analysis, which becomes more difficult! For the latter, you should now consider the electron-backscatter diffraction (EBSD) technique using a bulk specimen in an SEM to give better statistics (Schwartz et al.).

In this chapter, we'll concentrate on the hands-on approach to SAD analysis and leave CBED to Chapters 20 and 21. We'll also introduce hollow-cone and precession diffraction which make your SADPs more useful at times. We can't give you a foolproof guide since the best technique(s) will depend on your specimen.

## 18.2 EXPERIMENTAL SAD TECHNIQUES

By now you should know how the experimental camera length ( $L$ ) compares to the value you read from the microscope. You also know how the SADP is rotated with respect to the image as the magnification changes (unless your particular TEM automatically compensates for this rotation). You've checked that you haven't missed a  $180^\circ$  inversion; leading researchers have missed this in the past. Go back to Sections 9.3–9.6 and 11.9 if you need to refresh the details of the practical steps involved in obtaining SADPs.

You can vary  $L$  but your pattern may rotate as you do so. We generally use a value of  $\sim 500$  mm for SAD, but that will depend on your TEM, whether you want to see detail in the HOLZ and on the interplanar spacings in your specimen. It's good practice to choose a particular value of  $L$  and always use that value for your SADPs with a particular instrument/specimen combination. You may want to increase  $L$  for special high-resolution diffraction, but you'll give up a large number of other reflections and enlarging the photographic film will almost always provide the magnification you need. This is where a wide-angle CCD camera (Chapter 7) that captures a much larger area of reciprocal space than standard TEM film can be really useful.

*Tilting and rotating your specimen.* One of the biggest assets of the TEM is that you can monitor the DP as you tilt or rotate your specimen. Rotating the pattern requires a rotation holder (Chapter 8), which is ideal if you want to align a particular reflection parallel to the tilt axis, especially for a side-entry holder. This alignment is particularly helpful in stereomicroscopy (see Chapter 29). Tilting the specimen is far more common than rotating, since all side-entry holders automatically have one tilt axis parallel to the specimen rod. We discussed the importance of eucentricity in Chapter 9.

### TILTING

Tilting the specimen changes the diffraction conditions and may change the focus.

It is good practice to note the tilt settings whenever you are recording images. If you want to use these settings to give a rough estimate of how far you're tilting the specimen, you should remember that there may be some backlash due to mechanical hysteresis. So you will always need to approach a particular setting from the same tilt direction if you need to be exact. In the next chapter, we'll describe how we use Kikuchi maps to guide us as we tilt the specimen. If you don't have Kikuchi lines because your specimen is too thin, or too bent, you can still use the idea. Select a particular strongly diffracted beam and then tilt the specimen so that that particular beam remains excited. What you are doing is tilting the specimen so that the same plane remains nearly parallel to the electron beam (think about what this means and the crystallographic information that it can give you).

*Tilting the beam.* If you are really interested in examining the detail present in the DP and the image is less important, you can change the diffraction conditions in a very controlled and reversible way by tilting the beam using the DF deflection coils. You can be much more precise than mechanical tilting with the goniometer since there is no problem with backlash. To increase your accuracy, you may want to increase  $L$ . This technique is particularly helpful when you want to examine the effect of small changes in  $s$  on the appearance of diffraction spots.

For example, if you want to excite the third-order reflection  $3\mathbf{g}$  in BF, you could use the approach shown in Figure 18.1. (You wouldn't, but this exercise is useful!)

- Use the beam tilt (dark-field deflection coils) to put  $\bar{\mathbf{g}}$  on the optic axis (where  $\mathbf{0}$  was) (Figure 18.1A). Now tilt the sample so that  $\mathbf{g}$  is excited. Then tilt the beam to put  $\mathbf{0}$  back on the optic axis.  $3\mathbf{g}$  is now excited.

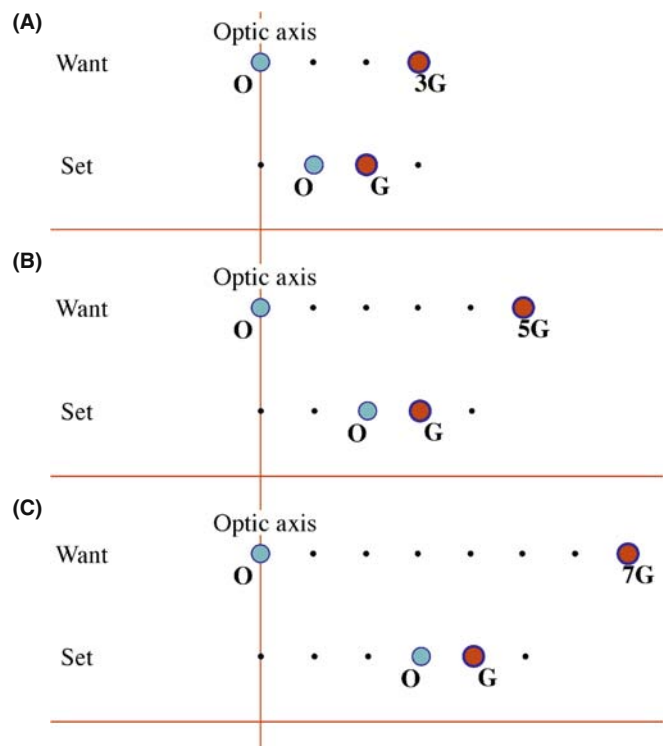


**FIGURE 18.1.** Exercises in exciting high-order reflections. (A) To excite  $3\mathbf{G}$  in BF, tilt the beam so  $-\mathbf{G}$  is on axis with  $\mathbf{G}$  strongly excited, then tilt  $\mathbf{O}$  back onto the optic axis. (B) To excite  $5\mathbf{G}$  in BF, tilt the beam so  $-2\mathbf{G}$  is on axis with  $\mathbf{G}$  strongly excited, then tilt  $\mathbf{O}$  back onto the optic axis. (C) To excite  $7\mathbf{G}$  in BF, tilt the beam so  $-3\mathbf{G}$  is on axis with  $\mathbf{G}$  strongly excited, then tilt  $\mathbf{O}$  back onto the optic axis.

Next, repeat the exercise but with the aim of exciting  $5\mathbf{g}$ .

- Use the beam tilt (dark-field deflection coils) to put  $2\bar{\mathbf{g}}$  on the optic axis (where  $\mathbf{0}$  was) (Figure 18.1B). Now tilt the sample so that  $\mathbf{g}$  is excited (as before). Then tilt the beam to put  $\mathbf{0}$  back on the optic axis.  $5\mathbf{g}$  is now excited.

Repeat the exercise again but with the aim of exciting  $7\mathbf{g}$ .

- Use the beam tilt (dark-field deflection coils) to put  $3\bar{\mathbf{g}}$  on the optic axis (where  $\mathbf{0}$  was) (Figure 18.1C). Now tilt the sample so that  $\mathbf{g}$  is excited (as before). Then tilt the beam to put  $\mathbf{0}$  back on the optic axis.  $7\mathbf{g}$  is now excited.

Now you can see that if you want to excite  $11\mathbf{g}$ , but you won't be able to see  $11\mathbf{g}$  on the DP, start by moving  $5\bar{\mathbf{g}}$  to the optic axis. You should now appreciate the possibilities.

We'll develop other variations of this technique in Chapter 19, and we'll see in Chapter 27 that the situation in Figure 18.1 does arise in weak-beam microscopy at higher voltages. Computerized control of the beam tilt is essential to hollow-cone and precession diffraction methods which we'll discuss toward the end of the chapter.

### 18.3 THE STEREOGRAPHIC PROJECTION

DPs not only tell us the direction of the electron beam but also the complete orientation of that region of the specimen illuminated by the beam. If we have a grain boundary or interphase interface (or indeed any planar defect) present in the specimen, we can determine the orientation of both grains and the plane of the interface. As we show in great detail in the companion text, what we often want to know is how the two crystals are related to one another. But first, we need a method for visualizing this relationship; this is where the stereographic projection or stereogram is an invaluable aid. Unfortunately the classic materials texts by Johari and Thomas and by Smallicki are out of print, so to get an in-depth appreciation of this technique, you'll have to resort to crystallography texts, such as those listed in the general reference section or a dedicated stereographic-projection text in another field (e.g., Lisle and Leyshon). Like other tools, you'll have to understand it and use it before you fully appreciate its value. We strongly recommend that you take time out to do this if you're not already familiar with the construction. Any introductory crystallography text is a good place to start and several are listed in the references.

*The construction.* Imagine a crystal located inside a sphere as shown in Figure 18.2. Draw a line normal to each crystal plane from the center of the sphere (the

sphere of projection) to intersect the sphere at point P in the northern hemisphere; the cross section view may be easier to visualize. Now draw a second line from the south pole to point P.

This second line cuts the equatorial plane at the point P'. The disk of the equatorial plane is the stereographic projection and the point P' *uniquely* represents the plane whose radial normal cuts through P. If P is in the southern hemisphere, we draw the line from the north pole instead and identify this P' on the projection with a circle instead of a dot.

Look again at the crystal; it's cubic to keep it simple but the construction is completely general. The normals to the planes (100), (111), (011) and ( $\bar{1}11$ ) all lie on the circumference of a circle around the sphere of projection. In this special case, all of the points on this circumference project onto the same great circle on the stereographic projection whose circumference we call the 'primitive' great circle. The Wulff net in Figure 18.3 shows 90 such great circles all passing from the north pole to the south pole and another around the equator: a great circle always passes through opposite ends of a diameter in the projection. These are the familiar lines of longitude on the globe. Circles on the sphere which do not contain the center of the sphere are smaller; they also project as circles called the small

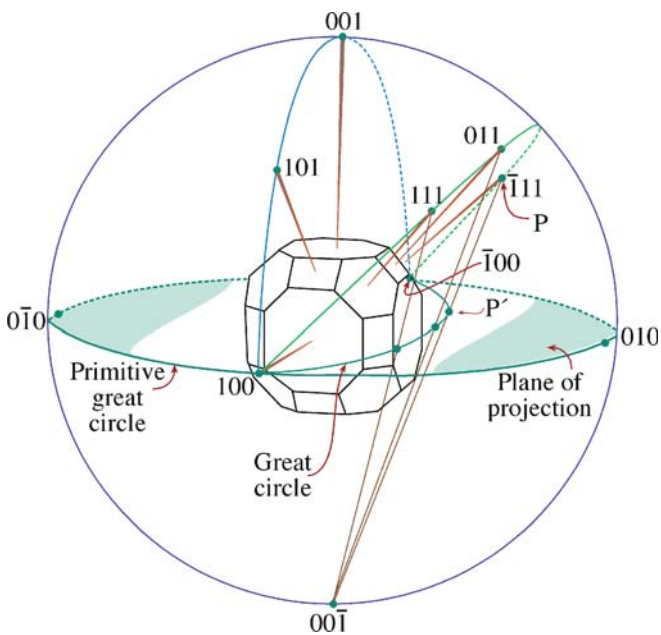


**FIGURE 18.2.** The stereographic projection. The crystal is at the center of the sphere. Normals to the crystal planes are projected until they intercept the sphere at P, then projected back to the south pole ( $00\bar{1}$ ) of the sphere. Where this projected line crosses the equatorial plane at P' is the point that uniquely represents the original plane in the crystal. Note that planes in the same zone on the crystal project as a great circle in the stereographic projection. An example of such a great circle is its diameter (or line of longitude); another is the circumference in the equatorial plane.

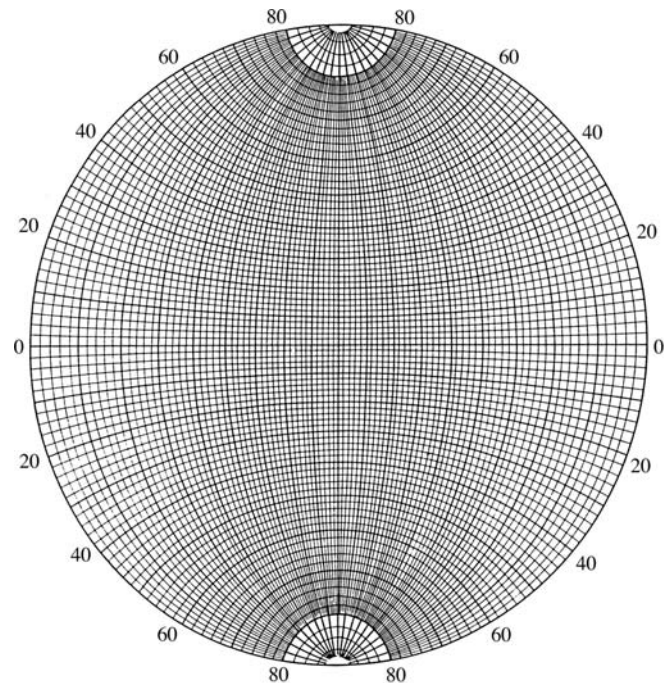


**FIGURE 18.3.** A Wulff net which contains 90 great circles like the one in Figure 18.2; each great circle is  $2^\circ$  apart so the net covers  $180^\circ$ . The only great circle that actually appears as a circle in the net is the circumference of the projection, called the primitive great circle. Points on the primitive represent planes whose normals are  $90^\circ$  from the north pole (which projects in the center of the Wulff net). Thus all distances on the net are proportional to angles in real space but only correspond exactly to angles around the primitive.



circles which, if concentric with the primitive, are familiar as lines of latitude. (Note, however, that most small circles are not concentric with the primitive.) We can then rotate the Wulff net, as we wish, to realign our great circles.

- We can represent plane normals (also called poles) and directions on the same projection even if they are not parallel to one another. Better still, we can read off the angles between them. Remember that, in general, the normal to the plane  $(hkl)$  is parallel to the direction  $[hkl]$  only for cubic materials.
- The zone axis is always  $90^\circ$  away from any plane normal that is in its zone. All the plane normals in a particular zone,  $[UVW]$ , will lie on a single great circle.
- The angle between any two planes is the angle between their plane normals, measured along a great circle using the Wulff net.
- We can use the same construction to summarize all the symmetry elements of any particular crystal system.

These poles at the  $UVW$  zone axis represent the possible diffracting planes for that zone;  $[UVW]$  is the beam direction. So if  $[UVW]$  is in the center of the projection, the  $hkl$  reflections will be around the circumference of the projection (the primitive great circle). Now you should appreciate why stereograms can be so useful in interpreting DPs.

Several examples of stereographic projections are shown in Figure 18.4. Look at the Wulff net and check some simple facts. For example, for the cubic system, check which poles are  $90^\circ$  away from the  $[001]$  direction. How large is the angle between  $(0\bar{1}1)$  and  $(011)$ ? How would this angle change if the material were forced to be tetragonal with  $c/a > 1$ ? What happens in this case to the  $(1\bar{1}1)$  pole or the  $(1\bar{1}0)$  pole? Now consider the more extensive plot shown in Figure 18.5. If the specimen is cubic with the  $[001]$  foil normal, what pole would you tilt

to if you wanted to form an image with the  $0\bar{2}2$  reflection? (One answer is the  $[011]$  zone axis, but why?). For the same specimen, if you want to excite the  $\bar{1}11$  reflection, you could tilt toward the  $[0\bar{1}1]$  zone axis keeping the 200 reflection excited, not toward the  $[011]$  zone axis.

- You could work this out using equations, but the stereographic projection tells you what to do while you are sitting at the microscope.
- If you are working with a non-cubic material, buy a large Wulff net and construct your own stereographic projection; you can buy standard projections for cubic materials so, as usual, it's easier to be a metallurgist than a ceramist or mineralogist.
- Use a program like EMS to help you plot the points, or download appropriate software from the Web (e.g., URL #1).
- Wulff nets and plotting software are also available on-line (e.g., URL #2).

## 18.4 INDEXING SINGLE-CRYSTAL DPs

Remember the fundamental relationship in a DP (Section 9.6.B).

$$Rd = \lambda L \quad (18.1)$$

Any distance between the direct beam and a specific diffraction spot or the radius of a diffraction ring,  $R$ , which we measure on the DP, is related to a specific spacing between planes in the crystal,  $d$ . Since  $\lambda L$  is a constant, we can measure several values of  $R$  and know that

$$R_1d_1 = R_2d_2 = R_3d_3 = R_4d_4 = \dots \quad (18.2)$$

If you know the lattice parameter of your crystal, then you know the allowed reflections and only certain  $d$ -spacings will be associated with diffraction spots.

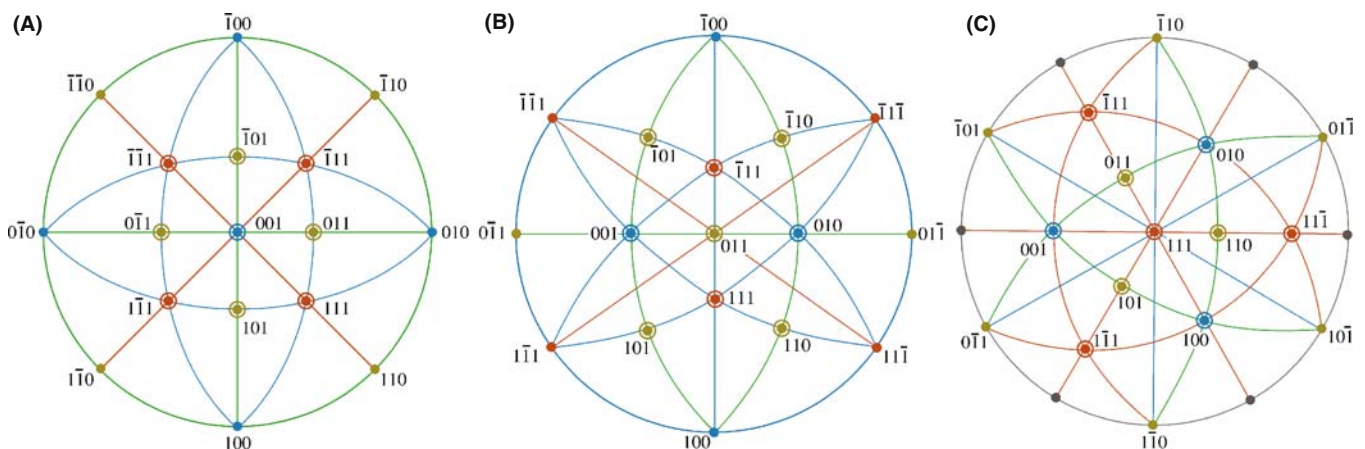
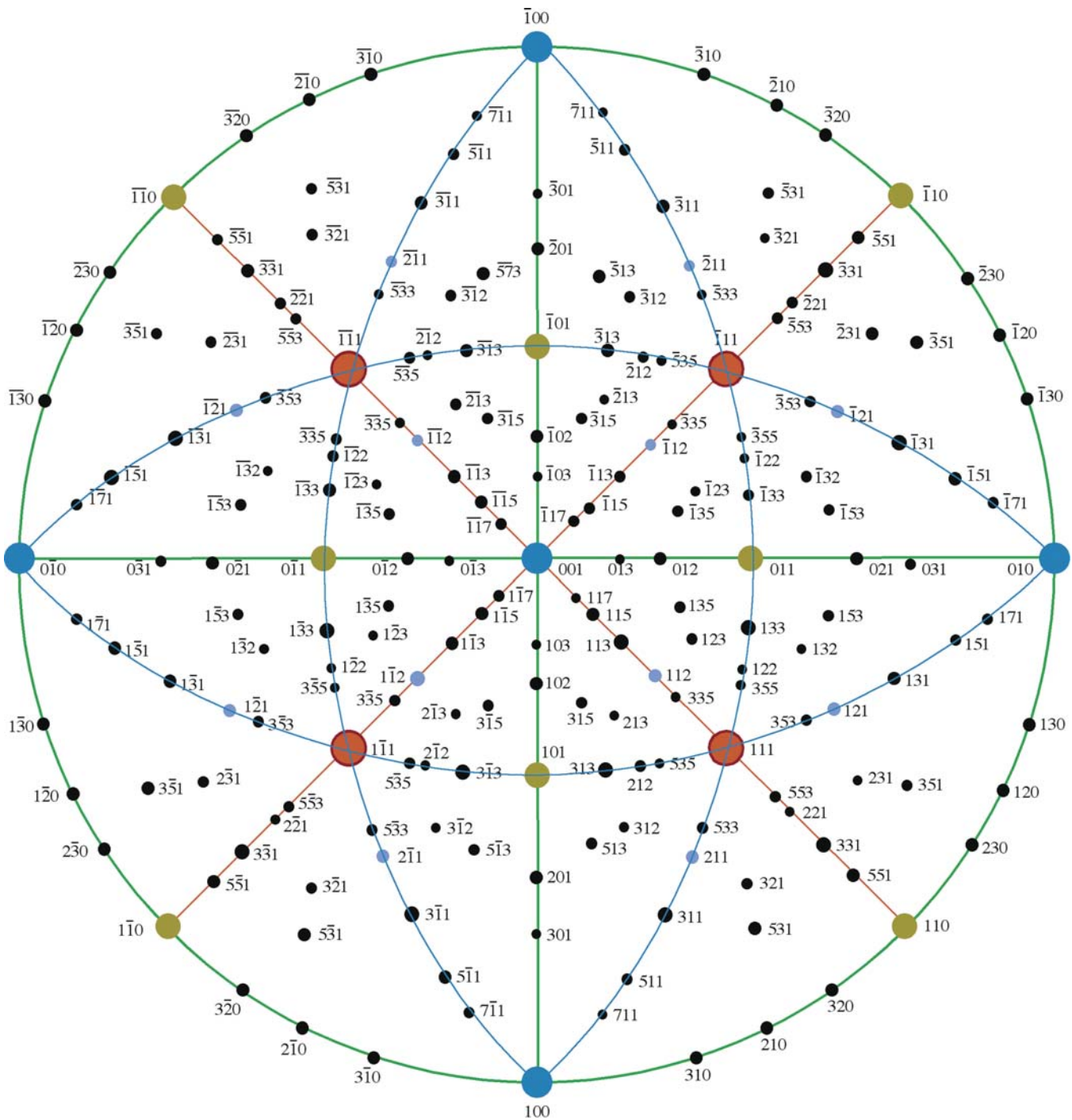


FIGURE 18.4. Some standard cubic stereographic projections. The pole in the center defines each projection, so these are 001, 011 and 111.



**FIGURE 18.5.** The stereographic projection for a cubic foil with a [001] normal, assuming the beam is down [001] also. If you want to form an image with the 022 reflection, you need to tilt the specimen so the 0 $\bar{1}$ 1 pole rotates until it is on the primitive, i.e., it is 90° from the beam direction. To do this, you need to tilt about a pole that is 90° from the 0 $\bar{2}$ 2 reflection, such as the [100], [111] or [311] zone axes.

Table 18.1 lists allowed and forbidden reflections for some cubic systems. Rules for more crystal systems are given in Table 16.2.

### R AND *d*-SPACINGS

The ratio of any two *R* values gives the inverse ratio of the *d*-spacings.

Once you have tentatively identified possible values for  $g_1$  and  $g_2$ , you need to cross-check your answers using the angles between the  $g$  vectors (i.e., the angles between the plane normals). The fully indexed patterns at the end of this chapter (Figures 18.19–18.21) show the principal interplanar angles and the principal ratios of  $g_1/g_2$ . Hence, in practice, you will rarely have to measure more than two or three spacings in order to index a



**TABLE 18.1. The Selection Rules for Cubic Crystal Structures**

bcc		fcc		Diamond cubic	
$h^2 + k^2 + l^2$	$hkl$	$h^2 + k^2 + l^2$	$hkl$	$h^2 + k^2 + l^2$	$hkl$
2	110				
		3	111	3	111
4	200	4	200	4	200
6	211				
8	220	8	220	8	220
10	310				
		11	331	11	331
12	222	12	222		
14	321				
16	400	16	400	16	400
18	411				
	330				
		19	331	19	331
20	420	20	420		
22	332				
24	422	24	422	24	422
26	431				
		27	511	27	511
		27	333	27	333
30	521				
32	440	32	440	32	440

particular zone-axis DP. However, if your specimen is not oriented close to a zone axis, you'll need to look ahead to Section 18.10.

**WEISS ZONE LAW**

Check the consistency of your indexing using the Weiss zone law. Each  $hkl$  reflection must lie in the  $[UVW]$  zone, i.e.,  $hU + kV + lW = 0$ .

The Weiss zone law only holds for diffraction into the zeroth layer of the reciprocal lattice and the diffraction spots that we see here are called the zero-order Laue zone (ZOLZ). There are circumstances when we can see diffraction from higher-order Laue zones (HOLZ) and we'll talk a lot more about this phenomenon in Chapters 20 and 21. All SADPs, particularly those that we talk about and index in this and the next chapter, are ZOLZ patterns.

The angle between normals to the planes  $(h_1k_1l_1)$  and  $(h_2k_2l_2)$  is  $\phi$ ; the angle between directions  $[U_1V_1W_1]$  and  $[U_2V_2W_2]$  is  $\rho$ . You can work these out and cross-check them with your DPs. These are standard equations in many texts (e.g., those by Edington and Andrews et al.). You'll probably find that the equations for the cubic system are the most useful.

$$\cos \phi = \frac{h_1h_2 + k_1k_2 + l_1l_2}{(h_1^2 + k_1^2 + l_1^2)^{1/2} (h_2^2 + k_2^2 + l_2^2)^{1/2}} \quad (18.3)$$

$$\cos \rho = \frac{U_1U_2 + V_1V_2 + W_1W_2}{(U_1^2 + V_1^2 + W_1^2)^{1/2} (U_2^2 + V_2^2 + W_2^2)^{1/2}} \quad (18.4)$$

Remember that you can always work out these expressions for any crystal system using the equation for the dot product of the two appropriate vectors.

In principle, if we don't know the crystal structure, we can still work out the  $d$ -spacings of the diffracting planes using equation 18.1. However, you should remember that SAD is not the most accurate method for determining the spacing of lattice planes,  $d_{hkl}$ , or the angles between them,  $\phi$ . SAD is generally very good at distinguishing patterns, but it completely fails when the difference between the two patterns is a  $180^\circ$  rotation, as occurs in some patterns of polar material, like GaAs or GaN.

To summarize

- Tilt your specimen to a low-index pole.
- Set  $s = 0$  for the innermost reflections.
- Record the SADP.
- Repeat the exercise using higher-order reflections after tilting the specimen to set  $s = 0$ . These measurements will be more accurate, but only if you make sure that  $s = 0$ .

The discussion on relrods in Chapter 16 told you that both  $d$  and  $\phi$  could be seriously in error if reflections are not set to have  $s = 0$ , especially since you've probably tilted the specimen.

So far, you have only indexed one DP. You'll probably need more than one to determine orientation relationships. While you're at the microscope, tilt to pole #2 keeping  $g_1$  (see Figure 18.6) strongly excited. Repeat the

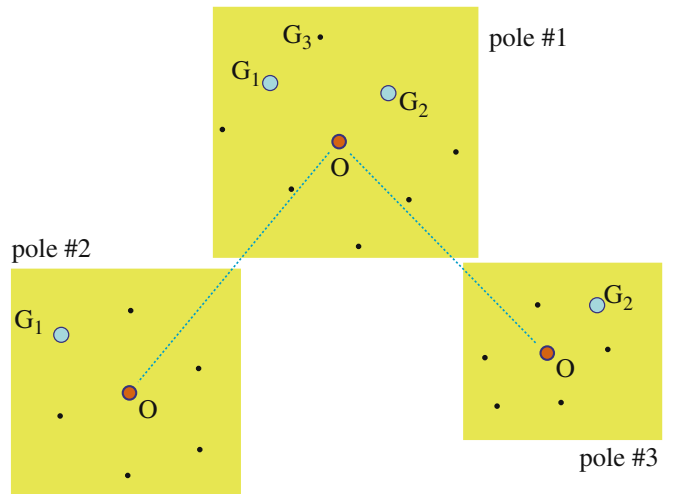


**FIGURE 18.6.** How to confirm your indexing of reflections and poles by tilting to other poles. Start with  $g_1$  and  $g_2$  strongly excited at pole #1. Tilt to pole #2 keeping  $g_1$  strong, then go back to pole #1 and tilt to pole #3, keeping  $g_2$  strong. Index all the strong reflections each time, measure the tilt angles between each reflection and estimate the tilt between poles.

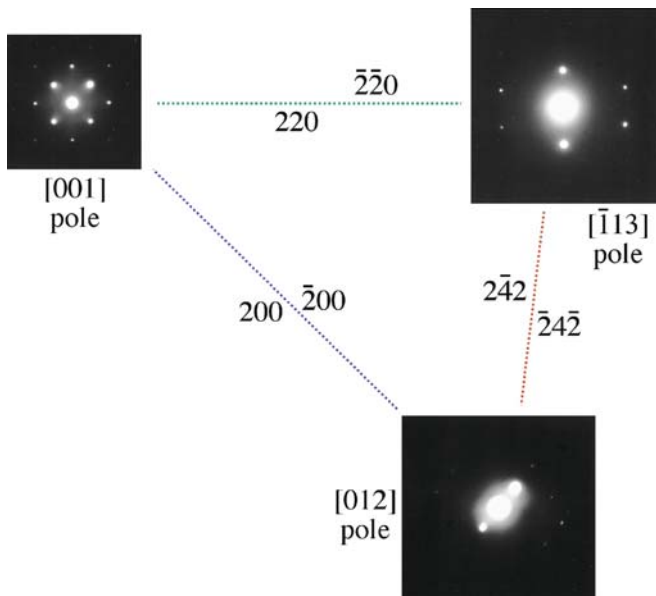


FIGURE 18.7. A practical illustration of the procedure described in Figure 18.6 for an fcc material, in this case MgO.

indexing procedure. Go back to pole #1 and tilt to pole #3 keeping  $\mathbf{g}_2$  strongly excited. You can repeat this indexing as many times as you wish. The important idea is that you now have angular measurements allowing you to cross-check your determination of both  $\mathbf{g}_1$  and  $\mathbf{g}_2$  and the zone axes. Of course the task is simple for an fcc crystal, as you can see in Figure 18.7, which is an experimental illustration of this procedure. The challenge comes when the crystal has less symmetry. If you already know the crystal structure, then you should plot out the most important poles, relating their orientations to one another (more on this in Section 18.11 and Chapter 19) and pay particular attention to the information from systematic absences which occur when the structure factor is zero (go back and check Section 3.9 and Chapter 13).

### THE GOLDEN RULE

Make the task as easy as possible. Record *ALL* the DPs you might need and how they relate to one another (draw road maps) while you're at the microscope.

## 18.5 RING PATTERNS FROM POLYCRYSTALLINE MATERIALS

Diffraction from polycrystalline specimens (especially when the grain sizes are at the nanoscale) can be viewed in much the same way as X-ray diffraction from powders. For a completely random polycrystal, we rotate the reciprocal lattice about all axes and produce a set of

nested spheres. When we intersect these spheres with the Ewald sphere (which, in the TEM, approximates to a plane) we will see the rings which are recorded in powder patterns.

### NANO AND DPs

Smaller grains give broader spots in the DP. Nanocrystals should give the largest spots, or...

If a polycrystal is textured, then there is usually one special plane which is common to nearly all the grains. Since the grains are small, all the reciprocal-lattice points will be broadened by the shape effect; so will the sphere or circles for the polycrystals. This situation will be exacerbated for nanocrystals.

If we then rotate the reciprocal lattice about the lattice vector normal to the texture plane, we produce a set of circles in reciprocal space, as shown in Figure 18.8. If we are examining cubic materials, the reciprocal-lattice vector  $\mathbf{g}_{hkl}$  will be parallel to the direction  $[hkl]$  in real space. Otherwise this will not generally be the case.

The DP in either of these examples appears as shown in Figure 18.9A and B which differs because the grain

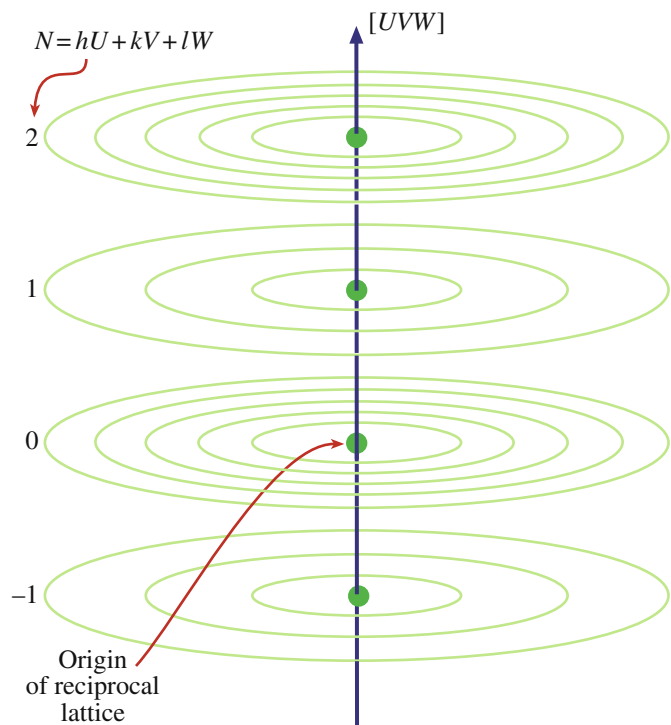
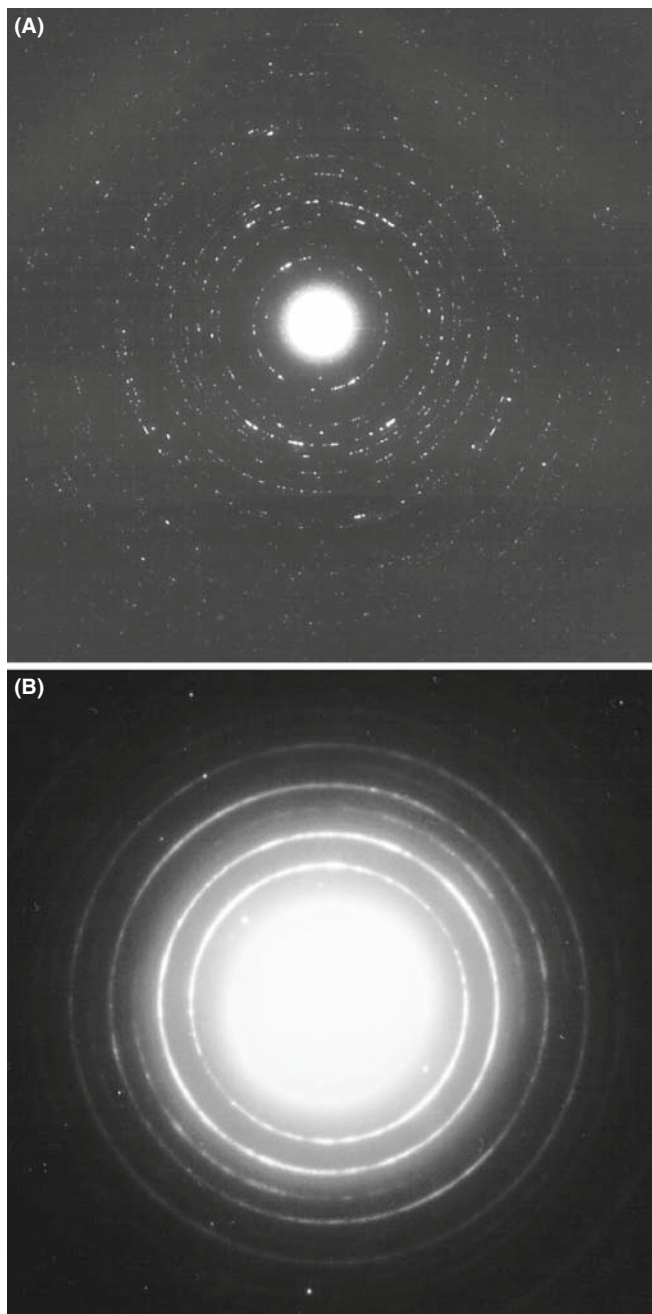


FIGURE 18.8. The generation of a set of circles in reciprocal space by a textured polycrystal. When the reciprocal lattice is rotated about a particular direction  $[UVW]$  (in this case the normal to the texture plane) each Laue zone ( $N = 1, 2$ , etc.) produces a set of concentric circles for each allowed reflection in each zone.



**FIGURE 18.9.** (A) and (B) Ring DPs from polycrystalline foils. In (A) the grain size is larger than in (B) so the rings are made up of discrete spots. A finer grain size, as in (B) produces a more continuous ring pattern, but the width of the rings of diffracted intensity in fact becomes broader and can be used as an inverse measure of the grain size.

size is different. A larger grain size gives a more speckled pattern.

You can distinguish the pattern produced by a textured specimen from one produced by a random polycrystal by tilting. If your specimen is textured, the rings become arcs as shown in the pattern in Figure 18.10A together with the Ewald-sphere construction in Figure 18.10B. You can locate the grains which give rise to the arcs by forming a

CDF image with the arc of diffracted intensity. In Figure 18.10C, these oriented grains are uniformly distributed, but you might encounter a situation where this is not the case. Think how the pattern might differ in this case.

Figure 18.10D and E emphasizes that these ring patterns can be quite varied. In this case the specimen is  $\alpha$ -Ag<sub>2</sub>Se, which is textured about an axis *inclined* to the beam. When the Ewald sphere cuts the circles now, it produces elongated spots which lie on an ellipse. Vainshtein et al. point out that all the ‘spots’ on one ellipse can be indexed with the same  $hk$  indices but a different  $l$ , and call such a pattern an oblique-textured electron DP. You should also be careful in indexing these textured patterns since not all possible  $d_{hkl}$  values need be present, depending on the texture plane.

There is more information in ring patterns than spot patterns. Like a powder pattern, you could estimate the grain size from the width of the rings, but it’s more direct (and more reliable) to just look at the DF image. You can see kinematically forbidden rings because you don’t necessarily have single scattering from each grain but there are ways around this problem.

Nanocrystalline materials, which fall into our smallest range of  $\sim 10$ -nm grain size, are very challenging because there’s probably always more than one grain through the foil thickness. Careful DF imaging combined with HRTEM or CBED with the smallest possible probe (often called nanodiffraction, see Section 21.8.B), is probably optimal, but you need to look for clustering of similarly oriented grains.

## 18.6 RING PATTERNS FROM HOLLOW-CONE DIFFRACTION

We can combine the advantages of ring patterns from small-grained materials with individual spot patterns from larger-grained materials. As we noted back in Section 9.3.D, if you have a nano/microcrystalline specimen, it is rather inefficient to get a DP from one grain at a time by carefully tilting your specimen and then getting individual DF images of single areas, or of phases within a single grain, by carefully tilting the incident beam. So we can use a computer to continuously change the beam orientation so it samples many angles of incidence and gather DPs from all the crystals superimposed on one another (i.e., get a ring pattern, even from a relatively large-grain material). This is the principle behind hollow-cone (sometimes called ‘conical’) diffraction (go back and look at Figure 9.15). In the same section we also introduced the idea of hollow-cone DF imaging. In earlier TEMs, before computer control of the beam, hollow-cone illumination was achieved by using an annular C2 aperture rather than a circular hole. Thus the beam that came through the annulus irradiated the specimen from a fixed angle

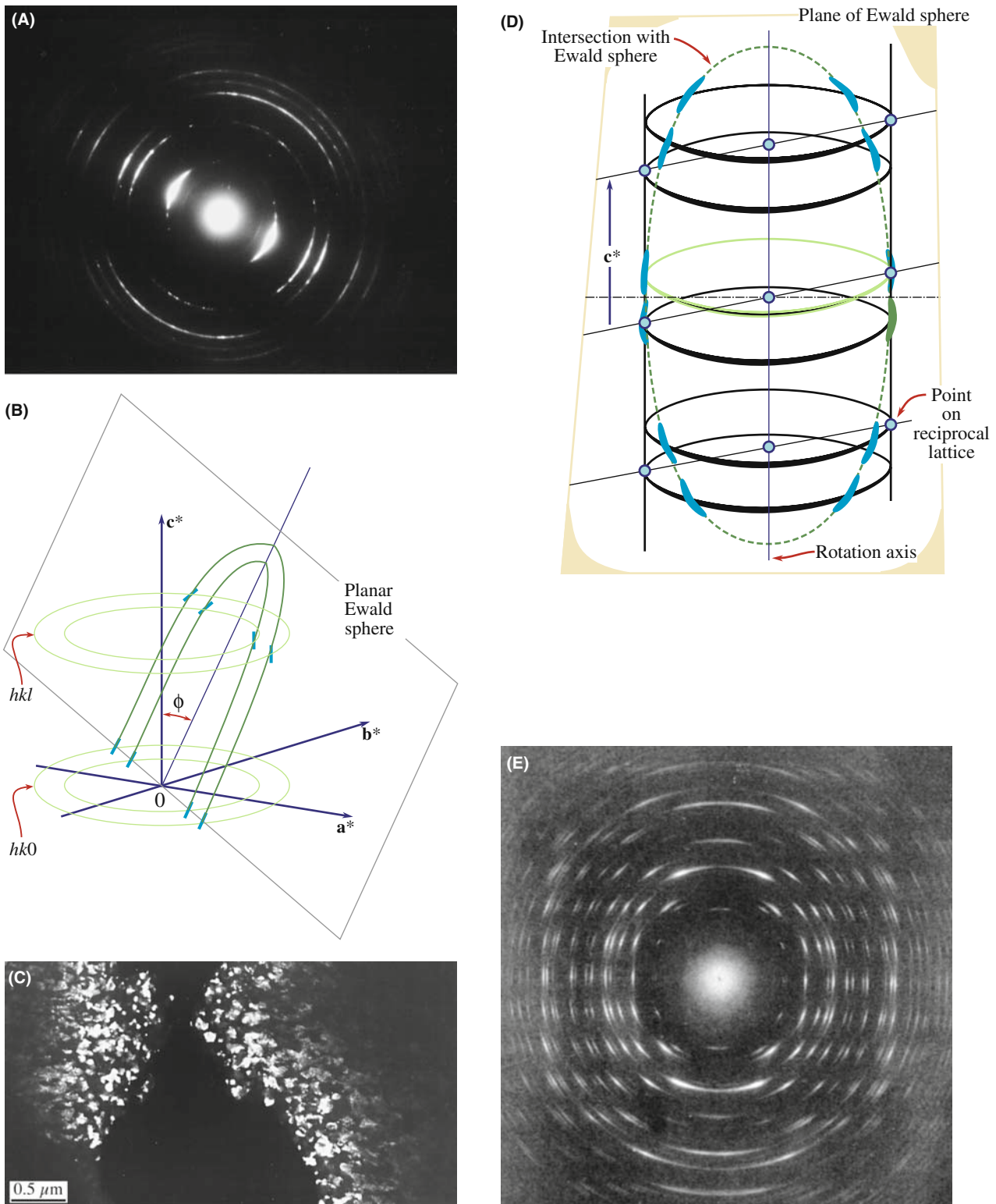


**FIGURE 18.10.** (A) A textured ring pattern where the rings are more intense over a certain angular range. (B) The corresponding interception of the Ewald sphere (plane) with the reciprocal lattice. (C) A DF image of the textured grains, taken from a brighter portion of one of the  $hkl$  rings, showing an equiaxed structure. In (D) the specimen is textured about a direction at an angle to the beam, so the Ewald sphere creates elongated spots or arcs in the DP (E).



around the optic axis, as shown schematically back in Figure 9.15A. It's much easier and more flexible to use the computer to control the pre-specimen scan coils and bring the beam onto the specimen at a fixed (or a range of) conical scan angle and a typical conical-scan DP is shown in Figure 9.15B. (If you look ahead, you can see another example of a hollow-cone DF image from an amorphous DP in Figure 18.14C.) Of course, we index the rings in exactly the same way as we described in Section 18.5 for ring patterns obtained from a polycrystalline specimen where the grain size is much smaller than the beam size.

With hollow-cone illumination, we can create a DF image of *all* the crystals in a film that are diffracting from their  $\{hkl\}$  planes, rather than imaging only that small fraction diffracting into the part of the diffraction ring that happens to be selected by the aperture. The difference in information content between these two approaches is shown back in Figure 9.15B and C. The hollow-cone technique is widely used in CBED (see Chapter 21) and has more recently been used as the basis for precession diffraction (see Section 18.8.)

## 18.7 RING PATTERNS FROM AMORPHOUS MATERIALS

Amorphous materials used to represent somewhat of a fringe field in materials science but the rapid growth in glass technology over the last decade, fueled by the optical-communications bubble, the development of bulk metallic glasses and the increased awareness of the role of glassy films at interfaces (particularly the gate oxide in semiconductors) have all conspired to crystallize the following question: *is the material really amorphous or is it (sub) nanocrystalline?* Actually this question is still debated when discussing both amorphous materials and, more intensely, oxide and metallic glasses because there's still no broadly accepted definition of when grains become small enough that a determinable crystal structure no longer exists. At best we should think of a continuum of states from nanocrystalline to amorphous.

### DPs AND AMORPHOUS MATERIALS

The DP from an amorphous material looks similar to that from polycrystalline material but the rings are broader and there is no speckle.

Rudee and Howie showed that electron scattering from regions of  $\leq 1.5$  nm diameter could be coherent. Graczyk and Chaudhari proposed modeling these materials as random networks. If we are careful, we can learn quite a lot about the structure of amorphous

materials, but we should first say what we mean by 'amorphous.'

An amorphous material is one where the locations of the neighboring atoms are defined by a probability function such that the probabilities are never unity.

This idea is best illustrated by a plot of the probability which we call the *radial distribution function* (RDF). The RDF,  $\rho(r)$ , is the probability, per unit element of volume, that an atom will be found at a distance  $r$  from another atom. The first example in Figure 18.11A compares the curves for liquid sodium and crystalline sodium; the numbers on the crystalline curve remind us that in the crystal each sodium has eight nearest neighbors, etc. The second plot, Figure 18.11B, shows the RDF for vitreous silica. This time the peaks are associated with distances

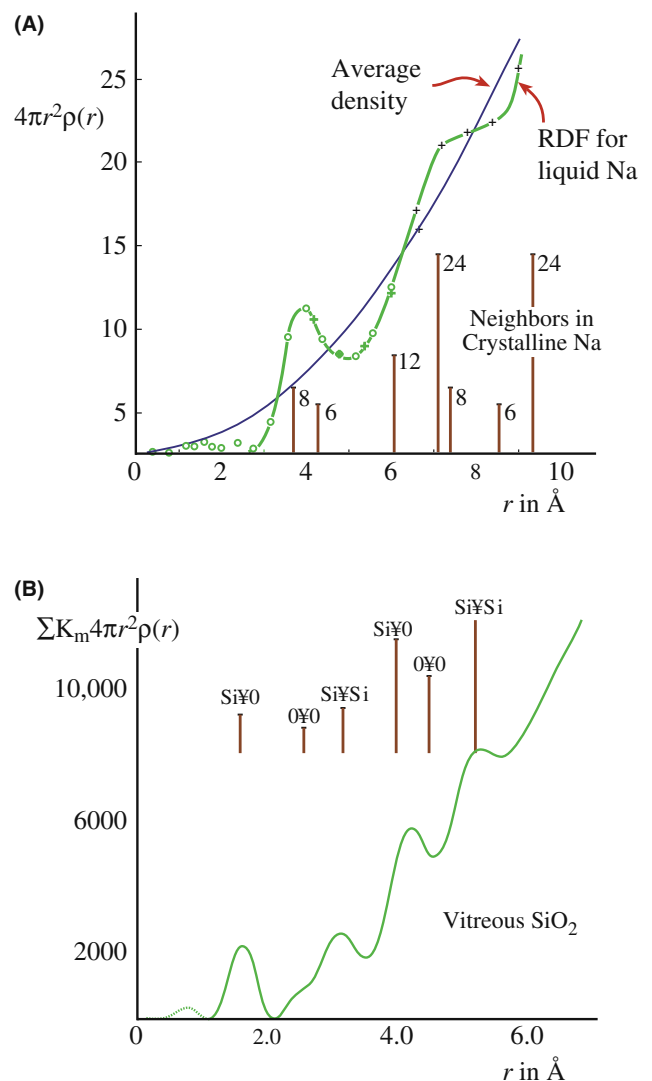


FIGURE 18.11. (A) Radial distribution functions for liquid Na and the average density curve superimposed on the distribution of the nearest neighbors in crystalline Na (vertical lines). (B) The RDF for vitreous SiO<sub>2</sub> is peaked at a distance that represents spacings between Si and O atoms.



between different pairs of Si and O atoms. The features to notice are

- The two curves both show definite peaks.
- The two curves are different.

*Some diffraction theory.* Since these materials are so different, we'll give a brief introduction to the theory of scattering from amorphous materials. We make the assumption that the electron beam is only scattered once; this is kinematical, but it's more realistic than for crystals at the Bragg condition. Following Howie, we express the kinematical intensity,  $I(\mathbf{k})$ , by the expression

$$I(\mathbf{k}) = |f(\mathbf{k})|^2 \sum_{i,j} e^{i2\pi\mathbf{k}\cdot(\mathbf{r}_i-\mathbf{r}_j)} \quad (18.5)$$

Here we assume that there are  $N$  identical atoms contributing to the scattered intensity and they are located at the different positions ( $\mathbf{r}_i$  or  $\mathbf{r}_j$ ).

The  $f(\mathbf{k})$  terms are the atomic scattering amplitudes, with  $\mathbf{k}$  reminding us that there is an angular dependence to  $f$ . If the material is isotropic, we can simplify equation 18.5 as follows

$$I(\mathbf{k}) = N|f(\mathbf{k})|^2 \left(1 + \frac{F(\mathbf{k})}{k}\right) \quad (18.6)$$

where

$$F(\mathbf{k}) = \sum_{i \neq j} e^{i2\pi\mathbf{k}\cdot(\mathbf{r}_i-\mathbf{r}_j)} \quad (18.7)$$

$$F(\mathbf{k}) = k \int \rho(r) e^{i2\pi\mathbf{k}\cdot\mathbf{r}} dV \quad (18.8)$$

$$F(\mathbf{k}) = 4\pi \int_0^\infty \rho(r) \sin(2\pi kr) r dr \quad (18.9)$$

The term  $\rho(\mathbf{r})$  is the RDF. Equation 18.9 can be inverted to give an expression for  $\rho$

$$\rho(\mathbf{r}) - \rho_0 = \frac{1}{r} \int_0^\infty F(\mathbf{k}) \sin 2\pi kr dk \quad (18.10)$$

This equation means that, in principle, the RDF can be obtained directly from DPs. This process is enhanced if the patterns are energy-filtered to remove inelastic contributions (see Chapter 37 and the work of Cockayne et al.) as shown graphically in Figures 18.12 and 18.13. Compare these figures with Figure 2.13A. Other ways to determine the RDF include extended X-ray absorption fine structure (EXAFS) studies in a synchrotron X-ray and, less expensively but more noisily, via EXELFS (see Chapter 40). Alternatively, we can rearrange equation 18.6 again to give a 'reduced-intensity function' as illustrated by the work of Graczyk and Chaudhari who

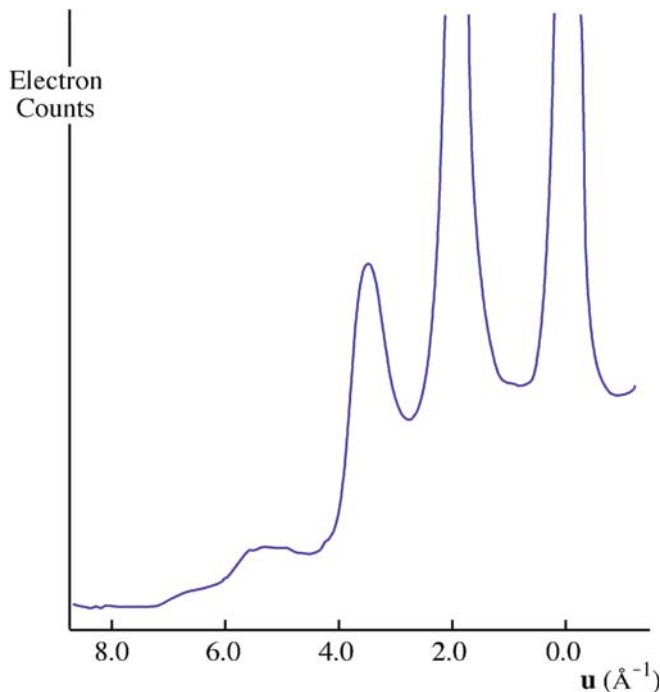


**FIGURE 18.12.** An intensity profile across an energy-filtered DP from amorphous Si obtained by scanning the pattern across the entrance slit to a serial EELS spectrometer and recording only the elastic (on-axis) electrons.

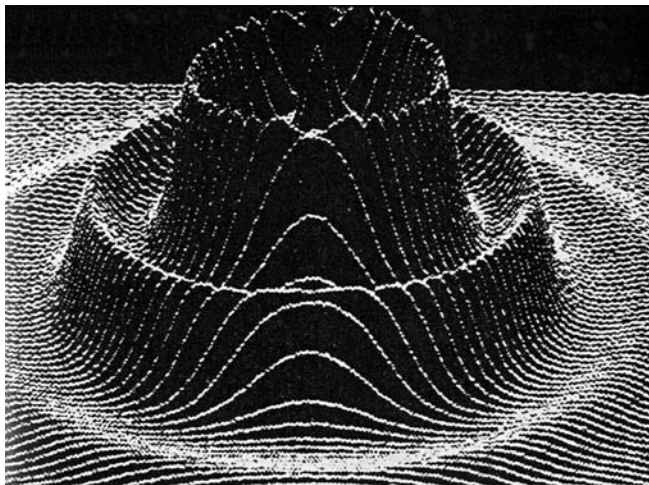


**FIGURE 18.13.** A computer plot of the diffracted intensity distribution from an amorphous structure, showing diffuse rings of intensity. The direct-beam intensity is off-scale.

showed clearly that the structure correlation can extend to 1.5 nm or more. Life gets more interesting as we explore the structure out beyond the nanometer level and Treacy et al. review a new imaging technique called fluctuation microscopy which is a hybrid imaging/diffraction technique sensitive to the presence of medium-range order in amorphous materials. We'll discuss this technique more in Chapter 29. If you get the idea that

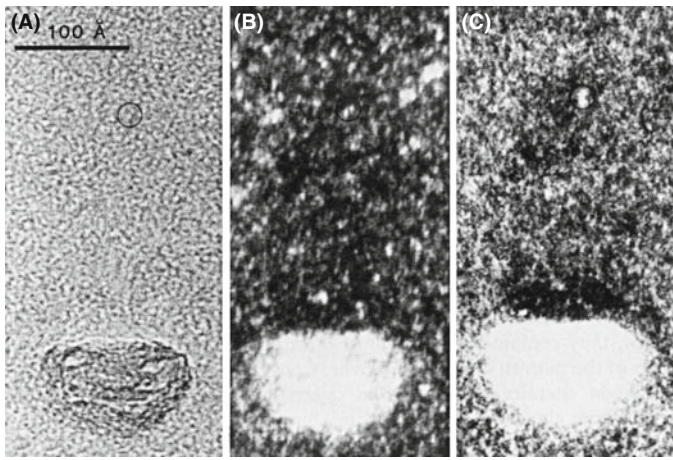


**FIGURE 18.14.** (A) BF image of amorphous carbon. (B) DF image from the diffuse diffracted intensity taken with a defocused beam and (C) hollow-cone image showing more structure.

the study of amorphous materials is at the frontiers of TEM materials-structure determination, you are right!

To summarize this discussion, the scattering theory is well known but the capability for routinely removing the inelastic contribution is only now becoming available and is still not commonplace. Probably the best way to answer whether a material is nanocrystalline or amorphous will come from a combination of SAD and EELS. A BF image of amorphous material is generally uninformative (Figure 18.14A), but if you try to form a DF image you will see a speckle of white spots against a dark background, as shown in Figure 18.14B. The size of the speckle increases as the defocus increases, so be wary of interpreting the image in terms of the size of regions in the amorphous structure. Hollow-cone DF imaging, as shown in Figure 18.14C, gives even more and finer ‘structure’ in the image. The fact that you can produce this type of speckled contrast is important because you may well want to study small particles (e.g., catalysts) supported by an amorphous film. In such a case, you need to know what the image of the support film looks like before you add a new component.

*Glass at interfaces and grain boundaries.* Another area where it is important to know whether or not an amorphous material is present, occurs in the analysis of grain boundaries in ceramic materials or gate oxides in semiconductor devices. Answering this problem severely taxes the limits of HRTEM when the film thicknesses are  $< 1$  nm, which is the case for the gate oxide in the latest semiconductor devices. For somewhat thicker films we can use conventional HRTEM and another technique, known as diffuse-dark-field (DDF) imaging, which essentially forms an image from the region in the SADP where the amorphous ring would be, if glass were present. We’ll return to DDF imaging in Chapter 29.

## 18.8 PRECESSION DIFFRACTION

Precession is a relatively new approach to performing electron diffraction; it is similar to the X-ray method which goes by the same ‘name’ (although in XRD the crystal, rather than the beam, is precessed) and it is closely related to hollow-cone diffraction that we just talked about. The main advantage that precession brings is to remove strong dynamical effects from the patterns leaving high-quality kinematical data, eliminating, e.g., extra spots due to dynamical effects. Precession diffraction can also be used for crystal structure and full symmetry determination. While the method was first tried in a TEM by Vincent and Midgley, recent advances in both CCD cameras and (you’ve guessed it) aberration correction make both the operational aspects and the interpretation of precession DPs much easier.

In precession diffraction we double-deflect the incident beam (either parallel or convergent) using the usual DF scan coils in a circular hollow cone (radius  $G$  and angle  $C$ ) about a centered zone-axis direction (Figure 18.15) and de-scan the beam onto the plane of the DP. So it is really a double conical beam-rocking system.

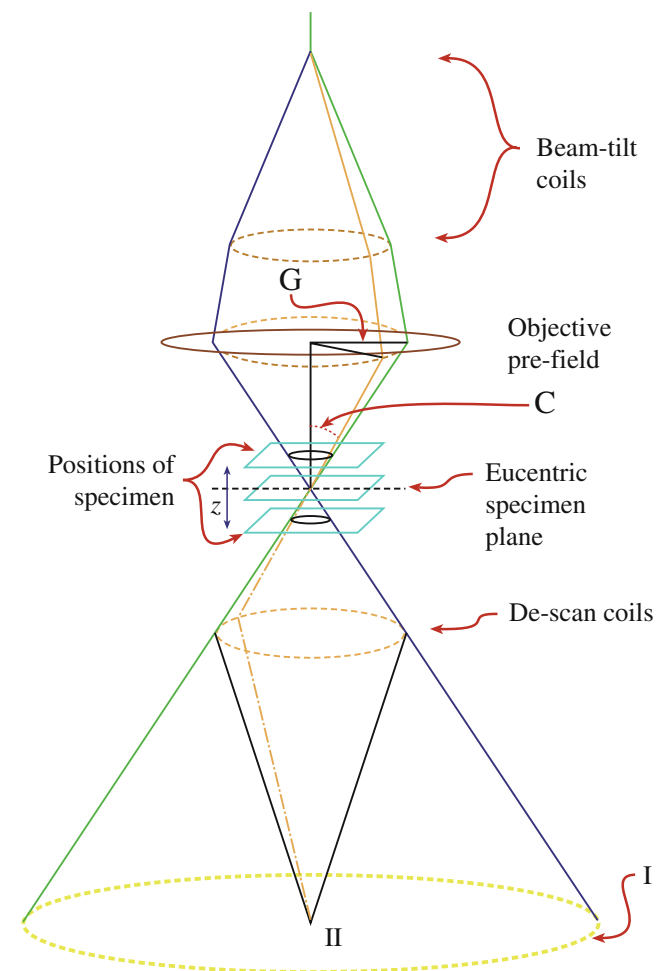


**FIGURE 18.15.** Schematic ray diagram for precession diffraction.

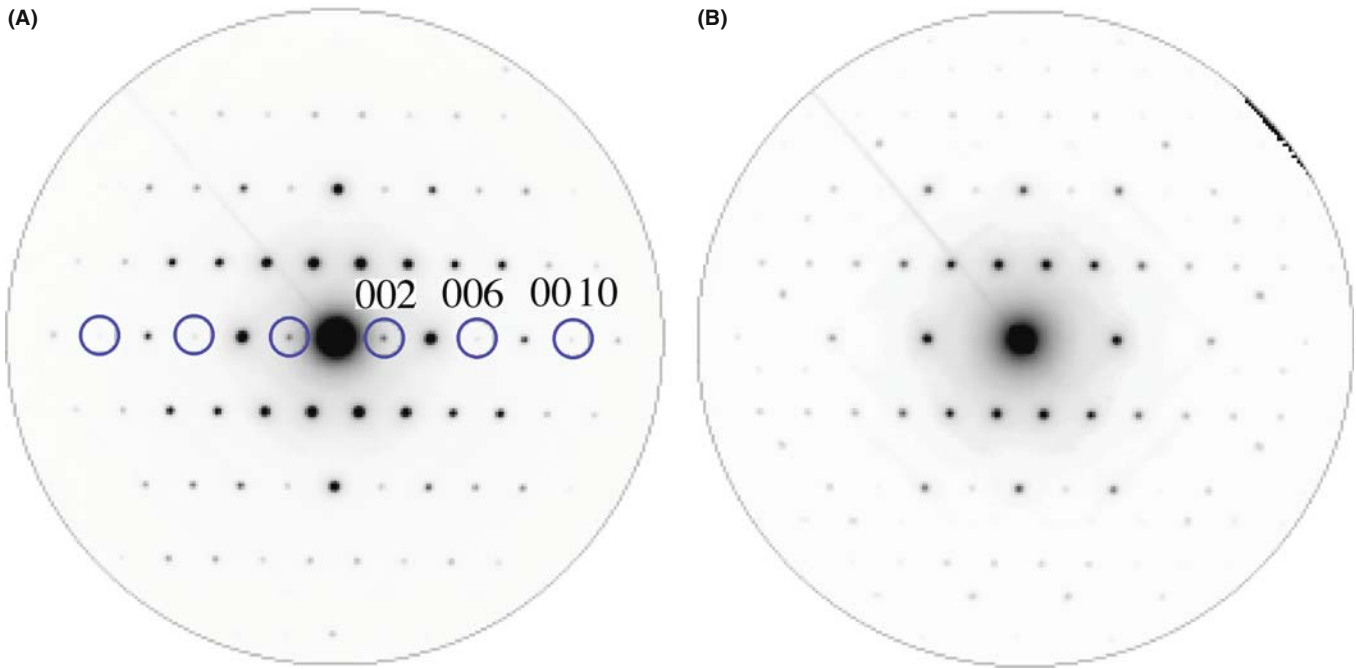


**FIGURE 18.16.** Si  $\langle 130 \rangle$  DP taken (A) with a small precession angle ( $1^\circ$ ) and (B) with a large precession angle ( $3^\circ$ ). The kinematically forbidden reflections 002, 006, 0010 disappear at the larger precession angle. Note also the appearance of strong differences in the intensity of individual  $hkl$  maxima.

Unlike standard TEM hollow-cone where we are seeking to get multiple (i.e., ring) patterns sampling many grains, in precession mode we are usually trying to average out the diffraction conditions within a single grain and obtain a single-crystal pattern in which dynamical effects are reduced. If the hollow-cone angle is large enough, all the diffraction data correspond to a two-beam condition and show reduced dynamical diffraction because not many reflections are simultaneously excited off the zone-axis condition. When we precess the beam, we integrate the diffracted intensities through the Bragg condition, so small specimen-tilt changes are averaged out and we can more reliably interpret crystal-symmetry information in the DP. Continuous changing of the precession angle over several degrees can help with point and space-group determination (see Chapter 21, the companion text and Morniroli et al.'s paper). Figure 18.16A and B shows, respectively, the differences between small and large precession-angle DPs from a Si single crystal. The larger angle removes the kinematically forbidden reflections that are present in the smaller-angle DP because the multiple-diffraction paths to them are unlikely to occur during the precession movement. Most of the time, only the direct beam and one diffracted beam are strongly excited as the beam precesses. This does not mean that the dynamical interactions disappear, they just occur between the direct beam and one diffracted beam (as in the two-beam case).

Precession is an area of electron diffraction that is seeing a rapid growth in applications across many fields. Commercial retrofits are available for any TEM (e.g., URL #3) but, if you want to do it on your own, then Own et al. give good detailed instructions.

## 18.9 DOUBLE DIFFRACTION

Double diffraction occurs when a diffracted beam traveling through a crystal is rediffracted either within the same crystal or when it passes into a second crystal. If the initial diffraction vector of the beam is  $\mathbf{g}_1$  and it is rediffracted by reflection  $\bar{\mathbf{g}}_2$ , then the resultant diffraction vector of the double-diffracted beam is  $(\mathbf{g}_1 - \bar{\mathbf{g}}_2)$ . If  $\bar{\mathbf{g}}_2$  is not an allowed reflection in the first crystal, the double-diffracted beam is characteristic of neither the first nor the second crystal.

Reflections attributable to double diffraction are a common feature of DPs recorded from two-phase materials exhibiting epitaxy or topotaxy including, e.g., oxidized metallic specimens. Quite complicated patterns may be formed, requiring careful analysis to distinguish the 'real' reflections from the double-diffraction reflections. Double diffraction is directly responsible for the moiré effect in the electron images that we will discuss in Chapter 23. As an example of this effect, we'll consider small  $\alpha\text{-Fe}_2\text{O}_3$  (hematite) islands grown on a single-crystal  $\alpha\text{-Al}_2\text{O}_3$  (alumina or sapphire) substrate as



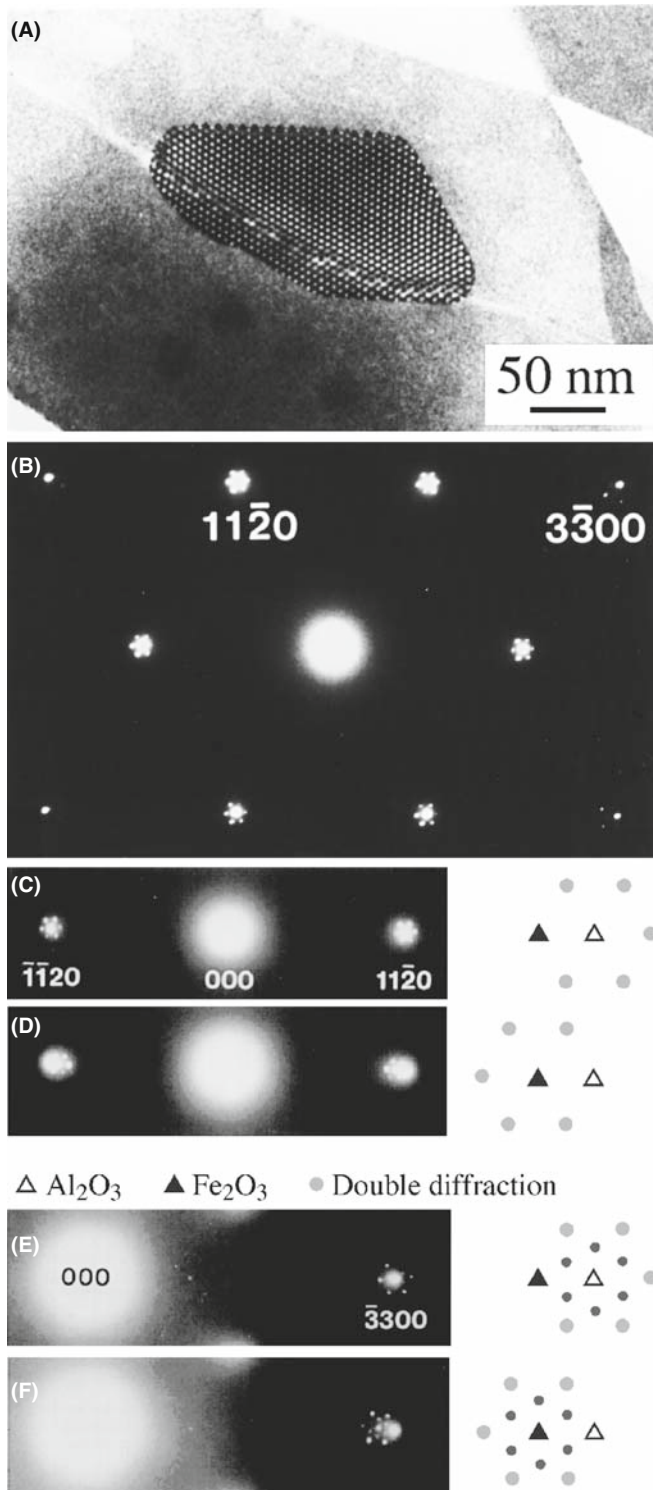


**FIGURE 18.17** (A) BF on-axis image of a particle of  $\alpha\text{-Fe}_2\text{O}_3$  on  $\alpha\text{-Al}_2\text{O}_3$ . (B)  $[0001]$  SADP from  $\alpha\text{-Fe}_2\text{O}_3$  showing double-diffraction spots around the  $\{11\bar{2}0\}$  and  $\{3\bar{3}00\}$  reflections. (C) Enlargements of regions near the  $\{11\bar{2}0\}$  reflections when the hematite island is on the top surface. (D) Enlargements of regions near the  $\{11\bar{2}0\}$  reflections when the hematite island is on the bottom. (E) Enlargements of regions near the  $\{3\bar{3}00\}$  reflections when the hematite island is on the top surface. (F) Enlargements of regions near the  $\{3\bar{3}00\}$  reflections when the hematite island is on the bottom.

shown in Figure 18.17A. The position of the double-diffraction spots relative to the hematite and alumina reflections actually changes depending on whether the islands were on the top or bottom surface of the specimen. This particular top–bottom effect can be derived from simple geometry; however, dynamical diffraction effects must also be considered when the materials are thicker.

Figure 18.17B shows the  $[0001]$  SADP recorded from one of these  $\alpha\text{-Fe}_2\text{O}_3$  particles. The closest reflections to the direct beam are the six  $\{11\bar{2}0\}$  reflections. The next closest reflections are the six  $\{3\bar{3}00\}$  reflections, only four of which are visible in the figure. Double-diffraction spots are visible around each of these primary reflections. They also surround the direct beam, although they are hidden by the flare from that beam in Figure 18.17B.

Figure 18.17C and D shows enlargements of regions near the  $\{11\bar{2}0\}$  reflections in the  $[0001]$  SADPs recorded when the hematite island was on the top surface in (C) and on the bottom surface of the sapphire in (D). Both  $\mathbf{g}$  and  $\bar{\mathbf{g}}$  reflections are shown for the two cases. In (C) the ring of six double-diffraction spots surrounds the  $\text{Al}_2\text{O}_3$  reflection while in (D) the double-diffraction spots surround the  $\text{Fe}_2\text{O}_3$  reflection.

The same observation can be made for the  $\{3\bar{3}00\}$  regions of the SADPs as shown in Figure 18.17E and F. In this case, an inner ring of double-diffraction spots (small filled circles) with the same spacing and orientation as the double-diffraction reflections in Figure 18.17C and D are still visible, as are the outer rings of spots (large filled circles). In general, the outer ring of double-diffraction spots is more intense than the inner ring.

This top-bottom effect in particular, and double diffraction in general, can be explained by the simple geometric analysis we show in Figure 18.18; the bottom crystal is  $\text{Al}_2\text{O}_3$ , which has the smaller lattice parameter and therefore has the larger reciprocal-lattice vectors. Double-diffraction spots can be formed around the primary hematite reflection,  $\mathbf{g}_H$ , by two different routes

- $2\mathbf{g}_H + \bar{\mathbf{g}}_A$  (A: alumina, H: hematite) giving the double-diffraction spot just inside  $\mathbf{g}_H$ .
- $\bar{\mathbf{g}}_H + 2\mathbf{g}_A$  gives a double-diffraction spot just outside  $\mathbf{g}_H$ .

These two routes at first appear to be equivalent. However, if we take into account the curvature of the Ewald sphere, then the deviation parameters of the two routes are very different. In the case of diffraction through the upper crystal, the deviation parameter of the  $2\mathbf{g}$  beam is slightly more than twice that of the  $\bar{\mathbf{g}}$  beam. This difference will not significantly affect the intensities from a very



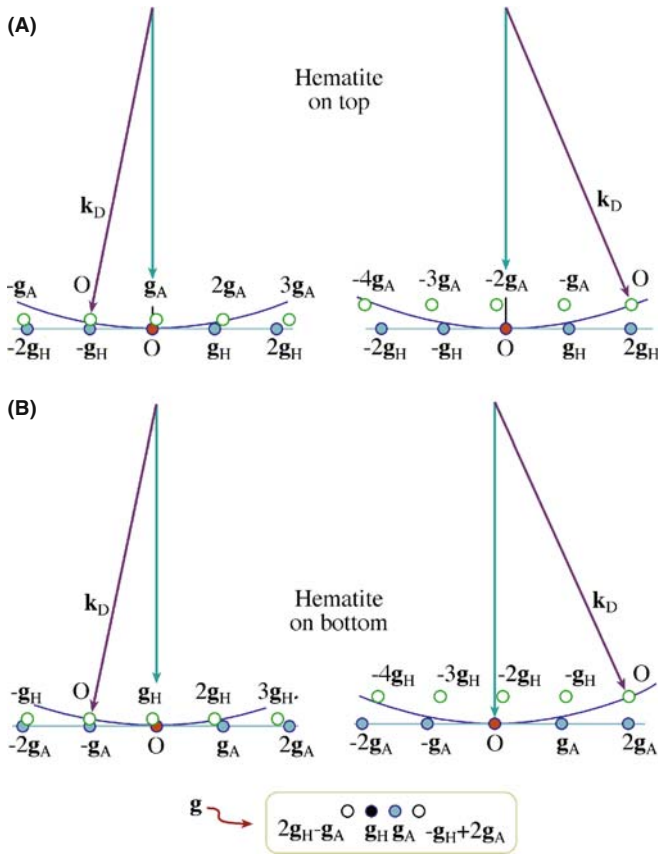


**FIGURE 18.18.** Top-bottom effect in double diffraction. The pattern depends on which of the two crystals is on top. In this case  $\alpha\text{-Fe}_2\text{O}_3$  particles are on top of the  $\text{Al}_2\text{O}_3$  and the two (non-equivalent) paths (A) and (B) for double diffraction are shown. NOTE:  $\mathbf{g}_A$  is for alumina and  $\mathbf{g}_H$  for hematite.

thin epilayer due to streaking of the reciprocal-lattice spots parallel to the beam direction (the shape-factor effect).

Now we can analyze the effects of diffraction through the lower crystal

- Draw the reciprocal lattice with the origin of the Ewald sphere at  $2\mathbf{g}_H$  for the first case and on  $\bar{\mathbf{g}}_H$  in the second.
- Keep the radius of the Ewald sphere unchanged since only elastic interactions are considered.
- The incident beam for the lower crystal is in the  $2\mathbf{g}$  or  $\bar{\mathbf{g}}$  directions for the two cases.
- The height of the ZOLZ is slightly different in the two cases since the deviation parameter at the origin must be zero.

You can see from Figure 18.18A that the deviation parameter for  $2\mathbf{g}_A$  is approximately zero, whereas for  $\bar{\mathbf{g}}_A$  it is of the same order as  $\mathbf{g}_H$ . The total deviation parameter is thus much smaller for the second route than the first. A similar analysis for the inverted structure is shown in Figure 18.18B. In both cases, the deviation parameter for the route  $\bar{\mathbf{g}}$  (upper) plus  $2\mathbf{g}$  (lower) produces a much smaller deviation parameter than the route  $2\mathbf{g}$  (upper)

plus  $\bar{\mathbf{g}}$  (lower). So the double-diffraction spot, which occurs on the same side of the diffraction spot from the upper crystal as the diffraction spot from the lower crystal, will be more intensely excited than the double-diffraction spot which occurs on the opposite side. In two dimensions, for thin films, the strongest double-diffraction spots will always be those arranged symmetrically around the diffraction spot from the lower crystal.

For thicker layers, the relative intensity of the  $\bar{\mathbf{g}}$  and  $2\mathbf{g}$  beams will vary as dynamical diffraction effects occur. We can simulate the DPs from these structures using the MacTempas program (see Chapter 30 and Section 1.6.B) The top-bottom effect is evident in the case of 2.7 nm of hematite on 13 nm of alumina, but only just discernible for the case of 2.6 nm of alumina on 13.5 nm of hematite. In the latter case, the dynamical diffraction effects are stronger.

We will meet this topic in Chapter 23 when we discuss moiré fringes. We have made this analysis a little more complicated than usual since we have considered the details of where the spots will actually be found. You can make this process simpler

- Trace the patterns from each crystal (if you know what tracing paper is).
- Then construct a new pattern using each diffracted beam from the upper crystal as an incident beam for the lower crystal.

The extent of the moiré pattern gives you an idea of just how strong dynamical scattering is, even for thin films!

## 18.10 ORIENTATION OF THE SPECIMEN

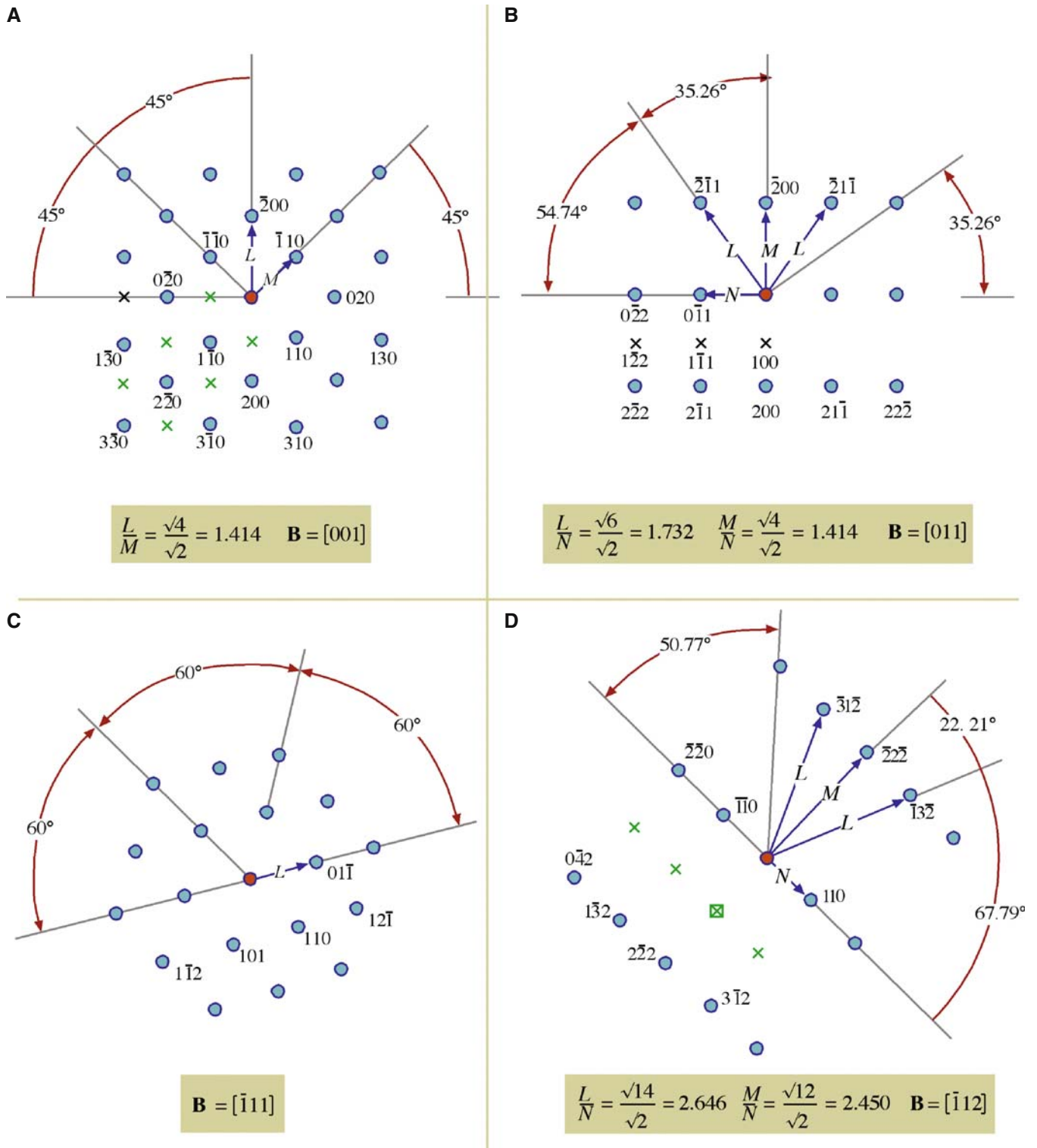
Once you have identified three  $\mathbf{g}$  vectors  $\mathbf{g}_1$ ,  $\mathbf{g}_2$  and  $\mathbf{g}_3$  in a single-crystal DP, you can calculate the direction of the beam  $\mathbf{B}$ . You can actually estimate  $\mathbf{B}$  to within about  $10^\circ$  from the vector cross product as follows

$$\mathbf{B} = \mathbf{g}_1 \times \mathbf{g}_2 = \begin{bmatrix} \mathbf{i}_1 & \mathbf{i}_2 & \mathbf{i}_3 \\ h_1 & k_1 & l_1 \\ h_2 & k_2 & l_2 \end{bmatrix} \quad (18.11)$$

$$= (k_1 l_2 - k_2 l_1, l_1 h_2 - l_2 h_1, h_1 k_2 - h_2 k_1) \quad (18.12)$$

For the three-beam case, you can determine  $\mathbf{B}$  with an accuracy of  $\sim 3^\circ$ . You first need to make sure that the three vectors are taken in the correct order. Draw a circle through these three reflections: if O is inside the circle, then the  $\mathbf{g}$  vectors should be numbered counter-clockwise; if O is outside, number them clockwise. Check your labeling; the determinant of the matrix in equation 18.13 should be positive

$$\mathbf{g}_1 \cdot (\mathbf{g}_2 \times \mathbf{g}_3) = \frac{1}{V} \begin{bmatrix} h_1 & k_1 & l_1 \\ h_2 & k_2 & l_2 \\ h_3 & k_3 & l_3 \end{bmatrix} \quad (18.13)$$



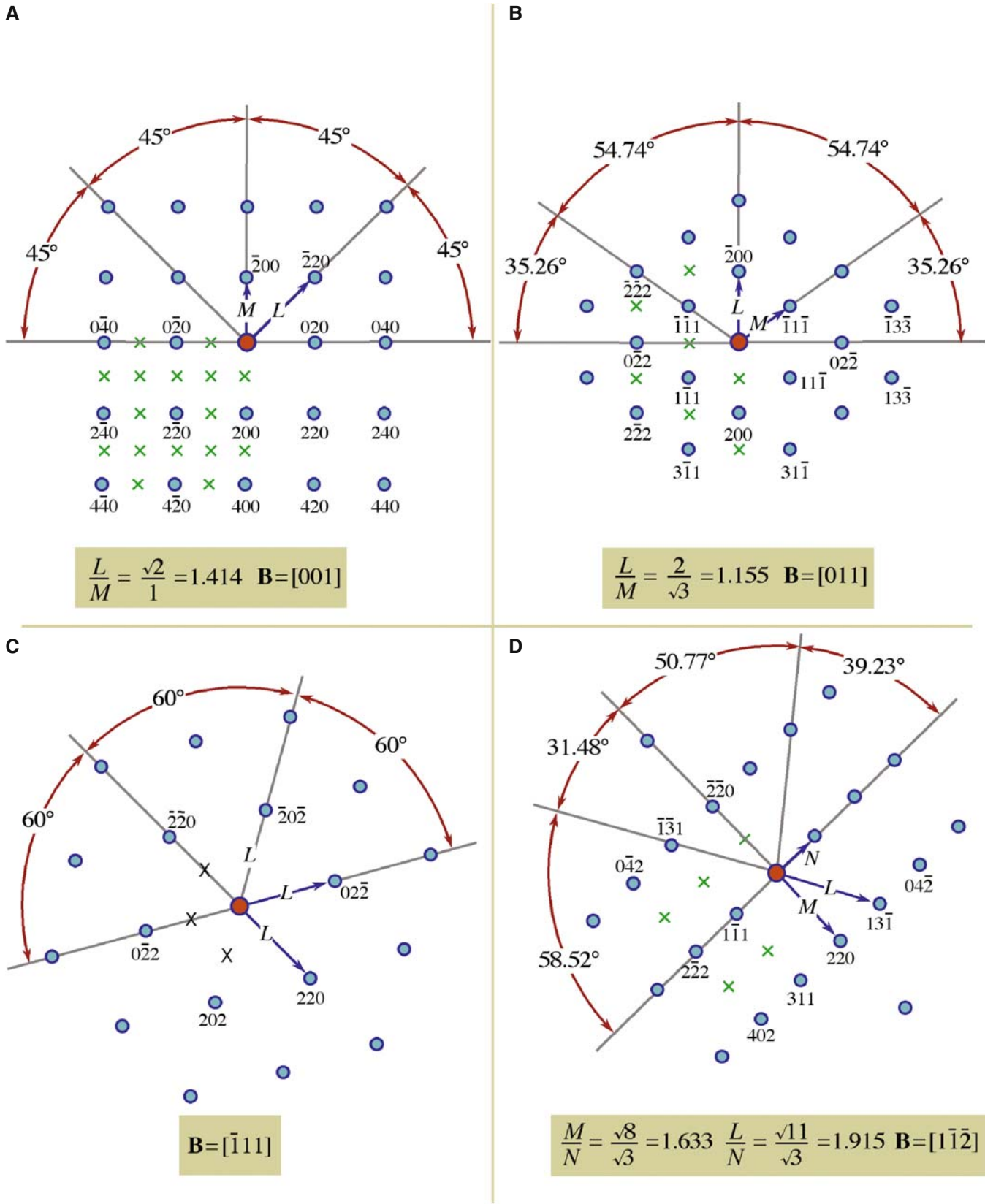
**FIGURES 18.19.** Four standard, indexed, DPs for bcc crystals in the [001], [011],  $[\bar{1}11]$  and  $[\bar{1}12]$  beam directions. Ratios of the principal spot spacings are shown as well as the angles between the principal plane normals. Forbidden reflections are indicated by x.

Now we can write a weighted-average expression for  $\mathbf{B}$

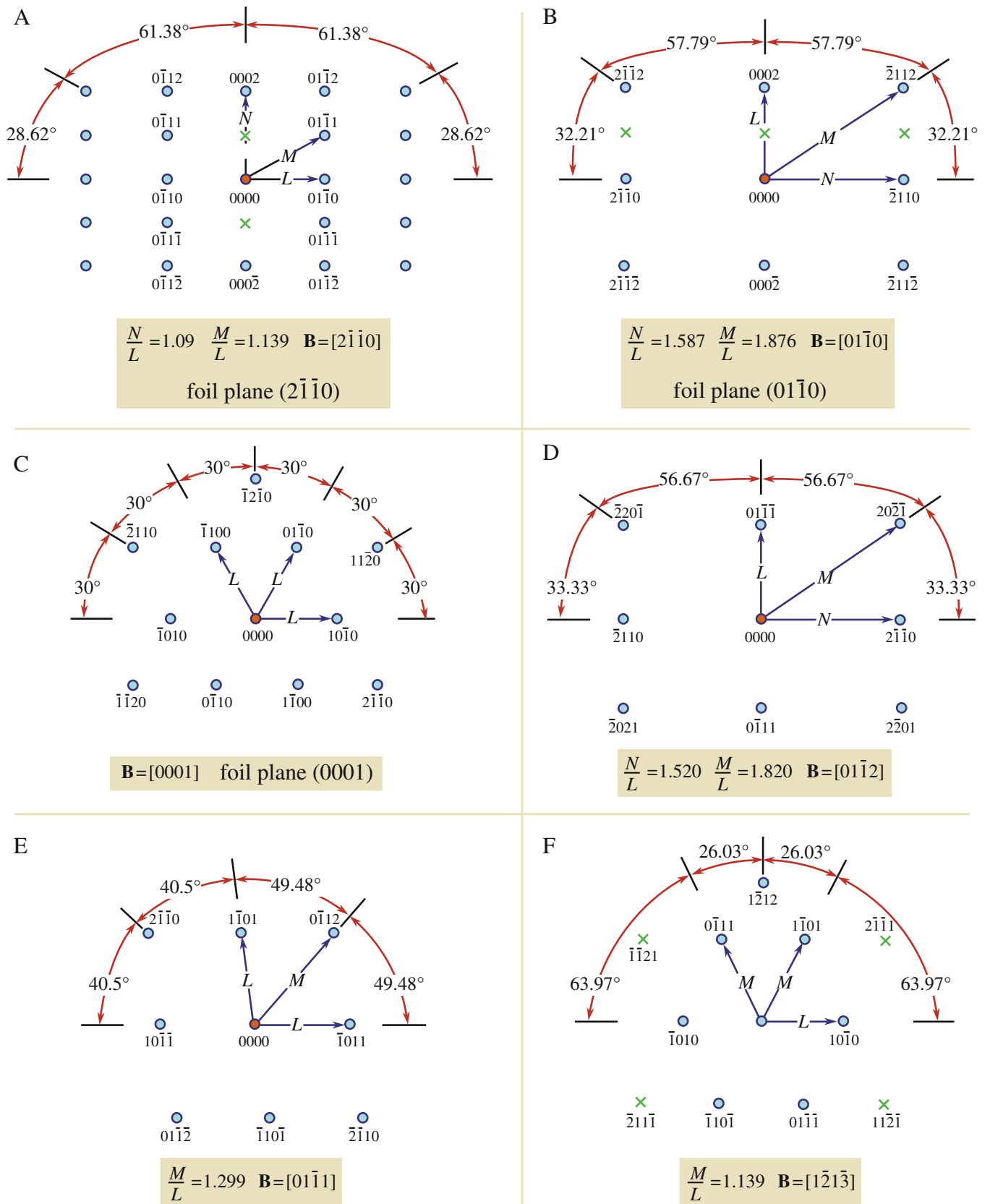
$$\mathbf{B} = \frac{\mathbf{g}_2 \times \mathbf{g}_3}{|\mathbf{g}_1|^2} + \frac{\mathbf{g}_3 \times \mathbf{g}_1}{|\mathbf{g}_2|^2} + \frac{\mathbf{g}_1 \times \mathbf{g}_3}{|\mathbf{g}_3|^2} \quad (18.14)$$

### OUR CONVENTION

The vector  $\mathbf{B}$  points up the column. It is normal to the emulsion side of a photographic negative. The electron beam travels along the direction  $-\mathbf{B}$ .



**FIGURES 18.20.** Four standard, indexed, DPs for fcc crystals in the [001], [011],  $[\bar{1}11]$  and  $[1\bar{1}\bar{2}]$  beam directions. Ratios of the principal spot spacings are shown as well as the angles between the principal plane normals. Forbidden reflections are indicated by x.



**FIGURES 18.21.** Six standard, indexed, DPs for hcp crystals in the  $[2\bar{1}\bar{1}0]$ ,  $[01\bar{1}0]$ ,  $[0001]$ ,  $[01\bar{1}2]$ ,  $[01\bar{1}1]$  and  $[1\bar{2}1\bar{3}]$  beam directions. Ratios of the principal spot spacings are shown as well as the angles between the principal plane normals. Forbidden reflections are indicated by x.



In Figures 18.19–18.21, we illustrate some of the most useful DPs for bcc, fcc and hcp crystals. You can extend these patterns as far as you wish using vector addition; remember the reflections correspond to reciprocal-lattice *vectors*. For example, in Figure 18.19C

$$(12\bar{1}) = (110) + (01\bar{1}) \quad (18.15)$$

You can extend the patterns in this way and then apply the selection rules to find the corresponding patterns for Si, etc., using the specific examples as a guide.

- bcc real space  $\rightarrow$  fcc reciprocal space.
- fcc real space  $\rightarrow$  bcc reciprocal space.

Take the example used by Edington, as shown in Figure 18.22 for an fcc crystal. Measure the distances to the reflections  $x$ ,  $y$  and  $z$ . Since the material is fcc, we can ratio  $d^2$  values to find suitable indices or use a calibrated camera length. Thus we find that plane  $A = (4\bar{2}0)$ ,  $B = (111)$  and  $C = (\bar{3}31)$ ; check that the angles are correct using

$$\cos(\phi_{AB}) = \frac{\mathbf{g}_A \cdot \mathbf{g}_B}{|\mathbf{g}_A| |\mathbf{g}_B|} \quad (18.16)$$

and so on for  $\phi_{BC}$  and  $\phi_{CA}$ . You should immediately recognize that this is the  $\pm[1\bar{2}3]$  pole, but continue. Now you can plug pairs of these indices into equation 18.11 or all of them 18.14 to show that  $B = [\bar{1}\bar{2}3]$ .

Finally, use the  $[001]$  stereographic projection. Draw a great circle that passes through the  $(111)$ ,  $(2\bar{1}0)$  and  $(\bar{3}31)$  points using your Wulff net: they all lie on one great circle because they are in the same zone. Now identify the zone axis directly by measuring  $90^\circ$  from all the poles. The result is, of course, the same in each case.

- Notice that if you used the stereographic technique with a non-cubic material, you would locate a direction, not a plane normal.
- You can make the determination of  $\mathbf{B}$  more accurate by making  $\mathbf{s} = 0$  for each reflection you use and then estimating your deviation from this idealized orientation. If the specimen is thicker, use Kikuchi lines (Chapter 19).

## 18.11 ORIENTATION RELATIONSHIPS

Once you've learned how to index a DP and determine  $\mathbf{B}$ , you can determine *orientation relationships (ORs)*, which are one of the most useful aspects of diffraction in the TEM for the materials scientist and nanotechnologist because the orientation between different grains, phases or crystals controls many properties of engineering materials. For example, the OR will determine how well the atomic planes in two different phases or grains fit together and this controls the nature of the interphase interface (e.g., coherent or incoherent) or grain boundary (special or random) which, in turn, governs the ways dislocations interact with the planar defect, thus controlling the mechanical behavior of the material. There are many other such effects of ORs; for example, we often want to know how a fiber is oriented to the surrounding matrix, a nanoparticle or a thin film to its supporting substrate. So the OR between two different crystals is important in many materials and can be described in one of two ways

- Two directions or plane normals (or two sets of parallel planes) can be parallel in the two crystals (the parallel-plane/direction relationship). We use this description for precipitate-matrix ( $\beta-\alpha$ ) orientation relationships where the crystal systems may be different.
- The two crystals have a common direction (axis) so that one crystal can be rotated through some angle

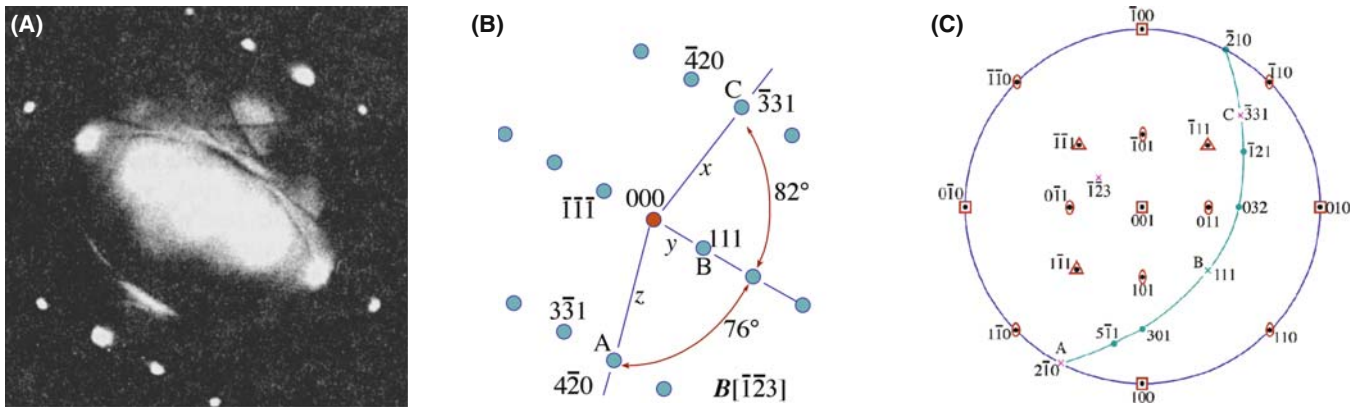


**FIGURE 18.22.** (A) An fcc pattern, indexed in (B) with the major indexed poles plotted on a stereographic projection in (C), identifying the pole of the great circle as  $\bar{1}23$  which is therefore the beam direction for the pattern in (A).

into exact alignment with the other (an axis-angle pair). We use this for GBs where the same material is present, either side of the boundary.

Record a set of three DPs, one from each crystal and one including the interface. If you're lucky you'll be able to index both single-crystal patterns directly. If one of them shows too few spots, you should try to record a complementary Kikuchi pattern (next chapter) or CBED pattern (subsequent two chapters) to provide more information. With CBED patterns from very small regions, you'll have to take a pattern in one crystal, translate the specimen or traverse the beam and take another pattern from the other grain.

We'll go through the experimental steps for analyzing the parallel-plane/direction relationship for two phases  $\alpha$  and  $\beta$

- Tilt to the zone-axis pattern (ZAP) 1 in phase  $\alpha$ , the matrix phase. Record and index it to determine  $\mathbf{B}_1(\alpha)$ .
- Translate the precipitate,  $\beta$ , onto the axis without touching the beam-tilt controls and record another DP. This pattern may not be exactly on a zone axis, so it may be more difficult to index; then Kikuchi lines may help considerably. Nevertheless, you need to determine a parallel-beam direction,  $\mathbf{B}_1(\beta)$ , for the precipitate.
- Translate back to the matrix. Tilt the specimen in a known direction until you find a different ZAP (again, Kikuchi maps will help you do this). Record and index ZAP 2 to give  $\mathbf{B}_2(\alpha)$ .
- Translate back to the precipitate, record the DP and index it, giving you  $\mathbf{B}_2(\beta)$ .
- Plot the position of  $\mathbf{B}_1$  and  $\mathbf{B}_2$  for both  $\alpha$  and  $\beta$  on a stereogram and construct the poles of the important planes that are normal to each  $\mathbf{B}$ . These will be the low-index planes that you indexed in each pattern.

So now you know that  $\mathbf{B}_1(\alpha)$  is parallel to  $\mathbf{B}_1(\beta)$  and  $\mathbf{B}_2(\alpha)$  is parallel to  $\mathbf{B}_2(\beta)$ . You can also see which plane normals are parallel (if any) from the stereogram. So you can quote the OR in terms of these two pairs of parallel directions, or a pair of directions and a pair of plane normals in the zone of each  $\mathbf{B}$ . It may well be the case that you can't find two low-index planes or directions that are parallel, in which case the orientation relationship is not a strong one. However, there are some well-known ORs between phases that you should know

- Best known is the *cube/cube* OR. If an fcc precipitate forms inside an fcc matrix (e.g.,  $\text{Al}_3\text{Li}$  ( $\delta'$ ) in an Al-Li ( $\alpha$ ) solid solution), then we find:

$$\begin{aligned} [100]_{\delta'} &\text{ is parallel to } [100]_{\alpha}, \\ (010)_{\delta'} &\text{ is parallel to } (010)_{\alpha}. \end{aligned}$$

Obviously, in these circumstances, any two  $\langle UVW \rangle$  directions or  $\{hkl\}$  planes in the cubic system would be parallel. It's just convention to choose the lowest-index planes or directions to define the OR. When the lowest-index planes and directions align, the surface energy between the phases tends to be lowest, so this configuration is thermodynamically favored.

- The Kurdjumov-Sachs OR is often found relating fcc and bcc crystalline grains. The close-packed planes (or closest packed in bcc) and close-packed directions are parallel, but these are not now identical

$$\begin{aligned} (111)_{\text{fcc}} &\text{ is parallel to } (011)_{\text{bcc}} \text{ (the closest-packed planes),} \\ [10\bar{1}]_{\text{fcc}} &\text{ is parallel to } [11\bar{1}]_{\text{bcc}} \text{ (the close-packed directions),} \\ (\bar{1}2\bar{1})_{\text{fcc}} &\text{ is parallel to } (\bar{2}1\bar{1})_{\text{bcc}}. \end{aligned}$$

- The Nishiyama-Wassermann OR is related to the Kurdjumov-Sachs OR

$$\begin{aligned} [0\bar{1}1]_{\text{fcc}} &\text{ is parallel to } [001]_{\text{bcc}}, \\ (\bar{1}11)_{\text{fcc}} &\text{ is parallel to } (\bar{1}10)_{\text{bcc}} \text{ (the closest-packed planes),} \\ (211)_{\text{fcc}} &\text{ is parallel to } (110)_{\text{bcc}}. \end{aligned}$$

If you plot this out on a stereogram, you'll see it's only a few degrees away from the Kurdjumov-Sachs relationship.

- The fcc and hcp systems also share an OR in which the close-packed planes and directions are parallel:

$$\begin{aligned} (111)_{\text{fcc}} &\text{ is parallel to } (0001)_{\text{hcp}} \text{ (the close-packed planes),} \\ [1\bar{1}0]_{\text{fcc}} &\text{ is parallel to } [1\bar{2}10]_{\text{hcp}} \text{ (the close-packed directions).} \end{aligned}$$

If you want to determine an axis-angle pair you proceed in a similar way. Obtain two indexed beam directions,  $\mathbf{B}_1$  and  $\mathbf{B}_2$ , in each crystal, and plot them on a stereogram. Then you need to determine from the stereogram which angle brings the directions and planes from one crystal into coincidence with the other crystal.

There's a full discussion of these methods in Edington's text; Randle and Ralph summarize the various methods available to determine boundary crystallography and many more examples of ORs are described in the companion text.

## 18.12 COMPUTER ANALYSIS

Although you must be able to analyze and index DPs 'by hand,' it's likely that you'll use one of the many available software packages, especially if your specimen is not cubic (see, e.g., Section 1.6 and URLs #1, 4-7). The main challenge comes when you have to index the

DP of a new material. Your laboratory should have the standard reference sources listed at the end of the chapter. The approach simply requires that you collect all the data you can and then search through the ICDD powder diffraction files, or better still the NIST/Sandia/ICPD electron-diffraction database (see URL #5), until you find a match. Yes, it is a lot of work and you have to remember some rules

- Measurements made on calibrated SADPs will be accurate to 1–2%. If you think you're more accurate, you may eliminate the material you're seeking from your database search!
- Check for multiple domains and double diffraction first. A schematic of such a DP is shown in Figure 18.23. As you can appreciate from the schematic, you must be careful not to confuse such patterns with those showing systematic absences.

A strategy for search-and-match procedures has been given by Lyman and Carr. The goal of the exercise is to identify all the possible compounds that could produce your DP. Then you can use other data (e.g., the chemistry deduced by XEDS or EELS) to make the final identification. Computers not only give us the speed to make such

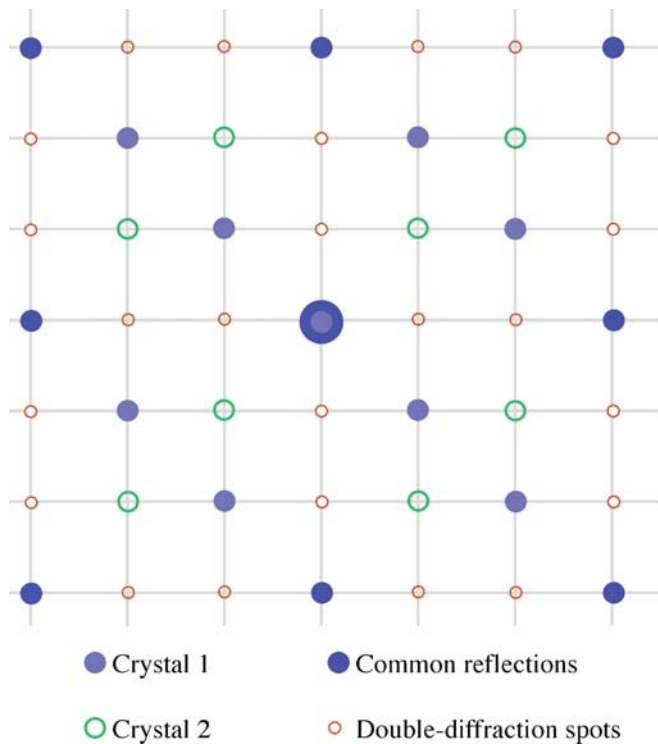


**FIGURE 18.23.** Care is needed to recognize diffraction from two similar domains which appears identical to diffraction from a real structure with a different symmetry. All the spots lie on a square array which may lead to erroneous indexing as a 100 pattern. The DP actually consists of separate patterns from two overlapping crystals plus double-diffraction spots as indicated.

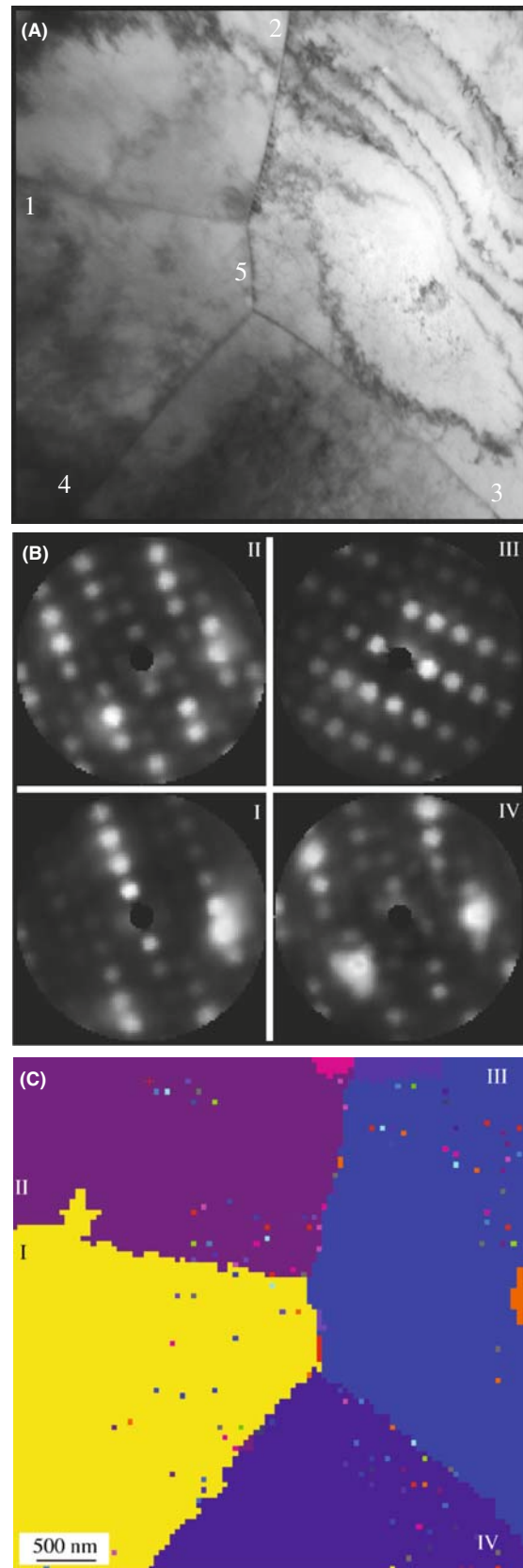


**FIGURE 18.24.** (A) STEM BF image of four grains in Cu. (B) A set of DPs produced from the grains as the beam scans across them. (C) A grain-orientation map in which different colors relate to different crystal orientations with respect to beam direction.

searches possible, but are also more objective. The procedure has four simple steps

- Obtain reliable data (and do not be too optimistic or overconfident in your accuracy).
- Search the database for possible matches. With the right database, chemical information will help.
- Test the matches you find. Are any of them possible given what you know about your specimen?
- Confirm the identification. Now you can go back to the microscope and use CBED to explore symmetry elements, improve your lattice-parameter measurements, etc. (Chapters 20 and 21).
- You should also simulate the DPs to confirm that the popular software packages do reproduce what you see. It's not a bad idea to carry out this exercise up front using known areas of your specimen or standard specimens before you attack the identification of unknowns.

### 18.13 AUTOMATED ORIENTATION DETERMINATION AND ORIENTATION MAPPING

In a parallel way to EBSD patterns in the SEM, a sequence of computer-indexed DPs can be transformed into an orientation map, which is an image in which the contrast or color links areas of similar orientation. One way to do this is via Automated Crystallography for TEM (ACT) developed by Dingley and available

commercially via EDAX. ACT gives you on-line orientation determination using hollow-cone DF imaging. As shown back in Figure 9.15A, the beam is tilted and rotated by the scan coils and strong diffracted beams travel sequentially down the optic axis as individual Bragg reflections occur. Digital DF images are collected at each beam position by an on-axis CCD camera as each grain diffracts at different orientations and a parallel-beam SADP is built up.

When the incident beam satisfies the Bragg condition for a given grain, the corresponding area in the DF image appears bright. After scanning, the recorded DF images are examined. In the DF images, recorded at different incident-beam positions, a specific pixel always corresponds to the same area in the specimen. The intensity of each pixel can be drawn as a function of beam tilt and rotation angle (i.e., a DP). Adjacent pixels having the same DP are from the same grain, and thus a grain map can be built. Figure 18.24A shows four grains with five grain boundaries in a specimen of Cu. Figure 18.24B shows a set of reconstructed DPs from four grains (I–IV). Once the DPs for all the grains are reconstructed, the orientation relationships across the boundaries (1–5) between the neighboring grains can be extracted and Figure 18.24C shows the orientation map for the four grains. As in the SEM it is easy to contemplate combining the diffraction data with elemental data gathered by XEDS and/or EELS and carrying out on-line phase identification.

## CHAPTER SUMMARY

This chapter has been concerned almost entirely with experimental technique.

- The stereographic projection is a very helpful aid. It's similar to projections we use to map the earth. Diffraction space (like global space) is three-dimensional. The stereographic projection gives us a two-dimensional map to guide us from pole to pole!
- How do you obtain the best DP from your specimen? Use the right exposure, always focus the DP and use the best technique (CBED or SAD  $\pm$  Kikuchis) for the size of the area of interest.
- Take the trouble and time always to get good DPs. You never know when you'll really need that information and an extra 9 or 29 seconds exposure time is not long, considering how long you'll spend analyzing the results!
- Which type of DP should you use? This depends on the characteristics of your specimen and what you want to know.
- Remember that reflections with moderately large values of  $g$  should give you the best value for both  $d$  and  $\phi$ , but *be absolutely sure* that  $s = 0$  for your chosen  $g$ .
- DPs from polycrystalline, nanocrystalline and amorphous materials contain a wealth of information. The added value that the various TEM techniques bring over X-ray diffraction is the spatial resolution and the accompanying images. TEM may not give the best statistics; XRD only gives statistics.



- Computer indexing of DPs should be the norm and should be automatic *if you know your material*. If you understand the principles discussed here, you will avoid a few pitfalls.
- Computer control of the beam and computer indexing can also be combined to form orientation maps of the distribution of different grain orientations or textures.

Finally, we'll repeat our word of caution: there is a very famous paper on interstitial defects in a ceramic and a follow-up paper on vacancy defects. The first paper missed the 180° ambiguity in the DP! Don't fall into such good company.

## REFERENCES

We list more references than usual in this chapter. You'll want to see many different examples so go to the originals where possible.

## CRYSTALLOGRAPHY AND DIFFRACTION

- Andrews, KW, Dyson, DJ and Keown, SR 1971 *Interpretation of Electron Diffraction Patterns* 2nd Ed. Plenum Press New York. An essential resource for anyone using electron diffraction.
- Burger, MJ 1978 *Elementary Crystallography* MIT Press Cambridge Massachusetts. One of the classics. Find it in the library.
- Champness, PE 2001 *Electron Diffraction in the TEM* Bios (RMS) Oxford UK. Superb, concise introductory text; full of great examples.
- Cullity, BD and Stock, SR 2001 *Elements of X-ray Diffraction* 3rd Ed. Prentice-Hall New York. The standard text on XRD.
- Edington, JW 1976 *Practical Electron Microscopy in Materials Science* Van Nostrand-Reinhold New York. Part 2 of the book is full of useful hints and examples on analyzing DPs.
- Giacovazzo, C, Monaco, HL, Artioli, G, Viterbo, D, Ferraris, G, Gilli, G, Zanotti, G and Catti, M 2002 *Fundamentals of Crystallography* 2nd Ed. Oxford University Press and IUCr Oxford. A comprehensive reference book.
- Glazer, AM 1987 *The Structure of Crystals* Adam Hilger Bristol United Kingdom. The essentials condensed into a 50-page monograph. Find it in the library
- Hammond, C 1992 *Introduction to Crystallography* 2nd Ed. Royal Microscopical Society Oxford United Kingdom. An excellent compact introduction to the subject with a nice section on the biographies of crystallographers.
- Johari, O and Thomas, G 1969 *The Stereographic Projection and Its Applications in Techniques of Metals Research* Ed. RF Bunshah Interscience New York. A very helpful book if you can find a copy in your library (it's out of print).
- Kelly, A, Groves, GW and Kidd, P 2000 *Crystallography and Crystal Defects* Wiley New York. Update of the classic 1970 edition. All materials scientists should already have one on their shelves. Not only the standard introductory text on this subject but also gives a good review of the stereographic projection.
- Klein, C and Hurlbut, CS 1985 *Manual of Mineralogy* Wiley New York. This is the modern version of the original classic by James D Dana. It gives an excellent readable review of the stereographic projection and its relation to the globe, plus basic crystallography.
- Lisle, RJ and Leyshon, PR 2004 *Stereographic Projection Techniques for Geologists and Civil Engineers* 2nd Ed. Cambridge University Press New York.
- Smaill, JS 1972 *Metallurgical Stereographic Projections* Adam Hilger Ltd London. Chapter 20 is another source for stereographic projections and the Wulff net if you can find a copy.
- Vainshtein, BK 1981 *Modern Crystallography I-IV* Springer-Verlag New York. No longer modern but more of a classic.
- Villars, P and Calvert, LD 1991 *Pearson's Handbook of Crystallographic Data for Intermetallic Phases* 2nd Ed. ASM Metals Park Ohio. This text is now in many volumes covering an ever-growing number of materials.
- Wells, AF 1984 *Structural Inorganic Chemistry* 6th Ed. Oxford University Press New York. The source for crystal-structure data in inorganic materials.

## AMORPHOUS MATERIALS

- Graczyk, JF and Chaudhari, P 1973 *A Scanning Electron Diffraction Study of Vapor-Deposited and Ion Implanted Thin Films of Ge. I* Phys. Stat. Sol. **B58** 163–179. Early modeling; you should check other papers by these authors if you're working in this area.
- Howie, A 1988 in *High-Resolution Transmission Microscopy and Associated Techniques* p 607 Eds. P Buseck, J Cowley and L Eyring Oxford University Press New York. On amorphous materials.
- McCulloch, DG, McKenzie, DR, Goringe, CM, Cockayne, DJH, McBride, W, Green, DC 1999 *Experimental and Theoretical Characterization of Structure in Thin Disordered Films* Acta Cryst. **A55**(2) 178–187.
- Rudee, ML and Howie, A 1972 *The Structure of Amorphous Si and Ge* Phil. Mag. **25** 1001–1007.
- Treacy, MMJ, Gibson, JM, Fan, L, Paterson, DJ and McNulty, I 2005 *Fluctuation Microscopy: a Probe of Medium Range Order* Rep. Prog. Phys. **68** 2899–2944.

## DIFFRACTION TECHNIQUES

- Dingley, DJ 2000 in *Electron Backscatter Diffraction in Materials Science* p1 Eds. AJ Schwartz, M Kumar and BL Adams Kluwer New York.
- Lyman, CE and Carr, MJ 1992 in *Electron Diffraction Techniques 2* p 373 Ed. JM Cowley Oxford University Press New York.
- Mornioli, JP, Redjaimia, A and Nicolopoulos, S 2007 *Contribution of Electron Precession to the Identification of the Space Group from Microdiffraction Patterns* Ultramicroscopy **107** 514–522.
- Own, CS, Marks, LD and Sinkler, W *Electron Precession: a Guide for Implementation* Rev. Sci. Instrum. 2005 **76** 33703-1-13.
- Randle, V and Ralph, B 1986 *A Practical Approach to the Determination of the Crystallography of Grain Boundaries* J. Mater. Sci. **21** 3823–3828.
- Schwartz, AJ, Kumar, M and Adams, BL (Eds.) 2000 *Electron Backscatter Diffraction in Materials Science* Kluwer New York.
- Tietz, LA, Carter, CB and McKernan, S 1995 *Top-Bottom Effects in Double Diffraction* Ultramicroscopy **60** 241–246. A challenge on 'double diffraction.'
- Vainshtein, BK, Zuyagin, BB and Avilov, AV 1992 in *Electron Diffraction Techniques 1* p 216 Ed. JM Cowley Oxford University Press New York.
- Vincent, R and Midgley, PA 1994 *Double Conical Beam-Rocking System for Measurement of Integrated Electron Diffraction Intensities* Ultramicroscopy **53** 271–282. Precession diffraction.

## URLs

- 1) Diffraction-Pattern Indexing – Start with the EM Yellow Pages and the EMS software <http://cimewww.epfl.ch/EMYP/emyp.html> and also the Web site for the International Union of Crystallography <http://journals.iucr.org/iucr-top/comm/ced/index.html>. Also try SingleCrystal<sup>TM</sup>; part of the extensive CrystalMaker<sup>®</sup> suite of DP and crystal structure software. For a free demo download go to [www.crystallmaker.co.uk/singlecrystal/index.html](http://www.crystallmaker.co.uk/singlecrystal/index.html).
- 2) [www.jcrystal.com/products/winwulff/index.htm](http://www.jcrystal.com/products/winwulff/index.htm) – WinWulff: a program for plotting stereographic projections onto a Wulff net.
- 3) [www.nanomegas.com](http://www.nanomegas.com) – Commercial retrofit for precession diffraction.
- 4) [www.icdd.com](http://www.icdd.com) – ICDD Powder Diffraction File is produced by the International Center for Diffraction Data (12 Campus Boulevard, Newtown Square, PA 19073). The latest installment of the historic Powder Diffraction File, Release 2006 contains data from the ICDD experimental powder data collection and data collected, edited and standardized from NIST and ICSD database in CD/DVD formats. Expensive, but your university or research lab should buy access.
- 5) <http://icsd.ill.fr/icsd/index.html> – Inorganic Crystal-Structure Database (ICSD): the world's most extensive database on inorganic crystal structures and contains information on all inorganic crystal structures (pure elements, minerals, metals and intermetallic compounds, including their atomic coordinates) that have been published since 1913. It is updated twice a year, each time adding approximately 3000 new records. Unlicensed users only have access to a demonstration version, with a 3592 structure subset of the 93,720 inorganic structures in release 2006-2. Access also comes with the ICDD CD.
- 6) <http://icsd.ill.fr/icsd/index.html> – NIST Crystal Data comprise standard cell parameters, cell volume, space-group number and symbol, calculated density, chemical formula, chemical name and classification by chemical type. The file includes reliable data from solid-state materials including inorganics, organics, minerals, intermetallics, metals and alloys. Comprehensive chemical, crystallographic and identification search software comes with the database. Access is also available via the ICDD CD.
- 7) <http://www.nist.gov/srd/nist15.htm> – NIST/Sandia/ICDD Electron Diffraction Database is thanks to the tireless efforts of M Carr. Designed for phase characterization by electron diffraction, this database and software permit highly selective identification of microscopic and macroscopic crystalline materials.

The database contains chemical, physical and crystallographic information on over 81,534 minerals, metals, intermetallics and general inorganic compounds. Available in CD-ROM format.

## THE COMPANION TEXT

Your skill in indexing diffraction patterns always benefits from practice. Energy filtering can improve the clarity of your DP but the geometry will be the same.

## SELF-ASSESSMENT QUESTIONS

- Q18.1 At what grain size does SAD begin to become useful?
- Q18.2 How would you excite a higher-order reflection?
- Q18.3 Why is it useful to use stereographic projections when analyzing DPs?
- Q18.4 In a stereographic projection, are the small or great circles similar to (a) latitude, (b) longitude?
- Q18.5 On the stereographic projection, if the zone axis is at the center of the circle, where are the poles of the planes in the zone?
- Q18.6 What kind of ring is seen in the DP from a large-grained polycrystal?
- Q18.7 How can we distinguish polycrystalline rings in the DP from those that would be caused by amorphous materials?
- Q18.8 Why does double diffraction complicate understanding a DP?
- Q18.9 When would you prefer SAD over CBED and vice versa?
- Q18.10 Why might grains smaller than 10 nm pose a problem for diffraction analysis in the TEM?
- Q18.11 How can you determine if a specimen is nanocrystalline (~1 nm grain size) or amorphous?
- Q18.12 Define the radial distribution function.
- Q18.13 How can you determine if a polycrystalline specimen is textured?
- Q18.14 When is it a good idea to tilt the beam rather than tilt the specimen?
- Q18.15 What is an orientation relationship (OR)?
- Q18.16 What are the big advantages of the TEM for studying DPs?
- Q18.17 How many DPs do you need to determine an OR?
- Q18.18 How can you distinguish between the pattern produced by a textured specimen from one produced by a random polycrystal?
- Q18.19 What is the best way to image an amorphous material?
- Q18.20 Will the DP always rotate as we change the camera length?
- Q18.21 Why will SAD not distinguish two patterns with 180° rotation?
- Q18.22 When will double diffraction not occur?
- Q18.23 What is the easiest way to examine the detail present in a DP?
- Q18.24 Why do we tilt from one direction to set a selected specimen orientation?
- Q18.25 Distinguish hollow cone and conical diffraction.
- Q18.26 Distinguish hollow cone and precession diffraction.

## TEXT-SPECIFIC QUESTIONS

- T18.1 Describe how you would excite 13g when O is on the optic axis if you can't see 13g on the screen.
- T18.2 Index the DPs in Figure 18.7 to be consistent with the (invisible) Kikuchi lines and with each other (after you've read Chapter 19).
- T18.3 We note in Section 18.6 that, unlike those from polycrystalline materials, DPs from amorphous materials do not show speckle. However, speckle from amorphous materials is the basis for the technique of fluctuation microscopy. How can these two statements be consistent? (Use the literature and Figure 18.14 to illustrate your answer.)
- T18.4 We note that indexing an OTEDP might be confusing if certain rings are missing due to the texturing. If you tilt the sample 30° these rings should reappear. Explain their absence in terms of a three-dimensional diagram like that shown in Figure 18.10D.
- T18.5 Discuss which of the techniques illustrated in Figure 18.14 is better for imaging amorphous carbon. Suggest regions for the large white area in B. Why are the images in B and C different?
- T18.6 Using the diagrams shown in Figure 18.17, explain the difference between Figure 18.17E and F. The argument is given in the text so try to put it into your own words or use a diagram to summarize the argument in the text.
- T18.7 Is the correct B given in each of Figures 18.19A–D?
- T18.8 Sketch Figures 18.21A and C on a sheet of paper so that you can describe how you would tilt from one pole to the other.
- T18.9 Notice that in Figure 18.21D–F you are only told B, not the foil plane. Assuming that B is normal to the foil plane, determine the foil plane.
- T18.10 Can the DP shown in Figure 18.23 actually happen? If so, give an example.

- T18.11 Draw the SADP that you would obtain from a  $45^\circ$  [100] twist grain boundary in Cu when viewed normal to the GB plane.
- T18.12 Generate the following DPs (to scale). Show all work and label reflections to a distance of  $2g$  in all directions about 000. For the following, assume only 1 atom per lattice site and each lattice site contains the same atom. (A) [123] beam direction; face-centered cubic;  $a = 3.68 \text{ \AA}$ ,  $\lambda L = 50 \text{ mm \AA}$ . (B) [011] beam direction; c-centered orthorhombic;  $a = 4.12 \text{ \AA}$ ,  $b = 3.15 \text{ \AA}$ ,  $c = 5.42 \text{ \AA}$ ,  $\lambda L = 50 \text{ mm \AA}$ . (C) [113] beam direction; body-centered tetragonal;  $a = 3.41 \text{ \AA}$ ,  $c = 3.0 \text{ \AA}$ ,  $\lambda L = 50 \text{ mm \AA}$ . Generate the following DPs (to scale). Show all your work and label reflections to a distance of  $2g$  in all directions about 000. For the following, assume only 1 atom per lattice site and each lattice site contains the same atom. (Courtesy Lucille Giannuzzi.)
- T18.13 Draw the same cubic stereograms as in Figure 18.4 but rotated  $90^\circ$  along the horizontal axis in each case.
- T18.14 Identify on Figure 18.5 the following poles:  $22\bar{1}$ ,  $01\bar{1}$ ,  $21\bar{2}$ . What is different about these three poles compared with all the others shown in Figure 18.5?
- T18.15 Why are the rings of diffracted intensity in the patterns in Figure 18.9 of varying intensity? Under what conditions could you infer something about the different thicknesses of foils that gave rise to each pattern?



# Kikuchi Diffraction

## CHAPTER PREVIEW

In this chapter and the following two, we will discuss two special cases of electron diffraction. We'll see that incoherently scattered, divergent beams of electrons give rise to paired arrays of lines in SADPs, known as Kikuchi patterns. In the next two chapters, we will form DPs with a convergent rather than a divergent (or, as in the previous chapter, parallel) beam. These two techniques have a lot in common. In the first, the electrons are initially being scattered by the atoms in the crystal so that they 'lose all memory of direction' and may also lose energy. We can then think of these electrons as traveling in diverging 'incident' directions into the specimen. When the direction is appropriate, these electrons can be scattered again, this time by Bragg diffraction. In the second technique, we intentionally form a convergent beam in the illumination system to make the electrons incident on the crystal over a range of different angles and create convergent-beam electron diffraction (CBED) patterns. In this case, we have another advantage in that we can focus the beam on a much smaller area of the specimen than in SAD. In both cases the information gained is enhanced if the specimen is thicker; in the case of Kikuchi patterns it has to be thick enough for inelastic scattering to occur and in CBED it has to be thick enough for dynamical scattering. So these next three chapters are particularly useful if you can't make your specimen thin enough for almost all other TEM techniques, which generally produce better quality information if the specimen is thinner.

In this chapter, we will show that these Kikuchi patterns can be used to give us much more accurate information on the beam direction than SADPs and can also give a direct link in reciprocal space to the stereographic projection. The topics we'll cover are basically experimental (although the phenomenon is well understood theoretically) and software for computer simulation of Kikuchi patterns is readily available and very useful. The ideas we develop in this chapter will carry over to the next two chapters when we discuss higher-order Laue-zone (HOLZ) lines in CBED patterns (where Kikuchi lines can also appear).

### 19.1 THE ORIGIN OF KIKUCHI LINES

The reason Kikuchi patterns form is that, if the specimen is thick enough, it will generate a large number of scattered electrons which travel in all (but mainly forward) directions; i.e., they have been *incoherently* scattered but not necessarily *inelastically* scattered (although obviously some of them will have lost energy). They are sometimes referred to as diffusely scattered electrons. These electrons can then be Bragg diffracted by the crystal planes. The rest of the story is merely geometry.

We'll discuss a little of the theory in Section 19.5, but for now we'll note the following experimental facts

- Since typical energy losses are small (15–25 eV) compared to  $E_0$  (100–400 keV) the diffusely scattered electrons can be assumed to have the same  $\lambda$  as the incident electrons. This assumption holds as long as the specimen is not too thick.
- When first formed, most of the diffusely scattered electrons travel close to the direction of the incident beam. You learned back in Chapter 3 that inelastic scattering is 'peaked in the forward direction.'

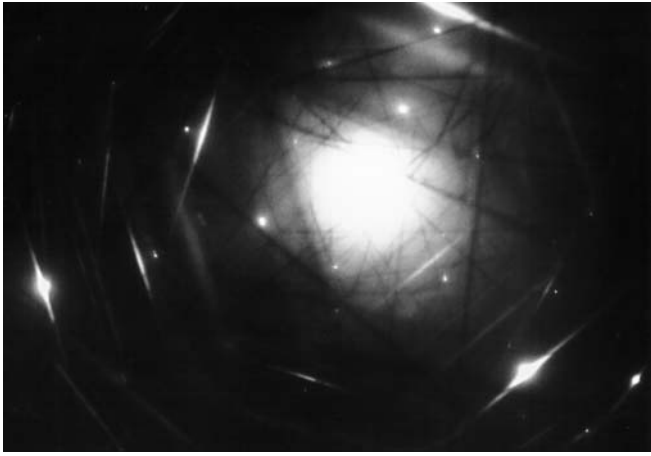


**FIGURE 19.1.** An ideal DP containing both well-defined spots and clearly visible pairs of bright (excess) and dark (deficient) Kikuchi lines.

- The ideal specimen thickness will be such that we can see both the spot pattern and the Kikuchi lines as illustrated in Figure 19.1. As noted, this is one of the few situations when thinner is not necessarily better.
- Although this phenomenon is related exclusively to electron scattering, Kikuchi described it in 1928, *before* the development of the TEM; it can occur in any crystalline specimen.

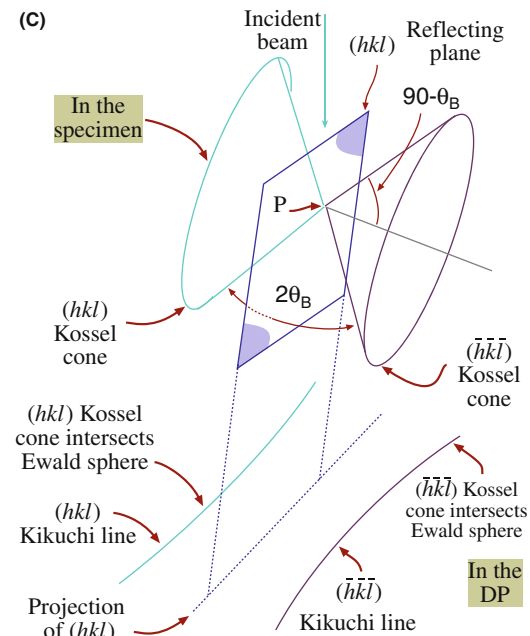
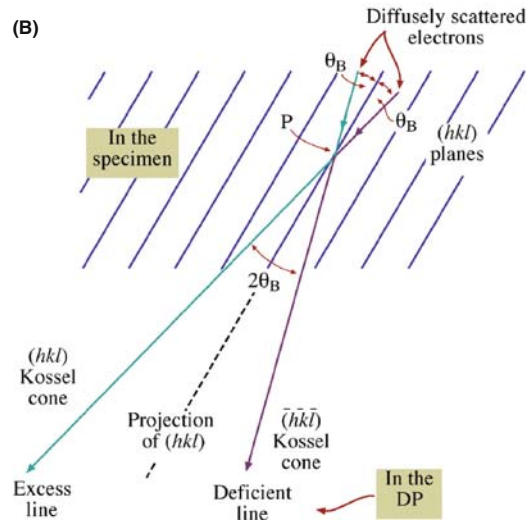
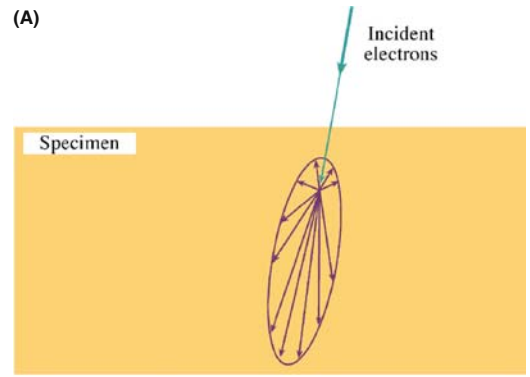
Diffuse scattering will again be important when we discuss forming images from these electrons in Section 31.5. We can select a region of reciprocal space containing diffusely scattered electrons to form the image and these electrons can be separated from the inelastically scattered electrons with an energy filter (see Sections 38.2 and 40.5). Your specimen needs to be thick enough but, if it is too thick, then there will be no Kikuchi lines because inelastic scattering then dominates and there is no detectable Bragg diffraction of these electrons. There will also be no Bragg spots and no useful DP!

## 19.2 KIKUCHI LINES AND BRAGG SCATTERING

The geometry of Kikuchi patterns can be understood from Figure 19.2 which relates what happens in the specimen to what we see in the DP. Let's imagine (Figure 19.2A) that electrons have been generated at the point shown and are scattered in all directions (but



**FIGURE 19.2.** (A) Schematic representation of all electron scattering localized at a single point in the specimen. In (B) some of the scattered electrons are diffracted because they travel at the Bragg angle  $\theta_B$  to certain  $hkl$  planes. The diffracted electrons form Kossel cones centered at P on the diffracting planes. The lines closest to the incident beam direction are dark (deficient) and the lines farthest away are bright (excess). In (C) the cones intercept the Ewald sphere, creating parabolas which approximate to straight lines in the DPs because  $\theta_B$  is small.



mainly forward). So we draw them as diverging from a point even though, in fact, they'll be scattered at different points throughout the specimen thickness. Some of these electrons will travel at an angle  $\theta_B$  to the  $hkl$  planes as shown in Figure 19.2B and then be Bragg diffracted by these specific planes. Since the scattered electrons are traveling in all directions, the diffracted beam will lie on one of two cones (Figure 19.2C). In other words, we see cones of diffracted electrons rather than well-defined beams because there is a *range* of incident  $\mathbf{k}$ -vectors rather than a single  $\mathbf{k}$ -vector. We construct the cones by considering all the vectors oriented at angle  $\theta_B$  to the  $hkl$  plane; these are called Kossel cones and the cone angle ( $90-\theta_B$ ) is very small (remember, angle really means semi-angle). There is a pair of Kossel cones for  $\pm\mathbf{g}$ , another pair for  $\pm 2\mathbf{g}$  and so on.

### SEEING KOSEL CONES

What we see in the DP is the intersection of these two cones with the screen or detector.

Since the screen/detector is flat and nearly normal to the incident beam, the Kossel cones appear as parabolas. If we consider regions close to the optic axis, these parabolas appear as two parallel lines. (Remember how close to  $90^\circ$  the cone angle is.) We'll sometimes refer to this pair of Kikuchi lines as a 'Kikuchi band' to include the lines and the region between them; the contrast associated with the region between the lines is actually quite complex (Section 19.6).

### FOR ANY PAIR OF KIKUCHI LINES

One line corresponds to  $\theta_B$  and the other to  $-\theta_B$ ; one is the  $\mathbf{g}$  Kikuchi line and the other the  $\bar{\mathbf{g}}$  Kikuchi line. *Neither* of them is the  $\mathbf{0}$  Kikuchi line.

We can make another important observation on the intensity of these lines by considering Figure 19.2 again. In Figure 19.2B you can see that the scattered beam which was initially closest to the optic axis, and therefore the more intense, is farther away from the axis after being Bragg diffracted. This beam then gives the excess (bright) line and the other the deficient (dark) line. You can see that this simple idea really does work in Figure 19.1.

The value of this result comes when we want to index a pair of Kikuchi lines: if you find a bright line, its partner must not only be parallel to it but must also be closer to O, and dark. The pair is separated by  $2\theta_B$ .

The cones shown in Figure 19.2C act as if they are rigidly fixed to the plane  $hkl$ ; they are thus 'fixed' to the crystal. We can draw a line half way between the two Kikuchi lines to represent the trace of the plane ( $hkl$ ). Remember our angles are all small. This simple

observation explains why we have a whole chapter on Kikuchi lines.

### TILTING AND KIKUCHI LINES

If we tilt the crystal through a very small angle, the Kikuchi lines will move but the intensities of the diffraction spots will hardly change and the positions of the spots will not change. So Kikuchi lines are much more sensitive to beam/specimen tilts than spots in SADPs.

The location of the Kikuchi line will also tell us whether  $\mathbf{s}$  is positive or negative. We can't usually deduce that from the spot pattern.

The distance in reciprocal space between the  $\bar{\mathbf{g}}$  and  $\mathbf{g}$  Kikuchi lines is  $\mathbf{g}$  (not  $2\mathbf{g}$ ) because the angle between the two Kossel cones is  $2\theta_B$ . This relationship is very valuable for the following reasons

- When the  $\mathbf{g}$  Kikuchi line passes through the reflection G,  $\mathbf{s}_g = 0$  (i.e., the Bragg condition is exactly satisfied) and the  $\bar{\mathbf{g}}$  Kikuchi line passes through O. So we can use the Kikuchi lines to set up specific diffraction conditions exciting specific reflections as we tilt the specimen (see Figure 19.3). We'll see later that we can also use Kikuchi lines to determine the exact value of  $\mathbf{s}_g$  when we are close to, but not exactly at, an exact Bragg condition.
- A corollary: if the direct beam is exactly parallel to the plane  $hkl$ , the  $\mathbf{g}$  and  $\bar{\mathbf{g}}$  Kikuchi lines are symmetrically displaced about O with the  $\mathbf{g}$  Kikuchi line 'passing through'  $\mathbf{g}/2$  and the  $\bar{\mathbf{g}}$  line 'passing through'  $\bar{\mathbf{g}}/2$ .

In this latter case, our simple explanation of Kikuchi-line formation breaks down, because Figure 19.2 predicts equal intensity in both excess and deficient Kikuchi lines and they would both, therefore, be indistinguishable from the diffuse-scattered background. So no Kikuchi lines should be visible if the beam is exactly down a zone axis, and this is patently not true. So the full Kikuchi-line explanation is more complex and (unfortunately) requires Bloch-wave theory. But we do understand the process in great detail.

## 19.3 CONSTRUCTING KIKUCHI MAPS

If instead of just taking pictures of Kikuchi-line pairs, we assemble a montage of all Kikuchi lines and spot patterns

### KIKUCHI MAP

Making a Kikuchi map is a highly recommended exercise if you are going to be doing detailed diffraction-contrast images/SAD experiments because familiarity with the Kikuchi map will help you to immediately identify the orientation of your specimen on your TEM screen.

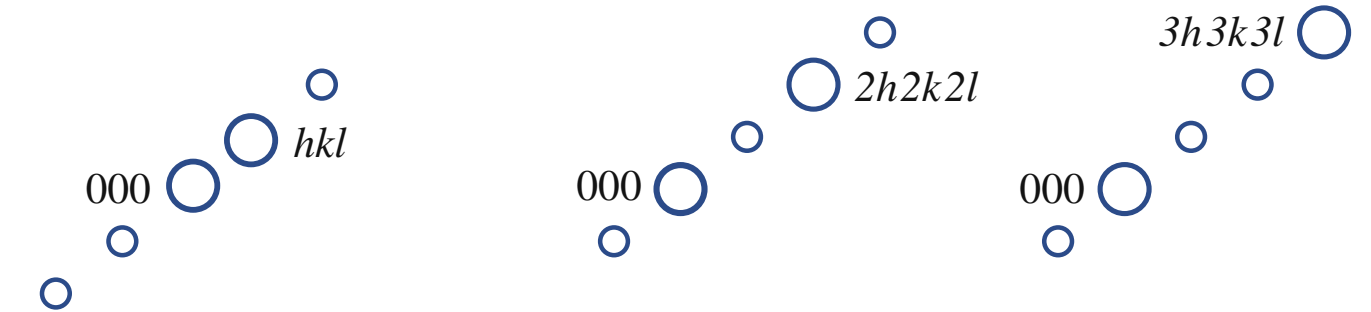
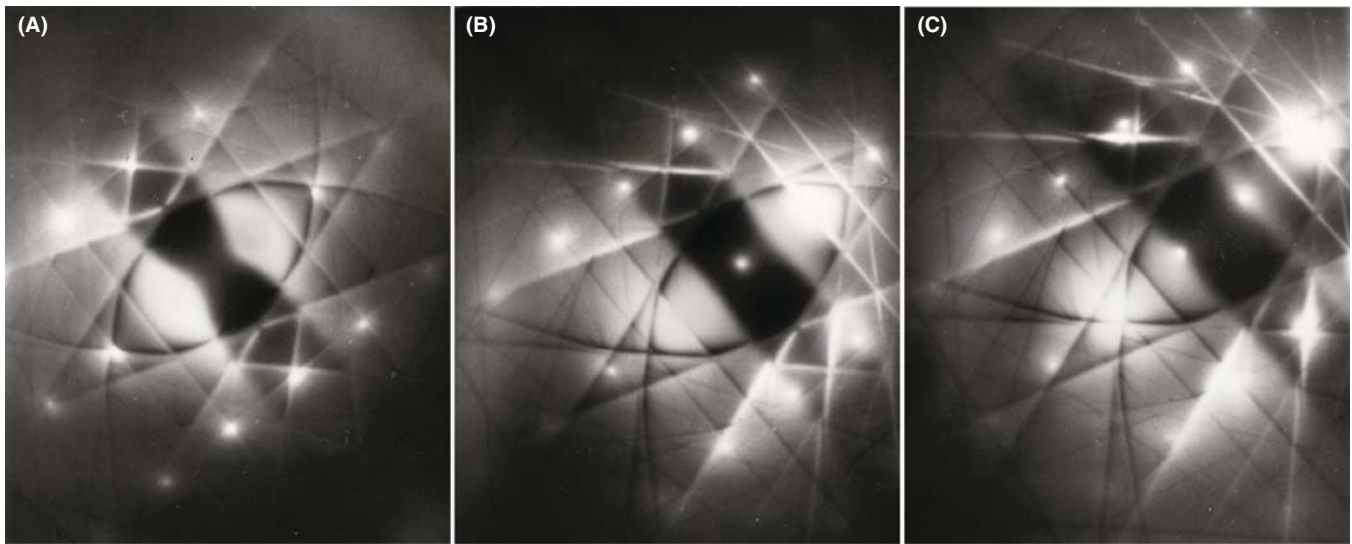


**FIGURE 19.3.** Three two-beam DPs from pure Al, obtained under different tilting conditions. As shown schematically below each figure, in (A) the  $hkl$  spot is at the exact Bragg condition (the excess Kikuchi line goes through  $hkl$ ). In (B) the  $2h2k2l$  and in (C) the  $3h3k3l$  spots, respectively, are strongly excited. Note that although we refer to these as ‘two-beam’ DPs, many other diffraction spots are visible.

over a wide array of reciprocal space, then we create a Kikuchi map.

The method for constructing Kikuchi maps is illustrated in Figure 19.4A. First, we draw the lines for the case where the  $[001]$  pole is exactly on the optic axis. The lines are then the perpendicular bisectors of every  $\mathbf{g}$ -vector you can find in the ZOLZ. The distance between each pair of lines is then automatically  $|\mathbf{g}|$ . We can then give each line a unique label  $\mathbf{g}$ .

Next, we can construct the map for the  $[101]$  pole. We start as shown in Figure 19.4B, keeping the common  $020$   $\mathbf{g}$ -vector pointing in the same direction. So, the  $020$  and  $0\bar{2}0$  Kikuchi lines are common to the two patterns. Although the angle between the  $[001]$  and  $[101]$  poles is  $45^\circ$ , we draw the  $020$  lines as parallel and straight because we are always looking at a small segment of the Kikuchi pattern. Notice that we can define all the distances in terms of their equivalent angles, as in any DP.

Now we add the  $[112]$  pattern. This pattern shares the  $2\bar{2}0$  and  $22\bar{0}$  reflections with the  $[001]$  pole and shares the  $\bar{1}\bar{1}1$  and  $11\bar{1}$  reflections with the  $[101]$  pole. The corresponding pairs of Kikuchi lines will then also be common, so we produce the triangle shown in

Figure 19.5A. We can add other poles and pairs of Kikuchi lines as shown in Figure 19.5B to get the full pattern.

A Kikuchi map for an fcc material is illustrated in Figure 19.6. The maps are available in the literature for fcc, bcc, diamond cubic and some hcp materials. Such maps are mainly from Thomas and co-workers (Levine et al. 1966, Okamoto et al. 1967, Johari and Thomas 1969), who developed the technique. Edington (1976) presents several Kikuchi maps in the appendices. Maps can also be downloaded from the Web using EMS (URL #1).

You can appreciate the value of Kikuchi maps in non-cubic materials from the map shown in Figure 19.7. The map has been drawn for  $\text{Ag}_2\text{Al}$ , which has the same  $c/a$  ratio as Ti. The Kikuchi bands are labeled (remember that they correspond to planes). The zone axes are also labeled: they correspond to directions. Thinking back to our brief discussion of Frank’s paper on four-index notation in Chapter 16, you should see an obvious application here.

- For cubic materials you need only the  $[001]$ ,  $[101]$ ,  $[111]$  triangle shown in Figure 19.5B.
- For hcp materials, the angles will generally depend on the  $c/a$  ratio of your material and you’ll need a larger area of the map.



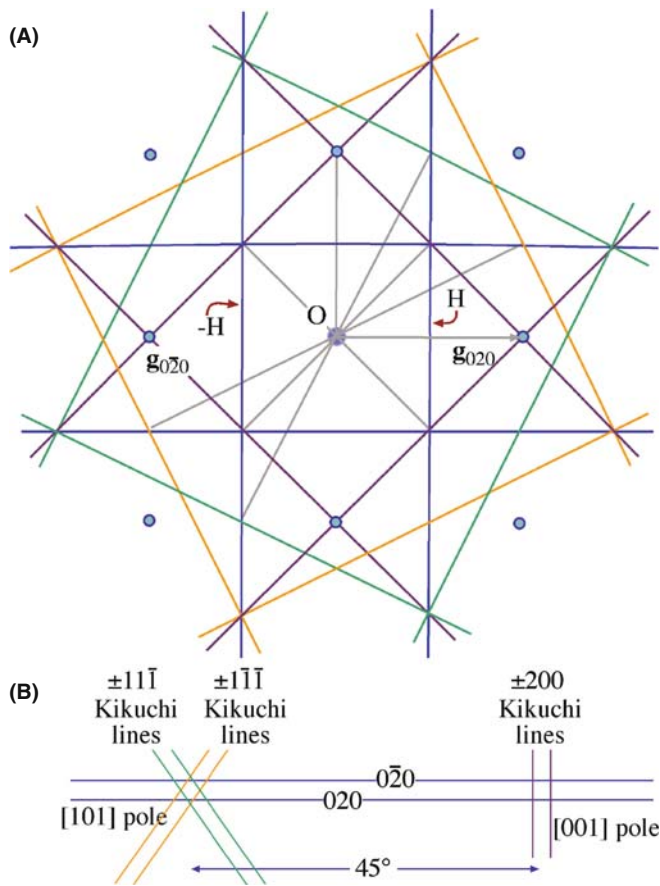


**FIGURE 19.4.** (A) To construct a Kikuchi pattern, draw pairs of lines each bisecting the  $\pm\mathbf{g}$ -vectors. For example, when the  $[001]$  fcc pole is on axis, the vector  $\mathbf{g}_{020}$  is bisected by the vertical line at H (020); the other Kikuchi line in the pair is at  $-H$  (020). All other Kikuchi-line pairs can be constructed for any  $\mathbf{g}$ -vector. (B) From one Kikuchi pattern we can extend the lines to create a second pattern. For example, knowing the  $[001]$  pattern we can construct the  $[101]$  pattern since a pair of lines is common to both. So we draw the  $0\bar{2}0$  and  $020$  lines from the  $[001]$  pole  $45^\circ$  to the  $[101]$  pole.

- For most non-cubic materials and particularly if you are working with monoclinic or triclinic crystals, it's not practical to construct the complete map experimentally. It's probably easier to become a metallurgist!

We can use the following procedure to generate a valuable experimental aid for any material.

- Construct segments of the map to scale as we've illustrated in Figure 19.5B. You can use one of the software packages to help you in this task. Make two copies of each map.
- While you're at the TEM, record the Kikuchi pattern for several special low-index poles along with the spot pattern.
- Index the DPs consistently.
- Print both DPs for each zone axis at the scale you used in your line drawing of the Kikuchi map.

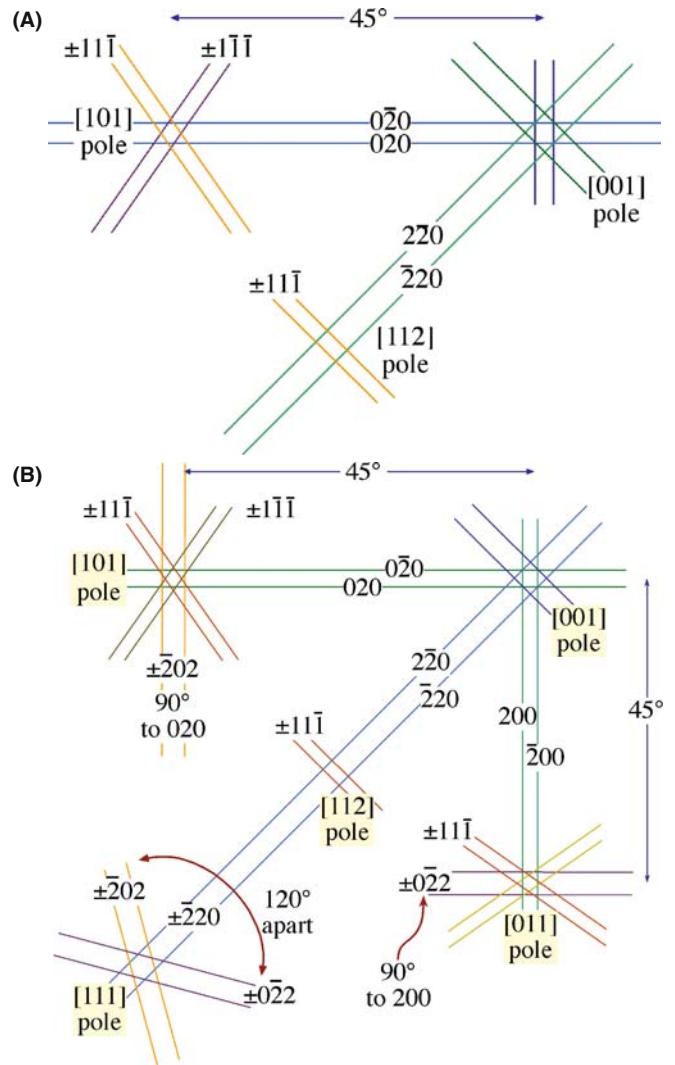


**FIGURE 19.5.** (A) Construction of the  $[112]$  pattern from the  $[001]$  and  $[101]$  patterns by extending the Kikuchi lines common to each pair of patterns. The  $[111]$  pair is common to the  $[001]$  and  $[112]$  patterns and the  $220$  pair is common to  $[001]$  and  $[112]$  patterns. (B) Other poles can be added such as  $[011]$  and  $[111]$ . Note that the Kikuchi-line pairs are not straight lines connecting poles. They are curved because over large angles their parabolic shape is evident. Nevertheless we draw them as straight lines where possible.

- Now add the experimental patterns to the line diagrams and you have two very useful experimental aids. An illustration is given in Figure 19.8.

When discussing Kikuchi maps, we like to use the road-map analogy. (Repeatedly!) What we just recommended is that you record the maps of the towns with pictures so that you'll recognize them. When you're on the highway traveling from town to town, you don't much care what the road looks like although you do want to know how far you've traveled and how much farther you have to go.

By now you will appreciate even more the value of the stereographic projection we introduced in Chapter 18.

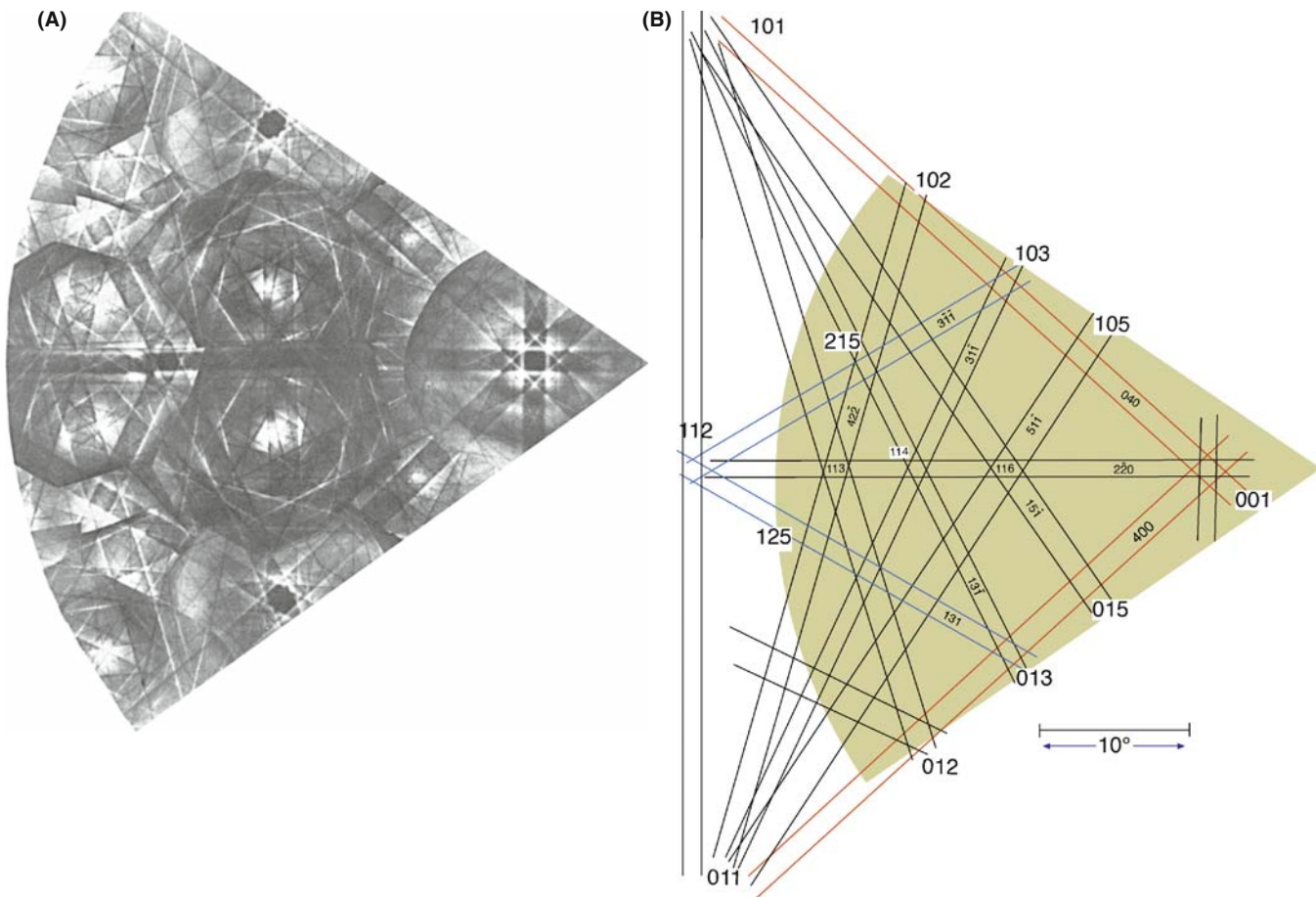


FIGURE 19.6. (A) Experimental Kikuchi map for fcc crystals and (B) indexed Kikuchi lines in the schematic map.

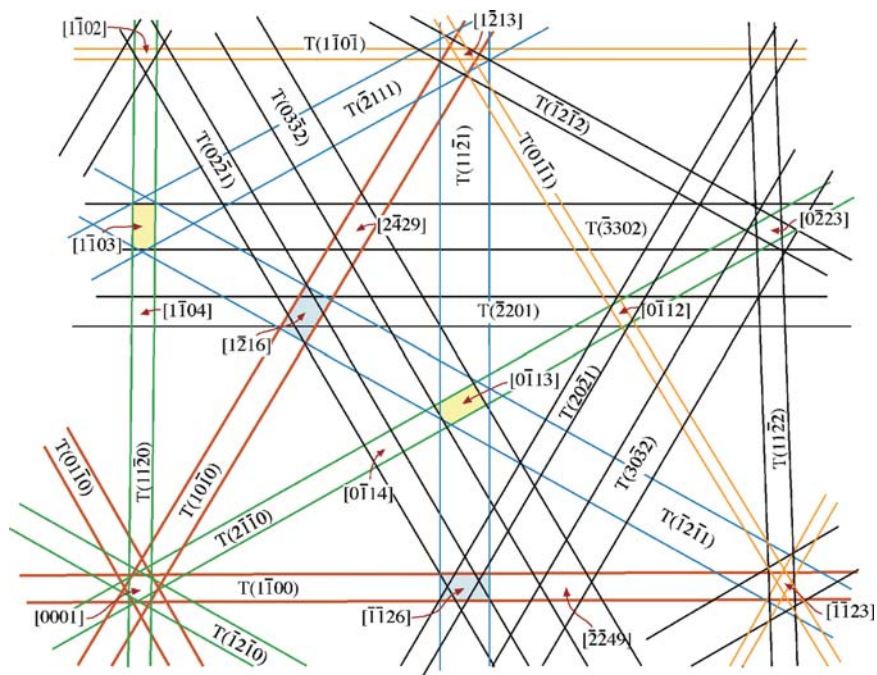
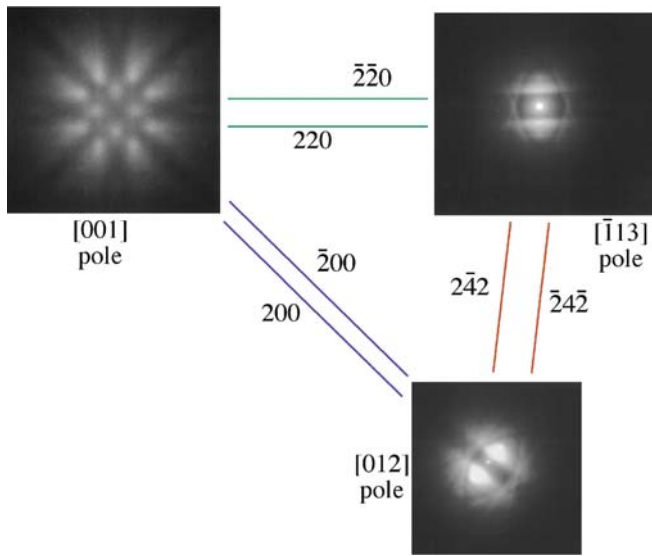


FIGURE 19.7 Part of the Kikuchi map for hexagonal  $\text{Ag}_2\text{Al}$  with the principal poles and pairs of lines indexed.



**FIGURE 19.8.** Experimental Kikuchi patterns around three principal poles in MgO with the common Kikuchi lines between each pole drawn in. You should compare this figure with the DPs in Figure 18.7.

Use the stereographic projection and the Kikuchi map together. The stereographic projection concisely summarizes all the relative locations of all the plane normals and the zone axes. Use the stereographic projection to relate Storrs and Huntsville, but use the Kikuchi map to locate the Benton Museum of Art and the Von Braun Center.

## 19.4 CRYSTAL ORIENTATION AND KIKUCHI MAPS

In the previous chapter we showed how you could use SADPs to estimate the orientation of the beam relative to the crystal with an accuracy of  $\pm 3^\circ$ . Using Kikuchi patterns you can increase this accuracy to  $\pm 1^\circ$ .

A routine method for orientation determination was developed by Thomas and co-workers (e.g., Okamoto et al.); they pioneered the use of Kikuchi maps in TEM analysis. The beam direction  $[UVW]$  lies along the optic axis  $O$  in Figure 19.9.  $A$ ,  $B$  and  $C$  are major poles (i.e., zone axes) which we can determine by observation and measurement. Let the indices of  $A = [p_1 q_1 r_1]$ ,  $B = [p_2 q_2 r_2]$  and  $C = [p_3 q_3 r_3]$ . Having indexed these poles, we can check our result by measuring the angles  $\alpha$ ,  $\beta$  and  $\gamma$  between the traces of the planes in Figure 19.9A (which equals the angle,  $\phi$ , between the plane normals in all systems); we must calculate each angle using equation 18.3 if the specimen is cubic.

### SPECIMEN ALIGNMENT

Kikuchi lines transform SADPs from an approximate to a very precise alignment technique.

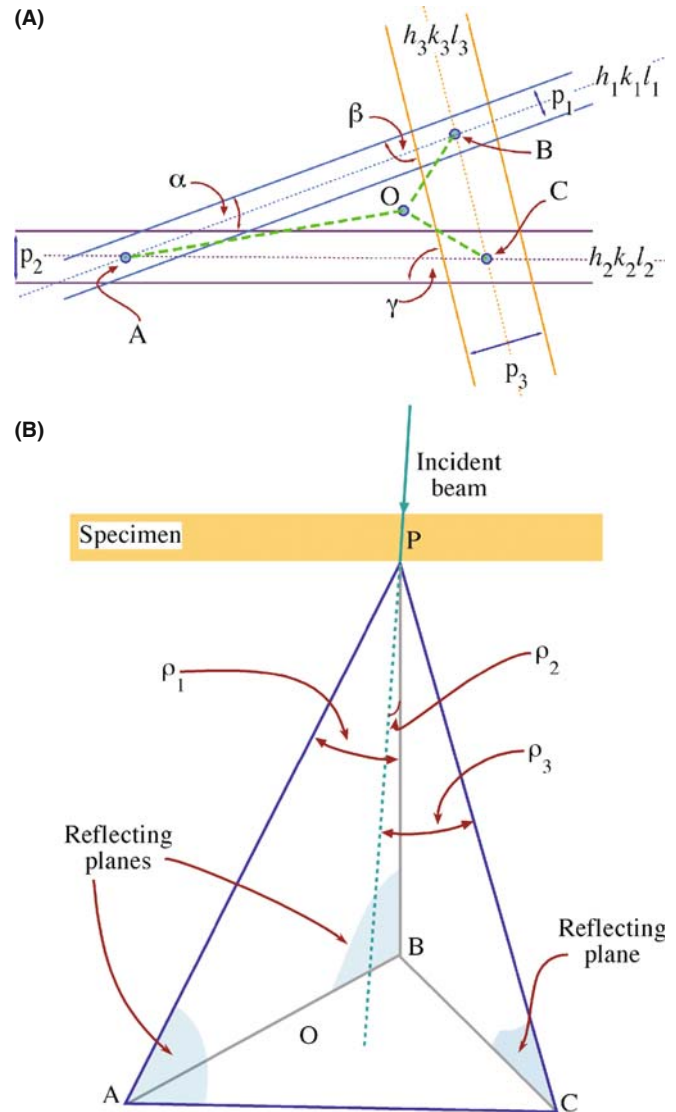


**FIGURE 19.9.** In (A) pairs of Kikuchi lines from the reflecting planes also intercept at points  $A$ ,  $B$ ,  $C$ . The distances from  $O$  to the points  $A$ ,  $B$ ,  $C$  correspond to the angles between the beam direction and the three zone axes while the angles  $\alpha$ ,  $\beta$ ,  $\gamma$  correspond to the angles between pairs of plane normals. The angle  $\alpha$  is between the  $(h_1k_1l_1)$  and  $(h_2k_2l_2)$  plane normals, etc. (B) Three reflecting planes in the specimen with traces  $AB$  ( $h_1k_1l_1$ ),  $AC$  ( $h_2k_2l_2$ ) and  $BC$  ( $h_3k_3l_3$ ), around the direct beam,  $O$ ; the traces of pairs of planes intercept at  $A$  ( $AB$ ,  $AC$ ),  $B$  ( $AB$ ,  $BC$ ) and  $C$  ( $AC$ ,  $BC$ ).

If we measure the distances  $OA$ ,  $OB$  and  $OC$  in Figure 19.9A, we can convert them into angles  $\rho_1$ ,  $\rho_2$  and  $\rho_3$  (which are defined in Figure 19.9B) by using our calibrated camera length. If  $[UVW]$  is the direction of the beam, then we can use the same vector-dot-product approach (equation 18.4 for the cubic case) to give equations for  $\rho_1$ ,  $\rho_2$  and  $\rho_3$ . Notice we are distinguishing between  $\rho$  and  $\phi$  (see Section 18.4). The angles  $\alpha$ ,  $\beta$  and  $\gamma$  in Figure 19.9A are slightly distorted values of  $(90 - \phi)$ .

We can solve these three equations for the three unknowns  $U$ ,  $V$  and  $W$  and hence we have  $\mathbf{B}$ . Finally, you should always check the sign of  $\mathbf{B}$ , as we described in Section 18.10.



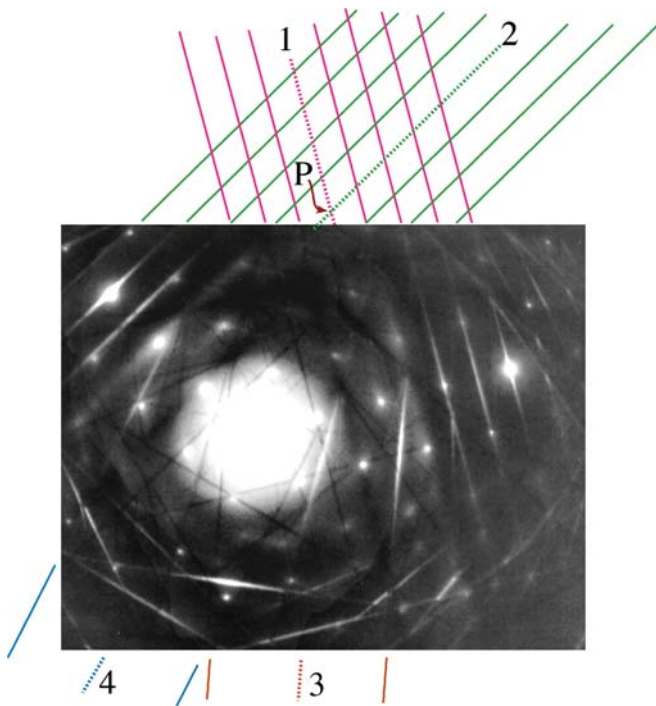


**FIGURE 19.10.** To index a DP well away from a low-index zone axis, extend the Kikuchi lines. The dark lines 1–4 represent the traces of the diffracting planes which intercept at a pole (P). For Kikuchi lines 1 and 2, the higher-order extensions are also drawn. From the  $d$ -spacings, index the Kikuchi-line pairs. The angles between the beam direction and the poles, P, can then be measured directly.

It is possible that the DP you have to work with is not obviously near a zone axis. All is not lost if you can just find pairs of Kikuchi lines as shown in Figure 19.10. If you see an excess line you will find the deficient line quite easily, closer to 000. Now trace these lines in both directions and you have found the poles. Use your knowledge of the  $d$ -spacings to index the pairs of Kikuchi lines. Remember that the zone axis lies parallel to each plane so it's defined by where the two plane traces meet. Now, if you can index three poles, you can obtain **B** as in Figure 19.9.

**DO REAL-TIME CRYSTALLOGRAPHY**  
 Normally, while you are at the TEM, tilt along the different Kikuchi bands until you find the appropriate poles to ease your task later.

### 19.5 SETTING THE VALUE OF $S_g$

Since the Kikuchi lines are 'rigidly attached' to the crystal, they give us a very accurate measure of the excitation error  $s_g$ . The diffraction geometry is shown in Figure 19.11 following Okamoto et al. When  $s_g$  is negative, the **g** Kikuchi line is on the same side of **g** as **O**;

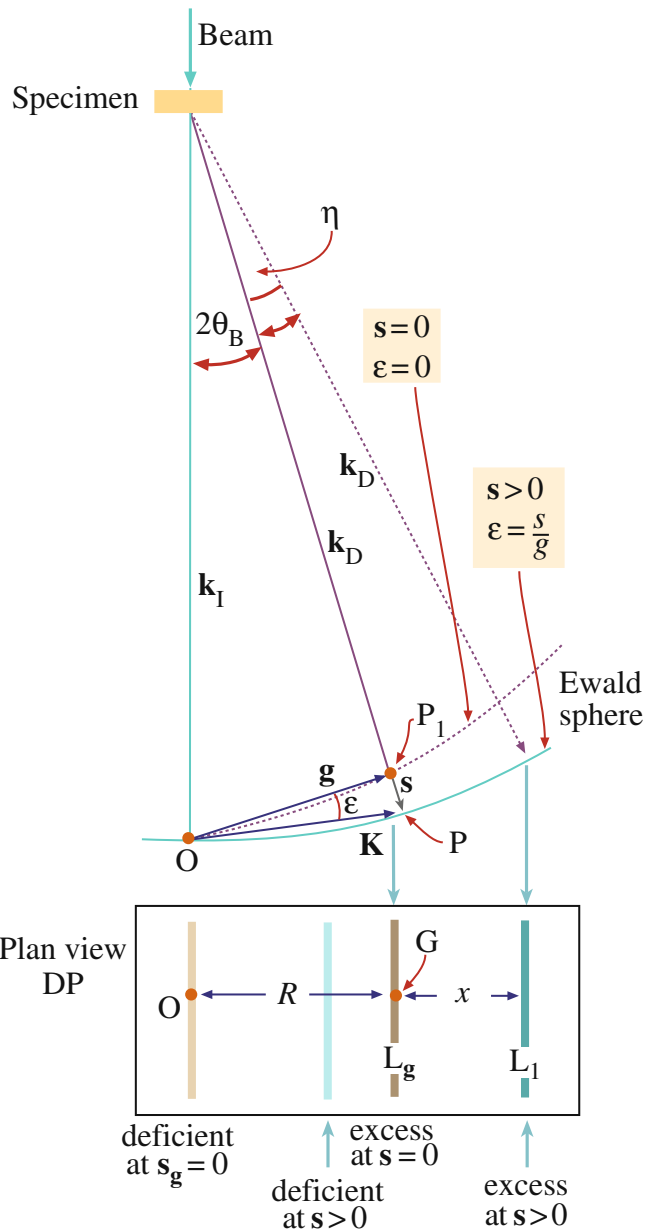


**FIGURE 19.11.** The distance between the diffraction spot and its Kikuchi line gives a direct measure of  $s$ . The angle  $\epsilon$  is  $s/g$  and is zero at the exact Bragg condition. In the box: measure  $x$ , the spacing between **O** and the deficient line (or **G** and the excess line) to determine  $s$ .

when  $s_g$  is positive, the line lies on the opposite side of **g**. If you look at Figure 19.10 you'll see that the bright diffraction spot at the top LH corner of the DP is under  $s_g$  positive conditions (excess Kikuchi line outside the spot), the bright spot at the middle/upper RH side is under  $s_g$  zero conditions (the excess Kikuchi line through the spot) and the bright spot toward the bottom of the DP is under  $s_g$  negative conditions (the excess Kikuchi line inside the spot).

For high-energy electrons, and knowing the camera length  $L$ , we can write an expression for the angle  $\eta$  in Figure 19.11



$$\eta = \frac{x}{L} = \frac{x\lambda}{Rd} \quad (19.1)$$

where  $d$  is  $|\mathbf{g}|^{-1}$ . The distances  $x$  and  $R$  are measured on the photographic negative.

The angle  $\varepsilon$  is given by

$$\varepsilon = \frac{s}{g} \quad (19.2)$$

Now we can set  $\varepsilon = \eta$  to give

$$s = \varepsilon g = \frac{x}{L} g = \frac{x}{Ld} \quad (19.3)$$

Again, with our small-angle approximation, the distance between the excess and deficient Kikuchi lines,  $R$  (the distance  $g$  measured on the DP), is equivalent to  $2\theta_B L$ . So, using Bragg's law, we have

$$\frac{R}{L} = 2\theta_B = \frac{\lambda}{d} \quad (19.4)$$

Hence the expression for  $s$  is

$$s = \frac{x}{Ld} = \frac{x}{d} \cdot \frac{\lambda}{Rd} \quad (19.5)$$

$$s = \frac{x}{R} \frac{\lambda}{d^2} = \frac{x}{R} \lambda g^2 \quad (19.6)$$

We'll reconsider this equation when we discuss weak-beam microscopy in Chapter 27.

Ryder and Pitsch have given a method for determining  $\mathbf{B}$  using the approach we described in Section 19.4 with the accuracy given by equation 19.6. Their expression for  $\mathbf{B}$  is

$$\mathbf{B} = \alpha_1 |\mathbf{g}_1|^2 (\mathbf{g}_2 \times \mathbf{g}_3) + \alpha_2 |\mathbf{g}_2|^2 (\mathbf{g}_3 \times \mathbf{g}_1) + \alpha_3 |\mathbf{g}_3|^2 (\mathbf{g}_1 \times \mathbf{g}_2) \quad (19.7)$$

where  $\alpha_i$  is given by

$$\alpha_i = \frac{R_i + 2x_i}{R_i} \quad (19.8)$$

where  $R$  and  $x$  are defined in Figure 19.11.

## 19.6 INTENSITIES

We'll conclude with a few remarks for further thought

- Tan et al. have shown experimentally that the distance between a pair of Kikuchi lines may change at larger specimen thicknesses due to dynamical scattering.

- Kikuchi lines can also be produced by the backscattered electrons. In the SEM these patterns are termed electron-backscatter DPs (sometimes EBSPs) and the technique as EBSD. They were regarded as a curiosity until it was shown (see Dingley's paper) that you can map out the texture of polycrystalline materials using these patterns, without thinning the sample. Not much happened for a decade or more until new detection systems, using CCD cameras and fast computer algorithms led to the development of orientation imaging microscopy (OIM) (see Dingley's review). As we saw in Section 18.13, similar techniques are available for automatic indexing of TEM DPs and Kikuchi maps. They aren't as automated, nor can they index as many patterns as EBSD software because there are usually far fewer thin grains in our specimens than crystals in an SEM specimen. But TEM can, in principle, give the interface plane much more accurately, so the two techniques will become more complementary with time.
- In the next chapter, we'll discuss HOLZ lines; HOLZ lines are very closely related to Kikuchi lines but are a little more complicated, since the Bragg planes are always inclined to the direct beam.
- In Chapter 24, we'll discuss ZAPs, or zone-axis patterns, in *images*; these ZAPs are, in many respects, the real-space version of Kikuchi lines. However, you'll see that their physical origin is *completely different*; the most important features of ZAPs are *not* associated with incoherent, inelastic or diffuse scattering.
- Bloch waves with vector  $\mathbf{k}^1$ , for example, are more strongly scattered than those corresponding to branch 2 of the dispersion surface. Therefore, we can expect anomalous absorption (see Chapter 24) to influence the intensity of Kikuchi patterns. Such effects do in fact lead to excess and deficient Kikuchi bands. Since we haven't yet found any use for the information in these bands we'll leave them as an exercise for further reading!
- We mentioned earlier that the contrast between the Kikuchi lines, i.e., the Kikuchi band, is complex. The contrast is strongly influenced by anomalous absorption of the Bloch waves which are formed by coherent scattering of the incoherently scattered electron, so all is clear.
- There are strong similarities between the Kikuchi process and the operation of a monochromator in optics: both select and diffract a particular wavelength or frequency.
- You can appreciate that the scattering is quite complex by considering what happens when the diffracting plane is exactly parallel to the incident beam: as we've mentioned, the two Kikuchi lines will both be visible although you might have guessed otherwise.

Back in Chapter 6 we noted that electron ray paths rotate through the objective-lens field, but in all our

discussion on diffraction (including Kikuchi lines and the CBED patterns in the next two chapters) we draw all the electron paths as straight lines, ignoring any rotation. However, particularly in a modern condenser-objective lens TEM, the lens field is relatively strong and can introduce a significant rotation into the off-axis incident and diffracted electrons (we described c/o

lenses and their effects on ray paths back in various sections of Chapter 9). An interesting consequence of this effect is that Kikuchi lines in modern TEMs may be less sharp than in older TEMs, unless you illuminate only a very small area of the specimen. If you're intrigued by this problem then you must read "Skew thoughts on parallelism" by Christenson and Eades.

## CHAPTER SUMMARY

Pairs of Kikuchi lines define the road and, taken together, the roads make up a map of reciprocal space. However, the key is different from real-space road maps because in our Kikuchi maps, narrow roads are the most important! What is the relevance of the roadside curbs? Well, they define the roads and tell us when we are standing on them, but we are not too interested in their detailed appearance. You should by now be under the (correct) impression that we view Kikuchi lines and maps as an invaluable tool for the microscopist. The key points are

- The Kikuchi lines arise from Bragg diffraction of divergent, incoherent electrons scattered within the specimen.
- The Kikuchi lines consist of an excess (bright) line and a deficient (dark) line. In the DP, the excess line is farther from the direct beam than the deficient line.
- The Kikuchi lines are effectively fixed *to the crystal* so we can use them to determine orientations accurately.
- The trace of the diffracting planes is midway between the excess and deficient lines.
- We can use the Kikuchi lines to set up specific (e.g., two-beam) diffracting conditions which are central to diffraction-contrast imaging.
- We can control and determine the value of  $s_g$  by measuring the separation between the  $g$  Kikuchi line and the  $G$  reflection (the separation is 0 when  $s_g = 0$ ). The precise value of  $s_g$  is also very important in controlling diffraction contrast.

Kikuchi lines and maps are two of the most important aids you have when orienting (or determining the orientation of) crystalline specimens. Knowing the orientation of your specimen is essential for any form of quantitative TEM, whether you're analyzing dislocation Burgers vectors by diffraction contrast, imaging grain boundaries with lattice resolution or measuring chemistry variations by EELS or XEDS. Kikuchi maps are especially useful when combined with the map of zones and poles (directions and plane normals) on the stereographic projection. Use a computer to check or to assist you in constructing such a map for your material but if you're doing any serious crystallography, never leave home or sit at your TEM without a map to guide you.

## IN GENERAL

Edington, JW (1976) *Practical Electron Microscopy in Materials Science*, Van Nostrand-Reinhold New York. Part 2 of the book is still an excellent source of guidance if you are doing hands-on DP acquisition and analysis and the Appendix has great Kikuchi maps.

Schwartz, AJ, Kumar, M and Adams, BL (Eds.) (2000) *Electron Backscatter Diffraction in Materials Science*, Springer NY. Kikuchi patterns in the SEM: an insight into what could really be done in terms of orientation determination in TEM, if we put our minds to it.

Thomas, G (1978) in *Modern Diffraction and Imaging Technique in Materials Science* p 399 Eds. S Amelinckx, R Gevers and J Van Landuyt North-Holland Amsterdam. Still the best reference because no one has really done anything of significance with Kikuchi patterns in TEM since Gareth Thomas, 40 years ago (check out the other references below).

## SOME HISTORY AND APPLICATION

Christenson, KK and Eades, JA 1988 *Skew Thoughts on Parallelism* Ultramicroscopy **26** 113–132.

Dingley, DJ 1984 *On-Line Determination of Crystal Orientation and Texture Determination in an SEM*. Proc. Royal Microsc. Soc. **19** 74–75. The idea of texture mapping developed for the SEM can be applied to the TEM.

- Dingley, DJ 2004 *Progressive Steps in the Development of Electron Backscatter Diffraction and Orientation Imaging Microscopy* J. Microsc. **213** 214–224.
- Johari, O and Thomas, G 1969 *The Stereographic Projection and its Applications in Techniques of Metals Research* Ed. RF Bunshah Interscience New York.
- Kikuchi, S 1928 *Diffraction of Cathode Rays by Mica* Japan J. Phys. **5** 83–96.
- Levine, E, Bell, WL and Thomas, G 1966 *Further Applications of Kikuchi Diffraction Patterns; Kikuchi Maps* Appl. Phys. **37** 2141–2148.
- Okamoto, PR, Levine, E and Thomas, G 1967 *Kikuchi Maps for H.C.P. and B.C.C. crystals* J. Appl. Phys. **38** 289–296.
- Ryder, PL and Pitsch, W 1968 *On the Accuracy of Orientation Determination by Selected Area Electron Diffraction* Phil. Mag. **18** 807–816.
- Tan, TY, Bell, WL and Thomas, G 1971 *Crystal Thickness Dependence of Kikuchi Line Spacing* Phil Mag. **24** 417–424.

## URLS

- 1) [http://cimewww.epfl.ch/EMYP/comp\\_sim.html](http://cimewww.epfl.ch/EMYP/comp_sim.html)

## THE COMPANION TEXT

The main chapters in the companion text that relate to this topic are those on CBED and EFTEM.

## SELF-ASSESSMENT QUESTIONS

- Q19.1 When viewing different regions of your specimen, the intensity of the Kikuchi lines changes. Could the reason be the variation in thickness?
- Q19.2 Why is the Kikuchi line nearer 000 brighter than its partner that is farther away?
- Q19.3 You record a series of DPs as you tilt along a Kikuchi band. You paste the DPs together but the Kikuchi lines appear to be slightly curved Kikuchi lines, but Kikuchi lines are drawn straight. Explain.
- Q19.4 When viewing another DP, a pair of parallel lines is present where one line is dark and the other is bright. Why does this happen, and how do we name each line?
- Q19.5 You're writing your dissertation on the beach in Aruba so you don't have crystallography software available but the crucial DP of a certain fcc specimen stored on your laptop is only showing Kikuchi lines. Can you determine the orientation? If so, how can you do it?
- Q19.6 Where is the  $\mathbf{g}$  Kikuchi line relative to O and G if the excitation error,  $\mathbf{s}_g$ , is less than zero?
- Q19.7 How does the distance between Kikuchi lines vary with specimen thickness?
- Q19.8 How accurately can you determine orientations using Kikuchi lines?
- Q19.9 Will a conventional TEM with a LaB<sub>6</sub> filament give better Kikuchi lines than a new FEGTEM at the same orientation and thickness?
- Q19.10 We say that Kikuchi lines arise due to incoherently scattered electrons? This statement is a little oversimplified. Why?
- Q19.11 Why are Kikuchi patterns used for setting the value of  $\mathbf{s}$ ?
- Q19.12 What are Kossel cones?
- Q19.13 What is the distance between a pair of Kikuchi lines?
- Q19.14 Can you just read off  $\mathbf{s}$  from where the Kikuchi line cuts the systematic row?
- Q19.15 Why is there an ideal thickness for a specimen when viewing Kikuchi diffraction?
- Q19.16 How can we trace the location of a plane from Kikuchi lines?
- Q19.17 Briefly describe how you can find poles using Kikuchi lines.
- Q19.18 Is EBSD possible in the TEM?
- Q19.19 What is the distance in reciprocal space between the  $-5\mathbf{g}$  and  $+5\mathbf{g}$  Kikuchi lines?
- Q19.20 How do HOLZ lines and Kikuchi lines differ? (Read Chapters 20 and 21 before answering this.)
- Q19.21 Construct a Kikuchi map where the [001] pole is exactly on the optic axis.
- Q19.22 Why do we only need the Kikuchi map for the [001], [101] and [111] triangle in fcc crystals but have to map much more of reciprocal space for hcp, and what is the largest area we would have to map for any crystal?

## TEXT-SPECIFIC QUESTIONS

- T19.1 Assuming that Figure 19.1 was obtained from a cubic material, determine the approximate orientation of the specimen.
- T19.2 Redraw Figure 19.4A for the [011] and [111] poles but arrange for two low-index reflections to be excited in each figure.
- T19.3 Consider Figure 19.6. Sketch and label the Kikuchi bands which pass through the 115 pole.
- T19.4 Using Figure 19.6 draw consistent DPs for the 102, 116 and 013 poles as you would expect to see them as you tilt your fcc sample. (So you have to align them appropriately too.)

- T19.5 Using Figure 19.7 draw consistent DPs for the  $\bar{1}\bar{2}13$ ,  $1\bar{1}02$  and  $0\bar{1}12$  poles as you would expect to see them as you tilt your hcp sample. (So you have to align them appropriately too.)
- T19.6 In Figure 19.10, determine what the pole is and how far it is inclined relative to the electron beam. How would you tilt the sample to bring P onto the optic axis (assuming O is on the optic axis)?
- T19.7 Consider Figure 19.10. Identify and index 10 pairs of Kikuchi lines (even if you can only see one of the lines).
- T19.8 In Figure 19.11, where are the diffracting planes? Why can we see the Ewald sphere in two places? Which one is correct as the diagram is drawn?
- T19.9 Sketch Figure 19.7 for Be showing the  $1\bar{1}02$ ,  $\bar{1}\bar{2}13$ ,  $0\bar{2}23$  and  $\bar{1}\bar{1}23$  poles. Now superimpose on this figure the one for Ti as if the Ti had grown in perfect alignment on 0001 Be.
- T19.10 Choose a 010 sample of olivine and construct the Kikuchi pattern to a radius of  $45^\circ$  about this pole. Label the Kikuchi bands and sketch the main DPs you will find. (You should use the Web or ICDD files to help you with this question.)
- T19.11 An Al-crystal (fcc) is observed exactly along a [011] direction. Draw the corresponding DP with the associated Kikuchi lines (bands). After a small tilt of the crystal, the Kikuchi lines pass through three of the low-index reflections. How far has the crystal been tilted and what was the tilt axis? The lattice constant for aluminum is 0.405 nm. The wavelength for the electrons is 0.0025 nm. (Courtesy Anders Tholen.)
- T19.12 Explain how you would deduce the accelerating voltage of the TEM using a DP from Si.



# Obtaining CBED Patterns

## CHAPTER PREVIEW

We know that SAD, while giving us useful information about the specimen, has two severe limitations.

- We have to be very cautious in interpreting SADPs from areas which are  $< \sim 0.5 \mu\text{m}$  in diameter because the information in the pattern may not be limited to that region. This scale is still large compared to the dimensions of many crystalline features that interest us in materials science and much larger than nanotechnology dimensions.
- SADPs contain only rather imprecise 2D crystallographic information because the Bragg conditions are relaxed for thin specimens and small grains within the specimen (see Chapter 17).

The technique of CBED overcomes both of these limitations and also generates much new diffraction information which we will introduce to you in Chapter 21 and expand in greater depth in the companion text.

In this chapter, we will show you how simple it is to use the versatility of modern TEMs to create a range of CBED patterns containing a variety of very useful contrast effects such as higher-order Laue-zone (HOLZ) spots and lines. In Chapter 21 and the companion text, you will see why these HOLZ features are so useful. They can give us a complete 3D crystallographic analysis of our specimens. By now you are well aware that a major advantage of doing anything in TEM is that we can get the information at high spatial resolution at the same time as we are looking at the TEM image. CBED is no exception. For most TEM operations, thinner specimens are better, but CBED patterns, like Kikuchi patterns, are generally more useful from thicker specimens in which dynamical scattering is occurring. Finally, as with many other sophisticated analytical techniques, CBED uses various obscure initials and acronyms which we will attempt to clarify as we introduce them.

### 20.1 WHY USE A CONVERGENT BEAM?

Historically, CBED is the oldest electron-diffraction technique used in the TEM. It was originally developed by Kossel and Möllenstedt, well before LePoole developed SAD. While SAD is the classic way to relate the diffraction-contrast information in the TEM image to the specimen orientation, it has a notable disadvantage. Remember, we saw back in Chapters 9 and 11 that the diameter of the smallest area you can select by SAD is  $\sim 0.5 \mu\text{m}$ , with an uncertainty of similar dimensions. However, if you have an intermediate-voltage HRTEM with a very low  $C_s$  you may be able to extend the range of SAD to analyze areas  $\sim 100 \text{ nm}$  in diameter, which is still too large for examining any nanoscale material

(particles, films, devices) as well as all crystal defects and most second-phase precipitates which influence the properties of conventional engineering materials. All these features are much smaller than  $0.1 \mu\text{m}$ . As we described back in Figure 9.4, one way we can overcome this limitation is to use a convergent beam of electrons. The region sampled by the convergent beam is a function of its size and the beam-specimen interaction volume, which increases with specimen thickness but is generally a lot smaller than the spatial limitations of SAD. In fact, several so-called micro- and nanodiffraction methods have been developed over the past 40 years to overcome the spatial-resolution limitations of SAD in a TEM. But CBED is by far the most simple and versatile of these techniques and easily

penetrates the nanotechnology domain ( $< 100$  nm), in fact all the way down to single unit-cell dimensions (truly nanodiffraction).

In addition to offering improved spatial resolution, CBED patterns contain a wealth of crystallographic and other data which are difficult or impossible to obtain via SAD and we'll describe much of this new information in the next chapter and in the companion text.

With such capabilities, CBED has transformed diffraction in the TEM from the 'poor relative' of X-ray and neutron diffraction to a more versatile and, in some senses, a unique technique. CBED has already begun to intrude significantly into XRD's traditional domain of quantitative crystallography, as a cursory reading of the contents of *Acta Crystallographica* will show.

Some would argue persuasively that CBED should be the diffraction method of first choice when operating a TEM and this is not surprising given all the new information you can access via CBED. However, much of diffraction theory, indexing methods, etc., were historically developed for parallel-beam SADPs, and standard BF/CDF and other imaging techniques build on such patterns. So we have chosen to construct the text starting with SAD and treat CBED as an 'enriched' variant of SAD.

### THE CBED ADVANTAGE

...over all other diffraction techniques is that most of the information is generated from minuscule regions beyond the reach of other diffraction methods.

In this chapter, we will concentrate on how you can control the experimental variables to acquire and index CBED patterns. In the next chapter, we will introduce to you, among other things, how to perform the basics of what is known as 'electron crystallography.' All the advantages of CBED can simultaneously be coupled with TEM images and spectrometry data thus allowing you to achieve a remarkable degree of characterization of the same region of your specimen at the same time.

There are two potential drawbacks which you should always keep in mind

- The focused probe may generate contamination which can cause localized stresses.
- The convergent beam may heat or damage the chosen region of your specimen.

In early probe-forming TEMs, the operator only had a few seconds to observe and record the CBED pattern before carbon contamination built up to a thickness which masked all the information. Modern TEMs, particularly UHV instruments, should not suffer from this problem (see Chapter 8). You should be able to study small regions of a clean specimen for many minutes or even hours without contamination.

### CONTAMINATION

Most contamination is caused by the specimen-preparation process or your careless handling of your specimen.

As we described in Chapter 4, beam heating/damage may be a problem in materials with poor thermal conductivity but this can be minimized by applying a thin conductive coating or, preferably, by using a liquid-N<sub>2</sub> cooling holder. This latter approach has other advantages for CBED, as we'll see.

You will probably find that it is experimentally easier to do CBED rather than SAD. SAD is used if your primary interest is the image. In CBED, there's no inserting and removing of diaphragms and more information is almost always obtained, invariably from smaller regions. You might not find this fact reflected in your reading of the TEM literature, but remember that researchers (including the authors) often use the technique with which they are most familiar, rather than the best one available. It's also appropriate here to mention why we include the 'E' in CBED but rarely in SAD; it's only so we can pronounce the initials as "see-bed." (Happily no one ever says "sad" or "said" for that matter.) But if the world were logical then all men would ride sidesaddle.

### THE CBED HOLDER

A double-tilt, cooling, low-background holder is really useful for CBED.

## 20.2 OBTAINING CBED PATTERNS

*First, which holder should you use?* As with SAD you will need to do a lot of tilting so a double-tilt holder is required. Some of the diffraction phenomena we will be describing become more visible if the specimen is cooled to liquid-N<sub>2</sub> temperatures. If you want to carry out XEDS and CBED simultaneously then you'll also need a low-background holder.

Single-tilt rotation holders can sometimes be advantageous (e.g., to line up interfaces in certain directions) and again are best if they can be cooled and are low background (for XEDS).

*Second, which kV should you use?* In diffraction, unlike most other TEM techniques, there is often an advantage to using lower kVs since the elastic-scattering cross section is higher. So the patterns are more intense. Also the Ewald sphere is more curved at lower kVs and so it intercepts more electrons scattered at higher angles than those in the ZOLZ. However, higher kVs give higher-resolution information from smaller volumes of your specimen and you can 'see' through thicker specimens. So you may have to compromise and gather patterns over a range of kVs.

Third, how thick should your specimen be? As we already mentioned, unlike most other TEM techniques, thicker specimens can be more useful than thinner specimens since more dynamical scattering occurs. Much of the undesirable diffuse scattering that hides the dynamical information can be filtered out in an EFTEM (much more about this later and in Section 38.2).

### 20.2.A Comparing SAD and CBED

Now let's consider the differences in the electron optics of SAD and CBED. In SAD the electron beam incident on your specimen is parallel (fixed incident vector  $\mathbf{k}$ ) and relatively large (usually  $\sim 1\text{--}10\ \mu\text{m}$  in diameter). In CBED, the beam is convergent (range of  $\mathbf{k}$  vectors) and relatively small (usually  $\sim 1\text{--}100\ \text{nm}$  in diameter) as shown in Figure 20.1. (Compare this situation with Kikuchi patterns which are generated by a divergent beam of electrons within the specimen.) We've already seen in Chapters 11 and 16 that parallel illumination means that the SADP consists of an array of sharp maxima (or spots) in the BFP of the objective lens and, as mentioned in Chapter 9, the beam convergence in CBED gives rise to a pattern of disks of intensity. Figure 20.2A shows an SADP from pure Si and Figure 20.2B is a CBED pattern from a much smaller region of the same Si specimen. While it isn't obvious that the CBED pattern comes from a smaller region of the specimen (i.e., has better *spatial* resolution), you can certainly see that it contains a wealth of contrast detail not present in the SADP. The dark lines within the 000 disk and between the diffraction

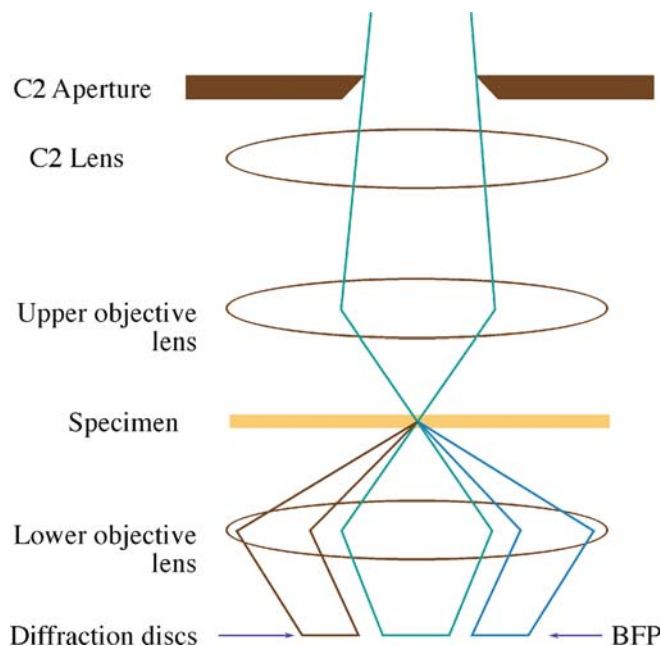


**FIGURE 20.1.** Ray diagram showing CBED pattern formation. If the c/o lens system focuses the beam at the specimen, the illuminated area is very small compared with parallel-beam SADP formation. A convergent beam at the specimen results in the formation of disks in the BFP of the objective lens.

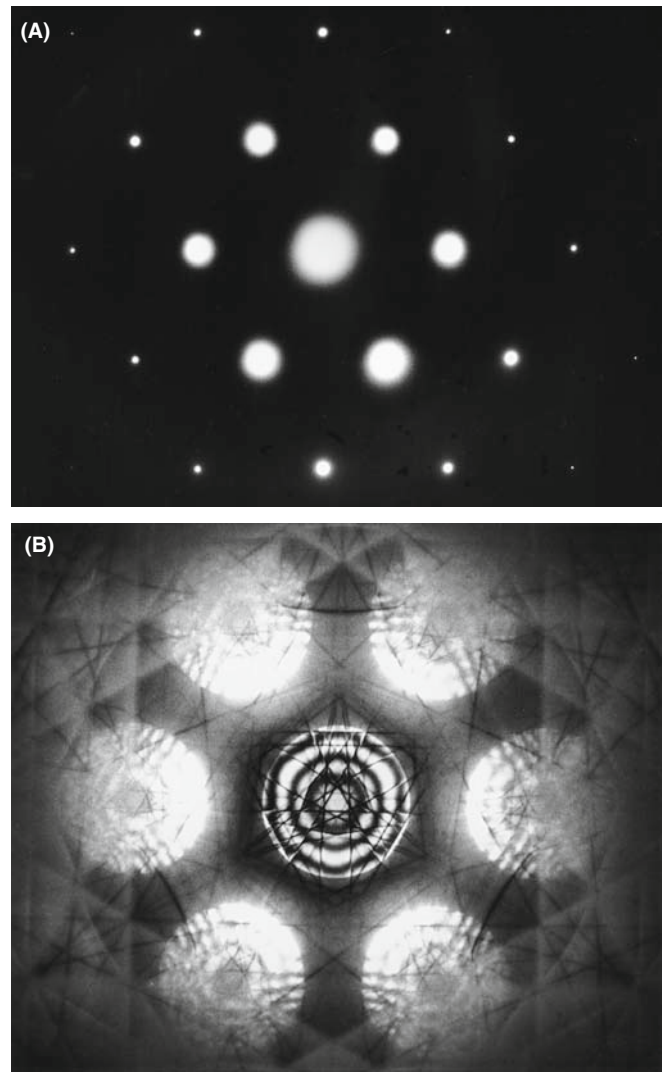


**FIGURE 20.2.** (A) SADP from [111] Si showing the first few orders of diffraction spots and no visible Kikuchi lines. (B) CBED pattern from [111] Si showing dynamical contrast within the disks as well as diffuse Kikuchi bands and sharp, deficient HOLZ lines.

disks are HOLZ effects which we'll return to many times throughout this and the next chapter. Converging the beam, in effect, opens up a greater angular range of reciprocal space for you to look into and in doing so it reduces the *angular* resolution of the DP (which is not something we worry about too much).

#### RELATING SAD AND CBED

You can imagine CBED as magnifying the information within the spots in the SAD. Like SAD, CBED is most useful when you either orient the beam along a zone axis in the crystal to give a symmetrical zone-axis pattern (ZAP) or when you tilt to strong two-beam conditions. Unlike SAD, CBED is also even more useful when the probe is deliberately under- or overfocused.

From Figure 20.1 you can see that we need a condenser/objective (c/o) lens (i.e., a strong upper-objective polepiece) to create a convergent beam, so any probe-forming TEM or dedicated STEM can generate such patterns. We've already described the lens systems and ray diagrams associated with forming a convergent beam in Chapters 6 and 9, so here we will emphasize the experimental variables that you can control. The various steps we describe below are covered in far greater detail, both operationally and in terms of extraordinarily detailed ray diagrams, in the essential text by Morniroli. We'll start with TEM mode and then describe STEM operation.

## 20.2.B CBED in TEM Mode

It's a good idea to start practicing CBED with a thin, single-crystal Si specimen or a stainless steel foil with large grains, since these specimens give immediately useful patterns containing many of the features that we'll be describing (without the need for cooling). The Si is a little easier since the parent wafer will be in a specific orientation such as  $\langle 111 \rangle$  and you'll invariably get a pattern like Figure 20.2B.

When you converge the beam in image mode, you'll lose any useful image contrast and you'll just see a bright spot on the TEM screen or computer display. But if you aligned the condenser system correctly then the beam will be focused on the region you chose. You will develop your own procedure as you gain experience. Basically the approach is as follows:

- Start with your specimen in the eucentric plane, as usual. Weaken C2 to give a broad, parallel beam, then focus an image with the feature from which you want to obtain the CBED pattern in the middle of the screen. It helps if you can do this without the objective diaphragm inserted. If you need it, then you'll have to take it out later (see below).
- Select a large C2 aperture about 100–200  $\mu\text{m}$  in diameter, carefully center it, then adjust the C2 lens to converge the beam to a focused spot on the area of interest.
- Keep C1 weakly excited to give a relatively large spot, about 100 nm FWTM (see Chapter 5) which should contain sufficient current to give a high-intensity pattern.
- Select a small camera length,  $< 500$  mm to give a wide-angle view of the pattern.
- To observe the CBED pattern, just switch to diffraction mode, making sure the objective and SAD diaphragms are retracted.

Remember that you control the minimum illuminated area on the screen (i.e., the beam diameter at the specimen) by the strength of the C1 lens, so after these initial steps, you might want to select a smaller probe size by increasing the C1 strength.

## 20.2.C CBED in STEM Mode

You should first get a focused STEM image of the specimen as we described in Section 9.4.

The procedure is quite simple because in STEM you're always operating with a focused probe and you don't have imaging-system diaphragms to worry about

- First, stop the beam scanning (i.e., select 'spot' mode on the STEM control system).
- Second, position the spot on the STEM screen on the region of interest.

A CBED pattern should then be visible on the TEM screen, but to see it you may have to remove the STEM detector if it sits above the TEM screen, or lower the TEM screen if the detector is below. The CBED pattern is present because the TEM is operated in the diffraction mode during STEM operation. As before, you may have to reduce  $L$  to ensure that several orders of diffraction maxima are visible on the screen. The other variables are the same, except that in STEM, the C2 lens in some TEMs is automatically switched off. This means that the C2 aperture alone governs  $\alpha$  and you can only focus the pattern with the objective lens.

### STEM AND CBED

In TEM you can't see the area of the specimen you have chosen without spreading the convergent beam; in STEM you can always scan the convergent beam to see the image.

In a DSTEM you can see both image and DP at the same time because the CBED pattern can be viewed by introducing a screen after the last post-specimen lens and viewing this screen with a TV camera. A hole in the screen allows any selected portion of the pattern to travel through the EELS to the BF detector and thus both image and DP can be viewed simultaneously. If you don't have post-specimen lenses then you can't vary  $L$ ; the CBED pattern is then viewed either directly using a TV camera to image the BFP of the objective lens or by scanning the pattern across the BF detector using post-specimen scan coils (see Section 21.8).

If you send the CBED pattern through the EELS before viewing it, then you can switch on the EELS and use it to filter out energy-loss electrons, or form the patterns with electrons of a specific energy. Energy-filtered CBED (which you can do in a TEM as well as a STEM) is a most powerful technique, as we'll see (look ahead to Figure 20.10).

The choice of operating mode then is really up to you; TEM and STEM both have their advantages.



## 20.3 EXPERIMENTAL VARIABLES

To form CBED patterns, you have to create a small ( $< 100$  nm) beam with a convergence semi-angle ( $\alpha$ )  $\geq 10$  mrad. There are at least five microscope variables you need to control when forming a CBED pattern

- The beam-convergence angle  $\alpha$  (remember, we mean semi-angle)
- The camera length  $L$  (i.e., the magnification of the pattern)
- The size of the beam (the probe diameter)
- The thickness of the specimen
- The focus of the pattern (under/over or exact)

The last variable is the most complex because there are CBED techniques which require focused patterns and those where we deliberately defocus the beam out of the specimen plane to gain other advantages. So we'll deal with this last variable separately. You can also change the kV if you want and as we noted above, low kV gives better contrast, but this is more than offset by the drop in gun brightness and the increased beam spreading. So, for materials specimens, most CBED is done at the highest kV, as with most other TEM techniques.

### 20.3.A Choosing the C2 Aperture

After you've read the next few sections you'll probably conclude that any full CBED study should include patterns taken with a range of camera lengths, a range of exposures, a range of C2 apertures and that the more C2 apertures you have in your TEM the better. You'll be right on all counts!

Once the CBED pattern is visible on the screen you can adjust  $\alpha$  by changing the C2 aperture, making sure to center the aperture you finally choose. The size of the diffraction disks depends on  $\alpha$  as shown in Figure 20.3 (go back and check equation 5.6). Let's start by choosing a small aperture so we get a pattern of discrete disks, similar to an SADP and we'll use the terminology first introduced by Steeds.

#### KOSSEL AND MÖLLENSTEDT

The pattern of non-overlapping disks is a Kossel-Möllenstedt (K-M) pattern. The pattern of completely overlapping disks is a Kossel pattern.

To get a K-M pattern you must select a C2 aperture such that the disk size (governed by  $\alpha$ ) is less than the spacing of the disks (governed by  $\theta_B$ ) for the particular specimen and orientation. Typically, the Bragg angle is a few milliradians, and C2 apertures in the 10–50  $\mu\text{m}$  range will usually ensure that you have satisfied the K-M conditions.

If  $\alpha$  is large enough for substantial overlap of the disks to occur such that individual diffraction maxima are no longer discernible, then the term 'Kossel pattern' is used (although this can cause confusion with the classic use of the term for geometrically similar X-ray patterns). Figure 20.3A–C shows a series of ray diagrams illustrating the transition from a K-M pattern to a Kossel pattern by increasing  $2\alpha$ . Equivalent experimental patterns from pure Al are shown in Figure 20.3D–F. The patterns in Figure 20.3 were all taken at a small camera length and, although the contrast is not particularly strong, you can clearly see rings of intensity which arise from electrons scattered to quite high angles ( $\pm 10^\circ$ ). We'll continue to read more about these HOLZ diffraction effects throughout this chapter.

Kossel patterns are most useful when viewed with a small camera length (see next section) because they display a relatively extensive area of reciprocal space, and the large value of  $\alpha$  gives rise to Kikuchi bands. For reasons we'll describe in Section 20.7, Kikuchi lines are much more prevalent in CBED than in SADPs and don't require the usual thick specimen. As we described in Chapter 18, the Kikuchi bands intersect in the center of the pattern when the beam is incident down a zone axis, as you can see in Figure 20.3F. Thus it is very easy for you to tilt to a particular zone axis, simply by following the bands until they intersect. So, to form a ZAP, it is best to start at very small  $L$  with a large  $\alpha$ . Later, you can worry about the best choice of C2 aperture, best choice of  $L$  and focusing the pattern. Because these Kossel patterns cover a large angular range in reciprocal space they are also an example of a whole class of large-angle CBED or LACBED patterns (see Section 20.4.B below) in which we defocus the beam to enhance the contrast compared with the Kossel patterns.

Because we need to be able to vary  $\alpha$ , a range of C2 apertures from about 10  $\mu\text{m}$  up to 200  $\mu\text{m}$  is desirable, consistent with the needs of other techniques. A reasonable choice if you have only three C2 apertures: one of about 200  $\mu\text{m}$  for routine TEM, EELS and Kossel patterns, a 50–70  $\mu\text{m}$  ultra-thick aperture for XEDS (which can also be used for STEM imaging and some K-M patterns) and a 10–20  $\mu\text{m}$  aperture for most K-M patterns. Some TEMs provide more than three apertures. More is better!

Because the C2 lens is excited in TEM mode, you can use it to change  $\alpha$ ; if you do, the objective lens has to be changed to maintain a focused pattern. You need to adjust C2 if you change the beam size with the C1 lens or if you want a value of  $\alpha$  between those given by the fixed C2 apertures.

#### STAY IN FOCUS!

Use the specimen-height ( $z$ ) control to maintain the specimen in the eucentric plane as you tilt. A computer-controlled stage is a great advantage.

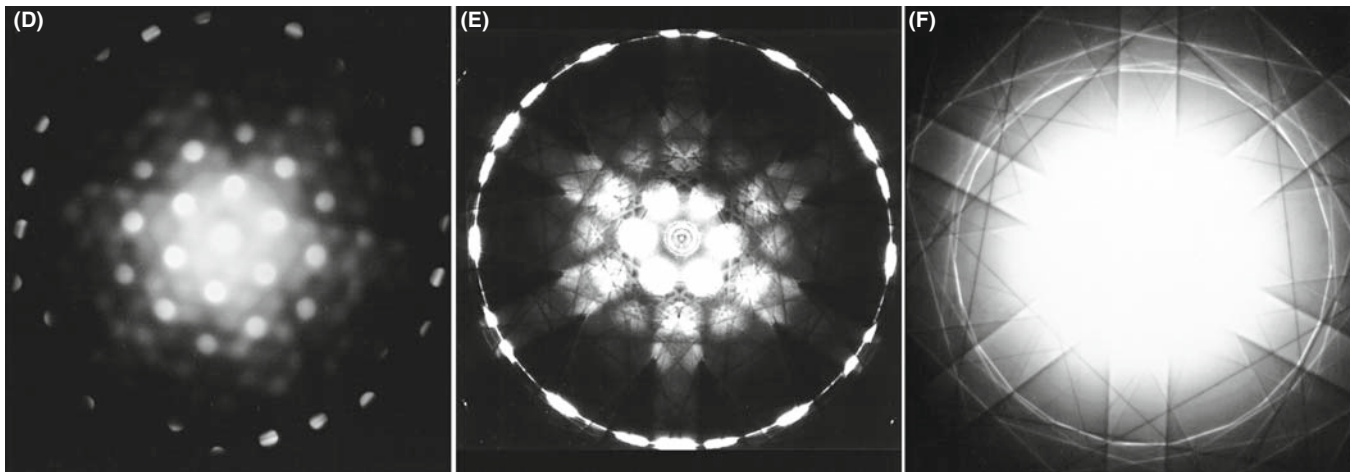
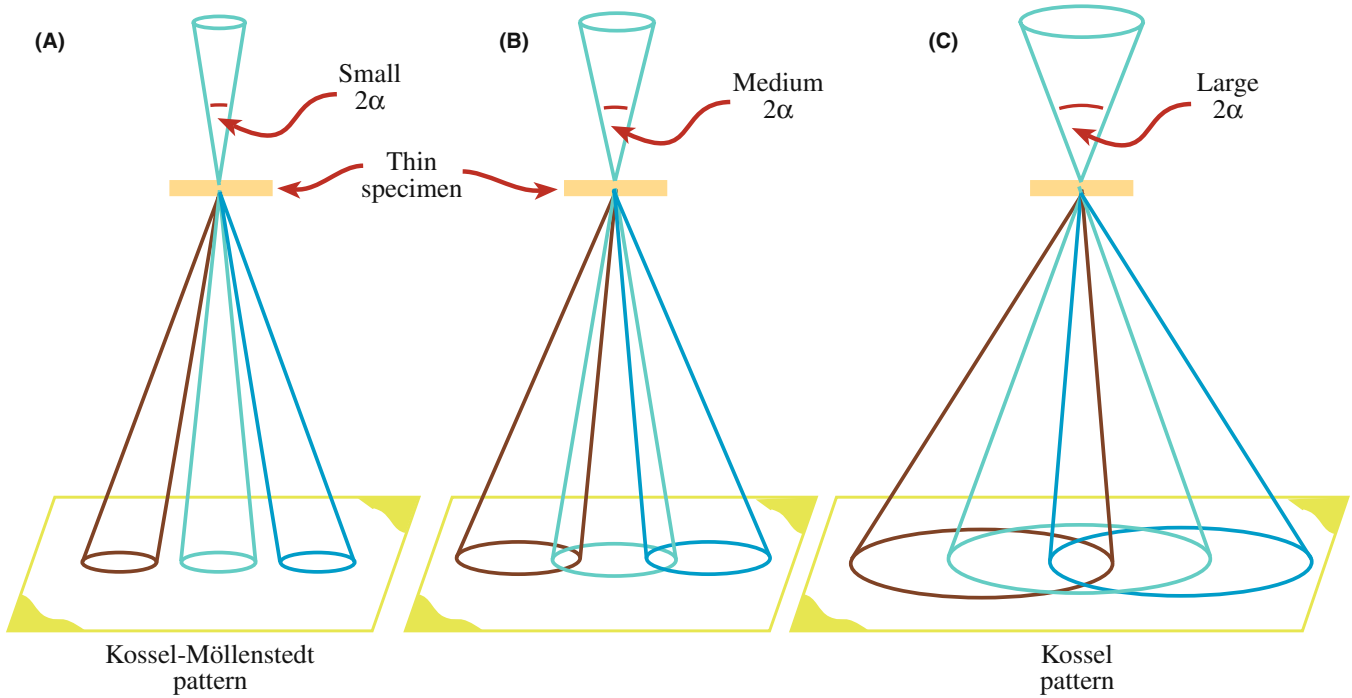


**FIGURE 20.3.** (A–C) Ray diagrams showing how increasing the C2 aperture size causes the CBED pattern to change from one in which individual disks are resolved (K-M pattern) to one in which all the disks overlap (Kossel pattern). (D–F) You can see what happens to experimental CBED patterns on the TEM screen as you select larger C2 apertures.

If you need to know the value of  $\alpha$ , you should use a known crystal to calibrate its variation with C2 aperture size for typical C2 lens excitations, as we described back in Section 9.1 and in equation 5.6.

### 20.3.B Selecting the Camera Length

The choice of  $L$  depends on the information that you want to obtain from the pattern and it's easy to be confused because  $L$  controls the magnification of the DP.

Typically we adjust the post-objective lenses in the imaging system to give  $L > 1500\text{--}6000\text{ mm}$  when we want to observe detail in the 000 (BF) disk at the highest

possible magnification. We reduce  $L$  to  $< 500\text{ mm}$  to view the low-magnification pattern, sometimes called (not surprisingly) the 'whole pattern' (WP) that contains electrons scattered out to high angles. Figure 20.4 shows three CBED patterns obtained over a range of  $L$  and you can see that if we start at a high  $L$  we can only see the 000 disk (Figure 20.4A), then we see the array of ZOLZ disks that is equivalent to an SADP (Figure 20.4B) but at the smallest  $L$  the HOLZ diffraction effects that we just mentioned become visible as a ring of intensity at high angles (Figure 20.4C). So it's often necessary to record your CBED patterns over a range of  $L$  (in addition to a range of  $\alpha$ ).

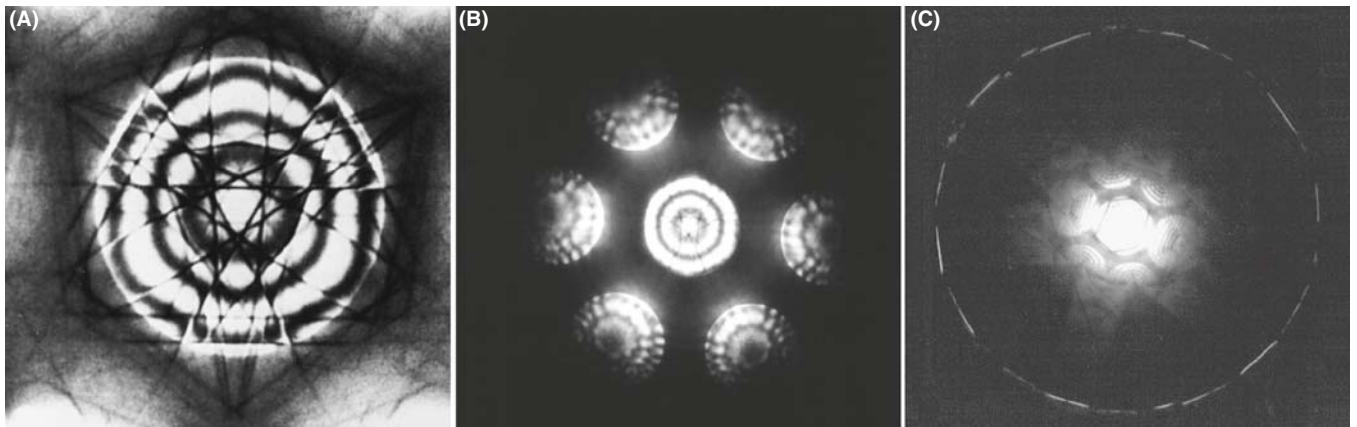


**FIGURE 20.4.** *Decreasing the camera length,  $L$ , increases our view of reciprocal space. (A) Starting at high  $L$ , we see a CBED pattern containing only the 000 diffraction disk. As  $L$  decreases, we see in (B) the distribution of electrons in the ZOLZ, similar to a typical SADP. At the shortest camera length, (C) a ring of HOLZ intensity is faintly visible surrounding the bright ZOLZ disks. Typically, we can record electrons scattered over an angular range of  $\pm 10^\circ$ .*

### LARGE $L$ , SMALL ANGLE

A large  $L$  gives a *high*-magnification view of the pattern but only spans a *small* angular range of reciprocal space.

In dedicated STEMs that don't have post-specimen lenses, the CBED pattern is projected onto the BF and/or ADF detector at a fixed magnification.

### 20.3.C Choice of Beam Size

We've already mentioned that you should start with a reasonably large beam with enough current to give a good intense pattern on the screen. Of course, a large beam size doesn't help if the crystal you're trying to analyze is small. The volume sampled by the beam defines the spatial resolution and so it is important to control the beam diameter. For the thinnest specimens, spatial resolution is close to the beam size but, in thicker specimens, elastic scattering will spread the beam and degrade the resolution in a manner similar to XEDS (see Chapter 36). Using the thinnest specimens and an FEG, CBED patterns can be obtained from extraordinarily small regions; we'll see in Section 21.8.B that sub-nanometer diffraction is possible. However, there is a drawback to using the thinnest specimens because they don't exhibit dynamical-diffraction effects which, as you'll soon see, are really useful.

### 20.3.D Effect of Specimen Thickness

If your specimen is very thin you may have kinematical-diffraction conditions. Then the diffraction disks have a uniform intensity and are devoid of contrast, as shown in the ZAP in Figure 20.5A. Moving to a thicker area of the specimen in the same orientation transforms the

pattern from an array of kinematically bland disks to a display of striking dynamical contrast (Figure 20.5B), which we'll discuss in great detail. So to get the most out of a CBED pattern, your specimen should be thicker than one extinction distance (see Chapter 16). As we've now mentioned many times, this requirement differs from that of almost all other TEM techniques, such as HRTEM, XEDS and EELS where the best information is obtained from the thinnest foils. So if your specimens are too thick for anything else, you can almost always get something useful out of them with CBED! As we'll discuss in Section 20.5, you can always energy-filter your CBED patterns from thick specimens and reduce the diffuse-scattering background to enhance the useful dynamical contrast.

## 20.4 FOCUSED AND DEFOCUSED CBED PATTERNS

There are times when you need to focus the CBED pattern and times when you have to defocus it. If you think about it, a focused CBED pattern will always come from the smallest possible region of your specimen and if you don't focus your patterns you will miss a lot of the fine detail! However, if the beam is defocused then what happens is that some image information appears in the CBED pattern (in an equivalent way to creating multiple DF images, which we used to calibrate the SADP rotation back in Section 9.6). Thus, in defocused CBED techniques we sample both direct and reciprocal space. In addition, slightly defocusing the objective lens increases the contrast in the patterns. Both of these advantages turn out to be particularly useful for direct analysis of crystal defects such as dislocations and grain boundaries using large-angle CBED (LACBED).



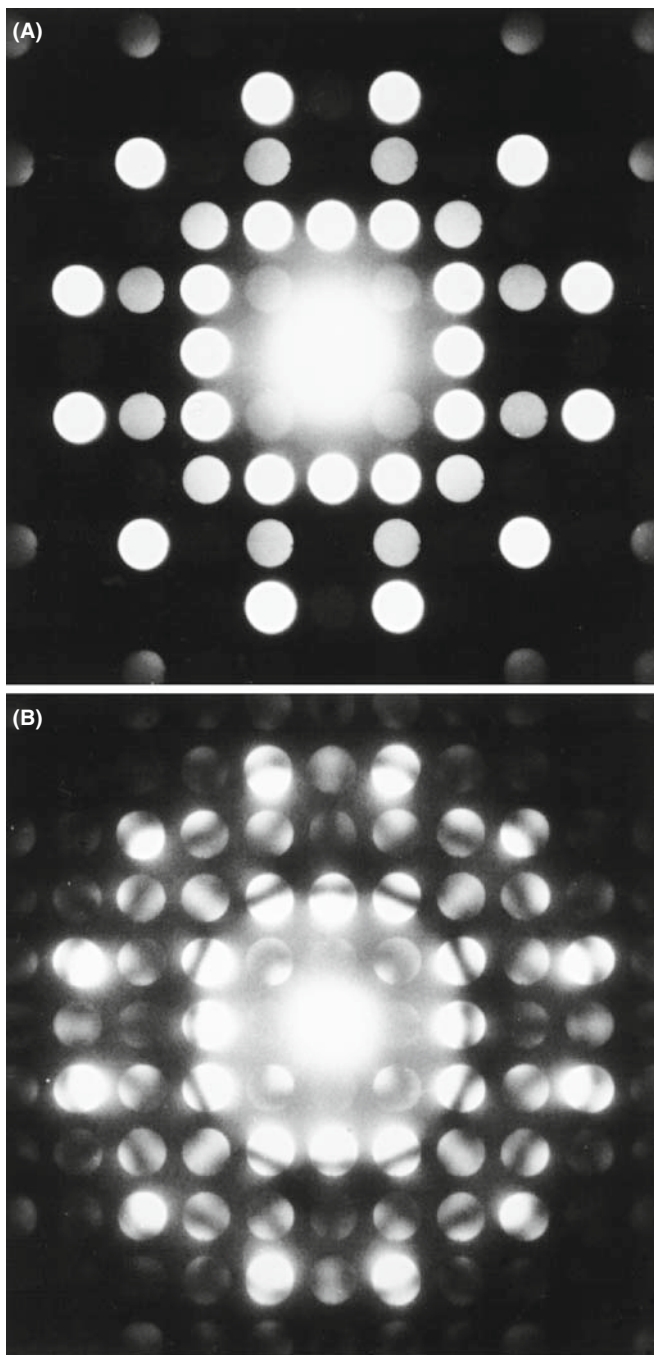


**FIGURE 20.5.** (A) CBED pattern under kinematical conditions. Such patterns give us no more information than SADPs, and their only advantage over SAD is that they come from a smaller region of the sample. (B) CBED pattern from a thicker area of the same specimen in (A) showing detailed dynamical-contrast phenomena.

### 20.4.A Focusing a CBED Pattern

Your TEM image is focused if your specimen is at the eucentric height and you can adjust the C2 lens to form the smallest spot on the TEM screen before switching to diffraction mode. To focus the CBED pattern

- Select K-M conditions (choice of C2 aperture) and choose a value of  $L$  so you can clearly see the 000 disk.
- Deliberately underfocus (weaken) the objective lens until a BF image is visible in the disk. This is because the beam is now spread at the plane of the specimen; see Figure 20.6A and the equivalent ray diagram back in Figure 6.5C.
- Strengthen the objective lens. As the beam crossover moves toward the specimen plane the image expands to higher magnifications until it goes through an inversion point at exact focus (see Figure 20.6B, which is equivalent to Figure 6.5B).
- Overfocus and again you can see a BF image in the 000 disk, inverted with respect to the underfocused image (Figure 20.6C). As you can see in Figure 20.6B there is non-spatial (i.e., diffraction-contrast) information in the 000 disk when you are at focus. (As we'll see in the next section, there are in fact several CBED techniques which deliberately use either an under- or overfocused beam).

If you leave the objective-lens current fixed and focus the beam on the specimen by adjusting C2 you'll see a similar effect to that shown in Figure 20.6, because the two lenses are coupled in a c/o system. If you use the second (non-eucentric) tilt axis or move to another region of the specimen, you will probably have to refocus the pattern with the  $z$  control, unless you have a stage that is fully computer controlled.

#### OBJECTIVE LENS CURRENT

Know the value of the objective-lens current that focuses the beam at the eucentric plane in your TEM. If your CBED pattern is focused at a different value, then adjust the lens current and refocus with the  $z$  control to maintain eucentricity.

The CBED pattern also has to be correctly focused in the BFP and you can do this in the conventional manner using the intermediate-lens fine focus to sharpen the image of the C2 aperture. As you'll see, you can also defocus the pattern by moving the specimen above or below the eucentric plane and this is just fine, unless you need to tilt the specimen to set up specific diffraction conditions, in which case the loss of eucentricity can make tilting tedious because the image will shift as you tilt.

### 20.4.B Large-Angle (Defocused) CBED Patterns

The reason we want to defocus the objective lens is that in some cases, as with TEM images, the contrast is minimized



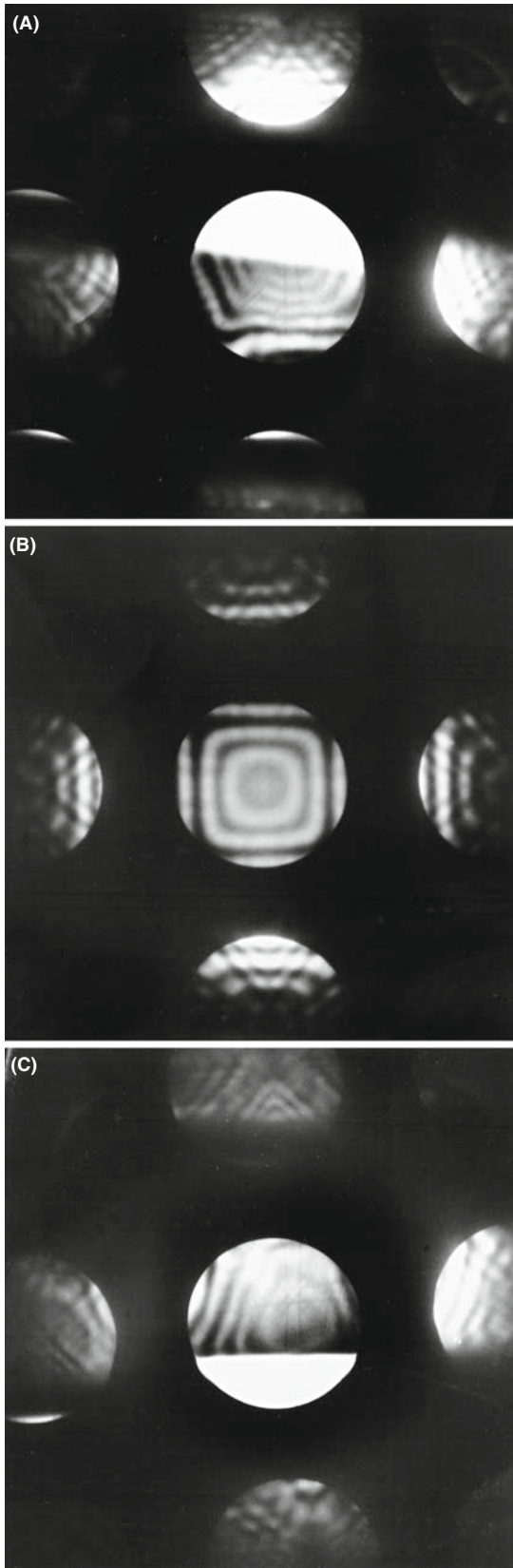


**FIGURE 20.6.** The procedure for correctly focusing the CBED pattern by adjusting the strength of the c/o lens through focus. In both underfocus (A) or overfocus (C) conditions, you see a BF image in 000 and DF images in the  $hkl$  disks, but at exact focus (B) the disks contain non-spatial, dynamical, diffraction contrast. Compare with Figure 6.5.

at exact focus. This is clear if you go back and look at the focused Kossel pattern in Figure 20.3F. At exact focus, the defect and excess Kikuchi lines overlap and reduce the overall contrast as shown in Figure 20.7A (although at the edge of the pattern, (i.e., where the electrons are traveling far off axis.) spherical aberration improves the contrast; a rare advantage for this otherwise-limiting lens defect). However, if you defocus the objective lens (either over or under) then the contrast in that same Kossel pattern is increased remarkably, as shown in Figure 20.7B. This

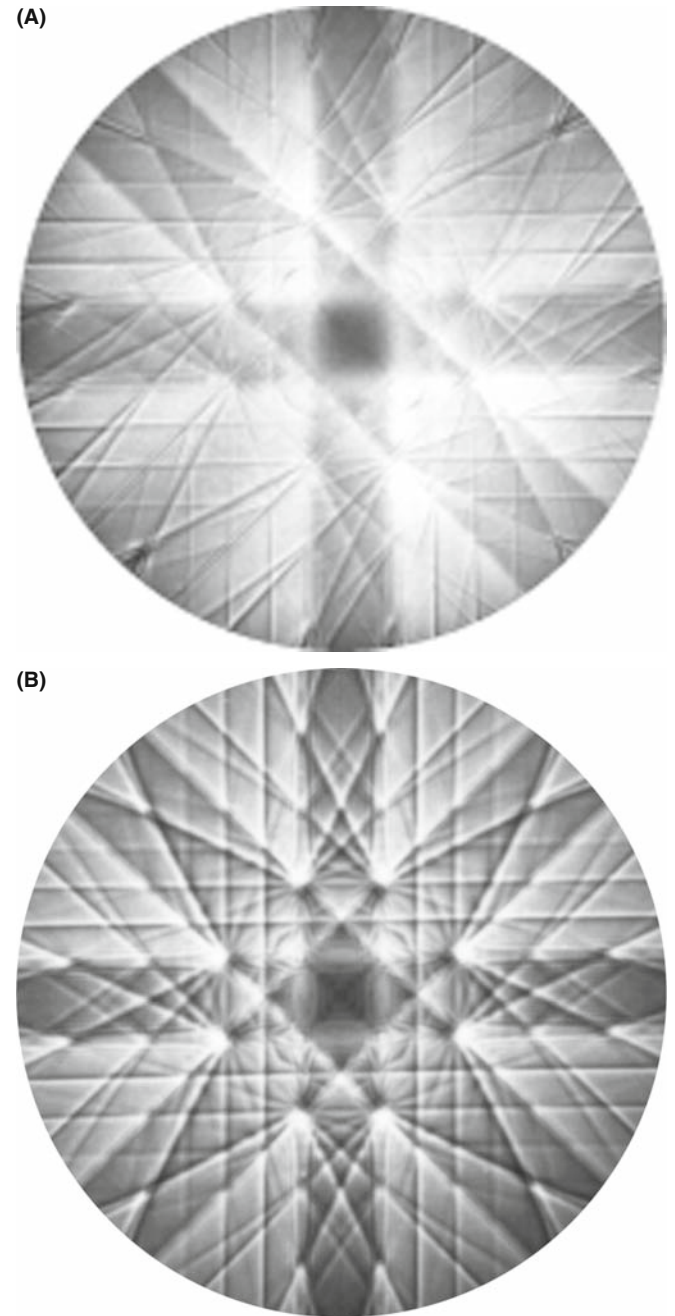


**FIGURE 20.7.** Kossel pattern from Si with the beam down a  $\langle 001 \rangle$  zone axis at (A) exact focus and (B) with the diffraction lens weakened to view a plane before the BFP of the objective lens (i.e., overfocus).

novel approach was pioneered by Tanaka and co-workers in Japan (see the references). There are several forms of defocused CBED patterns and we'll summarize three here and show you some applications of the techniques in the companion text.

The first and most common defocus technique is large-angle CBED or LACBED (Tanaka et al. 1980). These patterns are extraordinarily useful, as a perusal of Morniroli's book will confirm, and they are invaluable in analyzing line and planar crystal defects such as dislocations and interfaces (e.g., Spence and Zuo). There are a couple of ways that you can form LACBED patterns but they are based on Kossel patterns which, as we've noted, display the largest area of reciprocal space because they use the largest possible C2 aperture. Now if you want to defocus the pattern, as we just described in Figure 20.6, it's simple enough: you can either change the height of your specimen by adjusting the  $z$  control on the stage or you can defocus the C2 lens so that the beam does not form a crossover in the plane of the specimen as shown schematically in Figure 20.8A. This is a beautiful but initially daunting diagram, characteristic of many by Morniroli, but well worth taking the time to understand.

Start by looking at the cone of incident electrons in which two planes (ABE and CDE) are indicated where the electrons satisfy the Bragg condition for  $\pm hkl$  and these planes are bisected by the trace of the  $hkl$  plane itself. The beam is focused on the object plane of the objective lens and the specimen is raised a distance  $\Delta h$  out of that plane so it is illuminated by a disk of intensity. This has the effect of separating out the  $\pm \mathbf{g}_{hkl}$  diffracted electrons. The electrons incident along the lines  $A_E-B_E$  and  $C_E-D_E$  are Bragg diffracted and form  $\pm \mathbf{g}_{hkl}$  diffraction spots at K and L, respectively, in the object plane, and the direct-beam electrons form the 000 spot at E. All the electrons diverge through the spots and are re-focused by the objective lens to form spots in the image plane ( $K'$ ,  $L'$ , and  $E'$ ), respectively, and Figure 20.8B shows such a spot pattern. In the BFP there is a LACBED pattern consisting of a disk of intensity crossed by deficient lines (like Kikuchi lines but arising from elastic scattering) which are called Bragg lines (see Section 20.7 below). These deficient lines ( $A_F-B_F$  and  $C_F-D_F$ ) correspond to the lines in the specimen along which strong diffraction occurred from the  $\pm hkl$  diffracting planes as shown in Figure 20.8C and arise from the superpositioning of the  $h\bar{k}l$  excess lines on the  $hkl$  deficiency line ( $A_F-B_F$ ) and vice versa ( $C_F-D_F$ ). As you can see, there are lines from many diffracting planes in this figure while, for simplicity, Figure 20.8A only includes the ray paths for two strongly diffracting planes exactly at  $\mathbf{s} = 0$ .

Figure 20.8A shows that the key to getting the best LACBED patterns is careful use of the SAD

aperture. If you insert an SAD diaphragm into the image plane and permit only the direct beam to go through the aperture, the (BF) LACBED pattern you see on the screen is remarkably enhanced, as shown in Figure 20.8D (compare this with Figure 20.8C which is a LACBED pattern without the SAD aperture inserted). A DF LACBED pattern can be acquired simply by selecting one of the  $\mathbf{g}_{hkl}$  reflections in the image plane with the SAD aperture and such a pattern consists of just a single  $\pm hkl$  excess line of intensity. It is possible to improve the contrast in the LACBED pattern by choosing a smaller SAD aperture to cut out some of the inelastic, higher-angle scattering. If you look carefully at Figure 20.8D, you see that, as in all LACBED patterns, there is some real-space information about the specimen but the reciprocal-space information clearly dominates. Figure 20.9 shows a montage of BF and multiple DF LACBED patterns from Si in the [111] orientation. The beauty of such a pattern is only enhanced by the fact that the symmetry information can be used to determine the point group of the crystal directly; more about that in the companion text.

The second technique is called convergent-beam imaging or CBIM, which is a little younger than LACBED (Humphreys et al.). CBIM saw relatively little use because all it really did was give you an image of the area of your specimen from which you were obtaining the CBED pattern. If you include an objective aperture, a very small spot size and an energy filter the quality of the CBIM patterns is close to that of LACBED patterns although invariably CBIM emphasizes real-space over reciprocal-space information.

The last defocus technique in this acronym soup is parallel recording of dark-field images (PARODI) as a function of specimen thickness. The intensity variation in the multiple DF images visible in a systematic row of diffraction disks of a defocused CBED pattern (Wu et al.) can be recorded in a single exposure and, if you understand a lot of physics, you can use this approach to determine various properties of your crystalline specimens such as structure factors and valence-electron distributions.

There are several other mechanisms for obtaining LACBED patterns summarized by Morniroli, such as eucentric LACBED, specimen rocking, BF and DF LACBED and montages of CBED patterns, the last of which is illustrated in Figure 20.9.

### 20.4.C Final Adjustment

Sometimes, in either defocused or focused CBED patterns, it is quite difficult to make the ZAP exactly symmetrical as in Figure 20.2B. It often seems as if your last

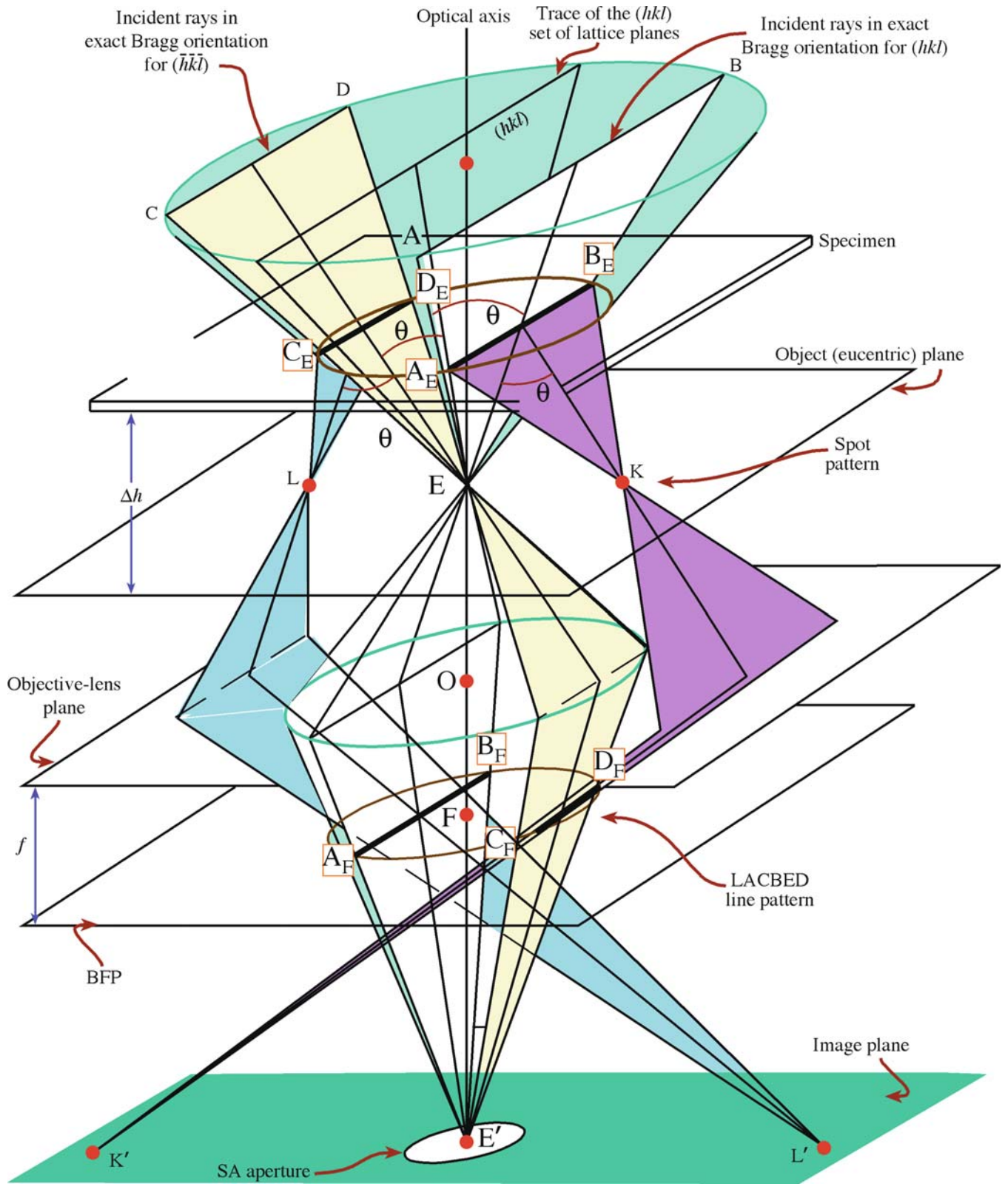
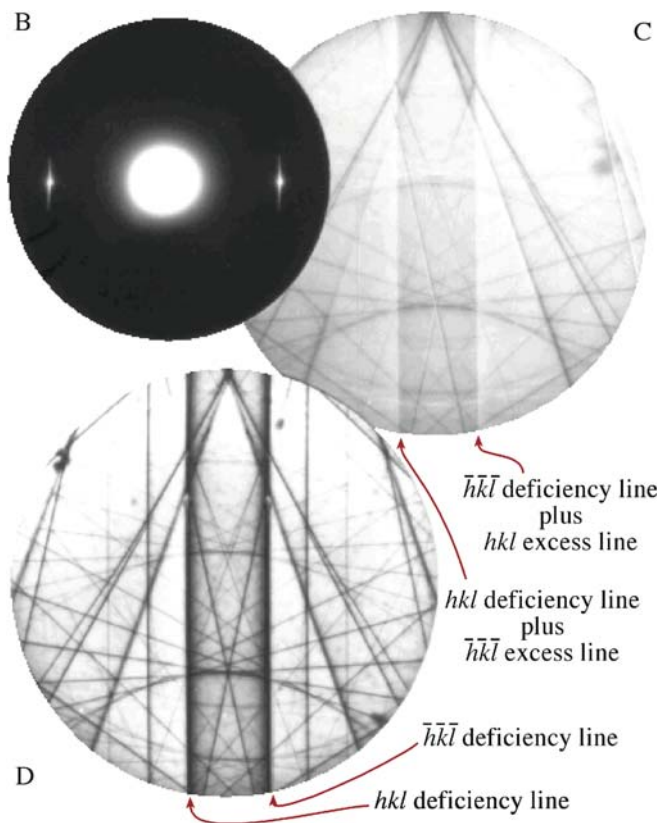


**FIGURE 20.8** (A) Ray diagram for LACBED formation under  $\pm h$  (three-beam) conditions. With the specimen raised by  $\Delta h$  from the eucentric plane in the objective lens, specific electrons in the incident cone are at the exact Bragg condition for diffraction from both sides of the  $hkl$  plane indicated, creating a spot pattern in the eucentric plane (B) and a LACBED pattern of lines in the BFP (C). The SAD diaphragm can be inserted to enhance contrast in the LACBED pattern by selecting only one beam to create (D) a BF LACBED pattern.





- Increase  $L$  to examine the 000 disk and focus the pattern.
- Defocus the pattern with the objective lens or raise/lower the specimen from the eucentric plane if you want to do LACBED, PARODI, CBIM or some form of defocused CBED.

## 20.5 ENERGY FILTERING

Every kind of DP contains electrons that have lost energy in going through the specimen. As we've seen already, these inelastically scattered electrons can be very useful if they cause Kikuchi lines, but if your specimen is thick enough, then the diffuse, inelastic scattering can raise the background intensity to levels that mask the useful contrast in the pattern. This is particularly the case in CBED patterns because, as we noted back in Section 20.2 and Figure 20.5, CBED is one of the few TEM techniques wherein more useful information is present in patterns from thicker specimens because they give rise to much more interesting dynamical contrast within the CBED disks.

So there's a balance here: we want thicker specimens to enhance dynamical effects but if the specimen is too thick the diffuse, inelastic scattering hides the useful contrast. If this is the case we can, in fact, have our cake and eat it at the same time. All we have to do is remove the diffuse-scattered electrons from the pattern using an energy filter.

### TO FILTER OR NOT?

If you can energy-filter your CBED patterns, you should always do so.

Now we'll talk a lot more about energy filtering when we discuss EELS in the last four chapters of Part 4 and the seminal text on filtering is edited by Reimer. Filtering can be achieved either with an in-column or post-column filter. If we remove inelastically scattered electrons, the CBED pattern contains electrons that have lost no energy. Thus, in effect we have removed any specimen-induced chromatic-aberration effects from the pattern, and all the contrast phenomena in the pattern appear much sharper because all the electrons are focused in the (same) BFP (or image plane if it is a LACBED pattern). All this text pales in comparison with the example shown in Figure 20.10. This improvement is so dramatic that it really never makes sense to do anything other than filter your CBED patterns if you have the necessary instrumentation.

FIGURE 20.8. (Continued).

minor tilt or traverse of the specimen is not precise enough, or mechanical backlash occurs. If this is the case, use the beam tilts or deflectors to make your final adjustments to obtain a symmetrical pattern. In Section 18.2, we used the same method to excite high-order reflections in SAD. You can also move the C2 aperture and center it on the zone axis, but this misaligns the illumination system so it should be the last resort.

As with SAD, a range of exposure times for all CBED patterns will give you the most information.

We can now summarize the experimental steps to obtain a CBED pattern

- Focus the beam to a crossover on your specimen at the eucentric plane and go to diffraction mode in TEM (or stop the beam from scanning in STEM).
- Decrease  $L$  to see the full pattern including HOLZ scattering and tilt to the desired orientation.
- Adjust the convergence angle with the C2 aperture.
- Increase the beam size if necessary with the C1 lens to make the pattern brighter.
- Decrease the beam size and/or go to a thinner portion of the specimen to select a smaller region (which generally increases the quality of the pattern).



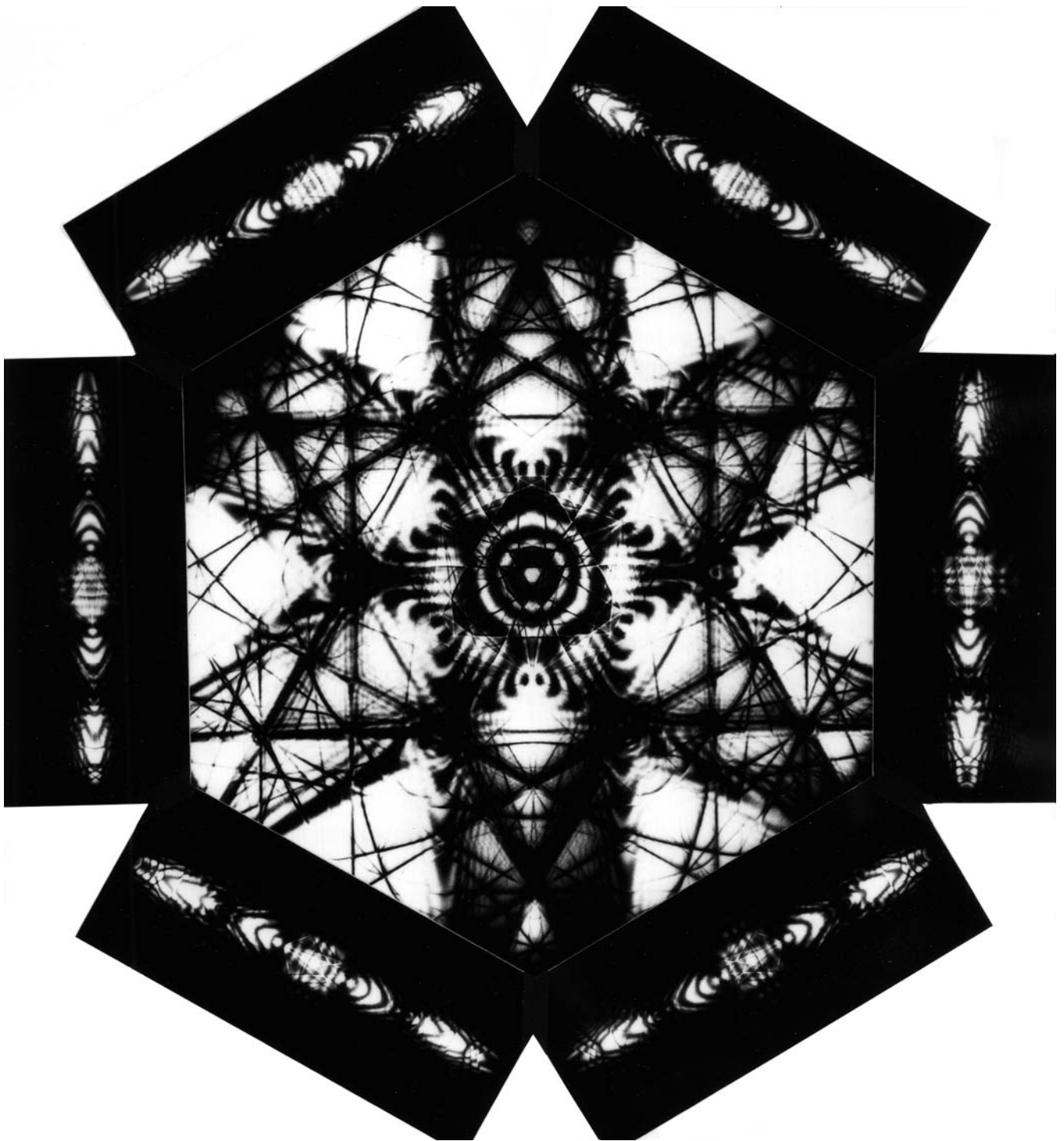


FIGURE 20.9. Montage of Si [111] BF LACBED pattern (center) surrounded by six  $\{2\bar{2}0\}$  DF LACBED patterns.

## 20.6 ZERO-ORDER AND HIGH-ORDER LAUE-ZONE DIFFRACTION

### 20.6.A ZOLZ Patterns

If you increase  $L$  above  $\sim 800$  mm you will magnify the pattern on the screen and only see the first few diffraction maxima, as shown in Figure 20.4A. Assuming the

C2 aperture is small enough, the CBED pattern consists of disks, similar to the array of spots in an SADP, i.e., discrete diffraction maxima surrounding the central 000 disk. Remember that such a pattern is termed a ZOLZ pattern (see Section 18.4) since the permitted  $hkl$  diffraction maxima must all satisfy the Weiss zone law  $hU + kV + lW = 0$ , where  $UVW$  is the beam direction. Remember also that all the  $hkl$  maxima in the DP

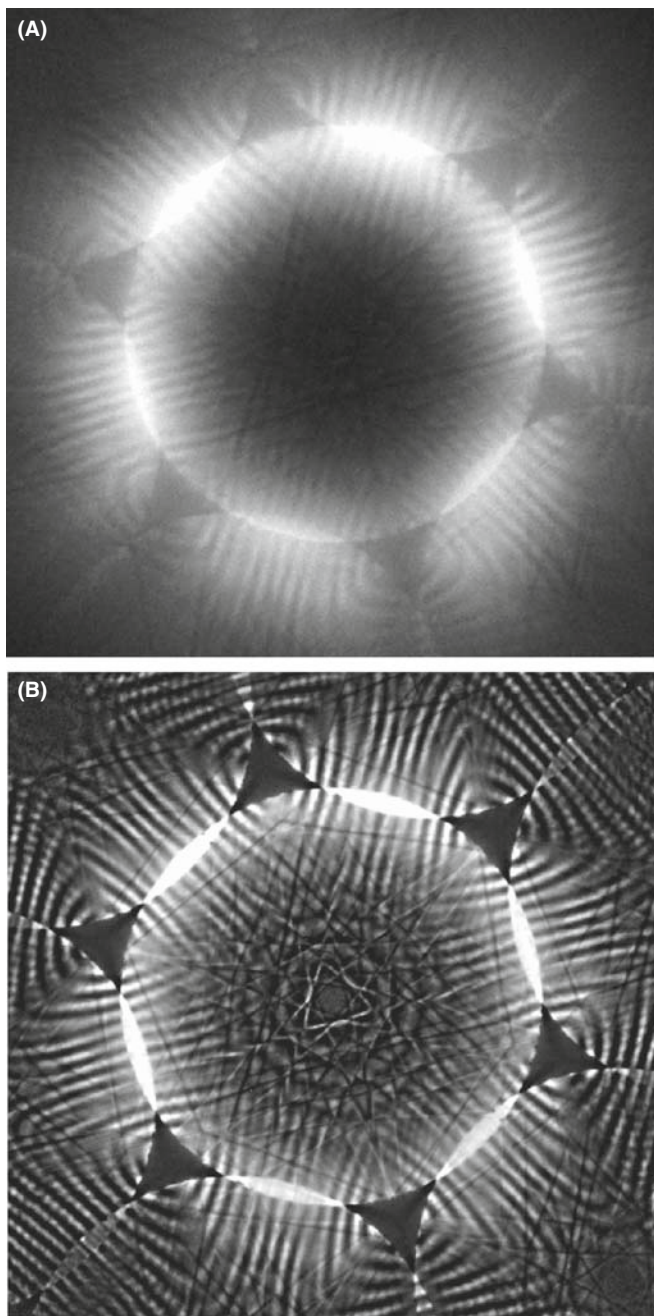


**FIGURE 20.10.** CBED pattern from a thick specimen of Si (A) without energy filtering and (B) with energy filtering. This figure is included only because it looks so striking, and similar patterns have been the basis of many TEM lab Christmas cards.

correspond to points in the reciprocal-lattice plane containing the origin, 000, of the reciprocal lattice, and this plane is also called the ZOLZ. So in fact SADPs are usually ZOLZ patterns, although we don't always describe them as such. From ZOLZ patterns, we can obtain the usual interplanar spacings and angles, the  $hkl$  maxima can be indexed and  $UVW$  identified, in exactly the same manner as we described in Section 18.4 for an

SADP. The two options are the method of ratios or using a calibration standard to determine the camera length.

Because of the finite size of the diffraction disks, you must take care to select equivalent points in each disk when measuring the  $hkl$  spot spacings. If  $\alpha$  is too large (Kossel conditions) you might not see individual maxima and you should then select a smaller C2 aperture (K-M conditions).

## 20.6.B HOLZ Patterns

The central portion of the CBED pattern is bright due to the relatively intense low-angle scattering (go back and check Figure 3.5). At higher angles, the ZOLZ intensity drops because the atomic-scattering amplitude,  $f(\theta)$ , decreases and the Ewald sphere no longer intercepts the relrods from the ZOLZ. However, the intensity increases again when the Ewald sphere intercepts the relrods from the HOLZ reciprocal-lattice points and a circle or ring of diffracted intensity is observed around the ZOLZ pattern as in Figures 20.3D–F and 20.4C. (You should recall that a circle can be defined geometrically as the interception of a sphere and a plane).

If you've chosen a small enough aperture for K-M conditions you'll see a ring of discrete HOLZ spots as in Figure 20.3D while a large C2 aperture gives a HOLZ ring of intersecting lines as in Figure 20.3F. The HOLZ intensity arises from relatively weak high-angle diffraction from crystal planes that are *not* parallel to the beam. Low temperatures increase the HOLZ scattering and also minimize the thermal-diffuse (phonon) scattering that, in some materials with a large Debye-Waller factor, masks the weak HOLZ intensity. So this is why you'll find a liquid-N<sub>2</sub> cooling holder very useful at times. You can't reduce the diffuse scattering via an energy filter because phonon scattering has a very small energy loss ( $\ll 1$  eV) and most of these electrons still contribute to the filtered pattern.

### SMALL $L$ , LARGE ANGLE

Remember that the radial distance from 000 in a DP is related to the angle of scattering; use a smaller  $L$  to see higher-angle scattering.

Consider the intersection of the Ewald sphere with the reciprocal lattice. The plane of HOLZ reciprocal-lattice points/relrods intercepts the sphere (unlike the zero layer which is tangential to the Ewald sphere). The first ring is called the FOLZ because the possible  $hkl$  reflections satisfy the relationship  $hU + kV + lW = 1$ , and so on. Where the Ewald sphere intersects the HOLZ relrods, diffracted intensity is expected, taking into account the usual structure-factor effects (see the next section).

Because the beam converges on the specimen over an angular range  $2\alpha$ , the Ewald sphere is effectively rotated  $2\alpha$  about the origin, and thus a range of angles along each HOLZ relrod is sampled, as shown in Figure 20.11A. This range of angles manifests itself as the CBED disk reflecting the effective angular broadening of the relrod, as shown in Figure 20.11B. Different interception points on the relrod correspond to different points in the disk as shown in Figure 20.11C. Figure 20.11D shows a K-M CBED pattern containing the expected distribution of diffraction maxima from the Ewald-sphere construction in Figure 20.11A.

### 3D

The most important point to remember is that there is 3D crystallographic information in the CBED pattern whenever significant HOLZ diffraction intensity is present.

We'll make use of this 3D information in the next chapter and in the companion text.

To observe HOLZ rings in addition to the ZOLZ pattern, choose a very small  $L$  ( $< 500$  nm) so that you can see the full angular range of the BFP permitted by the imaging system ( $\sim \pm 10^\circ$ ). As shown schematically in

Figure 20.11A, the Ewald sphere only intercepts relrods in HOLZs many orders of diffraction maxima away from the direct beam. Because of the large scattering angle, the intensity in the HOLZ spots is relatively low and the exposure time to reveal HOLZ maxima is usually long enough to ensure that the ZOLZ is overexposed on the negative (go back and see Figure 20.3). You might be lucky with your thin area; sometimes you can produce reasonable ZOLZ and HOLZ intensity on the same exposure as in Figure 20.11D. But generally, if you're still stuck with recording your patterns on film you will probably have to record at least two DPs: a relatively short exposure for the ZOLZ pattern containing only 2D crystallographic information and a longer exposure for the weak HOLZ reflections containing the 3D information. As we've already said, a range of exposures is useful for *all* DPs.

There are some alternatives

- A CCD camera will give a greater dynamical range making it easier to record a good pattern showing detail at both low and high scattering angles.
- You can use image-processing techniques on your computer to combine differently exposed patterns (see Chapter 31).

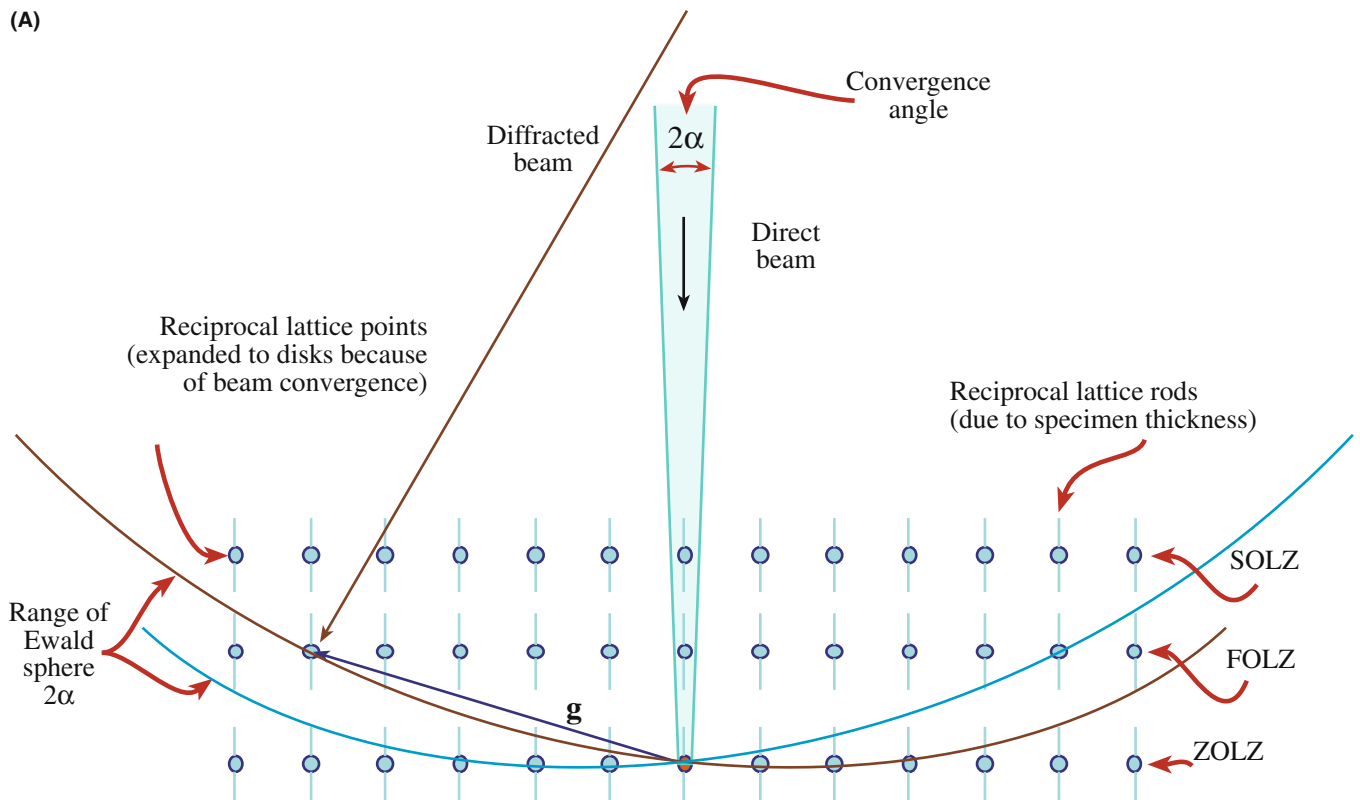


**FIGURE 20.11** (A) The Ewald sphere can intercept reciprocal-lattice points from planes not parallel to the electron beam whose  $\mathbf{g}$  vectors are not normal to the beam. The sphere has an effective thickness of  $2\alpha$  because of beam convergence and so intercepts a range of these HOLZ reciprocal-lattice points.



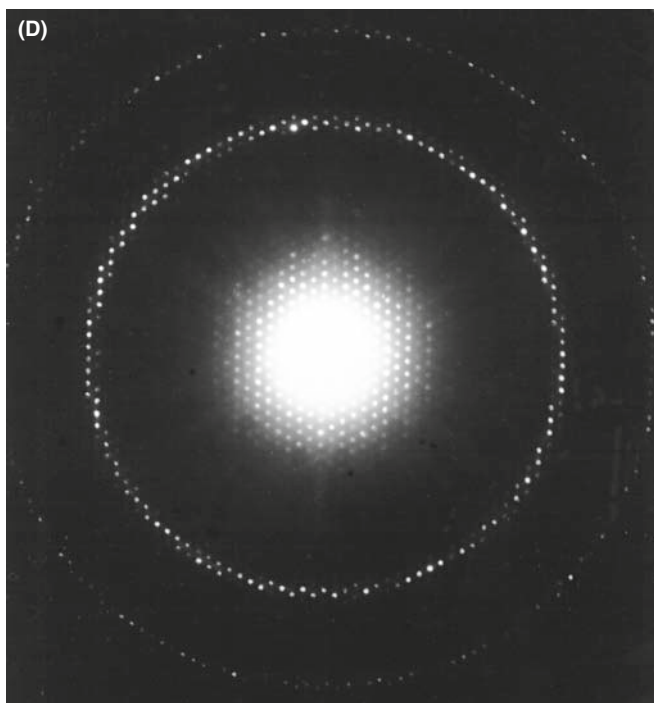
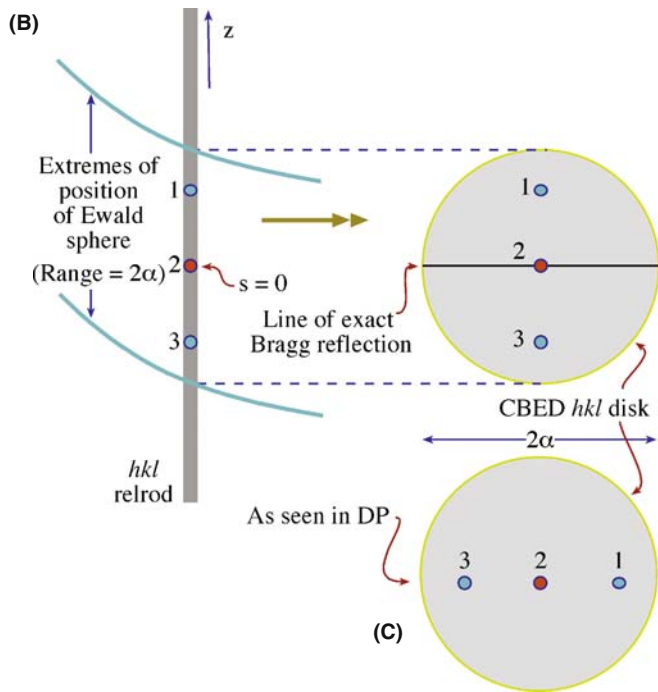


**FIGURE 20.11.** (Continued) The relrod has a shape shown in (B) and the intensity at specific points  $x_i$  in the relrod is directly related to equivalent points in the  $hkl$  disk (C). The interception of the Ewald sphere with the HOLZ layers gives rings: the first ring is called the FOLZ, the second the SOLZ and so on shown in the experimental pattern in (D).

The HOLZ ring radius is defined by the interception of the Ewald sphere with the allowed HOLZ relrods in the reciprocal lattice and so depends on the interplanar spacing in the crystal, the electron wavelength (i.e., the  $kV$ ),  $L$  and any off-axis lens distortion. Depending on

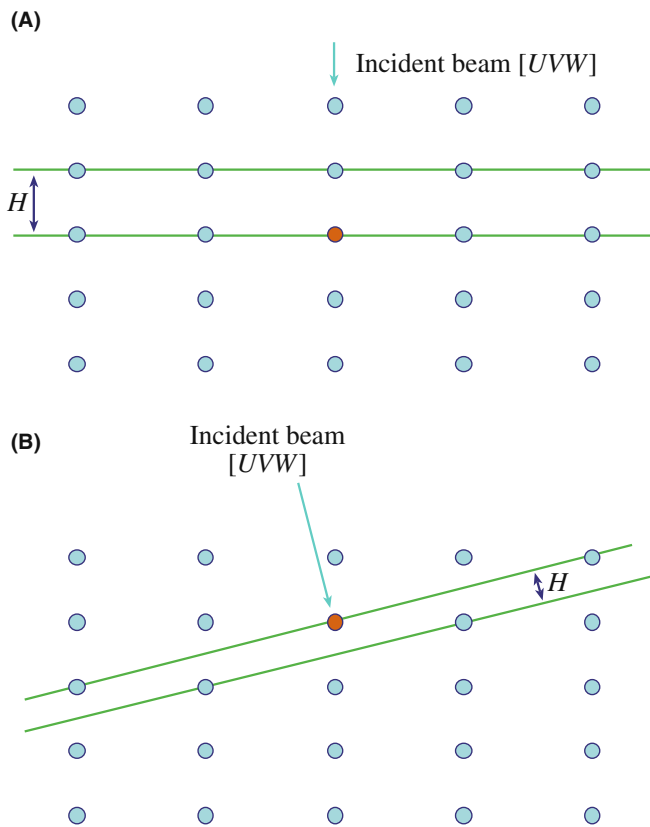


**FIGURE 20.12.** (A) The reciprocal-lattice spacing ( $H$ ) is large if the beam is down a major zone axis in the crystal. (B) The spacing is small if the beam is down a low-symmetry direction.

the crystallography of the specimen, the HOLZ rings may have very large diameters making them difficult to observe experimentally even at very small  $L$ . Under these circumstances, you should tilt to a *low-symmetry* zone axis (e.g.,  $\langle 114 \rangle$ ) since this gives you a better chance of observing the FOLZ than a high-symmetry zone axis such as  $\langle 001 \rangle$ . (If the reason for this is not clear, then look at Figure 20.12.) Cooling your specimen will reduce thermal-diffuse scattering that can mask HOLZ effects. If you still can't see a HOLZ ring, then the last thing you can try is increasing  $\lambda$  by lowering the  $kV$ . If all this fails, you need to pick another specimen!

In the next chapter, we will show you how to index HOLZ patterns and how HOLZ ring measurements can be used to deduce the lattice-repeat vector of the crystal parallel to the beam direction. You'll see that you can then determine the unit cell, the crystal system and also the type of lattice centering.

## 20.7 KIKUCHI AND BRAGG LINES IN CBED PATTERNS

In CBED patterns you almost invariably see sharp Kikuchi lines, while in SADPs Kikuchi lines are often rather diffuse or absent (see Chapter 19). This difference arises



in part because the convergent beam samples a much smaller region of the specimen than that selected by the SAD aperture. So, in the volume of specimen contributing to the CBED pattern, there is usually little or no strain, either elastic (due to specimen bending) or plastic (due to lattice defects). As a result, CBED Kikuchi lines will in general be sharper than SAD lines. This effect is shown in Figure 20.13A which is a conventional SADP containing very diffuse Kikuchi lines. This pattern was obtained from a large region of heavily deformed copper. By comparison, Figure 20.13B shows a CBED pattern from a much smaller region of the same specimen showing several pairs of well-defined Kikuchi lines. So you can use Kikuchi lines in CBED patterns to attack problems which are beyond the capability of SAD, for example, to determine accurate misorientation relationships between small grains in deformed materials (see Heilman et al.). However, if you put the probe right on a defect which has significant strain associated with it then even the CBED pattern may be blurred. On the positive side, this effect is used in LACBED patterns to characterize the crystallography of defects (e.g., the Burgers vectors) and this is explained in detail in the companion text. So, unless you want to study defects, always check the TEM image and tilt around to make sure that the area is clear of defects before getting your CBED patterns.

If the CBED pattern is not a ZAP, as in Figure 20.13B, the Kikuchi lines appear as pairs of excess (bright) and deficient (dark) lines, as in SADPs. But when you obtain a ZAP, the ZOLZ Kikuchi lines appear as bright bands. These bands increase in intensity and definition as you increase the convergence angle, as shown back in Figure 20.3D–F. A similar effect is seen in channeling patterns in the SEM that are generated by rocking a parallel beam around the optic axis. If you need to understand the difference between Kikuchi lines in SADPs and Kikuchi bands in CBED patterns, Reimer gives a clear discourse in his 1997 text.

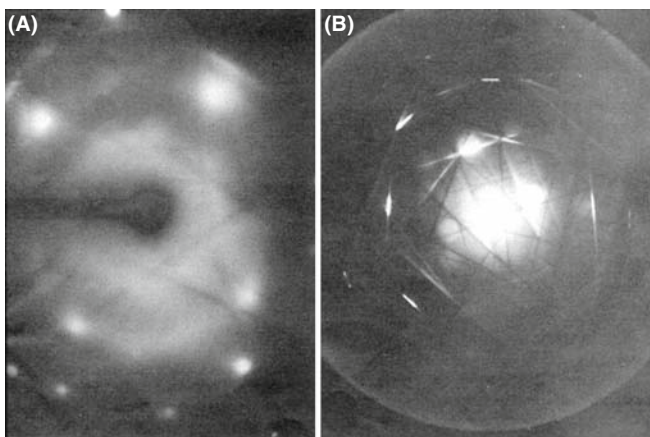


**FIGURE 20.13.** (A) Comparison of the poor quality of Kikuchi lines in an SADP and (B) the relatively clear distribution in a CBED pattern from deformed copper.

The generation of Kikuchi lines in a CBED pattern is marginally more complex than in an SADP. Remember how Kikuchi lines arise in a specimen illuminated by a parallel beam (see Chapter 19) and how a divergent beam of scattered electrons samples the various crystal planes (see Figure 20.14A). In Figure 20.14B you can see what happens when a convergent beam is used. In this case the incident rather than the scattered electrons span an angular range and therefore, just as in Kikuchi-line generation, some electrons in the beam will probably be at the exact Bragg angle to a ZOLZ plane (this is identical to the argument we used to explain the Kikuchi lines in LACBED patterns back in Figure 20.8A). Thus, there will be an elastic-scattering contribution to the Kikuchi lines where they cross the ZOLZ disks in CBED patterns. If you choose Kossel conditions (i.e.,  $2\alpha > 2\theta_B$ ) as in Figure 20.3F, there will *always* be electrons in the beam with the correct trajectory for exact Bragg diffraction from the planes in the *UVW* zone and so there will *invariably* be an elastic contribution to the Kikuchi lines.

Strictly speaking, we should only use the term ‘Kikuchi lines’ when inelastic scattering alone is responsible for their formation (i.e., the lines *between* any *hkl* disks). However, the term is used rather loosely in the literature to describe the ZOLZ intensity bands, despite the elastic contribution to the scattered intensity. Morniroli has proposed that this uncertainty be resolved by using the term ‘Bragg lines’ for the deficiency lines in CBED and LACBED patterns; this terminology is gaining wider acceptance.

## 20.8 HOLZ LINES

### 20.8.A The Relationship Between HOLZ Lines and Kikuchi Lines

As we just noted, Kikuchi lines can also arise from inelastic scattering by the HOLZ planes and HOLZ Kikuchi lines exist in many CBED patterns. You can see the array of deficient HOLZ Kikuchi lines between the ZOLZ maxima in Figure 20.2B. These HOLZ Kikuchi lines are, in principle, more useful than ZOLZ Kikuchi lines because they come from planes with much larger Bragg angles (and *g* vectors) so they are even more sensitive to changes in lattice parameter than the ZOLZ lines. Since

$$|\mathbf{g}| = \frac{1}{d}, |\Delta\mathbf{g}| = -\frac{\Delta d}{d^2} \quad (20.1)$$

then for smaller *d* values, the value of  $|\Delta\mathbf{g}|$  is much larger at the same  $\Delta d$ . We take advantage of this fact, not by using HOLZ Kikuchi lines specifically, but by seeking out a closely related phenomenon called HOLZ lines. HOLZ lines are simply the elastic part of the HOLZ Kikuchi lines, that is, they are the segments of the lines

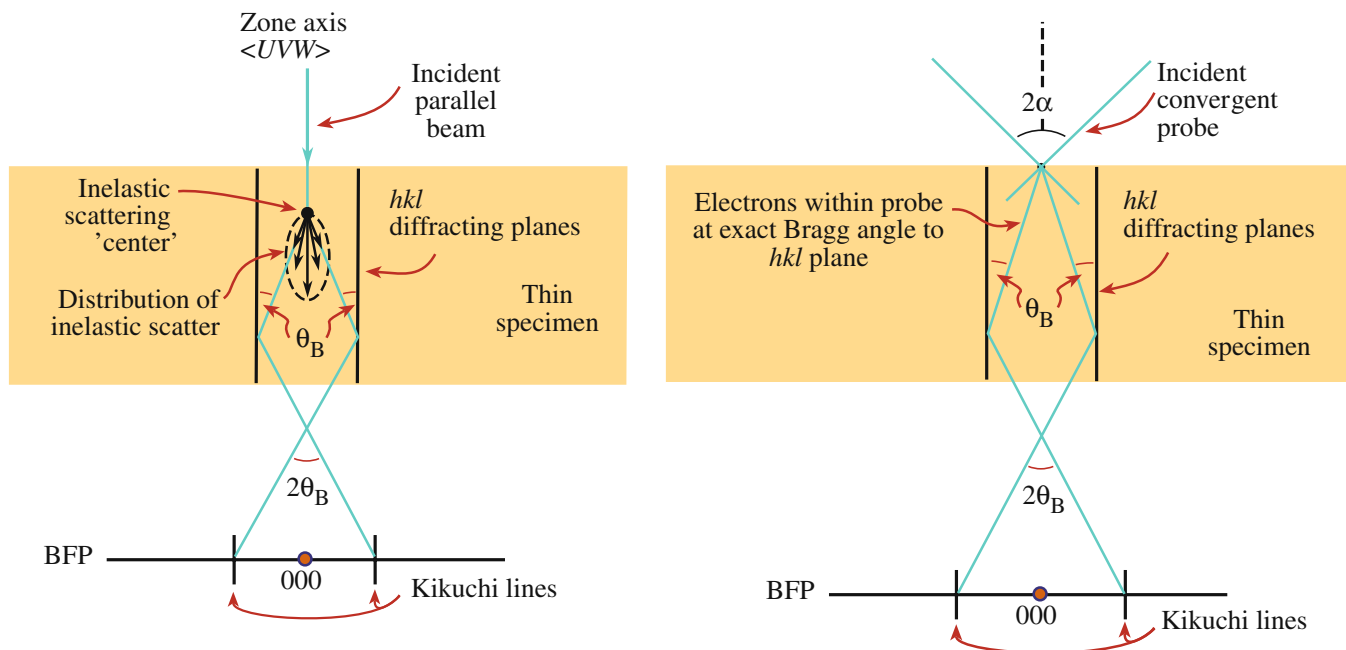


**FIGURE 20.14.** Comparison of the generation of Kikuchi lines (A) by inelastic scattering of electrons in a parallel beam and (B) by elastic scattering of electrons in a convergent beam when the convergence angle,  $\alpha$  is greater than the Bragg angle,  $\theta_B$ .

which appear *within* the diffraction maxima. By analogy with the production of Kikuchi lines and, as already shown in Figure 20.8A for LACBED patterns (although both these situations referred to ZOLZ diffraction), the HOLZ lines arise when electrons within the cone of the incident probe are at the correct Bragg angle for diffraction by a *HOLZ* plane. Therefore, these electrons are diffracted out to very high angles compared with ZOLZ diffraction. The result of this scattering is a bright line through the HOLZ disk and a dark line across the 000 disk. Not surprisingly, given what you've learned in the preceding nine chapters, the theory for the origin of HOLZ lines is much more complicated than this sparse summary. When you have time and the necessary inclination (tilt?) you should read the paper by Jones et al.

### PAIRS OF HOLZ LINES

HOLZ lines come in pairs, like Kikuchi lines, with the bright (excess) lines within the HOLZ *hkl* maxima and the dark (deficient) lines within the 000 disk.

An example of HOLZ lines is shown schematically in Figure 20.15, which compares with the experimental pattern in Figure 20.32B. Because these HOLZ lines contain 3D information they show the true, fcc, 3D, threefold  $\{111\}$  symmetry, while the ZOLZ Kikuchi lines and spots show sixfold, 2D,  $\{111\}$  symmetry. We will make use of

these differences when we discuss indexing such patterns and crystal-symmetry determination in Chapter 21 and in the companion text.

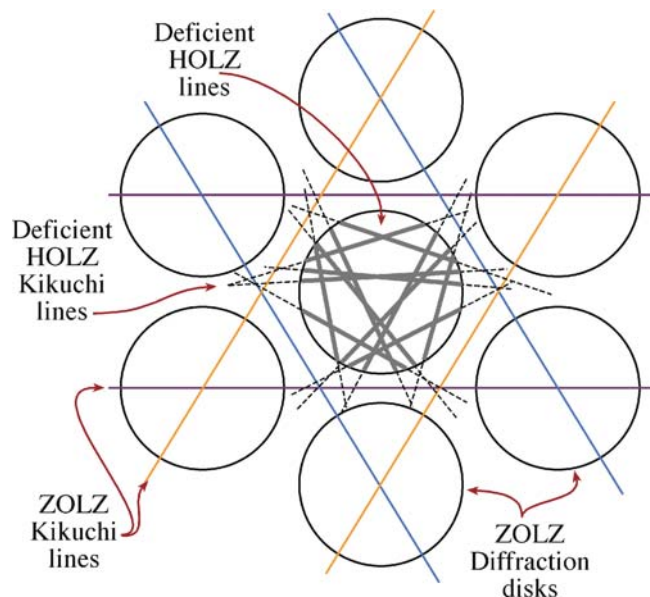


**FIGURE 20.15.** The relationship between Kikuchi lines and HOLZ lines is shown in this schematic of a  $\langle 111 \rangle$  CBED pattern from a cubic crystal. The three principal pairs of 220 ZOLZ Kikuchi bands show sixfold symmetry (characteristic of the 2D 111 planes) and bisect the  $\mathbf{g}$  vectors from 000 to the six 220 ZOLZ maxima. The *inelastic* deficient Kikuchi lines from the HOLZ planes are shown in the regions between the ZOLZ diffraction disks and the *elastic* deficient lines from the HOLZ planes are present within the 000 disk. In both cases, the HOLZ lines show threefold symmetry characteristic of looking down the  $\langle 111 \rangle$  direction in a 3D crystal.

## 20.8.B Acquiring HOLZ Lines

Steeds (1981) described the practical problems of recording HOLZ lines in some detail. Nothing much has changed in the intervening decades and the main points you have to consider are

- The lines are often only visible ‘on the negatives’ and not on the screen, so you should record all the DPs, not just ones on which you can see the lines. This poor visibility is less of a problem with a CCD because you can easily enhance the gain.
- You may have to make small changes in the operating voltage or the orientation in order to view the HOLZ rings, especially if the crystal has a small lattice-repeat spacing parallel to the beam and the angular view of the BFP is poor.
- Strains in the specimen from bending and thermal stresses smear out the HOLZ-line intensity. Choosing the smallest region (i.e., the smallest beam) may help this problem and will also minimize local thickness variations.
- Planar or point disorder as well as thermal (Debye-Waller) effects can reduce high-angle scattering. In practice, this means that cooling the specimen and reducing the kV can help to increase HOLZ-line visibility by reducing contamination and beam heating.
- Minor adjustments in HOLZ-line positions can help to distinguish HOLZ lines that overlap. To do this you need to change the kV by a small amount.

### CONTROLLING kV

Continuous kV control is an essential accessory to your TEM for serious CBED work.

The experimental procedure for observing HOLZ lines is quite straightforward but, since the lines themselves can be rather elusive, as we suggested at the start of the chapter, you should practice with a specimen such as Si or stainless steel in which the lines are almost always visible. The best way to search for the lines is

- Select the largest C2 aperture and go to the smallest  $L$  ( $\sim 3\text{--}500\text{ mm}$ ) at which you can see the full angular view of the BFP.
- Examine the Kossel/LACBED pattern (make  $2\alpha$  large) which should reveal Kikuchi bands intersecting at many poles, spanning a good fraction of the stereographic triangle as shown in Figure 20.16A.
- If you tilt to such a pole, as shown in Figure 20.16B, you should see the ring of HOLZ intensity.
- Tilt to a suitable zone axis for optimizing HOLZ effects. Remember, the best orientation for seeing the HOLZ lines in the 000 disk is *not* a low-index, high-symmetry pole such as  $\langle 100 \rangle$  or  $\langle 111 \rangle$ , but a higher-index, lower-symmetry one such as  $\langle 114 \rangle$ .
- To see the deficient lines, increase  $L$  to look in detail at the 000 region of the pattern, and if necessary, put in a

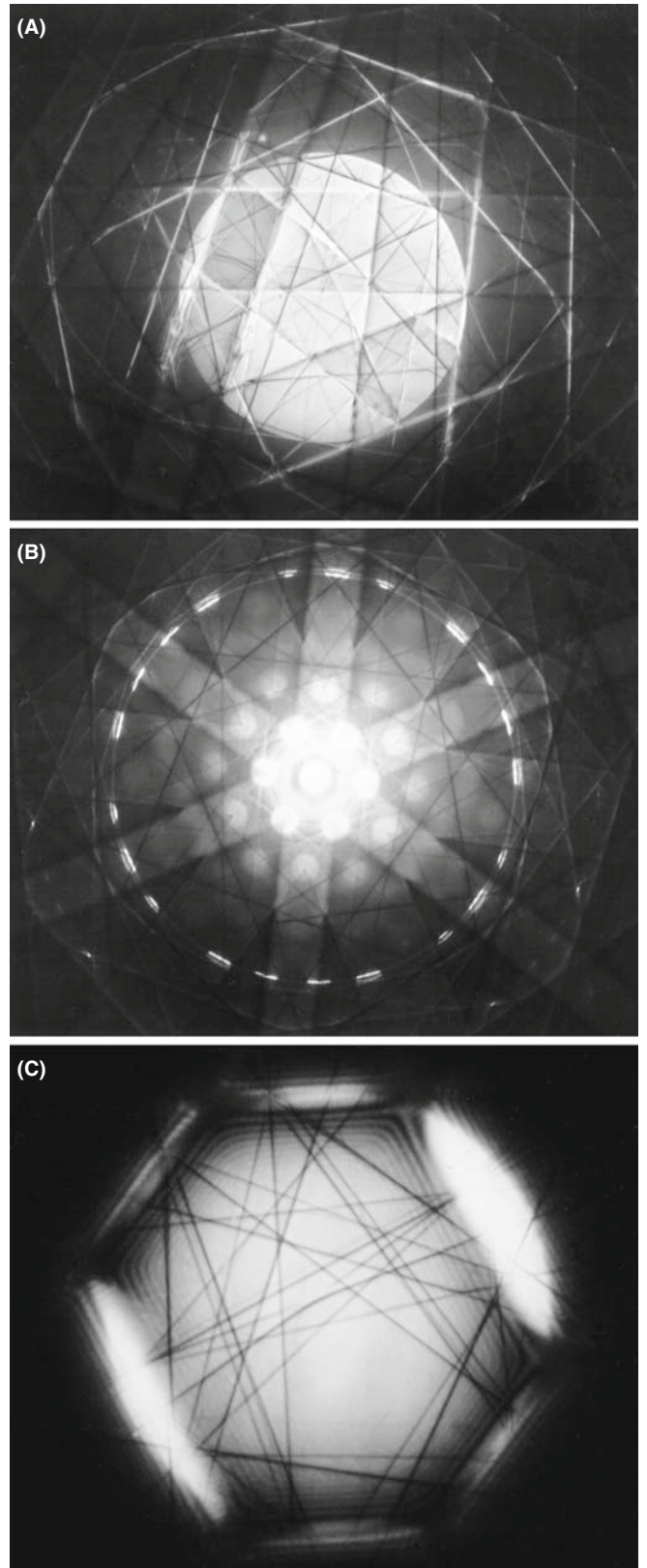


**FIGURE 20.16.** (A) Low- $L$ , large- $\alpha$  CBED pattern showing a wide area of reciprocal space, away from ZAP conditions. (B) When the specimen is tilted to a high-symmetry  $\langle 111 \rangle$  ZAP and a smaller C2 aperture is inserted, a ring of excess HOLZ lines appears. In (C) taken at high  $L$ , the deficient HOLZ lines are visible in the central 000 disk of the lower symmetry  $\langle 114 \rangle$  pattern.



smaller C2 aperture, center it and look for the fine dark lines crossing the bright disk as in Figure 20.16C. Usually, you'll just need this deficient-line distribution.

You have to use a range of  $L$  (from  $\sim 300$  to 1500 mm) to obtain all this information and this is easy in any post-1980 TEM. DSTEMs with sufficient post-specimen lenses are as versatile. Energy filtering improves everything that we've just described.

## 20.9 HOLLOW-CONE/PRECESSION CBED

As we described in Chapter 18, for SAD, we can acquire CBED patterns by rotating the incoming convergent beam about the optic axis in a hollow cone. Just as with SAD, hollow-cone CBED supplements the information we get in a stationary-beam pattern (i.e., all the patterns we've discussed so far). Remember, hollow-cone operation deflects the incident beam and rotates the pattern in the BFP while precession de-scans the beam so that the actual pattern is stationary. A good review of hollow-cone CBED and its relationship to other CBED methods is given in Tanaka's 1986 paper. Hollow-cone patterns do not show specific diffraction spots like CBED patterns since the rotating disk intensity is averaged out and the only stationary features are diffraction events at specific angles such as HOLZ lines. We can take advantage of this because if, for example, the cone angle is set to that of the FOLZ ring then the pattern consists predominantly of an array of excess HOLZ lines as shown in Figure 20.17. The ZOLZ disks, which would normally be so bright that they

might mask the excess lines, are removed because the rotation of the incident beam averages out the intensity.

Precession of CBED patterns has all the advantages of precession of SADPs as discussed in Section 18.8. A comparison of a precession DP and a standard DP under K-M conditions is shown in Figure 20.18. Precession extends the FOLZ ring into an annulus of width of  $\sim 10$  mrad. This dynamical background averaging can improve intensity measurements from DPs by considerably simplifying the problem of background subtraction.

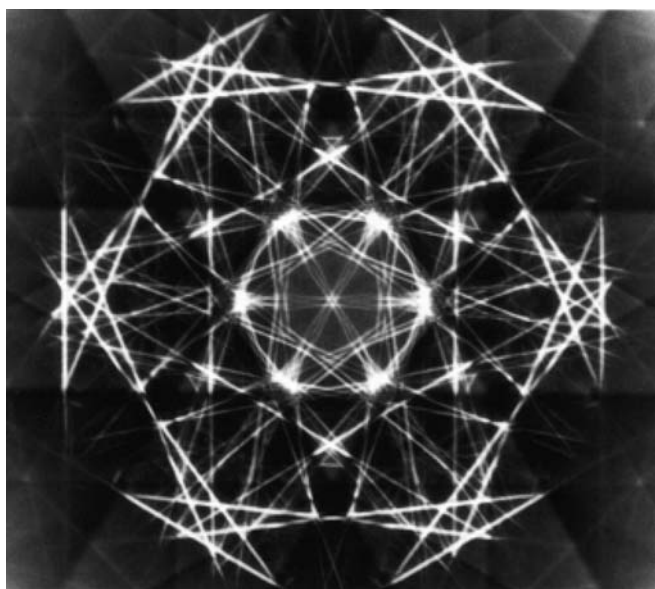


**FIGURE 20.17.** Hollow-cone CBED pattern showing bright, excess HOLZ lines only. All the usual diffraction-disk intensity is averaged out (Graphite 0001; 200 kV).

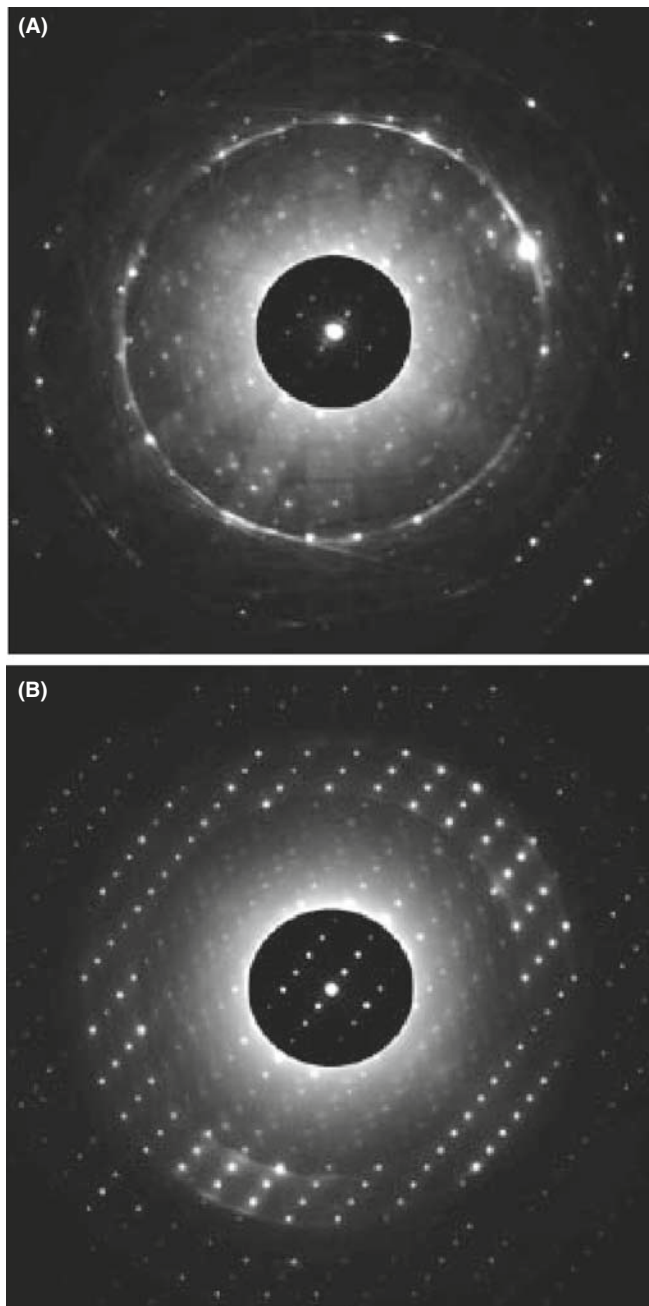


**FIGURE 20.18.** Comparison of (A) unprocessed and (B) precessed patterns from a very thick specimen of  $\text{Mg}_3\text{V}_2\text{O}_8$ . A small precession angle ( $\sim 5$  mrad) was used to form (B) and the reflections in the ZOLZ are more clearly defined. Dynamical scattering still contributes to the pattern so a thinner specimen would be better.



## CHAPTER SUMMARY

In this chapter we've covered how to obtain different CBED patterns experimentally. Particular points and terms that you should know are

- If you vary the specimen thickness,  $\alpha$ ,  $L$ , and the focus you can obtain CBED and LACBED patterns showing many different features. As with SAD, two-beam and zone-axis conditions are the standard operating conditions to get the most useful information.
- You'll probably have to record patterns at different values of  $\alpha$  and  $L$ , each with different exposure times.
- If you have an EELS then always filter your patterns.
- Even if you can filter the patterns, we strongly recommend using a double-tilt holder, cooled to LN<sub>2</sub> temperature.
- You must be able to change the kV by very small steps, if you are studying HOLZ lines.
- You can precess your CBED patterns or form them with hollow cones of incident electrons.
- Learn the meaning of such terms as ZAP, ZOLZ, FOLZ, HOLZ, K-M, and Kossel patterns.

In the next chapter, we'll show you how to use this contrast information to get the maximum amount of crystallographic information from your specimen.

### TEXTS

Champness, PE 2001 *Electron Diffraction in the Transmission Electron Microscope* BIOS Oxford UK. A concise and essential summary textbook full of useful examples often from non-cubic systems, since the author is a mineralogist not a metallurgist.

Morniroli, J-P 2002 *Large-Angle Convergent-Beam Electron Diffraction* SF $\mu$  (Société Française des Microscopies) Paris France. Highly recommended reading for serious students for whom CBED will be an important tool.

Reimer, L (Ed.) 1995 *Energy-Filtering Transmission Electron Microscopy* Springer-Verlag New York. For some specifics.

Reimer, L 1997 *Transmission Electron Microscopy; Physics of Image Formation and Microanalysis* (4th Ed.) Springer New York. For more specifics.

Spence, JCH and Zuo, JM (Eds.) 1992 *Electron Microdiffraction* Kluwer New York. *The book for the dedicated CBED researcher.*

Steeds, JW 1979 *Convergent Beam Electron Diffraction* in *Introduction to Analytical Electron Microscopy* 387–422 Eds. JJ Hren, JI Goldstein and DC Joy Plenum Press, New York. *The first book-chapter dedicated to the technique and still a superb introduction.*

### THE JEOL CBED ATLAS

This set of four volumes is perhaps the definitive work on CBED and describes an alternative approach to much of what is discussed in Chapters 20 and 21 and also in the companion text. The texts contain hundreds of beautiful and useful patterns.

Tanaka, M and Terauchi, M 1985 *Convergent Beam Electron Diffraction* JEOL Tokyo.

Tanaka, M, Terauchi, M and Kaneyama, T 1988 *Convergent Beam Electron Diffraction II* JEOL Tokyo.

Tanaka, M, Terauchi, M and Tsuda, T 1994 *Convergent Beam Electron Diffraction III* JEOL Tokyo.

Tanaka, M, Terauchi, M and Tsuda, T 2002 *Convergent Beam Electron Diffraction IV* JEOL Tokyo.

### HISTORY

Also see the references in Chapter 9.

Kossel, W and Möllenstedt, G 1938 *Elektroneninterferenzen im konvergenten Bündel* Naturwissenschaften 26 660–661.

### APPLICATIONS AND TECHNIQUES

Heilmann, P, Clark, WAT and Rigney, DA 1983 *Orientation Determination of Subsurface Cells Generated by Sliding* Acta Met. 31(8) 1293–1305.

- Humphreys, CJ, Maher, DM, Fraser, HL and Eaglesham, DJ 1988 *Convergent Beam Imaging – A Transmission Electron Microscopy Technique for Investigating Small Localized Distortions in Crystals* Phil. Mag. **58A** 787–798. CBIM.
- Jones, PM, Rackham, GM and Steeds, JW 1977 *Higher Order Laue Zone Effects in Electron Diffraction and Their Use in Lattice Parameter Determination* Proc. Roy. Soc. **A354** 197–222. When you have the time to really study HOLZ lines.
- Steeds, JW 1981 *Microanalysis by Convergent Beam Electron Diffraction in Quantitative Microanalysis with High Spatial Resolution* 210–216 Eds. GW Lorimer, MH Jacobs and P Doig The Metals Society London. For the terminology in Section 20.3.A.
- Tanaka, M, Saito, R, Ueno, K and Harada, Y 1980 *Large Angle CBED* J. Electr. Microsc. **29** 408–412.
- Tanaka, M 1986 *Conventional Transmission-Electron-Microscopy Techniques in Convergent-Beam Electron Diffraction* J. Electr. Microsc. **35** 314–323. Includes a good review of hollow-cone CBED.
- Wu, L, Zhu, Y and Taftø, J 1999 *Towards Quantitative Measurements of Charge Transfer in Complex Crystals Using Imaging and Diffraction of Fast Electrons* Micron **30** 357–369.

## APPLICATIONS AND TECHNIQUE

The companion text has a complete chapter devoted to CBED. Some of that material was in the original edition; it includes techniques that are still very powerful but that are not so widely used.

## SELF-ASSESSMENT QUESTIONS

- Q20.1 If CBED was invented before SAD, why did it only come into widespread use many years later?
- Q20.2 What advantages accrue when using a convergent rather than a parallel beam of electrons to create a diffraction pattern?
- Q20.3 What disadvantages are there to using CBED rather than SAD?
- Q20.4 How do you control the beam size in CBED?
- Q20.5 What are the advantages and disadvantages of using smaller beams to form CBED patterns?
- Q20.6 How do you control the size of the disks in the CBED pattern?
- Q20.7 Why would you want to change the camera length when viewing a CBED pattern?
- Q20.8 Define HOLZ, ZOLZ, FOLZ, K-M, ZAP, LACBED. Find any other acronyms from this chapter that are not in this list and define them.
- Q20.9 Explain why there is image information inside a CBED pattern disk when the pattern is not focused.
- Q20.10 Explain why this image effectively expands to infinite magnification when the pattern is focused.
- Q20.11 Why is it so important to align the C2 aperture when performing CBED?
- Q20.12 What is the role of thickness in CBED-pattern contrast?
- Q20.13 How can 3D information find its way into a 2D CBED pattern?
- Q20.14 Why is a higher-order ZAP preferable to a lower-order one for viewing a CBED pattern?
- Q20.15 Why do hollow-cone CBED patterns not show any diffraction disks, just HOLZ lines?
- Q20.16 What advantages accrue from precessing a CBED pattern?
- Q20.17 HOLZ lines within the 000 disk are continuous with lines outside this disk. What is the difference between the electrons contributing to the line within the disk and those in the line outside the disk?
- Q20.18 Why can we see Kikuchi lines in CBED patterns from specimens that are too thin to show such lines in SADPs or in specimens which are too deformed to show such lines in SADPs?
- Q20.19 Why do HOLZ lines appear more clearly at low temperatures?

## TEXT-SPECIFIC QUESTIONS

- T20.1 Look at Figure 20.1 and work out what would happen to the probe convergence angle if you switch on the C2 lens (a) weakly and (b) strongly enough to introduce a crossover before the upper objective lens. Sketch the ray diagrams for each case. Do the same for changing the size of the C2 aperture.
- T20.2 Look at the symmetry of the spots in Figure 20.2A and B and compare with the symmetry of the lines within the 000 disk in B. They are not the same. From what you know of the symmetry down the [111] direction in an fcc crystal, which pattern symmetry is correct? Why is the other symmetry observed?
- T20.3 Why does the intensity of the overall pattern increase from Figure 20.3D–F? Do you think the probe size has stayed constant as the C2 aperture has increased in size, and if not, why not? From what you know of lens limitations, what prevents us from keeping a very small probe size to localize the CBED pattern while increasing the current in the probe to generate a high-quality pattern? Are there experimental methods to overcome this problem?
- T20.4 Look at Figure 20.4 and explain why most of the intensity is in the 000 disk while it is barely possible to see the intensity scattered out to high angles in C. Is there anything you can do to increase the intensity scattered out to higher angles?

- T20.5 Draw schematic ray diagrams to explain the reversal in the image direction contained in the 000 disk in Figure 20.6 as the objective lens goes through focus.
- T20.6 List the pros and cons of forming CBED patterns in TEM versus STEM mode.
- T20.7 Why do you think that dynamical scattering causes regions of low (or zero) intensity to occur in CBED disks as in Figure 20.5B?
- T20.8 Explain what will happen to your CBED HOLZ intensity as you go to higher kVs. (Hint: look at Figure 20.11 and remember the effect of kV on  $\lambda$ .)
- T20.9 Compare and contrast HOLZ lines and Kikuchi lines in terms of their generation, intensity and distribution in low camera-length CBED patterns.
- T20.10 Since we know that the intensity of elastic scatter decreases rapidly with increasing angle away from the direct beam, where does the high intensity come from in the outer ring in Figure 20.16B?
- T20.11 Look at Figure 20.15. Explain what happens as the deficient HOLZ Kikuchi lines are extended such that they intercept other  $hkl$  disks in the ZOLZ.
- T20.12 Explain, with reference to Figure 20.8A, why it doesn't matter if you raise or lower the specimen out of the eucentric plane when forming a LACBED pattern. What experimental operation becomes increasingly difficult when you remove the specimen from the eucentric plane?
- T20.13 Why is the LACBED BF pattern so extensive while a LACBED DF pattern covers only a very small region of reciprocal space (e.g., see Figure 20.9)?

# Using Convergent-Beam Techniques

## CHAPTER PREVIEW

In the preceding chapter, we described how to obtain a variety of CBED patterns under various experimental conditions. In this chapter you will find out why these patterns are so useful: they contain a wealth of quantitative data, much of which you can't obtain by any other technique and many of which augment standard X-ray crystallographic methods (but always at higher spatial resolution). The established techniques largely depend on simple observation of the patterns whereas newer techniques involve quantitative simulations of the patterns.

CBED gives quantitative data on

- Specimen thickness
- Lots of crystallographic data such as the unit cell and associated lattice parameters, the Bravais lattice, crystal system, and full 3D crystal symmetry (point group and space group)
- Precise lattice-strain measurement (invaluable for semiconductors and other multilayer nanostructures)
- Enantiomorphism and polarity
- Valence-electron distribution, structure factors, and chemical bonding
- Characterization of line and planar defects

Between this chapter and in the companion text, we'll cover most of these applications of CBED. First, we'll show how to index the patterns and the HOLZ lines when they occur within those patterns. We'll also show you how to measure the specimen thickness, which is very useful in many aspects of TEM, particularly the spectrometry that we describe in Part 4. Next, we'll introduce the steps for a complete symmetry analysis of your specimen, which is fully described in the companion text. Then, we'll introduce you to methods of determining extremely small changes in lattice parameter which can be used to measure lattice strain and, indirectly, composition. Like any other TEM technique, we can simulate the contrast in CBED patterns in extraordinary detail and we'll tell you a little about how this is done. Other CBED methods are also available as well as different micro- and nanodiffraction methods, all of which offer better spatial resolution than SAD and we'll briefly summarize these at the end of the chapter.

We should warn you at this stage that some of the analyses we introduce here require a very good understanding of crystallography. Both the learning and the doing can be time-consuming processes, depending on your background. If you're a metallurgist, in a predominantly cubic world, then life is relatively easy, but in the rest of materials science, in functional materials, and in much of the nano-world, more complex crystal structures are common. In studying these materials, CBED is absolutely invaluable, but also really challenging. We suggest that you skim the chapter and see how many of the topics you can already relate to, given your current knowledge of crystallography and crystal defects. If you draw a blank, then it's time to read some of the basic texts listed in Chapter 18 before moving ahead.



## 21.1 INDEXING CBED PATTERNS

You've seen in the preceding chapter that, in addition to improved spatial resolution, CBED patterns often contain a wealth of new and sometimes spectacular contrast information not available in SADPs. However, before you do anything quantitative, you have to index the patterns. Indexing CBED ZOLZ patterns is no different to indexing SADPs, which we've already described back in Chapter 18. With indexed CBED patterns you can do exactly the same kind of orientation determination as with SADPs, but on a much smaller dimensional scale, suitable for crystallographic analysis of nanostructures, as shown in Figure 21.1, which also shows the power of CBED-pattern simulation.

What you need to learn now is how to index HOLZ spots, disks, and lines and understanding these requires a little extra thought since such diffraction effects come from lattice planes that, unlike those contributing to SADPs, are *not* parallel to the electron beam and, thus, are the key to obtaining 3D information about your specimen.

### 21.1.A Indexing ZOLZ and HOLZ Patterns

Remember that in a ZAP the HOLZ reflections appear as a ring of spots (or a ring of intensity) (see Figures 20.3, 20.4, 20.11, and many others). If you're not at a zone-axis orientation, the HOLZ spots might appear as an arc or somewhat randomly distributed, *but always farther away from the direct beam than the ZOLZ*

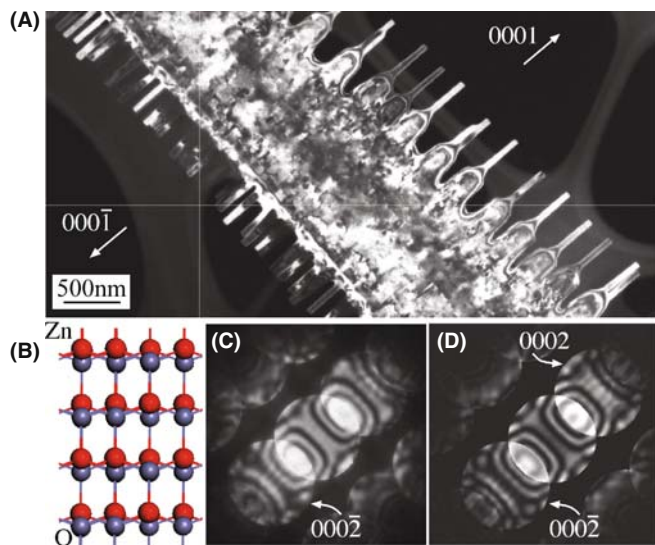


**FIGURE 21.1** (A) Dark-field TEM image recorded from a comb-like ZnO nanostructure. (B) A structural model of ZnO projected along 0110, showing polarity on the (0001) surfaces. (C) Experimental CBED pattern recorded from the ribbon. (D) Simulated CBED pattern using dynamical electron-diffraction theory. The simulation includes 127 beams in both the ZOLZ and HOLZ and the Debye-Waller factor at room temperature. The diffraction intensities are very sensitive to thickness. The best thickness match at 200 kV and beam direction  $\langle 0110 \rangle$  was 165 nm.

*reflections*. As with SAD, it's easiest to index ZAPs, so tilt around under Kossel conditions until you find a ZAP where Kikuchi bands intersect, then select a C2 aperture size to form diffraction disks (K-M conditions) in the HOLZ ring (like Figures 20.11D and 20.16B), which you can index as follows

- Index the ZOLZ for which  $hU + kV + lW = 0$  (see Section 18.4).
- Consult a stereographic projection to identify the poles of the principal planes constituting the FOLZ ( $hU + kV + lW = 1$ ) and SOLZ ( $hU + kV + lW = 2$ ), etc.
- Alternatively, you can just solve the Weiss zone law (see Section 18.4) for the appropriate  $UVW$ .
- Check to see if the poles on the stereographic projection constitute allowed reflections.
- Index the HOLZ maxima.

If you want to make use of a stereographic projection, see Chapter 18. Remember that the stereographic projection just gives you the major, low-index,  $hkl$  planes and ignores any systematic absences.

Examples of indexed ZOLZ, FOLZ, and SOLZ patterns are shown in Figure 21.2A–C for the fcc lattice under (a) [001], (b) [110], and (c) [111] beam directions; Figure 21.3A–C show similar patterns for the bcc lattice. Only the first few orders of diffraction maxima are shown in these figures but, paradoxically, you'll rarely find these reflections, and you'll never see them if you're under zone-axis conditions. This is because the Ewald sphere intercepts the HOLZ at large scattering angles (go back and check Figure 20.11) so relatively high orders of diffraction maxima are present in the HOLZs. Therefore, the schematic patterns in Figures 21.2 and 21.3 should be extended accordingly to match up with the experimental patterns. From the schematic HOLZ patterns in Figures 21.2 and 21.3, you can see that the symmetry of each  $\langle UVW \rangle$  zone is retained in each HOLZ pattern, but they are often shifted by a displacement vector relative to the ZOLZ because there is no allowed HOLZ reflection on the zone axis (i.e., directly above 000 in the ZOLZ). Note that in the HOLZ patterns we do not index the central spot. This displacement can be calculated for any zone axis using equations which we'll discuss in a while. So you should generate similar diagrams for the major zone axes of any specimen that you are going to study by CBED. You may have to generate less symmetrical patterns than those in Figures 21.2 and 21.3 (e.g., [233] or [114]), since these give rise to FOLZ rings with smaller radii (Figure 20.12), in which HOLZ phenomena are easier to see.

In some circumstances, the first ring of spots observed is from the second layer of the reciprocal lattice *but it is still called the FOLZ*. Well-known examples, as you can see in Figures 21.2 and 21.3, are the fcc (110) and bcc (111) patterns. You can't predict the total

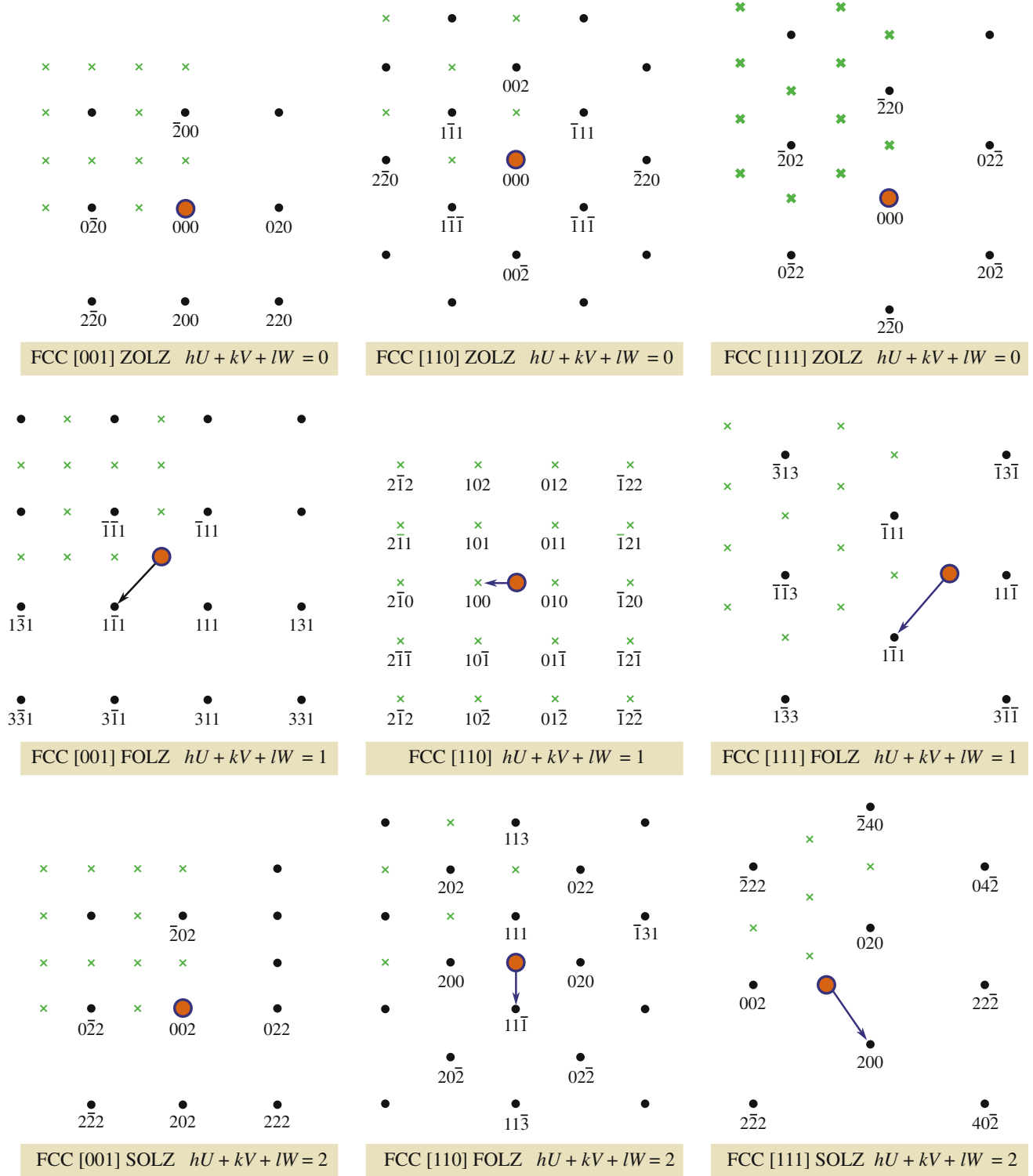


**FIGURE 21.2** The possible ZOLZ, FOLZ, and SOLZ reflections for the three principal zone axes of an fcc specimen. Allowed reflections are shown as black dots, forbidden reflections as crosses, the direct beam direction is a red spot, and the arrow indicates the displacement vector between the ZOLZ and FOLZ.

absence of a ring of HOLZ reflections just from the crystal symmetry, but it does vary with orientation. For example, in rhombohedral  $\alpha\text{-Al}_2\text{O}_3$ , which has trigonal symmetry, all HOLZ layers are present for the

[001] beam direction but, in other directions in this system, e.g., [121], [141], and [542] only every third Laue zone is present. (Ceramists would use 4-index notation for  $\alpha\text{-Al}_2\text{O}_3$  but remember the symmetry is

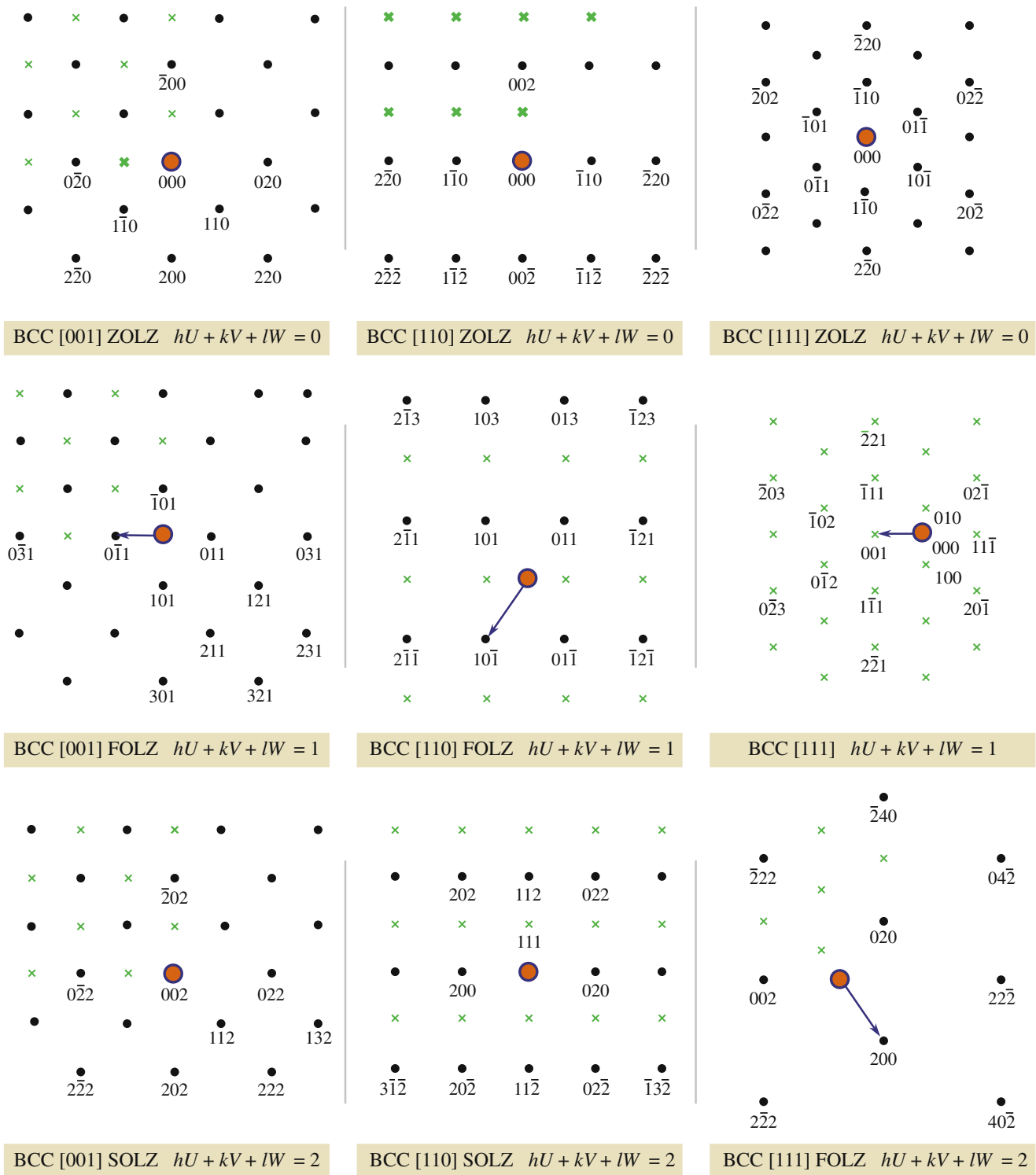


**FIGURE 21.3** The possible ZOLZ, FOLZ, and SOLZ reflections for the three principal zone axes of a bcc specimen. Allowed reflections are shown as black dots, forbidden reflections as green crosses, the direct beam direction is a red spot, and the arrow indicates the displacement vector between the ZOLZ and FOLZ.

only threefold.) A detailed explanation of this behavior is given by Raghavan et al. (1984). As with SADPs, computer indexing of HOLZ diffraction maxima is available on the Web. Once you are sure you can extend the principles you learned in Chapter 18 from the ZOLZ

to the FOLZ, then it's easy to use the commercial software available at any of the URLs #1–3 listed at the end of the chapter. There is also freeware available (URLs #4–7). One particularly good site is *WebEMAPS* (URL #4); Figure 21.4 illustrates computerized indexing of

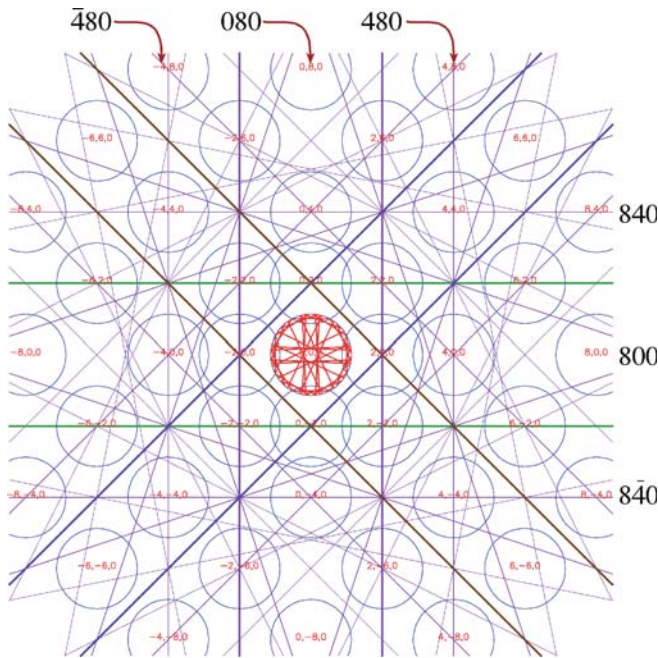


**FIGURE 21.4** Computerized indexing of ZOLZ disks and simulation of deficient HOLZ lines in the 000 disk (red) and Kikuchi lines in a 001 ZAP of GaAs (at 200 kV) using WebEMAPS. The indices for the ZOLZ disks are difficult to read because of the computer-output font size so several of the outer disks are indexed more clearly.

HOLZ and Kikuchi-line simulations of a GaAs ZOLZ CBED pattern.

### FOLZ WARNING

Be aware when you are indexing HOLZ rings that structure factors can cause *every* reflection in a FOLZ to be forbidden. So then we call the SOLZ the FOLZ!

### 21.1.B Indexing HOLZ Lines

When you're recording the pattern containing the deficient HOLZ lines, you must also record another pattern with a small  $L$  and a small  $\alpha$  to show the FOLZ disks. The first thing you have to do is index the FOLZ  $hkl$  maxima in the manner we just described. Then observe which maxima show the clearest HOLZ excess lines. Each HOLZ-line pair will be perpendicular to the  $\mathbf{g}$  vector from 000 to the FOLZ disk. There should be a parallel deficient HOLZ line in the 000 disk, and this line must be assigned the same indices as the FOLZ disk. If you repeat this exercise around the FOLZ ring, most of the HOLZ lines should be indexed, as shown in Figure 21.5. Below the schematic pattern is a magnified drawing of the 000 disk and you should be able to see the association of each HOLZ line with a corresponding FOLZ maximum (Ecob et al.).

In some cases you may find it difficult to associate a specific HOLZ deficient line in 000 with a specific FOLZ reflection due to strong excitation of two diffraction

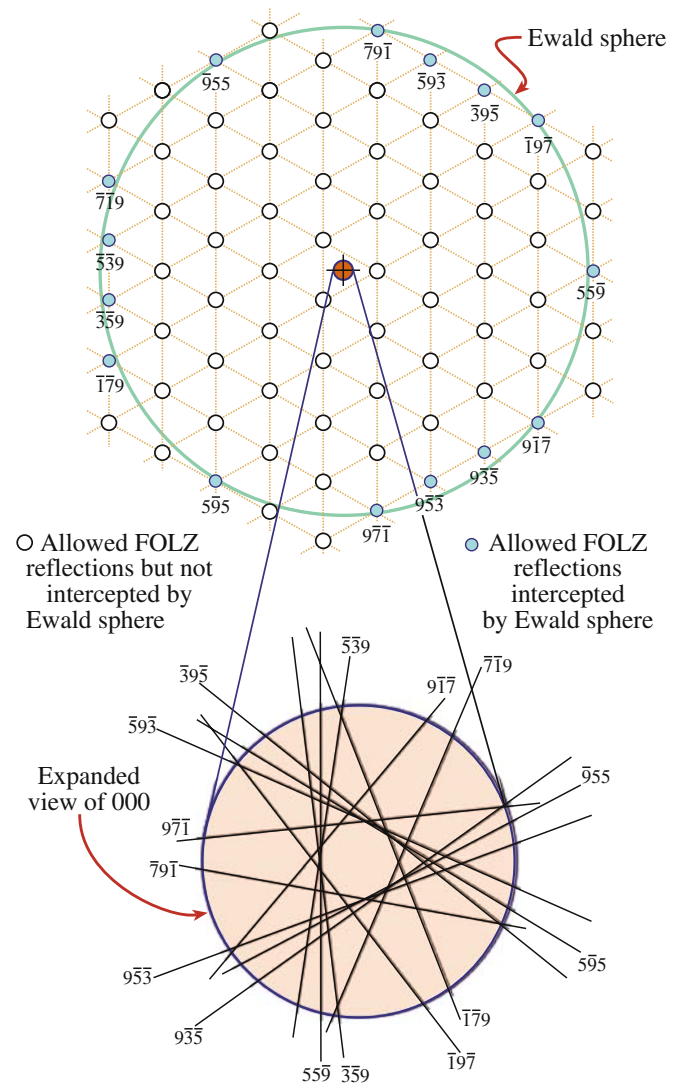


**FIGURE 21.5** How to relate deficient HOLZ lines to the HOLZ maxima; the indexed FOLZ reflections in this [111] pattern are shown as full circles and the open circles are the rest of the FOLZ reciprocal lattice points that don't intercept the Ewald sphere. The  $\mathbf{g}$  vector from 000 to each  $hkl$  FOLZ disk is normal to the  $hkl$  HOLZ line and the lines are shown in the expanded 000 disk below.

maxima. Under these circumstances, the two deficient lines may merge and appear to form a hyperbola. If you make small changes in the kV, the overlaps may resolve into two discrete lines. You should also be aware that faint HOLZ lines in the 000 disk may sometimes arise from second-order or even third-order Laue zones; these very high order lines are even more sensitive than first-order HOLZ lines to changes in kV and lattice parameter. As with the HOLZ patterns themselves, the indexing of HOLZ lines also lends itself to computer assistance. As we just showed in Figure 21.4, such programs can generate simulated HOLZ line patterns for a given orientation, lattice parameter, and kV. Matching of the computer simulation with the experimental pattern then allows direct indexing. This procedure is also



the first step in measuring the lattice parameter of the specimen and we will discuss this, along with other applications such as composition and strain measurements later in this chapter. Fournier et al. give a clear introduction to the step-by-step indexing and you should read this and then practice indexing some patterns by hand once or twice, just to get the hang of it. New software continues to become available to refine the various methods of HOLZ-line indexing (e.g., Morawiec).

## 21.2 THICKNESS DETERMINATION

As you read through this book, you will become aware that a direct and accurate measure of the specimen thickness is essential for many aspects of TEM and AEM, such as the correction of X-ray intensities for absorption within the specimen (Chapter 35), determining the attainable X-ray spatial resolution (Chapter 36), and obtaining EELS data with reasonable P/B (Chapters 37 and 38). A most useful application of CBED patterns is that you can use them to measure the thickness of a crystal.

When you record a ZAP under conditions where  $2\alpha_S < 2\theta_B$  such as shown back in Figure 20.2B, the 000 disk usually contains concentric diffuse fringes known as Kossel-Möllenstedt (K-M) fringes. If you move the specimen under the beam and it is not too bent then you will see that the number of these fringes changes. In fact the number of fringes increases by one every time the thickness increases by one extinction distance,  $\xi_g$ ; if the specimen is  $< \xi_g$  in thickness, then you'll see no fringes and the 000 and  $hkl$  disks will be kinematical and uniformly bright and boring, as shown back in Figure 20.5A. So these fringes clearly contain thickness information. In fact, because the foil thickness can be measured at precisely the point you are doing diffraction and analysis, and because the method is very amenable to computerization, it has become a most popular use for CBED patterns. The region of the foil you select should be flat and undistorted (this is relatively easy when you are using a small focused probe, compared to a broad beam for SAD) and the beam must be focused at the plane of the specimen. The method is, of course, limited to crystalline specimens and it can be a bit tedious, but it is one of the best and, certainly for fully crystalline materials, the most accurate method of thickness determination.

In practice, to simplify the interpretation, we don't make thickness measurements under zone-axis conditions. You need to tilt to two-beam conditions with only one strongly excited  $hkl$  reflection. If you do this you will see that the CBED disks contain parallel rather than concentric intensity oscillations, as shown in Figure 21.6.

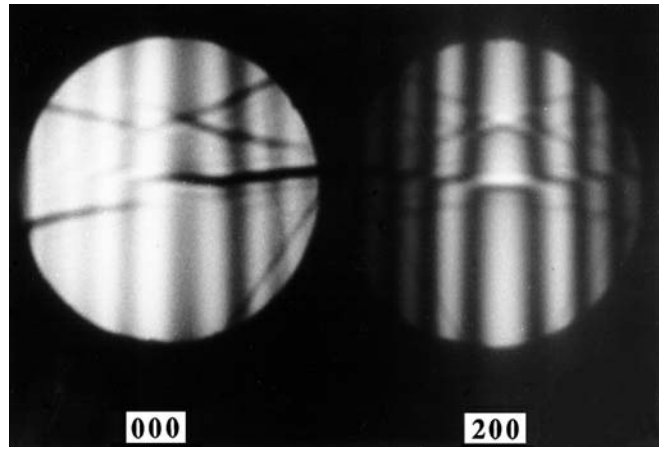


**FIGURE 21.6** Parallel Kossel-Möllenstedt fringes in a ZOLZ CBED pattern from pure Al taken under two-beam conditions with (200) strongly excited.

### FRINGES IN THE DISK

These oscillations are symmetric in the  $hkl$  disk and asymmetric in the 000 disk for two-beam conditions.

We'll see in Chapter 23 that these fringes are the reciprocal-space analog of rocking-curve intensity oscillations that occur across a bend contour in two-beam BF and DF images. We'll also see in Chapter 23 that bend contours arise when elastic deformation bends the diffraction planes and so an incoming parallel beam 'sees' a range of scattering angles across the bent region (see Figure 21.7A). In a similar manner, when you use a convergent beam and the illuminated region is undeformed, then the convergent beam provides a range of incidence angles to the diffracting  $hkl$  planes (see Figure 21.7B). The procedure to extract the thickness from the fringe pattern was first described by Kelly et al., refined by Allen, and is easily computerized. Energy filtering also helps to improve the clarity of the K-M lines.

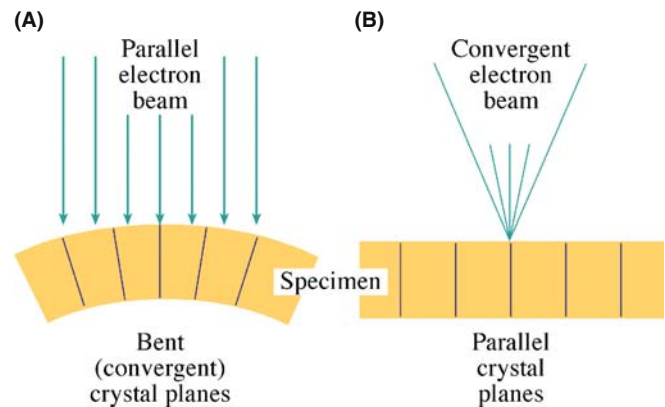


**FIGURE 21.7** The reciprocal relationship between electron ray paths during (A) the formation of bend contours in BF images and (B) the formation of K-M fringes in CBED disks.

But before you click on your Web browser, let's do it first by hand so you understand the process. If you look at the  $hkl$  disk through a  $10\times$  Lupe containing a graticule then it is easy to measure the distances between the middle of the central bright fringe and each of the dark fringes with an accuracy of about  $\pm 0.1$  mm. The central bright fringe is at the exact Bragg condition where  $\mathbf{s} = 0$ . The fringe spacings correspond to angles  $\Delta\theta_i$  as shown schematically in Figure 21.8A, and from these spacings you can obtain a deviation  $s_i$  for the  $i^{\text{th}}$  fringe (where  $i$  is an integer) from the equation

$$s_i = \lambda \frac{\Delta\theta_i}{2\theta_B d^2} \quad (21.1)$$

where  $\theta_B$  is the Bragg angle for the diffracting  $hkl$  plane,  $d$  is the  $hkl$  interplanar spacing, and we'll use the magnitude of  $\mathbf{s}$ , ignoring its sign. The angle  $2\theta_B$  in the CBED pattern is, of course, just the separation of the 000 and  $hkl$  disks. The specimen in Figure 21.6 is pure Al and the 200 reflection is excited. For Al,  $d_{200}$  is 0.2021 nm. If the extinction distance  $\xi_g$  is known, then you can determine the foil thickness  $t$  since

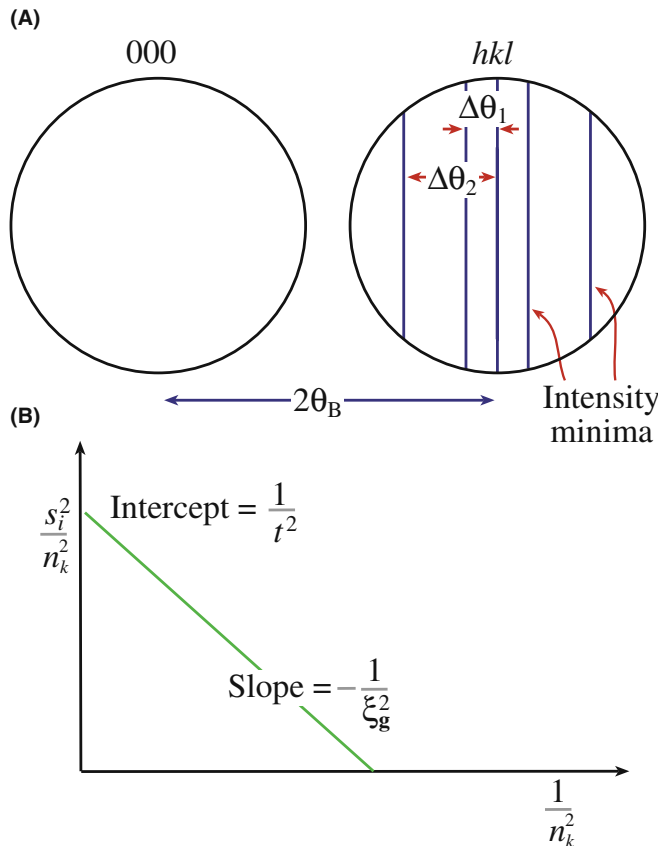


**FIGURE 21.8** (A) The measurements necessary to extract thickness ( $t$ ) from K-M fringes. From  $n_i$  measured spacings of  $\Delta\theta_i$ , determine the deviation parameters  $s_i$ , then (B) plot  $(s_i/n_k)^2$  against  $(1/n_k)^2$ . If the plot is a straight line, extrapolate to the ordinate to find  $t^{-2}$  and hence  $t$ .

$$\frac{s_i^2}{n_k^2} + \frac{1}{\xi_g^2 n_k^2} = \frac{1}{t^2} \quad (21.2)$$

where  $n_k$  is an integer ( $k$  is an integer identical to  $i$  or differing from  $i$  by a constant integer not related to  $\lambda$ ). If you don't know  $\xi_g$ , then you have to use a graphical method, plotting the measurements for several fringes as follows.

- Arbitrarily assign the integer  $n = 1$  to the first fringe, which corresponds to an excitation error  $s_1$ .
- Then assign  $n = 2$  to the second fringe,  $s_2$ , etc.
- Plot  $(s_i/n_k)^2$  versus  $(1/n_k)^2$ . If the result is a straight line, your arbitrary assignment was good. That is, the relationship between  $i$  and  $k$  is given by  $k = i + j$  where  $j$  is the largest integer  $< (t/\xi_g)$ .
- If your plot is a curve, then repeat the procedure by re-assigning  $n = 2$  to the first fringe.
- Continue to iterate until you find a straight line, as shown in Figure 21.8B.

You have to do all this because the minimum thickness may be  $> \xi_g$ . From the straight-line plot, the intercept is  $t^{-2}$  and the slope is  $-\xi_g^{-2}$ . We will now go through an example in detail.

**An example:** If we apply this method to Figure 21.6, we find that the first set of values of  $s_i$  for the three dark fringes are  $s_1$ ,  $s_2$ , and  $s_3$  given in Table 21.1. Now we guess the values of  $n$  as shown in column 2 to give the values for  $(s_i/n_i)^2$  in column 3.

These data do not plot as a straight line because both  $(s_1/1)^2$  and  $(s_3/3)^2$  are less than  $(s_2/2)^2$ . So we then assign the integer 2 to the first fringe, etc. We then find a second set of values as shown in Table 21.2, and these numbers plot as a straight line as shown in Figure 21.8B. The intercept of the line with the ordinate is  $1/t^2$ , and this

$s_i$ (nm <sup>-1</sup> )	$n_i$	$\frac{s_i^2}{n_i^2}$ (nm <sup>-2</sup> )
$s_1 = 0.84 \times 10^{-2}$	$n_1 = 1$	$0.7 \times 10^{-4}$
$s_2 = 2.1 \times 10^{-2}$	$n_2 = 2$	$1.1 \times 10^{-4}$
$s_3 = 3.0 \times 10^{-2}$	$n_3 = 3$	$1.0 \times 10^{-4}$

$s_i$ (nm <sup>-1</sup> )	$n_i$	$\frac{s_i^2}{n_i^2}$ (nm <sup>-2</sup> )
$s_1 = 0.84 \times 10^{-2}$	$n_1 = 1$	$1.7 \times 10^{-5}$
$s_2 = 2.1 \times 10^{-2}$	$n_2 = 2$	$4.9 \times 10^{-5}$
$s_3 = 3.0 \times 10^{-2}$	$n_3 = 3$	$5.6 \times 10^{-5}$

equals  $6.1 \times 10^{-5} \text{ nm}^{-2}$ . Therefore, we find that  $t^2 = ((6.1)^{-1} \times 10^5) \text{ nm}^2 = (1.64 \times 10^4) \text{ nm}^2$  and so  $t = 128 \text{ nm}$ .

Now you can see why this procedure lends itself to computerization. You can digitize the fringes by scanning the pattern on your TEM screen across the STEM detector or do it directly via a CCD camera. As we noted, software is available to do this analysis but this isn't difficult and you may even want to try writing the program yourself or incorporate equation 21.2 into a spreadsheet/graphing program. A good example of the relative strengths of CBED and EELS thickness measurements for a nanostructured material is given by Berta et al.

## 21.3 UNIT-CELL DETERMINATION

Before you start on the more esoteric aspects of crystal-structure determination, such as the analysis of point groups and space groups, you can make life much easier for yourself by determining the unit cell of your specimen. Remember

The unit cell is the smallest group of atoms or molecules which, when repeated in 3D, generates the lattice structure of the crystal.

The unit cell possesses the symmetry and properties of the lattice (assuming we could ever test a single, isolated unit cell!). In fact, determination of the unit cell is only possible if you already know the crystal system of the specimen. So don't start with an unknown structure! Remember

There are seven different axial/coordinate systems into which all crystals are classified: cubic, orthorhombic, tetragonal, hexagonal, trigonal, monoclinic, and triclinic.

Now in TEM investigations it is rare that we look at a totally unknown specimen and so, in this chapter, we'll assume that you know the crystal structure of your specimen. If in fact you don't know the structure, then you have to start with symmetry determination to find the point group/space group (also see the companion text) and then you can deduce the crystal system. Remember

The point group defines a set of 2D symmetry operations (rotations or reflections), acting through a point, which leaves the crystal unchanged. There are 32 unique point groups.

We can extend the definitions of symmetry to 3D. Remember

The space group is the complete set of 3D symmetry operations (rotations, reflections, translations, and combinations thereof) that leave the crystal unchanged. There are 230 space groups.

### WARNING

If you don't recognize any of these definitions then stop, do not pass this section. Return to the basic crystallography texts (referenced in Chapter 18).

So, assuming you know the crystal system, let's determine the unit-cell dimensions. We saw in the previous chapter that a CBED pattern at small  $L$  often reveals one or more rings of HOLZ intensity and you've just learned how to index the diffraction disks that make up these rings and the pairs of HOLZ lines that attach themselves to the HOLZ reflections. If you don't know the crystal structure, then, of course, it will be rather difficult to index the pattern since you don't know the appropriate systematic absences. But these rings are useful, even if you haven't indexed the individual disks.

If you measure the radii of the rings ( $G$ ), you can deduce the lattice-repeat vector of the crystal parallel to the beam direction.

So by tilting to an orientation in which the beam is coming down an axis of the unit cell such as [001] in an orthorhombic crystal, the disk spacings in the ZOLZ pattern will give you the [100] and [010] lattice parameters and the HOLZ-ring radius will give you [001]. (Now you see why you can't do this if you don't know the crystal system to start with, since you don't know what lattice spacings and angles to expect.)

So you should be able to determine all the lattice parameters of the unit cell from a single ZOLZ/HOLZ pattern. If you're not sure which pattern to choose, any low-index (i.e., high-symmetry) pattern is a good starting point. There are appropriate analytical expressions for calculating the spacing between atomic planes parallel to the beam and we'll discuss them next. These expressions give you the lattice parameters, since the lattice spacing is related to the lattice parameter by standard equations, given in basic crystallography texts (see Chapter 18). Then you have to look at differences between the ZOLZ and HOLZ disk patterns to determine the type of lattice centering. So we'll now show you how to utilize a unique aspect of CBED patterns, namely, that from a single 2D pattern, you can obtain 3D information about your crystalline specimen.

### 21.3.A Experimental Considerations

The first thing you have to do is get CBED patterns containing clear ZOLZ and HOLZ maxima. The patterns should have a small  $L$  to reveal one or more rings.

### TWO PATTERNS

It is good practice to record two patterns, one with a large  $C_2$  aperture (therefore large  $\alpha$ , Kossel conditions) and one with a small  $C_2$  aperture to show the individual disks (K-M conditions).

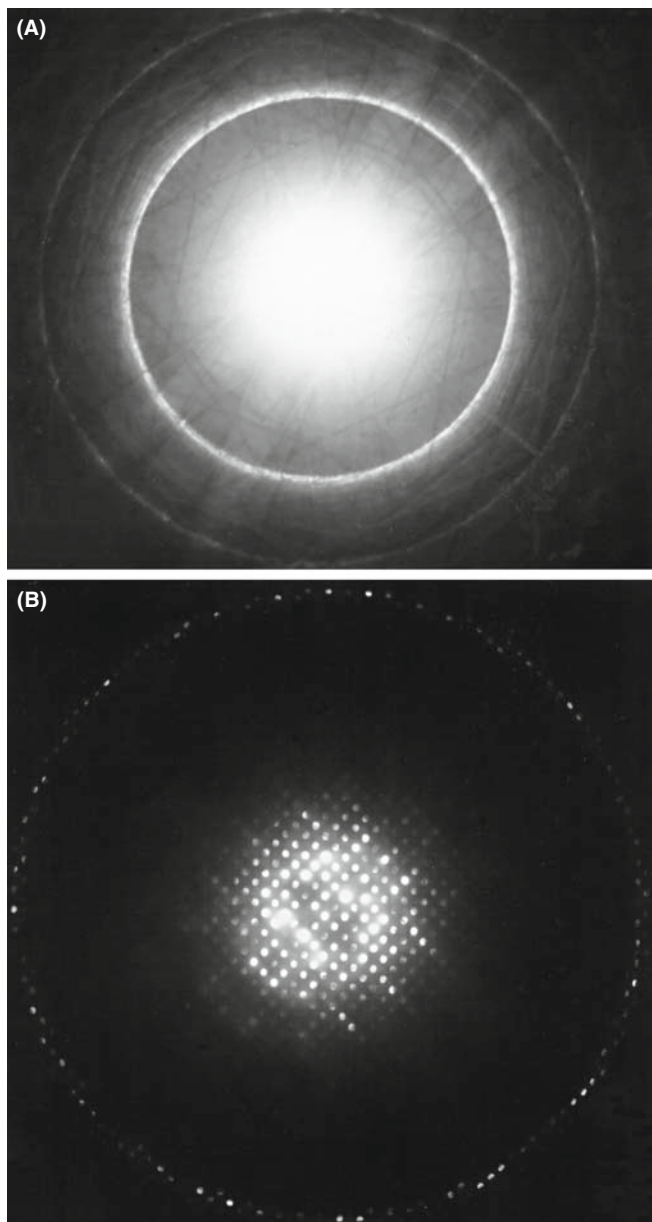


**FIGURE 21.9** (A) CBED Kossel pattern from a carbide particle taken with a 150- $\mu\text{m}$  C2 aperture showing the FOLZ ring of intensity surrounding the overexposed ZOLZ region. In (B) the same pattern taken with a 20- $\mu\text{m}$  aperture reveals individual reflections in both the ZOLZ and FOLZ.

Such a pair of patterns is shown in Figure 21.9A and B. We will use the ring pattern to measure  $G$  and the disk pattern to index individual HOLZ reflections and observe both the relative spacings and positions of ZOLZ and HOLZ reflections.

### 21.3.B The Importance of the HOLZ-Ring Radius

If you go back and look at Figures 20.11A–D and 20.12 you will be able to work out the simple geometrical relationship between  $H$  and  $G$ .

- $H$  in Figure 20.12 is the spacing of the reciprocal-lattice planes parallel to the electron beam.
- $G_n$  is the projected radius of a HOLZ ring that you measure on the recording of the pattern. If the HOLZ ring is split, always measure  $G_n$  using the innermost ring.
- If the order of the ring is high, then the electrons are scattered out to large angles ( $\geq \sim 10^\circ$ ), and your measurements may suffer from the effects of lens distortion because the electrons are traveling close to the polepiece. If this is happening, you must calibrate the distortion in reciprocal space using a known specimen from which  $G_1$ ,  $G_2$ , etc., can be calculated and compared with the values you obtain experimentally. Of course,  $C_s$  correction will minimize such distortion.

Experimentally, you'll find it much easier to measure  $G$  from a Kossel pattern because the HOLZ intensity appears as one or more rings as in Figure 21.9A. Since the radius of the Ewald sphere increases with decreasing electron wavelength  $\lambda$ , the value of  $G$  for any given orientation will increase as the accelerating voltage is raised, so it becomes increasingly difficult to see HOLZ rings at intermediate voltages.

From the geometry of Figures 20.11 and 20.12, and assuming that terms in  $H^2$  are negligible, the radii of the FOLZ and SOLZ rings,  $G_1$  and  $G_2$ , are

$$G_1 = \left( \frac{2H}{\lambda} \right)^{1/2} \quad (21.3)$$

And from a theorem you learned in high-school geometry

$$G_2 = 2 \left( \frac{H}{\lambda} \right)^{1/2} \quad (21.4)$$

where both  $G$  and  $H$  are in reciprocal-space units ( $\text{nm}^{-1}$  or  $\text{\AA}^{-1}$ ). Similar expressions can be developed, if you need them, for third- and higher-order zones. In practice, most people find it easier to think in real space rather than reciprocal space and so we rewrite these equations in terms of the spacing between Laue zones ( $H^{-1}$ ) in real-space units. We use the inverse relationship between real and reciprocal spaces to give, for the FOLZ

$$\frac{1}{H} = \frac{2}{\lambda G_1^2} \quad (21.5)$$

The value of  $H^{-1}$  can be expressed in real-space units (nm) through the measured radius  $R$  (mm) and the camera constant  $\lambda L$  (nm mm)



$$\frac{1}{H} = \left(\frac{2}{\lambda}\right) \left(\frac{\lambda L}{R}\right)^2 \quad (21.6)$$

You must take the time to measure  $\lambda L$  carefully (see Section 9.6) because this will minimize errors in  $H^{-1}$  which could be quite large due to the  $(\lambda L)^2$  dependence in equation 21.6. From the above equations and from Figure 20.12, you can see that a low-symmetry zone axis with a small  $H$  will give rise to a smaller HOLZ ring than for a high-symmetry zone. The smaller ring will be easier to observe at any chosen  $L$ .

*Summarizing the story so far:* by measuring  $R$  values, you can determine the real-lattice spacing ( $H^{-1}$ ) parallel to the beam direction. The next thing to do is compare this measured value,  $H_m^{-1}$  with calculated values  $H_c^{-1}$  assuming a certain unit cell. Now  $H^{-1}$  is directly related to the magnitude of the real-space direction vector

$$\frac{1}{H} = |[UVW]| \quad (21.7)$$

and so this magnitude can be calculated for a specific beam direction  $[UVW]$ .

**An example:** For an fcc crystal (Steeds 1979)

$$\frac{1}{H} = \frac{a_0(U^2 + V^2 + W^2)^{1/2}}{p} \quad (21.8)$$

where  $a_0$  is the lattice parameter,  $p = 1$  when  $(U + V + W)$  is odd, and  $p = 2$  when  $(U + V + W)$  is even. For bcc crystals  $p = 2$  if  $U$ ,  $V$ , and  $W$  are all odd, otherwise  $p = 1$ . These conditions for  $p$  just take account of structure-factor effects which cause systematic absences of some reflections, or in some cases whole rings. If a whole ring is absent, the calculated reciprocal-lattice layer spacing  $H_c^{-1}$  must be an integer multiple of the measured spacing  $H_m^{-1}$ . Thus

$$\frac{1}{H_c} = n \left(\frac{1}{H_m}\right) \quad (21.9)$$

where  $n$  must be an integer. If  $n$  is non-integral then your indexing is wrong. A generalized method for determining which Laue zone you should see has been given in Jackson's 1990 paper. If you have indexed the ZOLZ (i.e.,  $[UVW]$  is known),  $R$  is measured and  $\lambda$  is known, then you can determine  $H$  without the need to index individual spots in the HOLZ ring of intensity.

There are more generalized equations for  $H^{-1}$  than equation 21.8 (see Raghavan et al. and Ayer).

**Other examples:** In a crystal system with orthogonal axes (orthorhombic, tetragonal, or cubic systems, with lattice-repeat spacings  $a$ ,  $b$ ,  $c$ ) if there

are no absences of HOLZ layers ( $p = 1$ ) then for a given zone axis  $UVW$

$$\frac{1}{H} = (a^2U^2 + b^2V^2 + c^2W^2)^{1/2} \quad (21.10)$$

Similarly for hexagonal or rhombohedral systems using a three-index system

$$\frac{1}{H} = (a^2(U^2 + V^2 - UV) + c^2W^2)^{1/2} \quad (21.11)$$

and for the four-index system

$$\frac{1}{H} = (3(U^2 + V^2 + UV)^2 + c^2W^2)^{1/2} \quad (21.12)$$

and for the monoclinic system with a unique  $b$  axis

$$\frac{1}{H} = (U^2a^2 + V^2b^2 + W^2c^2 + 2UWac \cos \beta)^{1/2} \quad (21.13)$$

If you are working with a low-index, high-symmetry zone axis it may be just as easy to determine  $H^{-1}$  directly from reciprocal-lattice constructions rather than using equations. However, for lower-symmetry crystallographic directions, such constructions are effectively impossible to visualize and then you should use these equations.

So in summary we can give some guidelines

- Measure the radius of the HOLZ ring to give a value of the reciprocal of the spacing between the HOLZ and the ZOLZ,  $H_m^{-1}$ .
- Compare the measured spacing with the spacing calculated assuming a given unit cell,  $H_c^{-1}$ .
- The measured value should agree with, or be a multiple of, the calculated value. For example, if given a square ZOLZ DP, you assume a cubic crystal then the unit-cell repeat vector should be identical in all three dimensions. So the FOLZ ring diameter should give the same value of  $H^{-1}$  as that determined for the other two axes from the square  $[100]$  pattern. If  $H^{-1}$  is different, then the crystal is not cubic but another system, such as tetragonal.

### 21.3.C Determining the Lattice Centering

When you have measured  $H^{-1}$  from the Kossel pattern, the next thing to do is to compare the ZOLZ and FOLZ reflections in the K-M pattern obtained with a small C2 aperture such as Figure 21.9B. The superposition of the FOLZ and ZOLZ gives you information on the type of lattice you are dealing with, since centered lattices of all types will give different superposition patterns compared with a primitive lattice.

In a primitive lattice, the FOLZ will superimpose directly on the ZOLZ because there are no systematic absences. However, face-centered and body-centered lattices will give rise to displacements of the FOLZ pattern with respect to the ZOLZ in certain beam directions as illustrated schematically in Figure 21.10A. You can quite easily work out the displacement in terms of a shift vector for cubic crystal patterns in low-index orientations and we showed examples back in Figure 21.2 and 21.3. It is not so simple in more complex crystals but Jackson (1987) has developed a generalized method of determining the shift vector  $\mathbf{t}$  for all crystal systems and all orientations

$$\mathbf{t} = \mathbf{g} - \mathbf{u}^* \left( \frac{HN_L}{|\mathbf{u}^*|} \right) \quad (21.14)$$

where  $\mathbf{g}$  is the vector for the  $hkl$  HOLZ reflection,  $\mathbf{u}^*$  is the vector normal to the ZOLZ and parallel to  $H$ , and  $N_L$  is the number of the Laue zone containing  $hkl$ . To determine  $\mathbf{t}$  then all you do is look up values of  $H$ ,  $\mathbf{u}^*$ , and  $H/|\mathbf{u}^*|$ , tabulated by Jackson.

**An example:** We can illustrate the shift due to lattice type, by looking at Figure 21.10B, which is a series of schematic patterns for an orthorhombic cell (given by Ayer) oriented along the  $[001]$  axis. In each pattern the experimentally observed distribution of ZOLZ and FOLZ reflections is shown and adjacent to it is the same pattern but containing the FOLZ reciprocal-lattice points. So the FOLZ ring of spots is always coincident with the FOLZ reciprocal-lattice points. In the top pattern (P) the ZOLZ and FOLZ superimpose exactly and this would be the case for a primitive unit cell. In (A) the FOLZ lattice is displaced from the ZOLZ reflections by half the spacing of the ZOLZ reciprocal-lattice points in the  $[010]$  direction; this is the situation expected for an A-face-centered lattice. The next two patterns (B and I) show the expected displacements for a B-face-centered and an I (body-centered) lattice.

So you now know how to measure the lattice-repeat vectors in three dimensions and determine the type of lattice centering. This information should be sufficient to allow you to determine the correct unit cell of your specimen, particularly if you have further information, such as elemental analysis by XEDS or EELS.

## 21.4 BASICS OF SYMMETRY DETERMINATION

### 21.4.A Reminder of Symmetry Concepts

Before you study the following two sections in the companion text, you must have a basic understanding of crystal-symmetry elements (both rotational and

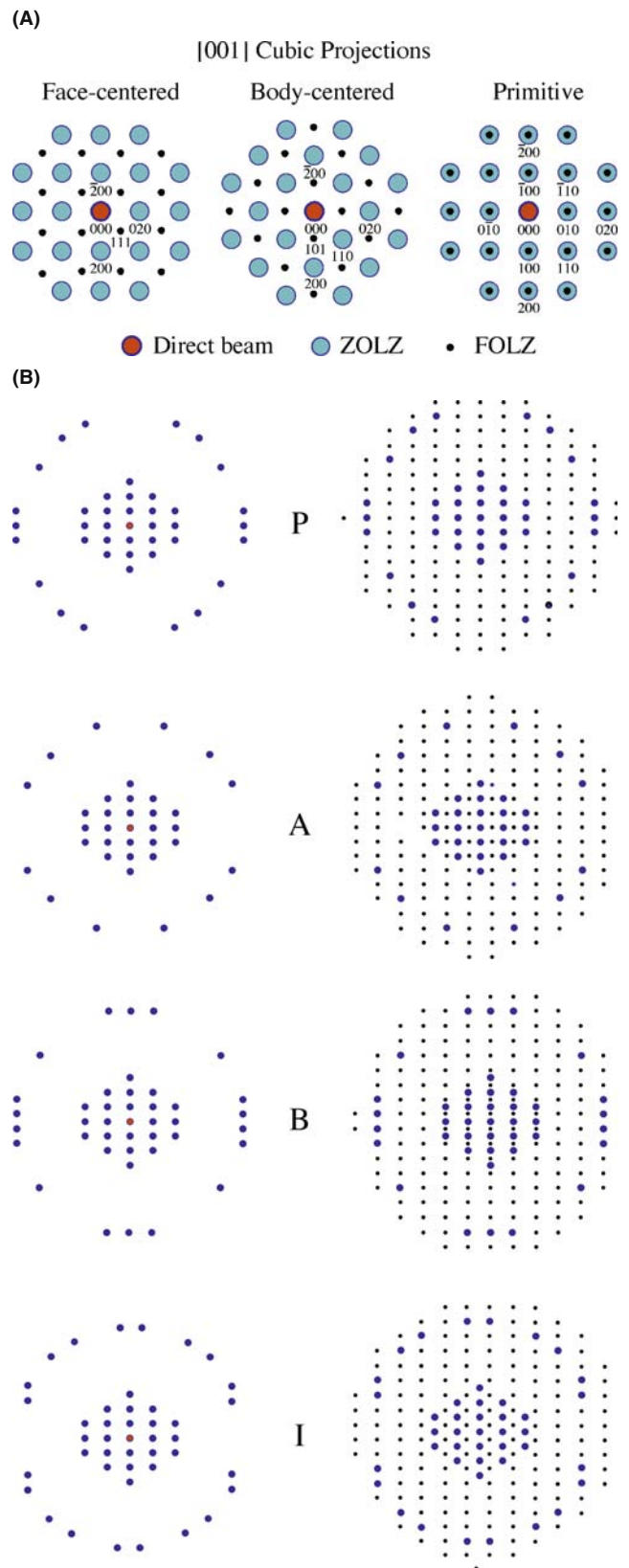


**FIGURE 21.10** (A) The overlap between the ZOLZ and the FOLZ when looking down the  $[001]$  axis of cubic crystals. In the fcc pattern, 111 is a FOLZ index, likewise 101 in bcc. In the primitive pattern, only the ZOLZ is indexed. (B) Schematic illustration of the superposition of the FOLZ pattern on the ZOLZ pattern for an orthorhombic crystal with the electron beam down  $[001]$  showing the differences in the superposition for (P) primitive, (A) A-centered, (B) B-centered, and (C) I-centered lattices.

translational) and be familiar with the standard international notation for point groups and space groups (see Section 16.10). You will also need to know how to represent the point-group symmetry of a crystal using the stereographic projection we discussed in Section 18.4. In Figure 21.11 we reproduce the standard point-group table familiar to any student of crystallography.

Historically, point-group determination has been the domain of X-ray crystallographers and electron microscopists have gladly avoided such concepts. However, the point group is not only useful for classifying crystals with common symmetry elements, but it is also an important indicator of many of the properties of the crystal, such as anisotropy in the electrical resistivity or the refractive index (all described in glorious detail in the classic text by Nye). With the availability of CBED you can determine the point group of a crystal directly in the TEM, simply by recording two or three low-index ZAPs.

This process has a tremendous advantage over classic X-ray techniques because

- We obtain this information from much smaller regions than is possible using X-rays.
- We can also distinguish all 32 possible point groups unambiguously, which is a non-trivial process using X-rays.

So as an electron microscopist, you must now master the details of point-group determination if you are to take full advantage of the capabilities of a modern TEM. This is described in detail in the companion text and you'll see that it's not too difficult an exercise, but there is no escaping the need to comprehend some of the basic principles of crystal symmetry. The exercises will require quite a lot of careful work and time. Therefore, if you can uniquely identify the unknown phase in your specimen through some other technique, such as XEDS or EELS, do so.

### 21.4.B Friedel's Law

Symmetry determination in crystals has evolved from the early work of Friedel and von Laue on the kinematical theory of XRD. We can summarize a fundamental aspect of Friedel's work by Friedel's law.

#### FRIEDEL'S LAW

Under kinematical diffraction conditions, the intensity of a reflection  $hkl$  is equal to the intensity in its opposite reflection  $\bar{h}\bar{k}\bar{l}$ .

If this law holds, then it is not possible to tell by diffraction whether an inversion center is present in the crystal or not. This is the case for most XRD patterns

from single crystals, because most XRD occurs under kinematical conditions.

So, under kinematical diffraction conditions, we cannot readily distinguish a mirror plane from a twofold rotational axis (diad) parallel to the mirror plane. That is equivalent to saying that *we cannot distinguish point groups  $m$  and  $2$* . Similarly, the presence of a fourfold rotation axis (tetrad) in a crystal, parallel to the  $c$  axis, results in  $I_{hkl} = I_{\bar{h}kl} = I_{h\bar{k}l} = I_{hkl}$  where  $I_{hkl}$  denotes the diffracted intensity of a reflection of type  $hkl$ . This DP cannot be distinguished from one containing two perpendicular mirror planes whose intersection is parallel to the rotation axis.

#### MIRROR PLANE

The presence of a mirror plane in a crystal, parallel to axes  $a$  and  $b$ , makes the intensity of all reflections of type  $hkl$  equal to the intensity of the corresponding  $\bar{h}\bar{k}\bar{l}$  reflection.

XRD is thus severely limited for point-group determination because of Friedel's law. Since crystals which do not possess true centers of symmetry (non-centrosymmetric crystals) still appear in X-ray DPs to possess a center of symmetry; they cannot be readily distinguished from centrosymmetric crystals. If you go back and look at the 32 point groups in Figure 21.11 and remove all those which do not contain a center of symmetry, then you are left with only 11 centrosymmetric point groups:  $\bar{1}$ ,  $2/m$  (equivalent to  $mm$ ),  $mmm$ ,  $\bar{3}$ ,  $\bar{3}m$ ,  $4/m$ ,  $4/mmm$ ,  $6/m$ ,  $6/mmm$ ,  $m\bar{3}$ , and  $m\bar{3}m$ . These 11 point groups are known as the *Laue classes* in XRD. Except under 'anomalous' scattering conditions, XRD can only determine these 11 symmetry groups.

#### WHEN FRIEDEL FAILS

In CBED patterns, *Friedel's law* breaks down because of dynamical scattering.

So, to get the full symmetry information, the crystal must be thick enough for you to see dynamical diffraction contrast within the CBED disks. If you then examine the intensity distributions within individual  $hkl$  reflections you can distinguish centrosymmetric and non-centrosymmetric crystals. Thus, in CBED patterns, the 32 crystal point groups are not reduced to the 11 Laue classes, as occurs in XRD.

### 21.4.C Looking for Symmetry in Your Patterns

You can't perform point-group determination without learning how to discern symmetry elements in

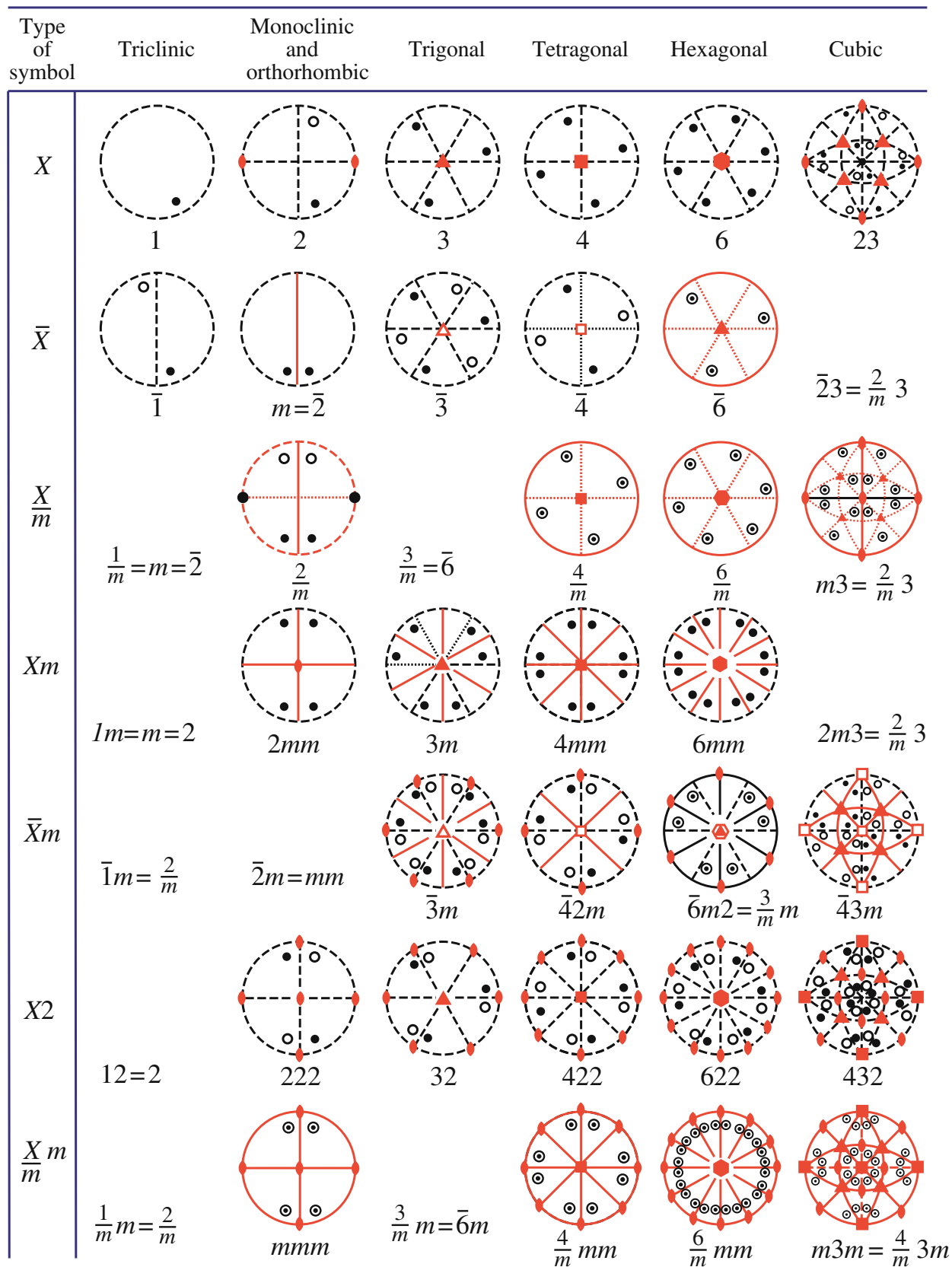
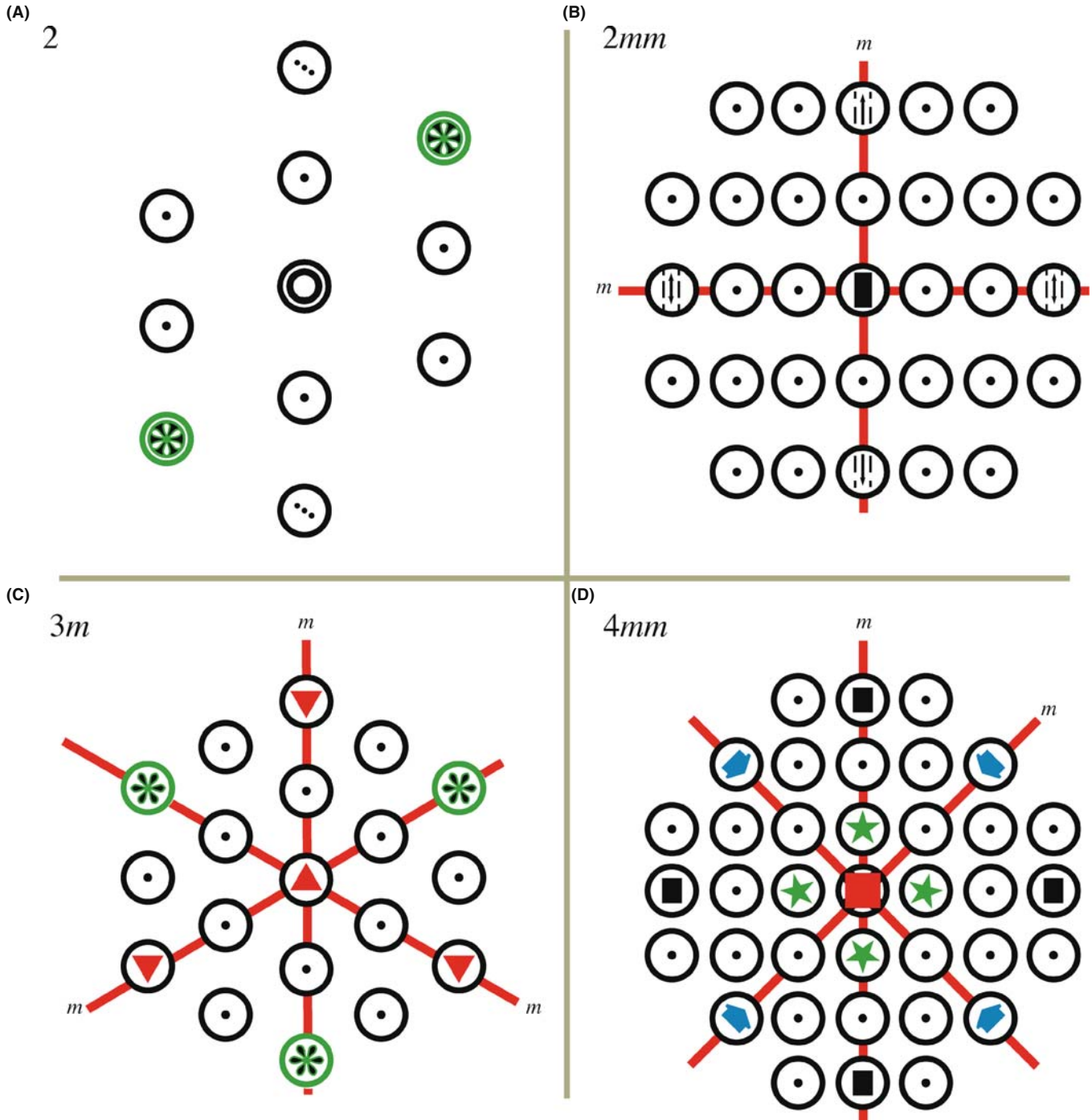


FIGURE 21.11 The 32 crystal point groups represented by stereograms showing the operation of rotational, mirror, and inversion symmetry elements on a general pole  $hkl$ . The international notation describing the point groups is given under each of the stereograms.



CBED patterns. When we look at CBED-pattern symmetry we use the same notation as for point groups, i.e., a number  $X$  ( $= 1, 2, 3, 4,$  or  $6$ ) for a rotation axis and  $m$  for a mirror plane parallel to the rotation axis and a second  $m$  for any independent mirror plane. Inversion symmetry or a mirror normal to the beam direction cannot be discerned and so the terms of the

form  $\bar{X}$  or  $X/m$  are not used. The only combinations we can get are the same as for the 10 2D point groups:  $1, 2, m, 2mm, 3, 3m, 4, 4mm, 6,$  or  $6mm$ . These symbols refer to the observable symmetry in the pattern, and four examples of different pattern symmetries are shown schematically in Figure 21.12.



**FIGURE 21.12** Four examples of symmetry in CBED patterns. (A) Symmetry 2 refers to a twofold (diad) rotation axis; i.e., the pattern has identical symmetry when rotated  $180^\circ$ . (B)  $2mm$  is a diad symmetry with two independent mirror planes parallel to the diad. (C)  $3m$  indicates threefold rotation (triad) symmetry with one mirror plane, i.e., rotational symmetry every  $120^\circ$  with one mirror plane present at each  $120^\circ$ . (D)  $4mm$  indicates a fourfold rotational symmetry (tetrad) with two independent mirror planes parallel to the tetrad.

Symmetry determination is generally carried out using ZAPs although there is useful information in off-axis patterns. Remember, to get a well centered ZAP

- You may find it easier to do the final adjustments to get an exact ZAP using the beam tilt/shift controls.
- As a last resort, you may have to displace the C2 aperture slightly off axis to center it precisely around the center of symmetry in the ZAP.

Once you've got a centered ZAP, there are specific kinds of symmetry for which to search

- Whole-pattern (WP) symmetry.
- Bright-field (BF) symmetry.
- Projection-diffraction symmetry.

The first and most important is the *WP symmetry*.

To be sure you get the correct symmetry, you should take a small camera-length pattern to include the HOLZ rings since HOLZ effects are not always visible in the ZOLZ (e.g., they may be hidden by the intense 000 disk). The pattern can be either a Kossel or a K-M pattern. The WP symmetry at any orientation must belong to one of the 10 2D point groups listed.

### WP SYMMETRY

The WP symmetry is just what it says: it's the symmetry of the whole pattern, including the relative positions of the HOLZ reflections and any HOLZ Kikuchi lines.

The second kind of symmetry is the *BF symmetry*.

In this case, the presence of the HOLZ lines ensures that the BF-disk symmetry contains 3D information. Take care to ensure that the C2 aperture is small enough so that you can see the 000 disk without any overlap from other diffraction disks. For example, the 000 disk back in Figure 20.2B has an array of deficient HOLZ lines which displays *3m* BF symmetry.

If there is only 2D diffuse intensity within the disk, or if you ignore the HOLZ lines, then the symmetry is more correctly called the *BF projection symmetry*. The symmetry in either of these latter cases should again be classified into one of the 10 2D groups just listed. You'll see in the companion text that combination of the WP and BF symmetry in three ZAPs is often sufficient to determine the point group.

### BF SYMMETRY

BF symmetry is the symmetry of the 000 disk only, when HOLZ lines are present.

On some occasions the *projection-diffraction symmetry* may be all that is available.

The diffuse contrast within these disks arises from dynamical interactions within the zero-order reciprocal-lattice layer of the crystal that give rise to K-M fringes, which we used above for thickness determination. The projection-diffraction symmetry is simply the symmetry displayed in SADPs. Since this symmetry is only 2D, it is not as useful as the WP and BF symmetry. If you go back and examine Figure 20.2B, the projection-diffraction symmetry is visible in the ZOLZ Kikuchi bands which show a sixfold rotational symmetry with two independent mirror planes, one within the Kikuchi bands and one between them, giving *6mm* symmetry. Similar symmetry is shown in the SADP from Si in Figure 20.2A.

### PROJECTION-DIFFRACTION SYMMETRY

This is displayed by the intensity in the direct 000 beam plus the *hkl* diffracted beams in the ZOLZ layer and corresponds to the projected 2D symmetry of the crystal down the zone axis that you have selected. It ignores any contributions from HOLZ layers, such as HOLZ lines and HOLZ reflections, but includes any diffuse intensity within these disks.

Now that you've learned the basics you should be able to breeze through the companion text which describes the process for point-group determination, step by step. After point-group determination you'll also be shown how to determine space groups. This exercise is a little more challenging and space groups are somewhat less important than point groups in terms of relating crystal symmetry to materials properties. Nevertheless, the space group of your specimen is an important crystallographic characteristic and since there are 230 of them it is a much more selective characteristic than the point group.

We'll now go on to discuss some more information that is available in HOLZ lines but, before you do this and before you read the CBED chapter in the companion text, we must warn you that symmetry determination from CBED patterns requires that you use your eyes to make a judgment on the presence or absence of certain symmetry elements and so this is not an exact science. There are 'error bars' in CBED symmetry and guidance on how to judge whether imperfections in the symmetry of the patterns can be ignored or not is also given in the companion text.

## 21.5 LATTICE-STRAIN MEASUREMENT

Strain arises from local changes in the lattice spacings of the material. Strain may arise from the presence of defects such as dislocations and coherent precipitates

or through local changes in chemistry. Such chemical changes can arise naturally or can be carefully introduced by controlling the deposition parameters for layered nanostructures formed by MBE or CVD methods. Either way, knowing the exact value of the strain is important in areas as diverse as mechanics, electronics, and optics. We can get a reasonably accurate measurement of the lattice constants ( $\sim 2\%$ ) by indexing the reflections in the ZOLZ and/or by measurement of the HOLZ-ring diameter. However, the best method is to use the positions of HOLZ lines in the BF disk which, because they arise from very high order reflections, are very sensitive to changes in lattice parameter. Results that are an order of magnitude more precise ( $\sim 0.2\%$ ) can be obtained by computer simulation of the position of the HOLZ lines using different lattice constants. The values that produce the best match with the experimentally observed HOLZ-line positions can be identified as the lattice constants of the crystal. So by measuring the HOLZ-line positions we can measure changes in lattice parameters. Materials scientists and nanotechnologists, particularly in the electronics industry, are most interested in changes due to lattice strain.

Local measurement of lattice strain has always been of interest to materials scientists and indeed we devote the whole of Chapter 25 to imaging of strain effects. Typically, direct lattice-strain measurements were performed by X-ray methods but the need for higher spatial resolution in semiconductor technology and nanostructured materials has created a tremendous market for CBED-based methods. For example, in semiconductor manufacturing and optical technologies, strain-layer superlattices (e.g., epitaxial layers of GaAs and AlGaAs which differ slightly in their precisely controlled lattice parameters) are widely used. Specific infrared sensors can be tuned, optical waveguides can be modulated, the

threshold voltages of lasers can be tweaked, and so on. Introducing local strain into the channel in semiconductor junctions to enhance carrier mobility and reduce the resistance between the source and drain has increased chip performance markedly, permitting Moore's law to be extended for yet a few more years. This concept is also referred to as 'strain engineering' and is central to the success of nanostructured electronics and optical devices.

Early CBED work in this area involved the measurement of strain around precipitates in thin foils (Rozeveld and Howe) and this has been extended down to nanometer-size probes coupled with sophisticated algorithms for matching the HOLZ-line patterns and extracting the strain measurement. Figure 21.13 shows the extraordinary match that can now be achieved between experiment and theory using Zuo's software which is a development of the early algorithms given in Spence and Zuo. Similar software is continuously being refined by many researchers and various forms are available on the Web at the URLs listed at the end of the chapter. As always, check the validity of the software by checking how well it simulates patterns from known specimens in known orientations: *caveat emptor* even if it's free!

In early computer programs, the position of the HOLZ lines in the simulation was derived from kinematical diffraction theory only, but dynamical effects may be important and should always be included, otherwise the match is incorrect (Eades et al.). The method is summarized in three steps.

- Start with a standard specimen of known lattice parameter to establish the exact electron wavelength for subsequent simulations.
- Adjust the continuous kV control. Since you know the lattice parameter, you can determine the exact kV.

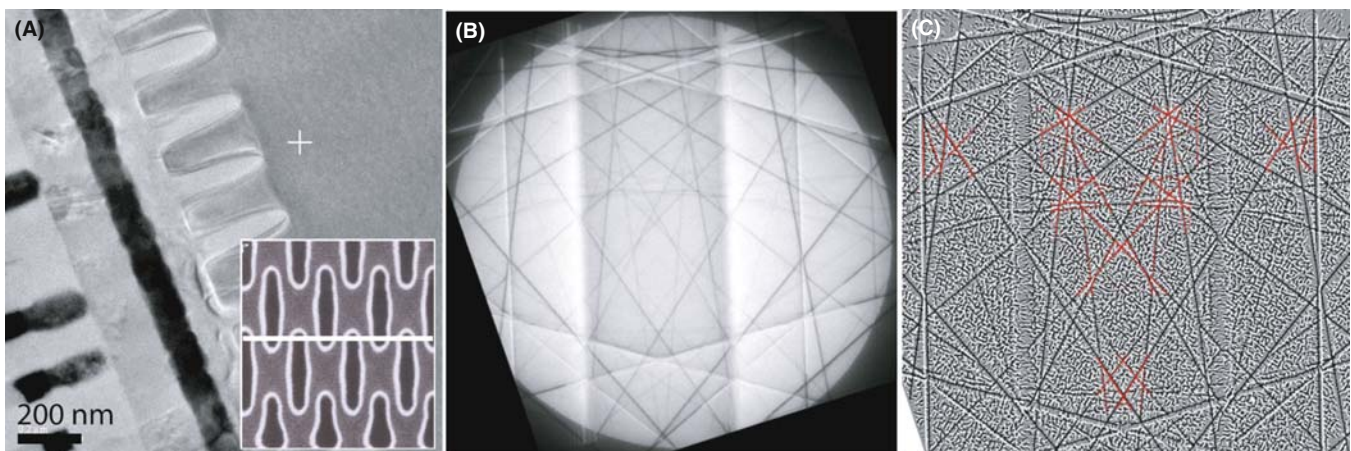


**FIGURE 21.13** (A) Cross-sectional BF image from a high-density, plasma-filled, shallow-trench isolation structure prepared along the line indicated on the SEM image (inset). (B) Experimental CBED HOLZ pattern taken at the cross in (A)  $\sim 10 \mu\text{m}$  away from the trench structure. (C) Simulation of a selected area of (B) where the HOLZ lines (highlighted in red) intersect showing the best fit for strain analysis. Both experimental and theoretical patterns were processed to enhance the contrast.



- At this predetermined kV setting, obtain a HOLZ-line pattern from the unknown and compare the experimental pattern with simulated patterns generated for a range of lattice parameters, until good matching is achieved between the simulated and experimental patterns (see Figure 21.13). Theoretically, an accuracy of 0.02% should be achievable but in practice an accuracy of 0.2% is generally obtained.

### LATTICE PARAMETERS FROM CBED

For determining precise values, compare the experimental HOLZ-line patterns to the computer-simulated version.

While this approach has demonstrated reasonable success in measuring lattice-parameter shifts as reviewed by Randle et al., you should be wary of other possible causes of HOLZ-line shifts and the difficulties of exact matching between theory and experiment. Often the HOLZ-line patterns display asymmetries which make matching difficult. Remember, you'll probably need to cool the specimen so you can see HOLZ lines in some materials. There are some necessary precautions you should take

- Compare your standard and unknown under identical conditions.
- Take account of any differences in thermal-contraction coefficient if you cool the specimen to liquid-N<sub>2</sub> temperatures.
- Watch for problems such as surface relaxation, or local strain, or the presence of dislocation lines which can give rise to spurious measurements of lattice parameter.

With this same approach we can also make localized measurements of strain around precipitates or defects, but the data are always averaged through the foil thickness and in one dimension and so the interpretation can be difficult. Furthermore, strain relaxation due to the presence of the surfaces of the specimen is an ever-present challenge. However, particularly in planar, thin-film layered structures it is often possible to tilt the specimen so that the local strain is projected along the beam direction. It is also feasible to use this HOLZ-line shift approach to infer, indirectly, the composition of a specimen by comparing the lattice parameter of an unknown with a standard of known composition and in the case of binary solid solutions, extrapolating to other compositions assuming that Végard's law applies. Such an analysis is not limited by elemental considerations or absorption, as is the case for XEDS, and does not require ultra-thin specimens as for EELS. However, this method is indirect and makes several assumptions that may not always apply. It's a last resort.

## 21.6 DETERMINATION OF ENANTIOMORPHISM

The terms 'handedness,' 'chirality,' and 'enantiomorphism' all refer to the same thing. We say that a crystal or molecule is 'handed' if two forms of the structure occur, and if we describe the atomic coordinates of one of them in a right-handed set of axes, the atomic coordinates of the other structure will be identical in a left-handed coordinate system. These two structures, termed 'enantiomorphic' or 'chiral,' are mirror images of each other and we refer to them as the right-handed and left-handed forms. (Look at your hands and try and rotate them into exact coincidence and all this should be clear.) If you go back and look at the section on symmetry concepts, you should be able to convince yourself that any crystal that contains a mirror (*m*), inversion center ( $\bar{1}$ ), or a fourfold inversion axis ( $\bar{4}$ ) cannot show chirality.

By the way, if you don't think such an esoteric topic as enantiomorphism is important then a salutary fact is that the drug thalidomide (2-(2,6-dioxo-3-piperidyl) isoindole-1,3-dione) comes in enantiomorphic crystal forms. One enantiomer (the *S*-form) causes catastrophic birth defects in children and the other (*R*-form) provides the desired therapeutic effects for women suffering difficult pregnancies and is particularly efficacious as a treatment for disfiguring skin lesions such as those arising from leprosy. Thousands of seriously deformed children were born because of the failure to distinguish the different effects of the two enantiomorphs. This tragedy gave rise to the whole field of single-enantiomer drug development (currently a \$100B/yr market in the USA alone), avoiding the common racemic mixture of both forms that is produced in most chemical processes.

So, although we don't often need to know which of the two-handed forms we are looking at, there are occasions when it is of the utmost importance, and several groups have worked hard on the determination of handedness from CBED.

Enantiomorphism is an essentially 3D phenomenon (again, look at your hands). Since the projection of a crystal is a 2D object, a projection of the structure cannot tell you anything about the handedness. This means that, in ZAPs, to see handedness, we must look at effects of HOLZ diffraction or, more generally, if your specimen is not at a zone axis, there must be diffraction involving at least three *non-coplanar* diffraction vectors in addition to the direct beam. This condition does not necessarily mean that we have to look at a HOLZ pattern. It means that we have to look at HOLZ diffraction effects which, as you now know well, may appear in the ZOLZ as well as in HOLZ directly. In the example given in Figure 21.14, the asymmetric effects are visible only in the reflections in the first HOLZ ring.

Looking at HOLZ effects, we can readily see the difference between enantiomorphs. But just observing



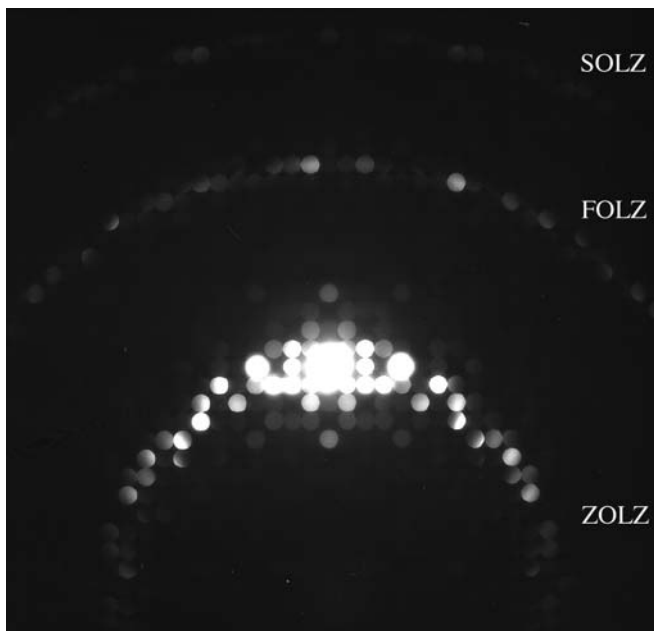


**FIGURE 21.14** CBED pattern from a specimen of  $\text{Ho}_2\text{Ge}_2\text{O}_7$ , tilted slightly away from the zone axis to improve the contrast. The ZOLZ (the bright spots just below the center of the figure) shows mirror symmetry but in the HOLZ ring (above the center) the reflections are clearly asymmetric. If the specimen had the other chirality, the HOLZ ring would be mirrored across the vertical axis of the pattern.

the difference does not let us to say which structure is which hand. It does allow us to say whether two crystals have the *same* or *opposite* handedness.

The determination of whether a particular crystal is right-handed or left-handed requires a dynamical calculation to simulate CBED patterns which you must then compare with the experimental patterns. But note

- You'll find that such a comparison with experiment is not always easy because there is often ambiguity in the indexing of the pattern and, if your indexing is wrong, the handedness will be wrong.
- To perform the simulation and thus to determine the handedness, you need to know the full crystal structure.
- Some authors have suggested that the dynamical calculations (needed to say which enantiomorph is which) can be done by hand, e.g., by calculating the phases of the structure factors and working out the effects of multiple-diffraction paths. However, this calculation requires considerable understanding of dynamical diffraction and it is surely easier, as well as more reliable, to perform a full dynamical *simulation* using some of the software we've already referenced.

Recently Inui et al. have systematically tabulated appropriate zone axes for the determination of handedness for all the point groups that can show handedness. In studies of enantiomorphism, it is crucial to determine

whether or not a CBED pattern contains mirror symmetry or not. You'll find that doing this is not always easy but, if you use off-axis patterns rather than ZAPs, the asymmetries tend to be stronger, as described by Jones (and also shown in Figure 21.14).

## 21.7 STRUCTURE FACTOR AND CHARGE-DENSITY DETERMINATION

When you read the literature about CBED and its applications, you'll often come across references to extraction of structure factor ( $F_{hkl}$ ) values via CBED. (Go back to Chapter 3 to remind yourself of the importance of structure factors in electron diffraction.) You should remember that  $|F(\theta)|^2$  is direct measure of the diffracted intensity. Direct, reproducible, and quantitative measurement of the diffracted intensity is basically impossible in SADPs but is quite feasible in CBED patterns, especially when they are energy-filtered. When we determine a specific crystal structure for our specimen, it is, in fact, equivalent to assigning a structure-factor phase to the diffraction disks in the pattern. There are

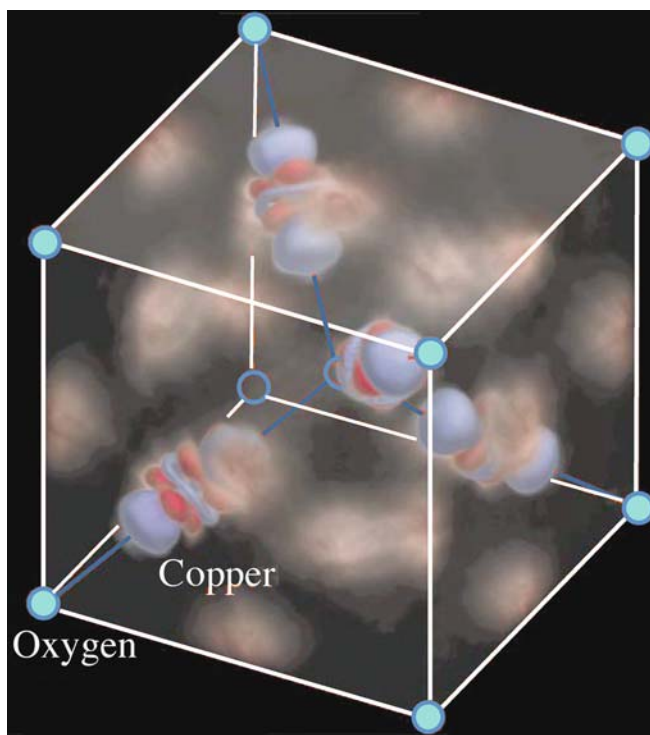


**FIGURE 21.15** A three-dimensional rendering of the experimental difference map between the static crystal charge density (determined from quantitative analysis of CBED patterns) and the superimposed spherical charge density of  $\text{O}^{2-}$  and  $\text{Cu}^+$  ions. The color scheme is blue where the difference in charge density is negative ( $\Delta\rho < 0$ ), white where it is zero ( $\Delta\rho = 0$ ), and red where it is positive ( $\Delta\rho > 0$ ). The difference would be zero everywhere if cuprite were purely ionic (i.e., the ions were indeed spherical). The non-spherical charge distortion on the Cu atoms shows the characteristic shape of d orbitals. The positive charge in the tetrahedral interstitial regions suggests Cu–Cu covalent bonding.

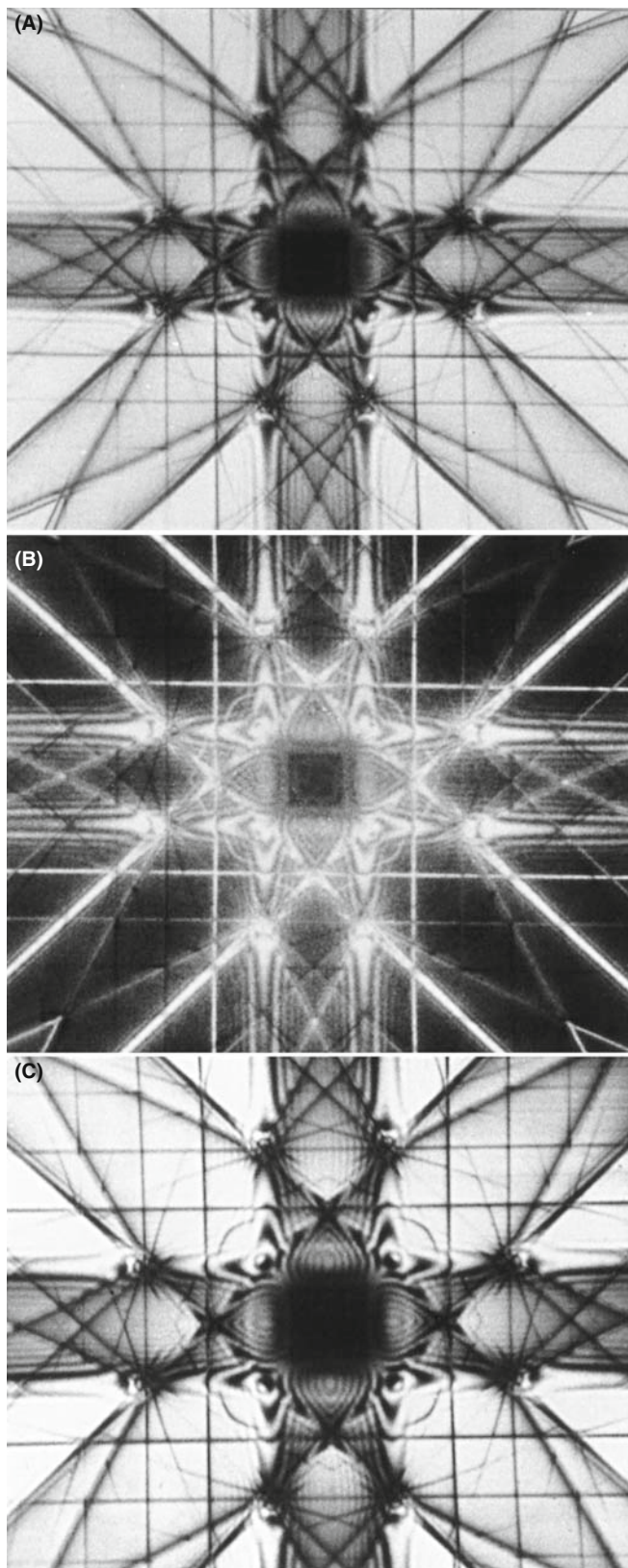


**FIGURE 21.16** Series of Eades double-rocking ZAPs obtained from a thin Al foil in the [001] orientation. (A) is the BF image, (B) is the 200 DF image, and (C) is an energy-filtered version of (A). The removal of energy-loss electrons sharpens the image.

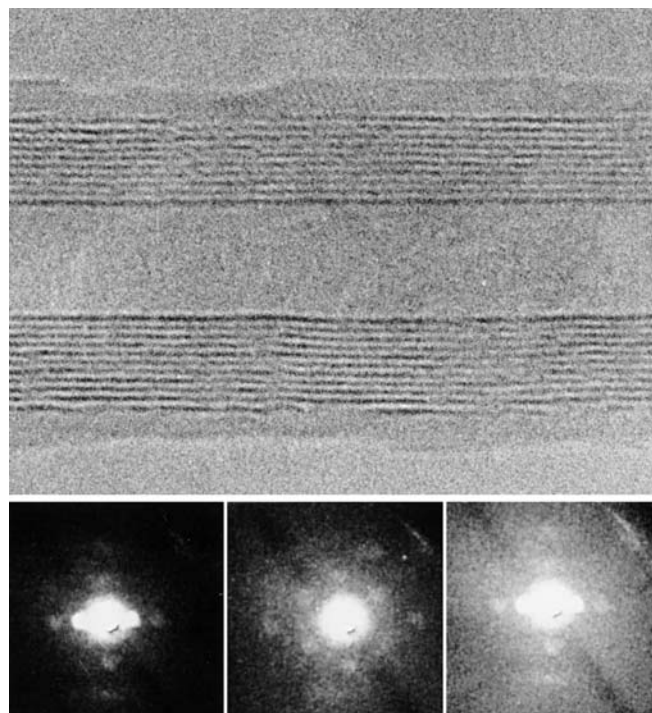


**FIGURE 21.17** Nanodiffraction patterns from a multi-walled carbon nanotube (top).

several ways to do this and advances in computer simulation and CCD cameras make the direct, quantitative interpretation of diffracted intensity much more tractable, but the essential steps were all described by Spence and Zuo. Basically, we match computer simulations of intensity variations in the CBED disks with the experimental patterns, assigning specific values of  $F_{hkl}$  to each of the reflections until the best fit is obtained. So it is computer-intensive, but that is not a problem today.

Once the structure-factor data are obtained, a very useful side effect is that the valence-electron density can be measured from the low-order structure factors and this characteristic is otherwise inaccessible experimentally for crystals without an inversion symmetry (Spackman et al.). Once measured, the valence-electron density can be mapped out and the culmination of much of this work was the first-ever direct imaging of an atomic bond (Zuo et al.) (Figure 21.15).

## 21.8 OTHER METHODS

### 21.8.A Scanning Methods

Diffraction is as useful in scanning-beam instruments as in TEM. As we discussed back in Chapter 18, electron-backscatter diffraction (EBSD) studies are as ubiquitous today as SAD and CBED and very complementary. Many more crystals can be studied by EBSD and the specimen does not need to be thinned. EBSD patterns contain HOLZ lines just like CBED patterns.



Historically, electron channeling was another way to obtain crystallographic information in the SEM but the patterns are of such low contrast that EBSD has rendered the channeling technique obsolete (for now).

Scanning DPs can be obtained in STEMs using either one or two sets of coils both before and after the specimen. In both cases the beam is stationary at the plane of the specimen and rocks back and forth in a manner similar to the hollow-cone or precession methods we described in Chapters 18 and 20. Using only one scan coil below the specimen partially ‘de-rocks’ the beam but two coils fully ‘de-rock’ the beam such that, instead of the DP scanning across the BF STEM detector and being recorded sequentially, the 000 disk is always on the optic axis and thus on the BF detector. However, the HOLZ lines, etc., move continuously across the detector because, like Kikuchi lines, they are ‘fixed’ to the specimen. The resulting double-rocking patterns, which are often named after their inventor, Alwyn Eades, cover several degrees in comparison with the fractions of a degree visible in a normal CBED disk. These patterns are very striking as you can appreciate from Figure 21.16; such patterns can be viewed in BF or DF and, as with all CBED patterns, can be sharpened by energy filtering. These scanning methods can be used to study the occurrence of forbidden

reflections which are important in crystal-symmetry determinations and more detail is given in the companion text.

### 21.8.B Nanodiffraction

Nanodiffraction, as the term implies, involves diffraction with a nanometer-scale beam and has been pioneered by Cowley. Nanometer beams have only a few picoamps of current so the patterns are noisy and require a FEG-TEM (or DSTEM), which also provides a coherent beam. If you scan the literature, you’ll find that nanodiffraction permits determination of local variations of crystallography within large individual unit cells, dislocation cores, grain-boundary segregant films, individual nanotubes or nanoparticles such as catalysts. Figure 21.17 shows nanodiffraction patterns from a single, multi-walled, carbon nanotube.

In addition, it is possible to assess crystallographic effects associated with medium-range ordering by correlating atom positions over distance of a few nanometers. Nanodiffraction methods have helped develop the new field of fluctuation microscopy which we mention again in Chapter 29; they are also essential for diffractive imaging with atomic resolution.

## CHAPTER SUMMARY

CBED patterns contain contrast information which gives a complete crystallographic characterization of small crystals, as well as other information such as thickness. To make the most of this capability you need detailed knowledge of crystal-symmetry concepts, stereographic projections, and the ability to produce ZAPs from a variety of orientations. In addition, the determined operator is often rewarded with patterns that are both very useful and stunningly beautiful. Before you go and read about CBED in the companion text, remember that, if you want to determine the point group and/or the space group from your CBED patterns, you need to determine

- WP symmetry
- BF symmetry
- Projection-diffraction symmetry

CBED symmetry information from the HOLZ-line distribution in the 000 disk is also very useful for measuring other characteristics of our specimens which cannot be determined, on a nanoscale, by other techniques. The examples we showed were lattice strain, an essential variable in the electronics and optical industries, enantiomorphism, structure-factor and charge-density determinations. If you’ve successfully worked your way through these two chapters, then you’re ready for the companion text and the more challenging aspects of CBED, such as measurement of defect crystallography, structure factors, Debye-Waller factors, polarity, and charge density which are discussed in depth in the essential texts by Spence and Zuo and by Morniroli.

### THE JEOL CBED ATLAS

By Tanaka, M et al, 1985-2002 *Convergent Beam Electron Diffraction I-IV* JEOL Tokyo. The details are in Chapter 20.

## TECHNIQUE

- Eades, JA 1989 (Ed.) *Journal of Electron Microscopy Techniques* **13** (I & II). Special issues on CBED with many useful papers covering much of the content of this chapter.
- Jones DN 2007 *Sensitive Detection of Mirror Symmetry by CBED Applied to LaAlO<sub>3</sub> and GdAlO<sub>3</sub>* *Acta Cryst.* **B63** 69–74. Using off-axis CBED patterns.
- Mansfield, JF 1984 *Convergent Beam Electron Diffraction of Alloy Phases* Adam Hilger Ltd. Bristol UK. A great collection of CBED patterns and proof that steel can still be beautiful.
- Morniroli, J-P 2002 *Large-Angle Convergent-Beam Electron Diffraction (LACBED)* SFμ. (Société Française des Microcopies) Paris, France. The essential instructional text full of great diagrams and practical examples along with an excellent bibliography
- Spence, JCH and Zuo, JM 1992 *Convergent Beam Electron Diffraction* Plenum Press New York. You will want a copy of this book if you use CBED extensively. You may find a reference to earlier CBED studies on your material here in the selective bibliography organized by material. Although now considered obsolete by some, the original code for plotting HOLZ lines is included in the appendices along with the Fortran code for one Bloch wave and one multislice program.

## THICKNESS DETERMINATION

- Allen, SM 1981 *Foil Thickness Measurements from Convergent-Beam Diffraction Patterns* *Phil. Mag.* **A43** 325–335.
- Kelly, PM, Jostons, A, Blake, RG and Napier, JG 1975 *The Determination of Foil Thickness by Scanning Transmission Electron Microscopy* *Phys. Stat Sol.* **A31** 771–780.

## APPLICATIONS

- Ayer, R 1989 *Determination of Unit Cell* *J. Electron Microsc. Tech.* **13** 16–26.
- Berta, Y, Ma, C and Wang, ZL 2002 *Measuring the Aspect Ratios of ZnO Nanobelts* *Micron* **33** 687–691.
- Cowley, JM 2001 *Electron Nanodiffraction Methods for Measuring Medium-Range Order* *Ultramicrosc.* **90** 197–206. Nanodiffraction.
- Kim, M, Zuo, JM and Park, G-S 2004 *High-Resolution Strain Measurement in Shallow Trench Isolation Structures Using Dynamic Electron Diffraction* *App. Phys. Lett.* **84** 2181–2183.
- Mansfield, JF 1985 *Error Bars in CBED Symmetry?* *Ultramicrosc.* **18** 91–96. As it says.
- Raghavan, M, Scanlon, JC and Steeds, JW 1984 *Use of Reciprocal Lattice Layer Spacing in Convergent Beam Electron Diffraction Analysis* *Metall. Trans.* **15A** 1299–1302.
- Randle, V, Barker, I and Ralph, B 1989 *Measurement of Lattice Parameter and Strain Using Convergent Beam Electron Diffraction* *J. Electron Microsc. Tech.* **13** 51–65. Accuracy in using HOLZ lines for determining lattice parameters.
- Steeds, JW 1979 *Convergent Beam Electron Diffraction in Introduction to Analytical Electron Microscopy* 387–422 Eds. JJ Hren, JI Goldstein and DC Joy Plenum Press, New York.

## CRYSTALLOGRAPHY

- Eades, JA, Moore, S, Pfullman, T and Hangan, J 1993 *Discrepancies in Kinematic Calculations of HOLZ Lines* *Microscopy Research and Technique* **24** 509–513. The importance of dynamical scattering for HOLZ line calculations.
- Inui, H, Fujii, A, Sakamoto, H, Fujio, S and Tanaka, K 2007 *Enantiomorph Identification of Crystals Belonging to the Point Groups 321 and 312 by Convergent-Beam Electron Diffraction* *J. Appl. Cryst.* **40** 241–249.
- Jackson, AG 1987 *Prediction of HOLZ Pattern Shifts in Convergent Beam Diffraction* *J. Electron Microsc. Tech.* **5** 373–377. Collected data.
- Jackson, AG 1990, *Identification of the Laue Zone Number in HCP Systems in Convergent Beam Electron Diffraction* *Ultramicrosc.* **32** 181–182.
- Nye, JF 1985 *Physical Properties of Crystals* (2nd Ed.) Oxford University Press New York.

## INDEXING AND LATTICE PARAMETERS

- Ecob, RC, Shaw, MP, Porter, AJ and Ralph, B 1981 *Application of Convergent-Beam Electron Diffraction to the Detection of Small Symmetry Changes Accompanying Phase Transformations – I. General and Methods* *Phil. Mag.* **A44** 1117–1133. Early HOLZ/FOLZ.
- Fournier, D, L'Esperance, G, Saint-Jacques, RG 1989 *Systematic Procedure for Indexing HOLZ Lines in Convergent Beam Electron Diffraction Patterns of Cubic Crystal* *J. Electr. Microsc. Tech.* **13** 123–149.
- Morawiec, A 2007 *A Program for Refinement of Lattice Parameters Based on Multiple Convergent-Beam Electron Diffraction Patterns* *J. Appl. Cryst.* **40** 618–622.
- Rozeveld, SJ and Howe, JM 1993 *Determination of Multiple Lattice Parameters from Convergent-Beam Electron Diffraction Patterns* *Ultramicrosc.* **50** 41–56.



## BONDS

- Spackman, MA, Jiang, B, Groy, TL, He, H, Whitten, AE and Spence, JCH 2005 *Phase Measurement for Accurate Mapping of Chemical Bonds in Acentric Space Groups* Phys. Rev. Lett. **95** 085502–05. Inversion symmetry.
- Zuo, JM, Kim, M, O’Keeffe, M and Spence, JCH 1999 *Direct Observation of d-Orbital Holes and Cu-Cu Bonding in Cu<sub>2</sub>O* Nature **401** 49–52. ‘Imaging’ atomic orbitals

## URLs

- 1) <http://cimewww.epfl.ch/people/stadelmann/jemsWebSite/DiffractionPatterns.html> (Stadelmann’s EM Yellow Pages at EPF Lausanne)
- 2) [www.gatan.com/imaging/dig\\_micrograph.php](http://www.gatan.com/imaging/dig_micrograph.php) (Gatan’s software suite)
- 3) [www.soft-imaging.net](http://www.soft-imaging.net) (Olympus’s Soft Imaging System)
- 4) <http://emaps.mrl.uiuc.edu> (Maintained by Zuo at UIUC)
- 5) <http://cimesg1.epfl.ch/CIOL> (Stadelmann’s JEMS for students) and <http://cimewww.epfl.ch/people/stadelmann/jemswebsite/jems.html>, the main site
- 6) [www.amc.anl.gov](http://www.amc.anl.gov) (Zaluzec’s Argonne National Laboratory site)
- 7) [www.public.asu.edu/~jspence/ElectrnDiffn.html](http://www.public.asu.edu/~jspence/ElectrnDiffn.html) (the IUCr site)

## SELF-ASSESSMENT QUESTIONS

- Q21.1 Why would you want to measure your specimen thickness with CBED?
- Q21.2 Why do you need a foil of a certain thickness before you see K-M fringes?
- Q21.3 Why do the K-M fringes increase in number as the specimen gets thicker?
- Q21.4 List the experimental factors that can limit the accuracy of your thickness determination.
- Q21.5 How can you create a continuous ring of HOLZ intensity rather than a distribution of HOLZ disks? Why would you want to do this, thus losing the distribution of individual disks in the pattern?
- Q21.6 Why might you have to record several CBED patterns to get all the useful information?
- Q21.7 Why is the HOLZ-ring radius important and what microscope parameters should you use to ensure that you can easily see the ring(s)?
- Q21.8 Distinguish A-, B-, C-, and I-lattice centering.
- Q21.9 What is Friedel’s law and why is it important when trying to infer symmetry from CBED patterns?
- Q21.10 Distinguish the BF symmetry and the whole-pattern symmetry.
- Q21.11 Distinguish diffraction groups and point groups.
- Q21.12 What distinguishes space groups from point groups?
- Q21.13 Define WP and CBIM.
- Q21.14 How can compositional changes manifest themselves in CBED patterns?
- Q21.15 Why would lattice strain effects appear in HOLZ-line patterns?
- Q21.16 What is enantiomorphism and why would this property affect the symmetry of DPs?
- Q21.17 Why might you want to form a DP while the beam is scanning rather than stationary?
- Q21.18 Why might it be useful to see both image and diffraction information in the same picture at the same time, as in CBIM?
- Q21.19 Why is the nanodiffraction pattern in Figure 21.17 noisy?
- Q21.20 List the main applications of CBED that cannot be performed with standard SAD techniques.

## TEXT-SPECIFIC QUESTIONS

- T21.1 We get parallel fringes in CBED patterns under two-beam conditions and also in TEM images under two-beam conditions. Explain why this is so and why the symmetry of the fringes changes in the 000 and the *hkl* disk in a similar manner to changes in BF and DF images. (Hint: go and look in the imaging chapters.)
- T21.2 Reproduce the data in Tables 21.1 and 21.2 from the information given in the chapter.
- T21.3 Given that the lattice parameter of stainless steel is 0.405 nm, work out the lattice spacing in the [111] direction from the HOLZ ring in Figure 20.16B.
- T21.4 Draw schematic diagrams like in Figure 21.12 to show threefold (triad) and *6mm* symmetry.
- T21.5 Go back and look at Figures 20.4A and 20.16C and state the BF symmetry in each case.
- T21.6 Why is the CBED technique seeing increasing usage for crystal structure determination, displacing some of the more conventional XRD techniques?
- T21.7 Why are there diffraction spots in Figure 21.17 when there are no visible crystal planes in the center of the image from where the pattern is taken?
- T21.8 Why does energy-filtering sharpen the DP in Figure 21.16C? (Hint: look ahead to the EELS chapters.)
- T21.9 If lattice strain disturbs the crystal plane spacing in three dimensions, how is it possible to deduce this strain from 2D HOLZ-line distributions?